



HAL
open science

Investigation of encapsulation of Aromatic pollutants by β -Cyclodextrin in presence of linear aliphatic alcohols

Shivalika Tanwar

► To cite this version:

Shivalika Tanwar. Investigation of encapsulation of Aromatic pollutants by β -Cyclodextrin in presence of linear aliphatic alcohols. Organic chemistry. Université Sorbonne Paris Cité, 2018. English. NNT : 2018USPCD076 . tel-02613822

HAL Id: tel-02613822

<https://theses.hal.science/tel-02613822>

Submitted on 20 May 2020

HAL is a multi-disciplinary open access archive for the deposit and dissemination of scientific research documents, whether they are published or not. The documents may come from teaching and research institutions in France or abroad, or from public or private research centers.

L'archive ouverte pluridisciplinaire **HAL**, est destinée au dépôt et à la diffusion de documents scientifiques de niveau recherche, publiés ou non, émanant des établissements d'enseignement et de recherche français ou étrangers, des laboratoires publics ou privés.

Université Paris 13-UFR SMBH

THESE

Pour Obtenir le grade de
DOCTEUR DE L'UNIVERSITE PARIS 13

Discipline : Chimie
Ecole doctorale Galilée

Présentée et Soutenue publiquement par

Shivalika TANWAR

Le 26 Novembre 2018

**Investigation of encapsulation of Aromatic pollutants by
 β -Cyclodextrin in presence of linear aliphatic alcohols**

Directrice de thèse: Prof. Nathalie DUPONT

JURY

Professeur. D LANDY

Rapporteur

Professeur. F PILARD

Rapporteur

Docteur. E GUENIN

Examineur

Docteur. F SCHOENSTEIN

Examineur

Docteur. S BLANCHARD

Examineur

Professeur. N DUPONT

Directrice de thèse

Acknowledgement

I would never have been able to complete my doctoral studies without my continuous faith in God along with the help and support from my family and friends. Thus, I would like to take the opportunity to express my greatest appreciation.

First of all, I would like to thank the members of the evaluation committee for their kind agreement to revise this work. Hence I would like to acknowledge Professor D. Landy and Professor F. Pilard for accepting to be referees. Thank you for your time to evaluate my thesis. Equally, I would like to express my gratitude to Doctor Erwann Guenin, Doctor S Blancard and Doctor Frédéric Schoenstein for their acceptance to be examiners.

I would like to acknowledge my mentor and advisor, Professor Nathalie DUPONT, for encouraging my growth and competence to become a more self-directed, self-motivated, and highly –independent scientific researcher. Thank you for having time to answer all my questions, for providing endless guidance toward the success and giving me constant motivation. Furthermore, I would like to thank our team members, SBMB for their timely help and advices on all matters. Your support made my three years easier.

Also, I would like to acknowledge Institute Galilée (University Paris 13) for funding my thesis. I would like to express my great thanks to IUT, Saint Denis for allowing me to use characterization techniques like Powder XRD and DSC.

Many thanks to past and present PhD students and engineers in the CSPBAT laboratory. I want to especially thank to Inga Tijunelyte, Raymond Gilibert, Hanane Moustouai and Agnès Victorbala for their discussions about science and help during the tough phases. Additional thanks to the master students who were present in our team during my thesis.

Last but not the least I thank you all my friends and family for understanding, support and encouragement. Lastly, I thank my husband Varun, for his love and care during these years. Thank you all!!

Abbreviations

α CD - Alpha cyclodextrin

β CD- Beta cyclodextrin

γ CD- Gamma cyclodextrin

δ CD- Delta cyclodextrin

CD(s)- Cyclodextrin(s)

BTEX- Benzene, Toluene, Ethylbenzene, Xylenes

PAH(s)- polycyclic aromatic hydrocarbon(s)

AH(s)- Aromatic hydrocarbon(s)

NMR- Nuclear magnetic resonance

PXRD- Powder X-ray Diffraction

DSC- Differential Scanning Colorimetry

BEN- Benzene

FB- Fluorobenzene

TOL- Toluene

TFT- α,α,α trifluorotoluene

PHE- Phenol

BA- Benzoic acid

NAP- Naphthalene

2NAP- 2-Naphthol/ β -Naphthol

ANTH- Anthracene

PYR-Pyrene

DFT- Density Functional Theory

E.U WFD- European Union water framework Directive

U.S EPA- United States Environment Protection Agency

CSD- Cambridge Structural Database

REF- Reference

MM- Molecular mechanics

MD- Molecular dynamics

QM- Quantum Mechanical

DNA- Deoxyribonucleic acid

HPLC- High pressure liquid Chromatography

LC- Liquid chromatography

HRGC-MS- High resolution gas chromatography-mass spectroscopy

LC-FD- Liquid chromatography fluorescence detection

USAEME- Ultrasound-assisted emulsification microextraction

DLLME- Dispersive liquid-liquid microextraction

D₂O- Deuterium Oxide

MW- Molecular weight

TMS- Tetramethylsilane

U.V- Ultra Violet

RT- Room temperature

mM-millimolar

TGA- Thermogravimetric analysis

FWHM- Full width half maxima

λ_{cu} – Wavelength of copper

Å- Angstrom

IR- Infrared

LUMO- Lowest unoccupied molecular orbital

HOMO- Highest occupied molecular orbital

Chapter wise listing of figures and tables

Chapter 1

Table 1.1 : Chronological summary on the development of Cyclodextrins.

Table 1.2 : List of Chemically modified CDs and their abbreviations.

Table 1.3 : Properties of natural cyclodextrins.

Table 1.4 : Compilation of the molecular modeling methods used in the study cases.

Figure 1.1: Glucopyranose unit.

Figure 1.2: Macrocyclic structures with cavity diameters of parent CDs. a) α CD, b) β CD and c) γ CD.

Figure 1.3: Exterior and Interior of the CD cavity.

Figure 1.4: Schematic diagram of CD showing the cavity, primary and secondary faces and the distribution of primary and secondary hydroxyl groups on the two CD faces.

Figure 1.5: CD Inclusion compounds and Stoichiometry.

Figure 1.6 : Views along c axis (right) and b axis (left) of CSD organization in the channel type structure CSD PUKPIU. Guest molecules are willingly hidden. Hydrogen atoms are not represented. Carbon atoms are represented in grey while oxygen atoms are represented in red.

Figure 1.7 : Views along b axis (right) and c axis (left) of CDs organization in the herringbone dual nested channel type structure CSD BCDEXD10. Guest molecules are willingly hidden. Hydrogen atoms are not represented. Carbon atoms are represented in grey while oxygen atoms are represented in red.

Figure 1.8 : Views along b axis (right) and c axis (left) of CDs organization in the brick dimer type structure CSD BOTBES. Guest molecules are willingly hidden. Hydrogen atoms are not represented. Carbon atoms are represented in grey while oxygen atoms are represented in red.

Figure 1.9. Repartition in term of space groups and structural types of the structures involving α CD, β CD and γ CD available in the CSD version 5.39 update 3 (May 2018).

Chapter-2

Table 2.1 : The different mixtures of solution prepared for β CD and linear alcohols.

Table 2.2 : The different mixtures of solution prepared for β CD and Aromatic hydrocarbons.

Table 2.3 : Experimentally Observed $^1\text{H-NMR}$ chemical shifts, (δ ppm), of C-H protons in unsubstituted CDs in D_2O .

Table 2.4: The position and multiplicity of the proton NMR peak in all alcohols studied.

Table 2.5 : Principal structural characteristics of the CSD structures used further as references.

Table 2.6 : Simulated X-ray pattern of CSD refcode BCDEXD10 for $4^\circ < 2\theta < 14^\circ$: Dual channel Herringbone structural type. ($\lambda_{\text{Cu}}=1.5405 \text{ \AA}$, FWHM = 0.1).

Table 2.7: Simulated X-ray pattern of CSD refcode CACPOM for $4^\circ < 2\theta < 14^\circ$: dual channels made with dimer brick structural type. ($\lambda_{\text{Cu}}=1.5405 \text{ \AA}$, FWHM = 0.1).

Table 2.8 : Simulated X-ray pattern of CSD refcode PUKPIU for $4^\circ < 2\theta < 14^\circ$: Channel structural type. ($\lambda_{\text{Cu}}=1.5406 \text{ \AA}$, FWHM = 0.1).

Table 2.9 : Simulated X-ray pattern of CSD refcode POHXUG for $4^\circ < 2\theta < 14^\circ$: Channel structural type. ($\lambda_{\text{Cu}}=1.5405 \text{ \AA}$, FWHM = 0.1).

Table 2.10 : Simulated X-ray pattern of CSD refcode ZUZOH for $4^\circ < 2\theta < 14^\circ$: Channel structural type. ($\lambda_{\text{Cu}}=1.5405 \text{ \AA}$, FWHM = 0.1).

Table 2.11 : Experimental X-ray pattern of β CD directly out of the box (Wacker) and CSD refcode reference assignment.

Table 2.12 : XRD peaks corresponding to different types of β CD Crystals.

Table 2.13 : Common characteristic frequencies of organic compounds.

Figure 2.1 : Energy levels of a nucleus with spin quantum number.

Figure 2.2 : Effect of magnetic field on the energy gap between two possible states adopted by a spinning nucleus.

Figure 2.3 : Spinning motion of a nucleus on its axis.

Figure 2.4 : Flipping of the magnetic moment on absorption of energy.

Figure 2.5 : Experimental setup for NMR.

Figure 2.6 : Graphical representation of job's plot showing (a)1:1 (b) 2:1 and (c) 1:2 complexations respectively.

Figure 2.7 : Glucopyranose unit with atoms numbering.

Figure 2.8 : Positions of different Hydrogens in a CD molecule.

Figure 2.9 : ^1H NMR experimental spectrum of β CD (10mM) solution in D_2O .

Figure 2.10 : Observed proton NMR spectrum of Hexanol.

Figure 2.11 : Schematic of crystal formation at liquid-liquid interface.

Figure 2.12 : Power Compensated DSC.

Figure 2.13 : Observed DSC thermogram of β CD.

Figure 2.14 : Bragg's Law reflection.

Figure 2.15 : Types of diffraction patterns obtained by different style arrangements of β CD while forming an inclusion complex. Simulation done with the Mercury software ($\lambda_{\text{Cu}}=1.5405 \text{ \AA}$, FWHM = 0.1).

Figure 2.16 comparison of diffraction patterns of experimentally observed and simulated herringbone structure (BCDEXD10) from literature of β CD. The CSD reference are BCDEXD10 and ZUZXOH. The experimentally observed β CD pattern can be seen to show peaks corresponding to both these structures.

Figure 2.17 : Observed powder XRD pattern of β CD co-precipitated in presence of octanol in comparison with the powder xray simulated pattern from 4° to 14° in 2θ for CSD CACPOM exhibiting a brick type dimers structural type.

Figure 2.18 : "Jablonski" style diagram of energetic transitions involved in Raman scattering. Rayleigh scattering is elastic; the incident photon is of the same energy as the scattered photon. Raman scattering is inelastic; in Stokes scattering, the incident photon is of greater energy than the scattered photon, while in anti-Stokes scattering, the incident photon is of lower energy.

Figure 2.19 : Observed Raman Spectrum of β CD.

Figure 2.20 : Manual docking procedure of a guest (herein a pentanol molecule) in β CD with the two orientations A and B. Carbon, oxygen and hydrogen atoms are respectively represented in grey, red and white.

Chapter-3

Table 3.1: Volume of β CD and Alcohols solutions mixed together to form inclusion complexes in D_2O to carry out NMR studies.

Table 3.2: Shows the significant shifts for the peak positions of H5 and H3 for lower alcohols for the stoichiometry 1:1

Table 3.3 : Shows the significant shifts for the peak positions of H5 and H3 for higher alcohols for the stoichiometry 1:1.

Table 3.4 : Shows the observed medium H3 and H5 R_{max} values for each β CD: Higher alcohols and the corresponding stoichiometry

Table-3.5: List of boiling point temperatures of different linear alcohols (from methanol to Butanol)

Table-3.6:List of boiling point temperatures of different linear alcohols (from pentanol to n-Undecanol)

Table-3.7:Vibrational regions assigned to alcohols

Table 3.8: Energies features. thermodynamic and electronic parameters of β CD:methanol complexes by PM3 method for the more thermodynamically favorable complex of each orientation.

Table 3.9: Energies features. thermodynamic and electronic parameters of β CD:ethanol complexes by PM3 method for the more thermodynamically favorable complex of each orientation

Table 3.10: Energies features. thermodynamic and electronic parameters of β CD:propanol complexes by PM3 method for the more thermodynamically favorable complex of each orientation

Table 3.11: Energies features. thermodynamic and electronic parameters of β CD:Butanol complexes by PM3 method for the more thermodynamically favorable complex of each orientation

Table 3.12: Energies features. thermodynamic and electronic parameters of β CD:pentanol complexes by PM3 method for the more thermodynamically favorable complex of each orientation

Table 3.13: Energies features. thermodynamic and electronic parameters of β CD:Hexanol complexes by PM3 method for the more thermodynamically favorable complex of each orientation.

Table 3.14: Energies features. thermodynamic and electronic parameters of β CD:Heptanol complexes by PM3 method for the more thermodynamically favorable complex of each orientation

Table 3.15: Energies features. thermodynamic and electronic parameters of β CD:Octanol complexes by PM3 method for the more thermodynamically favorable complex of each orientation

Table 3.16: Energies features. thermodynamic and electronic parameters of β CD:Nonanol complexes by PM3 method for the more thermodynamically favorable complex of each orientation.

Table 3.17: Energies features. thermodynamic and electronic parameters of β CD:Decanol complexes by PM3 method for the more thermodynamically favorable complex of each orientation

Table 3.18: Energies features. thermodynamic and electronic parameters of β CD: Undecanol complexes by PM3 method for the more thermodynamically favorable complex of each orientation

Table 3.19: Energies features. thermodynamic and electronic parameters of β CD: Dodecanol complexes by PM3 method for the more thermodynamically favorable complex of each orientation

Table 3.20 : Energetic features and thermodynamic parameters for linear alcohol inclusion complexes by PM3 manual docking method.

Figure 3.1: NMR spectra obtained for β CD: Lower alcohols for volume ratio 1:1 prepared in D_2O

Figure 3.2 : NMR spectra obtained for β CD: Propanol mixture solutions prepared in D_2O .

Figure 3.3 :NMR spectra obtained for β CD: Higher alcohols for volume ratio 1:1 prepared in D_2O

Figure 3.4:NMR spectra obtained for β CD: Heptanol mixture solutions prepared in D_2O

Figure 3.5: Job'plot obtained for β CD: Higher alcohol H3 and H5 protons complexes (a) β CD: Hexanol .(b) β CD: Heptanol. (c) β CD: Octanol . (d) β CD: Nonanol. (e) β CD: Decanol (f) β CD: Undecanol.

Figure 3.6: DSC curves for inclusion complex of β CD: lower alcohols in molar ratio 1:1

Figure 3.7: DSC curves for inclusion complex of β CD: Higher alcohols in molar ratio 1:1

Figure 3.8: Powder x-ray diffraction for inclusion complex of β CD: lower alcohols in molar ratio 1:1 compared with reference (BCDEXD10)

Figure 3.9: Powder x-ray diffraction for inclusion complex of β CD: Higher alcohols in molar ratio 1:1 compared with PUKPIU

Figure 3.10: Powder x-ray diffraction for inclusion complex of β CD: Higher alcohols in molar ratio 1:1 compared with reference CACPOM

Figure 3.11: Raman Spectra for inclusion complex of β CD: Lower alcohols in molar ratio 1:1

Figure 3.12 : Raman Spectra for inclusion complex of β CD: higher alcohols in molar ratio 1:1

Figure 3.13 : Evolution of the binding energy changes ΔE_{bind} (kcal/mol) in function of the starting position of methanol along Z-axis for the two orientations

Figure 3.14 : Evolution of the binding energy changes ΔE_{bind} (kcal/mol) in function of the starting position of ethanol along Z-axis for the two orientations.

Figure 3.15 : Evolution of the binding energy changes ΔE_{bind} (kcal/mol) in function of the starting position of propanol along Z-axis for the two orientations.

Figure 3.16 : Evolution of the binding energy changes ΔE_{bind} (kcal/mol) in function of the starting position of Butanol along Z-axis for the two orientations.

Figure 3.17 : Evolution of the binding energy changes ΔE_{bind} (kcal/mol) in function of the starting position of pentanol along Z-axis for the two orientations.

Figure 3.18 : Evolution of the binding energy changes ΔE_{bind} (kcal/mol) in function of the starting position of Hexanol along Z-axis for the two orientations.

Figure 3.19 : Evolution of the binding energy changes ΔE_{bind} (kcal/mol) in function of the starting position of Heptanol along Z-axis for the two orientations.

Figure 3.20 : Evolution of the binding energy changes ΔE_{bind} (kcal/mol) in function of the starting position of Octanol along Z-axis for the two orientations.

Figure 3.21 : Evolution of the binding energy changes ΔE_{bind} (kcal/mol) in function of the starting position of Nonanol along Z-axis for the two orientations.

Figure 3.22 : Evolution of the binding energy changes ΔE_{bind} (kcal/mol) in function of the starting position of Decanol along Z-axis for the two orientations.

Figure 3.23 : Evolution of the binding energy changes ΔE_{bind} (kcal/mol) in function of the starting position of Undecanol along Z-axis for the two orientations.

Figure 3.24 : Evolution of the binding energy changes ΔE_{bind} (kcal/mol) in function of the starting position of Dodecanol along Z-axis for the two orientations.

Figure 3.25 : Binding energy ΔE_{bind} (kcal/mol) (in green), ΔH (kcal/mol) (in blue) and ΔG (kcal/mol) (in orange) results from PM3 manual docking of a linear primary alcohol molecule in β CD. Energy axis is inverted to allow a better visualization of the results

Chapter-4

Table 4.1 : list of melting and boiling point values of all the guests (source: Wikipedia)

Table 4.2. Experimental X-ray pattern of β CD:BEN and β CD:FB with CSD refcode reference assignment.

Table 4.3 : Comparison of FB peak shifts and relative intensities (free FB and inclusion complex with β CD).

Table 4.4 : Comparison of TOL peak shifts and relative intensities (free TOL and inclusion complex with β CD).

Table 4.5 : Comparison of TFT peak shifts and relative intensities (free TFT and inclusion complex with β CD).

Table 4.6: Comparison of PHE peak shifts and relative intensities (free PHE and inclusion complex with β CD).

Table 4.7 : Comparison of BA peak shifts and relative intensities (free BA and inclusion complex with β CD).

Table 4.8 : Comparison of NAP peak shifts and relative intensities (free NAP and inclusion complex with β CD).

Table 4.9 : Comparison of 2-NAP peak shifts and relative intensities (free 2-NAP and inclusion complex with β CD).

Table 4.10 : Comparison of PYR peak shifts and relative intensities (free PYR and inclusion complex with β CD).

Figure 4.1 : Comparison of NMR spectra of β CD and β CD:BA complex showing shift in H3 and H5 positions.

Figure 4.2 : Job's plot for β CD:BA complex in D_2O for β CD protons.

Figure 4.3 : BA molecule with proton labelling.

Figure 4.4 : Displacement of peaks of Benzoic acid.

Figure 4.5 : Job's plot for β CD:BA complex in D_2O for BA protons.

Figure 4.6 : Comparison of NMR spectra of β CD and β CD:PHE complex showing shift in H3 and H5 positions.

Figure 4.7 : Job's plot for β CD:PHE complex in D_2O .

Figure 4.8 : PHE molecule with proton labelling.

Figure 4.9 : Displacement of peaks of Phenol.

Figure 4.10 : Comparison of NMR spectra of β CD and β CD:2NAP complex showing shift in H3 and H5 positions.

Figure 4.11 : Job's plot for β CD:2NAP complex in D_2O .

Figure 4.12 : 2-NAP molecule with proton labelling.

Figure 4.13 : Displacement of peaks of 2-Naphthol.

Figure 4.14. DSC curve of β CD and β CD:FB (1:1)

Figure 4.15 : DSC curve of β CD and β CD:TOL (1:1).

Figure 4.16. DSC curve of β CD and β CD:TFT (1:1)

Figure 4.17 : DSC curve of β CD and β CD:PHE (1:1).

Figure 4.18 : DSC curve of β CD:BA (1:1).

Figure 4.19 : DSC curve of β CD: NAP and β CD:NAP (1:1).

Figure 4.20 : DSC curve of bcd:2naphthol and β CD:2-NAP (1:1).

Figure 4.21 : DSC curve of bcd:2naphthol and β CD:PYR (1:1).

Figure 4.22 : Comparison of diffraction patterns of experimentally observed and simulated structures (PUKPIK and POXHUG) from literature of β CD inclusion complexes. The experimentally observed β CD: aromatic hydrocarbon pattern can be seen to show peaks corresponding to both these structures.

Figure 4.23 : Comparison of diffraction patterns of experimentally observed and simulated structures (PUKPIK and CACPOM) from literature of β CD inclusion complexes. The experimentally observed β CD: aromatic hydrocarbon pattern can be seen to show peaks corresponding to both these structures

Figure 4.24 : Comparison of diffraction patterns of experimentally observed and simulated structures (CACPOM) from literature of β CD inclusion complexes. The experimentally observed β CD: aromatic hydrocarbon pattern can be seen to show peaks corresponding to both these structures.

Figure 4.25 : Raman Spectrum of the β CD, BEN and of the inclusion complex obtained after mixing β CD with BEN in the molar ratio of 1:1.

Figure 4.26 : The vibrational modes of BEN which are most intense and have been impacted by the interaction with β CD.

Figure 4.27 : Raman Spectrum of the β CD, FB and of the inclusion complex obtained after mixing β CD with FB in the molar ratio of 1:1

Figure 4.28. The vibrational modes of FB which are most impacted on interaction with β CD.

Figure 4.29. Raman Spectrum of the β CD, TOL and of the inclusion complex obtained after mixing β CD with TOL in the molar ratio of 1:1.

Figure 4.30 : The vibrational modes of TOL which are most impacted by the interaction with β CD.

Figure 4.31 : Raman Spectrum of the β CD, TFT and of the inclusion complex obtained after mixing β CD with TFT in the molar ratio of 1:1.

Figure 4.32 : The vibrational modes of TFT which are most impacted by the interaction with β CD.

Figure 4.33 : Raman Spectrum of the β CD, PHE and of the inclusion complex obtained after mixing β CD with PHE in the molar ratio of 1:1

Figure 4.34 : The vibrational modes of PHE which are most impacted by the interaction with β CD.

Figure 4.35: Raman Spectrum of the β CD, BA and of the inclusion complex obtained after mixing β CD with BA in the molar ratio of 1:1.

Figure 4.36: The vibrational modes of BA which are most impacted by the interaction with β CD

Figure 4.37: Raman Spectrum of the β CD, NAP and of the inclusion complex obtained after mixing β CD with NAP in the molar ratio of 1:1.

Figure 4.38 : The vibrational modes of NAP which are most impacted by the interaction with β CD.

Figure 4.39 : Raman Spectrum of the β CD , 2-NAP and of the inclusion complex obtained after mixing β CD with 2-NAP in the molar ratio of 1:1.

Figure 4.40: The vibrational modes of 2-NAP which are most impacted by the interaction with β CD

Figure 4.41 : Raman Spectrum of the β CD, ANTH and of the inclusion complex obtained after mixing β CD with ANTH in the molar ratio of 1:1.

Figure 4.42 : The vibrational modes of ANTH which are most probably impacted by the interaction with β CD.

Figure 4.43 : Raman Spectrum of the β CD, PYR and of the inclusion complex obtained after mixing β CD with PYR in the molar ratio of 1:1

Figure 4.44 : The vibrational modes of PYR which are most impacted by the interaction with β CD.

Chapter-5

Table 5.1 : Volume of β CD and Aromatic hydrocarbons solutions mixed together to form inclusion complexes in EtOD as co-solvent to carry out NMR studies.

Figure 5.1 : Chronological order representation of aims and objectives of the thesis. (P.S- the images used are only for better understanding of the reader about the concept).

Figure 5.2 : Evolution of H3 and H5 peaks of β CD:BEN complexes when dissolved in 50% EtOD.

Figure 5.3 : Evolution of BEN peak when dissolved in 50% EtOD.

Figure 5.4 : job's plot for β CD: BEN complex in EtOD as co-solvent.

Figure 5.5 : Evolution of H3 and H5 β CD: TFT complexes peaks when dissolved in 30% EtOD.

Figure 5.6 : Evolution of TFT peak when dissolved in 30% EtOD.

Figure 5.7 : job's plot for β CD: TFT complex in EtOD as co-solvent.

Figure 5.8 : DSC curve of β CD and β CD:alcohol:BEN (1:1:1).

Figure 5.9 : DSC curve of β CD and β CD:alcohol:FB (1:1:1).

Figure 5.10 : DSC curve of β CD and β CD:alcohol:TOL (1:1:1)

Figure 5.11 : DSC curve of β CD and β CD:alcohol:TFT (1:1:1).

Figure 5.12 : DSC curve of β CD and β CD:alcohol:NAP (1:1:1).

Figure 5.13 : DSC curve of β CD and β CD:alcohol:ANTH (1:1:1).

Figure 5.14 : DSC curve of β CD and β CD:alcohol:PYR (1:1:1).

Figure 5.15 : Powder diffraction pattern of β CD:BEN and β CD:alcohol:BEN (1:1:1) in comparison to the references from the literature (CACPOM, PUKPIU and POHXUG).

Figure 5.16 : Powder diffraction pattern of β CD:FB and β CD:alcohol:FB (1:1:1) in comparison to the references from the literature (PUKPIU and POHXUG).

Figure 5.17 : XRD diffraction pattern of β CD:TOL and β CD:alcohol:TOL (1:1:1) in comparison to the references from the literature (CACPOM).

Figure 5.18 : XRD diffraction pattern of β CD:TFT and β CD:alcohol:TFT (1:1:1) in comparison to the references from the literature (CACPOM).

Figure 5.19 : XRD diffraction pattern of β CD:NAP and β CD:alcohol:NAP(1:1:1) in comparison to the references from the literature (CACPOM).

Figure 5.20 : XRD pattern β CD:alcohol:ANTH (1:1:1) in comparison to the references from the literature (PUKPIU).

Figure 5.21. XRD pattern of β CD: PYR and β CD:alcohol:PYR (1:1:1) in comparison to the references from the literature (CACPOM).

Figure 5.22 : XRD pattern comparison of β CD, β CD: Hexanol, β CD:PYR and β CD: Hexanol: PYR (1:1:1, 1:2:1 and 1:1:2).

Figure 5.23 : Raman spectra of β CD, β CD: Octanol, β CD:BEN and β CD: alcohol: BEN inclusion complexes (1:1:1).

Figure 5.24 : Raman spectra of β CD, β CD: Octanol, β CD:FB and β CD: alcohol: FB inclusion complexes (1:1:1).

Figure 5.25 : Raman spectra of β CD, β CD: Octanol, β CD:TOL and β CD: alcohol: TOL inclusion complexes (1:1:1).

Figure 5.26 : Raman spectra of β CD, β CD: Octanol, β CD:TFT and β CD: alcohol: TFT inclusion complexes (1:1:1).

Figure 5.27 : Raman spectra of β CD, β CD: Octanol, β CD:NAP and β CD: alcohol: NAP inclusion complexes (1:1:1).

Figure 5.28 : Raman spectra of β CD, β CD: Octanol, β CD:ANTH and β CD: alcohol: ANTH inclusion complexes (1:1:1)

Table of Contents

Introduction	12
Chapter -1 Non exhaustive state of the art	15
1.1 Host-Guest Chemistry	15
1.2 Cyclodextrins as Supramolecular Hosts	15
1.3 History of CDs.....	15
1.4 Molecular structure of CDs.....	18
1.5 Guest Inclusion	21
1.6 Crystal structures involving CDs	24
1.7 Molecular modelling of CDs and their inclusion complexes	29
1.8 Different Methods to prepare the complexes.....	32
1.9 Different spectroscopic techniques to analyse inclusion complexes	33
1.10 Aromatic hydrocarbons (AHs)	34
1.11 References	37
Chapter-2 Materials and Methods.....	53
2.1 Introduction	53
2.2 Liquid state studies: ¹ H NMR analysis of the Stoichiometry of the Host and guest complex	54
2.3. Sample preparation by Co-precipitation for solid state characterization	70
2.4 Solid State studies: Part 1: Thermal Characterization of the complexes.....	71
2.5 Solid State studies: Part 2: X-ray diffraction analysis of CDs	74
2.6 Solid state studies: Part-3. Raman Spectroscopy analysis of the inclusion complexes	84
2.7 Molecular Modelling studies.....	92
2.8 Conclusion.....	96
2.9 References.....	96
Chapter-3 Inclusion complexation studies of βCD: Alcohols	105
3.1 Introduction	105
3.2 NMR studies of βCD:alcohol complexation	106
3.3 DSC analysis of the inclusion complexes in the solid state	113
3.4 Powder X-ray diffraction studies of βCD: Alcohol inclusion complexes.....	116
3.5 Raman spectroscopic analysis of βCD: Linear alcohol complexes	118
3.6 Molecular modelling studies of βCD: Alcohol complexes	120
3.7 Conclusion.....	139
3.8 References.....	141
Chapter 4 : Inclusion complexes of βCD: Aromatic Hydrocarbons	143
4.1 Introduction	143
4.2 NMR studies of βCD: aromatic hydrocarbons	144

4.3 Thermal studies of β CD: Aromatic hydrocarbons	151
4.4 Powder X ray diffraction studies of β CD: aromatic hydrocarbon complexes	159
4.5 Raman Spectroscopy based analysis of β CD: Aromatic hydrocarbon complexes.....	161
4.6 Conclusion.....	186
4.7 References.....	186
Chapter 5. Inclusion complexes of βCD:Linear alcohols:aromatic hydrocarbons	192
5.1 Introduction	192
5.2 NMR studies: Ternary complexation in presence of co-solvent	193
5.3 Thermal studies of β CD: alcohol: aromatic hydrocarbon complexes	197
5.4 Structural studies of β CD: alcohol: aromatic hydrocarbon complexes	204
5.5 Raman spectroscopic studies of β CD: alcohol: aromatic hydrocarbon complexes.....	211
5.6 Conclusions	215
5.7 References.....	216
Conclusions and perspectives	217
Additonal informations	223
βCD:Aromatics and βCD:Alcohols:Aromatics complexes Normalised subtracted spectra	223

Introduction

Aromatic hydrocarbons or Polycyclic aromatic hydrocarbons (PAHs) are released to the environment through natural and man-made processes. One of the consequence - environmental water pollution by aromatic compounds, is an ongoing worldwide issue. Today, chemical pollution is one of the main causes affecting environmental water. However, certain chemicals which induce harm to the environment or living organisms have been identified by international agreements or regulations as being “priority chemicals for control” depending on various criteria such as toxicity, bioaccumulation, persistent and carcinogens. Mono-aromatic hydrocarbons referred as BTEX (benzene, toluene, ethylbenzene and xylenes) as well as polycyclic aromatic hydrocarbons (PAHs) are consistent with all these criteria. Due to their toxicity and carcinogenicity PAHs are listed as the priority substances to be detected in the environment by the E.U WFD (Water Framework Directive) and by the United States Environmental Protection Agency (U.S EPA)

The objectives of the REMANTAS project (approved by the National Research Agency under the ECOTECH 2011 program) were to address such issues. Initiated in 2012, it aimed in developing an original analytical tool allowing on-site measurements of organic contaminants in aquatic environments (fresh, surface, ground, coastal and transitional waters) and offering a better estimation of the spatial and temporal variability of water contamination. Our team¹ members were part of the REMANTAS project where they were successful in investigating aromatic hydrocarbon inclusion by CDs using Raman Spectroscopy and thermal analysis .The molecules targeted during my PhD are summarised in the table 1.

Monocyclic aromatic compounds and derivatives	Bi-/Polycyclic aromatic compounds and derivatives
Benzene	Naphthalene
Fluorobenzene	2-Naphthol
Toluene	Anthracene
α,α,α ,Trifluorotoluene	Pyrene
Phenol	
Benzoic acid	

Table 1 : List of the targeted substances for this thesis.

The concept of this thesis is based on a communication published in 1998 by Udachin² et al where the researchers prepared the crystals of β CD:Pyrene in presence of cyclohexanol and octanol separately. Our research team¹ was successful in encapsulating two of the aromatic hydrocarbons namely, Naphthalene and Fluoranthene. The results were determined by Raman Spectroscopy and thermogravimetric analysis.

On combining the above two ideas, the objectives of our work are:

1. To prepare inclusion complexes of β CD and different aromatic compounds (pollutants) in the presence of linear aliphatic alcohols.
2. To characterize the successful inclusion (if occurs) in liquid as well as in solid state by different characterization techniques like NMR, DSC, XRD and Raman Spectroscopic studies.

3. To prepare theoretical models in order to explain the phenomenon of inclusion complexation.

Our thesis is basically the advancements to the research previously done which aims at the detection of aromatic hydrocarbons in the naturally occurring water bodies.

The main objectives of our research were to first study in detail fundamentally and systematically the interaction between the different CDs and aromatic hydrocarbons or PAHs by combining experimental and theoretical methods. To achieve this, we need to have a better understanding and knowledge about the complex formation in solution as well as in the solid state, also the crystal structures obtained by them.

These structures obtained in the solid state can be used as starting point for molecular modelling complexation and can be considered as the basis of solid state organisation. This solid state organisation is the following result and tri-dimensional packing of the complex units obtained in solution. We start our study with the analysis of complexation in solution by ^1H NMR and determination of the stoichiometry. In the solid state, thermal analysis and powder x-ray diffraction are the most frequently used analytical methods which are known to verify the formation of new compounds based upon CD complexes. Raman spectroscopy is less favourable for such studies, but as it is the basic analytical method employed in the on-site analytical device developed by the team, it has to be considered. We are interested in the validity check of this method to study the solid state complexes obtained. Literature² have shown that two major structural types are obtained for CD complexes in solid state: cage type and channel type. Alcohols are mandatory to solubilize pure PAHs compounds in water. While extending our literature research in Cambridge Structural Database³, only few structures comprising CDs and alcohols are available and most of them involve short length chain alcohols like methanol or ethanol. On considering PAH, only two structures² involving a PAH, herein pyrene and β CD are available in the CSD. Now the prime question emerges: why lesser number of structures are available inspite of the frequent use of CDs? Is it possible to gather further explanation and understanding about those structures? Our first systematic and fundamental studies involving CDs and aliphatic linear alcohols indicate the predominant role of the alcohol chain length in the formation of either of the structural types. Channel types structural formation seem to be favoured for PAH inclusion by CDs. Then, we continue with the study of complexation of some polar aromatic derivative compounds by CDs. The complexation of PAHs in presence of alcohols by CDs is finally considered.

Chapter-1 gives the detailed idea about CDs, contributions of different scientists who have worked with CDs, their physical and chemical properties, applications in different fields, types of methods that can be used to prepare inclusion complexes, a brief idea about types of techniques to investigate inclusion complex formation. The last part gives an introduction about the aromatic hydrocarbons, their sources and existence in the environment, effect on human health and the detection techniques used so far.

Chapter-2 discuss in detail, the materials and methods used during this thesis. The principle of the analytical techniques like NMR, DSC, PXRD, Raman Spectroscopy are outlined with the help of mathematical theory behind their working and instrumental setup. The techniques differentiate the results for the liquid (in solution) and the solid (powder) states. It also includes the description about the first step of this thesis i.e to interpret the results obtained

for uncomplexed β CD by each technique for further comparison with inclusion complexation results in the later chapters.

Chapter-3 is based on the studies of β CD: Linear alcohols chemistry. The different techniques were used to exploit the complexation phenomenon. NMR was used to check the insertion of aliphatic part of linear alcohol inside the β CD cavity. Furthermore, method of continuous variation (job's plot) was applied on the results obtained by NMR technique to know about the stoichiometry of the inclusion complex formed. The next step was to confirm inclusion complexation by thermal (DSC) and XRD studies. Raman Spectroscopy, the next solid state characterization explained the vibrational behaviours the molecules before and after inclusion. A molecular modelling analysis concludes this chapter.

Chapter-4 brings the addition of aromatic hydrocarbons to the β CD cavity first in the absence of linear alcohols to form ternary complexes while chapter-5 considers their addition in presence of linear aliphatic primary alcohols. Most of the samples in chapter-4 do not provide any result because of the poor solubility of PAH in water. We also considered the inclusion of some polar aromatic derivatives such as phenol, benzoic acid, 2-Naphthol etc. Different stoichiometries were considered for β CD: Linear alcohol: aromatic hydrocarbon. The characterisation of the inclusion complexes prepared are done with the same techniques as described in chapter-2 and the results obtained are discussed with the conclusions made.

A part of the thesis was initially supposed to be devoted to the growing of suitable crystals for mono crystal X-ray diffraction analysis. We developed different methods to grow crystals described in the chapter 2. After a fire occurring in the laboratory on April 2017, all the crystal samples were destroyed and the structural determinations could not be correctly realized.

CDs are widely studied and extended literature is available that our work can't be considered as exhaustive.

Chapter -1 Non exhaustive state of the art

1.1 Host-Guest Chemistry

The phenomenon of complexation occurs when a molecule called as 'host' combines to another molecule called as 'guest' to form one large molecule or **supramolecule**. Generally, the host is either a large molecule or aggregate such as an enzyme, or a synthetic cyclic compound having a central cavity whereas the guest can be a small molecule such as 'water' molecule, a monoatomic cation or an inorganic anion. To form a stable inclusion complex, the host must possess binding sites, which mutually contact and attract the binding sites of guests without the presence of any strong non-bonded repulsion. In other words, we can say, the guest molecule is held within the host molecule by weak Van der Waals or hydrogen bonds. Importantly, no covalent bonds are formed^{4,5}.

The stability of the complex is related to different properties occur in the host-guest system. The intramolecular cavities present in the hosts like 'cavitands' are strictly intramolecular property of the host and exists in both solution and the solid state. On the contrary, clathrands possess extra molecular cavities, often a gap between the two or more hosts, more relevant in the crystalline or solid state^{6,7}.

1.2 Cyclodextrins as Supramolecular Hosts

From all other supramolecular hosts existing like Cucurbiturils, Calixarenes etc., Cyclodextrins (CDs) seem to be the most important⁸⁻¹¹ ones because of their production from natural material-starch, by a simple enzyme conversion, high production, low price, least toxicity and properties like functionalisation and derivatization.

Cyclic glucose oligosaccharides are non-reducing sugars are commonly known as '**Cyclodextrins**' (CDs). They belong to the family of cage type supramolecules. The periodic orientation of the glucose molecules in the structure makes the interior cavity of the molecule as hydrophobic and the exterior as hydrophilic building them as water soluble molecules. Hence, the hydrophobic nature of the cavity is capable of entrapping hydrophobic molecules leading to the formation of a 'host-guest' complex. Moreover, the properties of the hydrophobic guest changes upon encapsulation. Due to this remarkable quality of CDs, they have been extensively used in various fields like pharmaceuticals¹²⁻¹⁵, food technology¹⁶⁻¹⁸, cosmetics¹⁹⁻²¹, toiletries^{22,23}, biotechnology^{24,25}, textiles²³⁻²⁸ and many more.

1.3 History of CDs

1.3.1 Discovery period

CDs have a long history in terms of their production followed by their uses in different fields in today's world. CDs were first discovered in late 19th century (1891) by Antoine Villiers, who termed his findings as '**cellulosine**'. He obtained this crystalline substance from a culture medium of *Bacillus amylobactor* that was grown on a medium containing starch. He determined the composition to be $(C_6H_{10}O_5)_2 \cdot 3H_2O$. After the discovery of dextrin, a decade later, an Austrian microbiologist Franz Schardinger^{11,29}, observed that the role of microorganisms (*bacillus macerans*) that are responsible for the conversion of starch molecules into two different crystalline substances. The properties of these substances were found to be similar to already reported cellulosine so he named them as α - and β -dextrin. In those years CDs were named Schradinger dextrins in his honour.

1.3.2 Explanatory period

The further development in the studies of CDs were done by many scientists all over the world working independently like Freudenberg and co-workers started exploration structures of these two dextrans and found them to be cyclic in nature. Cramer and French^{30,31} described all the basic structural and physiochemical characteristics of α -, β - and γ - CDs, including their chemical structures, cavity size, solubility, reactivity, complexing abilities, and their effect on the chemical stability of guest molecules. These scientists have worked on the gradual developmental studies about CDs in different span of years starting from their discovery and characterization followed by a period of doubts and dis-agreements, exploration and eventually the utilization in different industrial applications mainly food industry^{16,32}, cosmetics, pharma industry^{12,33,34} and textile industry. Ongoing research are also adding on new directions of applications of these molecules.

1.3.3 Utilization period

The utilization period started right after detailed study of their toxicological behaviour. The different reasons responsible for their toxic effects could be:

- Complexes impurities
- Inadequate form of administration
- Extreme dosing

In 1981, the first International Symposium on CDs was organized. Derivatizations of molecules started leading to the production of more other CDs derivatives³⁵⁻⁴³ with applications in different fields.

Table 1.1 shows the chronological summary of development of CDs.

Years	Events
1891	Villiers published his discovery of cellulosine (CD)
1903	Schardinger published his first paper on α - and β -dextrins
1924	Methylation of CDs first described, later both Freudenberg and Meyer Delius (1938) and Szejtli (1980) prepared different grades of methylated CDs
1928-1932	The ability of CDs to form complexes with various organic compounds discovered.
1935	Freudenberg and Jacobi discovered γ -CD
1938-1952	The chemical structure of α -, β -, and γ - CD elucidated by Freudenberg, Cramer, Borchert, French and Rundle
1948-1951	Formation and structure of CD inclusion complexes discovered.
1953	The first CD patent entitled "method of preparation of inclusion compounds of physiologically active organic compounds" was issued in Germany to Freudenberg, Cramer and Plieninger.
1954	Cramer's book on inclusion complexes published
1957-1965	French described the existence of large natural CDs with upto 12 glucose units
1965	Higuchi and Connors publish their article on classification of complexes based on their phase-solubility profiles
1976	The parent α - and β -CDs officially approved as food additives in Japan
1976	The world's first pharmaceutical product, prostaglandin E2/ β CD (prostarmon ETM sublingual tablets), marketed in Japan Ono Pharmaceutical Co.
1981	The first international symposium on cyclodextrins was organised and held in Budapest by Szejtli.
1983-1985	Brauns and Muller (Europe) and Pitha (USA) filed patents on 2-Hydroxypropyl β CD
1988	Piroxicam/ β -cyclodextrin tablets (Brexin) marketed by Chiesi Pharmaceutical (Italy)
1990	Stella and Rajewski filed patent on sulfobutyl ether β CD

Table 1.1 : Chronological summary on the development of Cyclodextrins^{30,44}.

1.4 Molecular structure of CDs

CDs are cyclic molecules made up of glucopyranose units (Figure 1.1) which are linked together by α -1,4 glycosidic bonds. There are predominantly three types of CDs – α , β and γ containing 6, 7 and 8 glucopyranose molecules (Figure 1.2) respectively. Higher analogous members have also been reported namely δ CD⁴⁵⁻⁴⁸ (containing 9 glucopyranose units) but they are highly flexible and are less commonly used. Also, the lower analogous member (with five or less glucopyranose units) are highly unlikely to exist due to extensive steric strain for CDs. The three main CDs are crystalline, homogeneous and non-hygroscopic in nature.

The glucose residues in these systems are present in 4C_1 conformation (chair). The cyclic orientation of the molecules makes the structure as donut or toroidal shape. The C_1 conformation of the glucopyranose units promotes the existence of secondary hydroxyls (C2 and C3) on one of the two edges of the ring whereas all primary hydroxyls (C6) are present on the other side. The interior of the cavity is composed of hydrogens from C3 and C5 and the lone pairs of the glucose ring oxygen⁴⁹⁻⁵¹ (Figure 1.4). The presence of these hydroxyl groups on the surface and glycosidic oxygens inside of the cavity make the interior hydrophobic and exterior hydrophilic (Figure 1.3). This remarkable property is the fundamental basis of vast areas of applications of CDs.

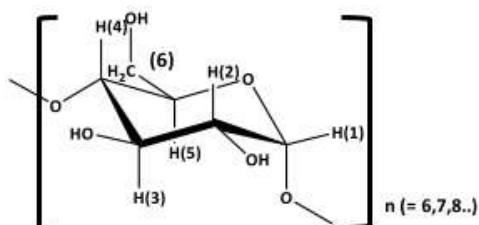


Figure 1.1 : Glucopyranose unit.

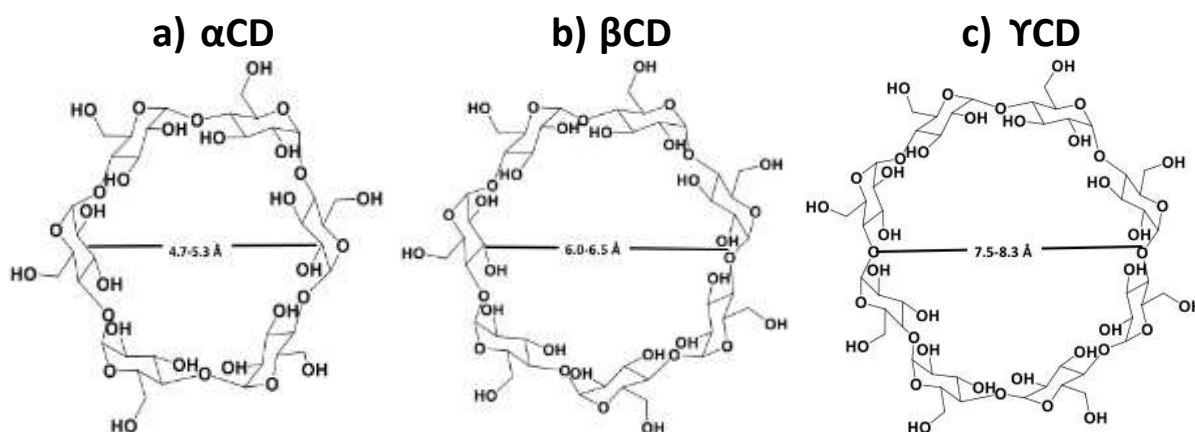


Figure 1.2 : Macroyclic structures with cavity diameters³¹ of parent CDs. a) α CD, b) β CD and c) γ CD.

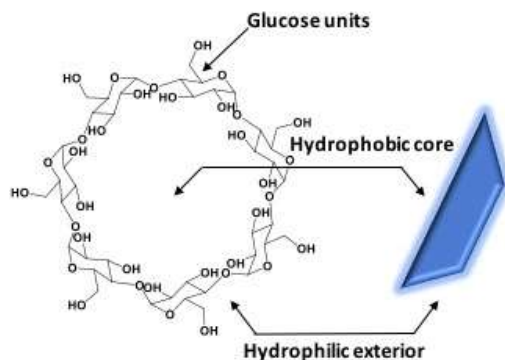


Figure 1.3 : Exterior and Interior of the CD cavity.

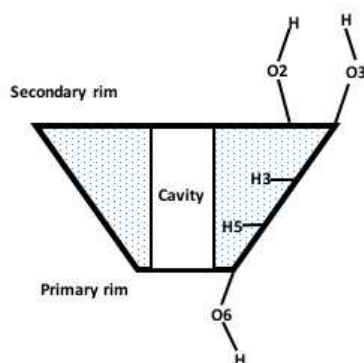


Figure 1.4 : Schematic diagram of CD showing the cavity, primary and secondary faces and the distribution of primary and secondary hydroxyl groups on the two CD faces.

Many researchers performed the NMR studies which indicated the formation of intramolecular hydrogen bonds in solution between the secondary hydroxyl group of adjacent glucopyranose units^{52,53}. The studies further suggested that the rotation of the glucopyranose units are restricted due to presence of these bonds, hence contributing to the structural rigidity of CD molecules.

The cavity diameters exist within the ranges- 4.7-5.3, 6.0-6.5 and 7.5-8.3 Å for α , β and γ CDs respectively. Cavity size variation enables CD to selectively incorporate hydrophobic guests based on size and geometry. γ CD is the most flexible among the three native CDs as the average bond distances between the O (2) and O (3) atoms of the adjacent glucopyranose units for α , β and γ CDs are 3.00, 2.86 and 2.81 Å respectively allowing weak intermolecular hydrogen bond interactions. On the contrary, the intramolecular hydrogen bond increases in strength for β CD resulting in decrease in aqueous solubility in comparison to α and γ CDs. Another reason for its low solubility could be its tendency to highly increase the local water structure in the cavity and around the molecule which eventually lead to the restrained macrocyclic motion²⁵.

The decreased solubility of CDs has restricted their use commercially. This is particularly the case of β CD. To overcome this problem, researchers have worked on structural modifications of β CD chemically. Many β CD derivatives have been synthesized because of their higher aqueous solubility than the native β -CD. Chemical modification of CD^{54,55} have produced CD derivatives which are amorphous, non-crystallisable CD derivatives. The advantages of these modifications are reduced parental toxicity, enhanced aqueous solubility, physical and microbiological stability. The primary and secondary hydroxyl groups are substituted by

different functional groups to synthesis derivatives. Some of the commonly used CD derivatives have been listed in the table 1.2.

Cyclodextrin (CD)	Abbreviation
Hydroxyethyl- β -CD	HE- β -CD
Hydroxypropyl- β -CD	HP- β -CD
Sulfobutylether- β -CD	SE- β -CD
Methyl- β -CD	M- β -CD
Dimethyl- β -CD	DM- β -CD (DIMEB)
Carboxymethyl- β -CD	CM- β -CD
Carboxymethyl ethyl- β -CD	CME- β -CD
Glucosyl- β -CD	G1- β -CD
Maltosyl- β -CD	G2- β -CD
Tri-O-methyl- β -CD	TRIMEB
Tri-O-ethyl- β -CD	TE- β -CD
Tri-O-butyryl- β -CD	TB- β -CD
Tri-O-valeryl- β -CD	TV- β -CD

Table 1.2 : List of Chemically modified CDs and their abbreviations.

The physical properties of three CDs are shown in the table 1.3.

CDs have different aqueous solubility due to strong binding interactions between C (2)-OH group of one unit to C (3)-OH of the adjacent unit. A new type of secondary belt is formed by these hydrogen bonds making them a rigid structure. This is the most probable reason observed for lowest solubility of β CD. For α CD, the hydrogen bond belt is incomplete due to distorted position of one of the glucopyranose unit. As a result, only four bonds are formed instead of 6. In case of γ CD, the structure is non-planar and more flexible making them the most soluble.

Properties	α - CD	β - CD	γ - CD
Number of glucose units	6	7	8
Molecular weight	973	1135	1297
Solubility in water (25°C, g/100ml)	14.5	1.85	23.2
Cavity Diameter (Å)	4.7-5.3	6.0-6.5	7.5-8.3
Melting temperature range (°C)	255-260	255-265	240-245
Water molecules in cavity	6	11	17

Table 1.3 : Properties of natural cyclodextrins²².

1.5 Guest Inclusion

CDs exhibit complexation in both solid and liquid phases.

The cavities of CDs are never empty; water molecules or solvent molecules are present in the cavity if guest molecules are absent²². The presence of hydrophobic cavity results in its capability to include guest molecules with lower polarity than water. The molecule to be included must have the appropriate shape and size. During the formation of guest:CD complex, no covalent bonds are formed or broken. For this phenomenon to occur, the main driving force could be the release of high enthalpy water molecules from the CD's cavity^{8,22}. The replacement of enthalpy rich water molecules by suitable guest lowers the energy of the system.

The event of complexation induces enthalpic and entropic changes driven by Van der Waals interactions or hydrophobic interactions. When there is no interaction between the CD and guest, ΔH and ΔS remain zero. But in case complexation is Van der Waal interactions driven the expected result would have large negative ΔH and Zero ΔS , whereas if hydrophobic interactions dominate the expected result is a large positive ΔS and zero ΔH ⁵⁶.

1.5.1 Orientation of the Guest in the CD cavity

The size and shape of the guest are the prime factors to determine the orientation and fit in the CD cavity even when it is partially included. CDs are rather flexible hosts which can adapt to the topologies of the guests embedded in their cavities. Some of the properties like the cavity diameter and number of glucose units are listed in the Table 1.3.

1.5.2 Complexation properties (Host: guest inclusion)

The study of CD inclusion complexes has gained interest over the past decades. An inclusion complex can be defined as a guest molecule occupying the interior space of the host. The properties of the resulting inclusion complex change from that of the native host and guest properties. The phenomena of complexation generally depend on the host/guest system where the complexation usually occurs in a manner that allows maximum exposure of the hydrophobic portion of the guest to the apolar host cavity.

There are number of factors which result in effective complexation:

- a) To initiate the CD/guest interaction, favourable energetics must be present.
- b) The host and the guest must have some affinity for each other.
- c) Size compatibility between the host's cavity and guest must exist to allow full or partial inclusion.

High energy water molecules play an important role in the driving force of CD complex formation with hydrophobic molecules in aqueous solution. They are released from the CD cavity upon guest inclusion. The process of replacement of these high energy molecules is favoured as CD ring strain reduces. Thus, complexation takes place from this decrease in the CD ring strain upon inclusion of the guest molecule.

Host: guest complexes are certain types of complexes where a host molecule recognizes and selectively binds a certain guest. In other words, the host must possess binding sites, which mutually join and attract the binding sites of guests without generating any strong non-

bonded repulsion. The forces taking part in the complexation are weak van der Waal forces or hydrogen bonds.

CD's cavity in pure form are generally considered as empty. When no guest molecule is present for complexation, there are usually solvent molecules are present. Complexation takes place when one of the guest molecule is present partially or fully inside the cavity depending on the size of the guest molecule. Complexation takes place not only in the solid state but also in the aqueous solutions by various methods. In case of aqueous solution, the cavity is filled with solvent molecules, appropriate guest molecule can substitute the water molecules in the cavity.

If the guest molecule fits well inside the cavity, the driving force of binding then depends on the thermodynamic interactions between the different component of the system: solvent, guest and CD. The solvent- water plays an important role in binding. The water molecules present inside the CD cavity, also the water molecules in the close proximity to the cavity, are energetically different from the bulk solvent. The second factor for binding is the guest. On binding to the host by weak Van der Waal forces, the highly organised water molecules surrounding the hydrophobic guest will be free to interact with the bulk solvent. In other words, there are many factors that include the force driving complexation is the release of high energy water molecules from the cavity and guest stabilization by weak Van der Waal interactions. Thus, inclusion formation in a polar solvent between the host and the guest leads to an increase of entropy through the hydrophobic effect. The inclusion complexes made can be obtained as stable crystalline product.

In conclusion, there are four main factors that contribute to energetically favorable binding interactions between CD and a guest. One, dislocation of polar water molecules by a guest from the apolar CD environment. Two, an increase of hydrogen bonds formed as trapped water molecules return to the bulk solvent. Three, reduction of non-favorable interactions between the bulk (polar) solvent and the apolar guest. Four, increase of Dipole-Dipole interactions between the guest and the CD cavity.

CDs form inclusion complexes with guest molecules having size compatible with dimensions of the cavity. Depending on the fit of the guest in the cavity, different stoichiometries⁵⁷ can be formed like 1:1, 1:2, 2:1, 2:2 (Figure 1.5) etc. The main objective of inclusion of guest is to change the physicochemical properties like solubility, bio-availability, decreased toxicity, chemical stability etc.

The inclusion complex formation can take place in the solid state also and these complexes are different from those formed in solution. In solution, the hydrophobic guest molecule is included in the cavity and the whole complex is surrounded by a shell of water molecules. But, in the solid state, the guest molecule can either form a complex within the CD cavity or within the intra-molecular cavities formed by the crystal lattice of the CD molecule. It has been observed that solid CD includes water molecules in its cavity^{8,22}. Different kinds of CDs contain different number of water molecules (ranging from 6 to 17) in the solid state. Water molecules can still be released from the CD cavity, therefore acting as driving force for CD solid complex. From the above discussion, it can be concluded that solid CD complex are seldom of stoichiometric composition.

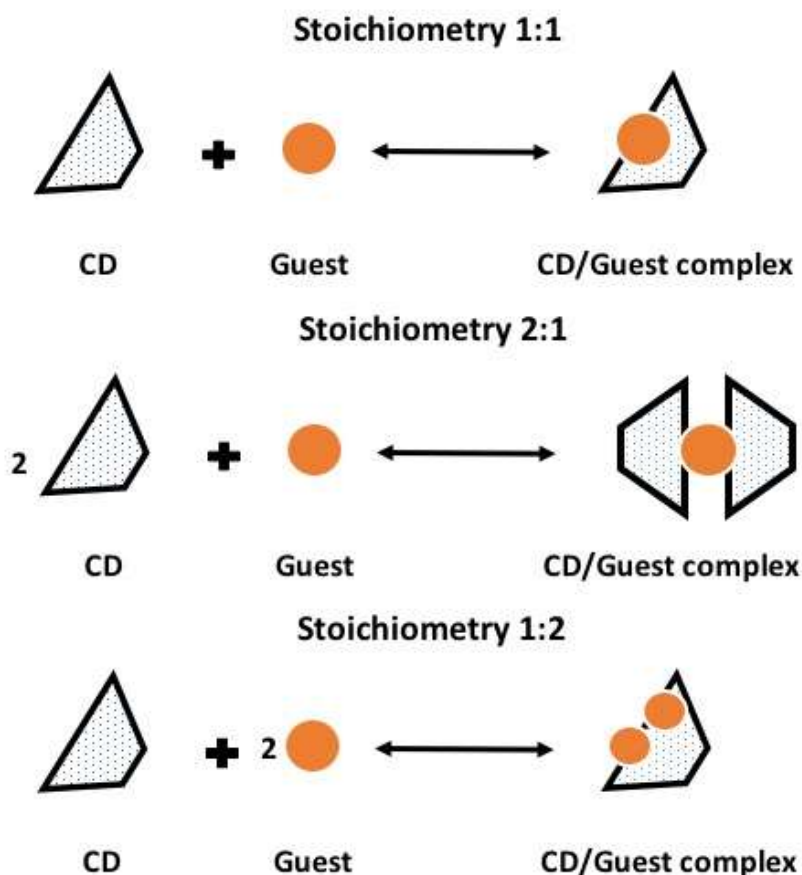


Figure 1.5 : CD Inclusion compounds and Stoichiometry.

The chemical kinetics of the system at equilibrium gives the stoichiometry of inclusion complexes of CD. The equilibrium of a 1:1 host-guest system can be written as:



Where the association binding constant, K_a , is expressed as:

$$K_a = \frac{[\text{CD} \cdot \text{Guest}]}{[\text{CD}][\text{Guest}]}$$

The Gibbs free energy can be calculated from K_a , and the entropic and enthalpic contributions to binding can be obtained from measuring K_a at different temperatures. The above equation indicates a 1:1 stoichiometry ratio between the CD and the guest, but other stoichiometric complexes such as 2:1 or 1:2 CD:Guest complexes also exist.



The other stoichiometry like 2:1 is favourable for encapsulation of a longer or a bulkier guest molecule by two CD molecules.

By complex formation, there occurs a relationship between enthalpy, ΔH and entropy ΔS . If the heat is generated during complexation, then ΔH is small and ΔS is large implying a higher degree of disorder after complex formation. On the other hand, if ΔH is large, the entropy is negative resulting in higher order of the complexation system. Calorimetric measurements can be used to calculate actual values of ΔH and ΔS ^{56,58}.

1.6 Crystal structures involving CDs

Established in 1965, the Cambridge Structural Database³ is the world's repository for small-molecule organic and metal-organic crystal structures. The software Conquest⁵⁹ allows research in the database on the basis of criteria such as molecular fragment. The software Mercury⁶⁰ allows among other uses, representations of the structures and simulations of the powder X-ray patterns. The simulated X-ray patterns are used as references further in the text and their use is detailed in the chapter 2.

Among the 900000 entries available today in the CSD, only 96 organic structures involve α CD molecules and derivatives, 226 organic structures involve β CD molecules and derivatives and 32 organic structures involve γ CD and derivatives. Saenger and al. have classified the structures involving CSD in three major structural types: channels⁶¹⁻⁶⁸, herringbone and brick-type^{23,69-77}. We have viewed and analyzed in Mercury all the structures available. Our observations tend to complete this description.

- a) **Channel type crystal packing mode:** In channel type structures, the CD molecules are vertically stacked on top of each other, with guest molecules embedded into these endless channels. The alignment of the channel can be 'head to tail' or 'head to head' type. Figure 1.6 represents two perpendicular views of CDs organization in such a structure.
- b) **Herringbone and brick-type crystal packing modes:** This type of crystal structure was initially described as cages with the cavity of one CD molecule blocked on both sides by adjacent CDs, thereby forming isolated cavities. In fact, only few structures present such isolated cavities and most of them consist in dual nested channels. In this type of arrangement, the molecules can be packed crosswise. E.g. –herringbone or brick type. In herringbone type structures, CD molecules are isolated and tilted from each other. Figure 1.7 represents two perpendicular views of CDs organization in herringbone type. In brick-type structures, CDs are arranged by dimers and can present tilted orientation from each other. Figure 1.8 represents two perpendicular views of CDs organization in brick type.

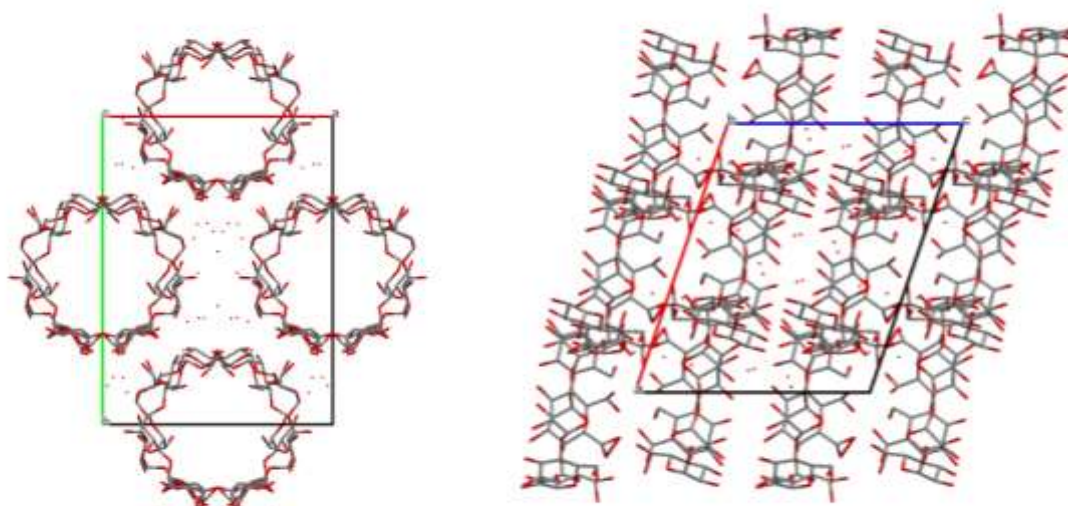


Figure 1.6 : Views along c axis (right) and b axis (left) of CSD organization in the channel type structure CSD PUKPIU². Guest molecules are willingly hidden. Hydrogen atoms are not represented. Carbon atoms are represented in grey while oxygen atoms are represented in red.

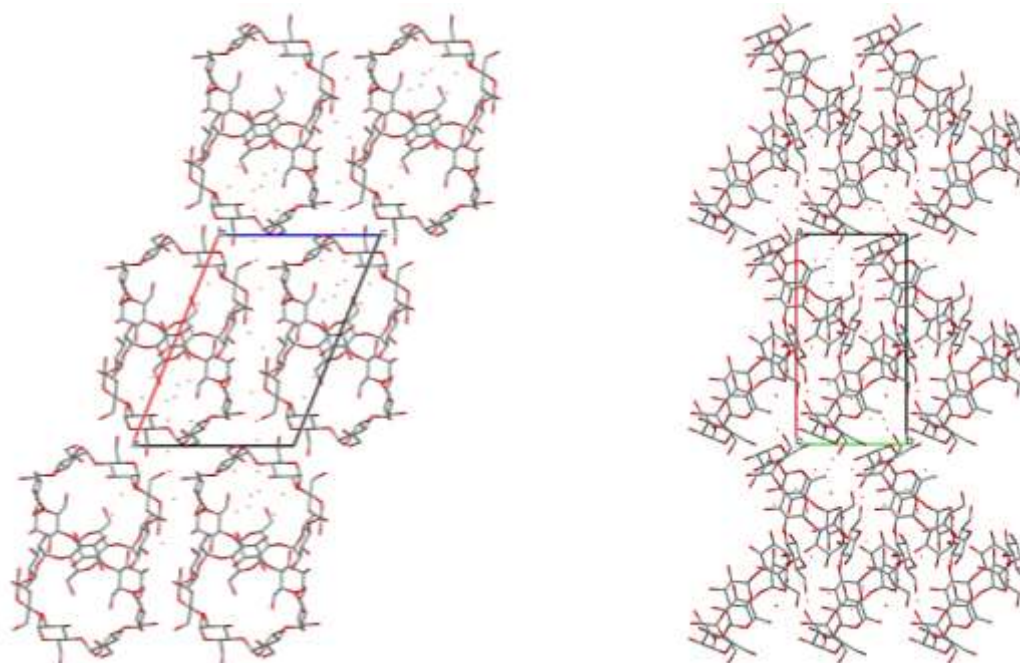


Figure 1.7 : Views along b axis (right) and c axis (left) of CDs organization in the herringbone dual nested channel type structure CSD BCDEXD10⁶⁹. Guest molecules are willingly hidden. Hydrogen atoms are not represented. Carbon atoms are represented in grey while oxygen atoms are represented in red.

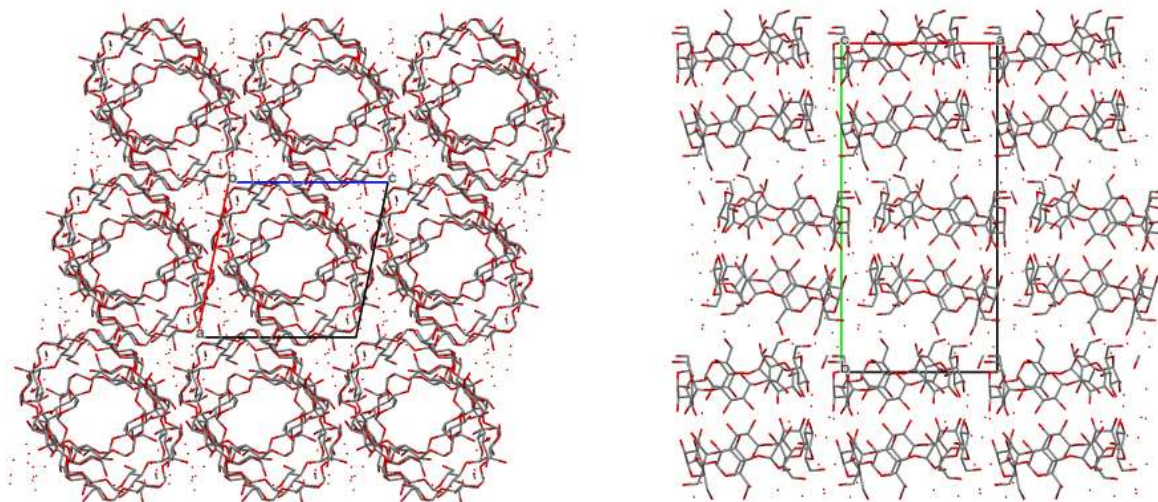


Figure 1.8 : Views along b axis (right) and c axis (left) of CDs organization in the brick dimer type structure CSD BOTBES⁷⁸. Guest molecules are willingly hidden. Hydrogen atoms are not represented. Carbon atoms are represented in grey while oxygen atoms are represented in red.

All the structures are very similar. Repartitions in term of space groups and structural types are represented in Figure 1.9 α CD and γ CD non-channels structures are in majority based upon isolated CDs although in the case of β CD, 98 brick-type structures on a total of 137 non-channels structures are based upon CD dimers.

Most of the structures involving β CD and small guests are obtained in presence of water and exhibit a non-channel herringbone or brick-type structural type. In presence of longer chain molecule, guest or co-solvent, β CD tends to form channel structural type.

In the case of α CD, 7 structures involve linear primary alcohol molecules. 3 structures are obtained in presence of methanol (CSD REF CODE ACDMSM⁷⁹, INUPEM⁸⁰ and CDEXME10⁸¹) 1 structure in presence of 1-ethanol (CSD REF CODE VEHQAA⁸²), 1 structure in presence of 1-decanol (CSD REF CODE TEXTIB) and 2 structures in presence of 1-undecanol (CSD REF CODE KEZGAZ and TEXTEX⁸³).

In the case of β CD, 23 structures involve linear primary alcohol molecules. 3 structures are obtained in presence of methanol (CSD REF CODE BOTBES⁷⁸, BOBPIR⁸⁴, GUXZOO⁸⁵), 19 structures in presence of 1-ethanol (CSD REF CODE LONGIE⁸⁶, WISREV, WISRIZ⁸⁷, CACPOM⁸⁸, UJEFEV⁸⁹, BURXOC⁹⁰, MAXTOW⁹¹, TAFZEG⁹², OFOWIQ⁹³, BOSZEP, BOSZIT⁷⁸, SADPOF⁹⁴, OFAXID⁹⁵, POHXUG⁹⁶, ZUZOH⁹⁷, IJOLUO⁶¹, KOLGAU⁹⁸, IQERON⁹⁹, XETNIW¹⁰⁰) and 1 structure in presence of 1-octanol (CSD REF CODE PUKPIU²).

In the case of γ CD, 6 structures involve linear primary alcohol molecules. 3 structures are obtained in presence of methanol (CSD REF CODE YAPROY, YAPRUE¹⁰¹ and NUNRIX¹⁰²) and 3 structures in presence of 1-propanol (CSD REF CODE CYDXPL¹⁰³, SIBJAO and SIBJES¹⁰⁴).

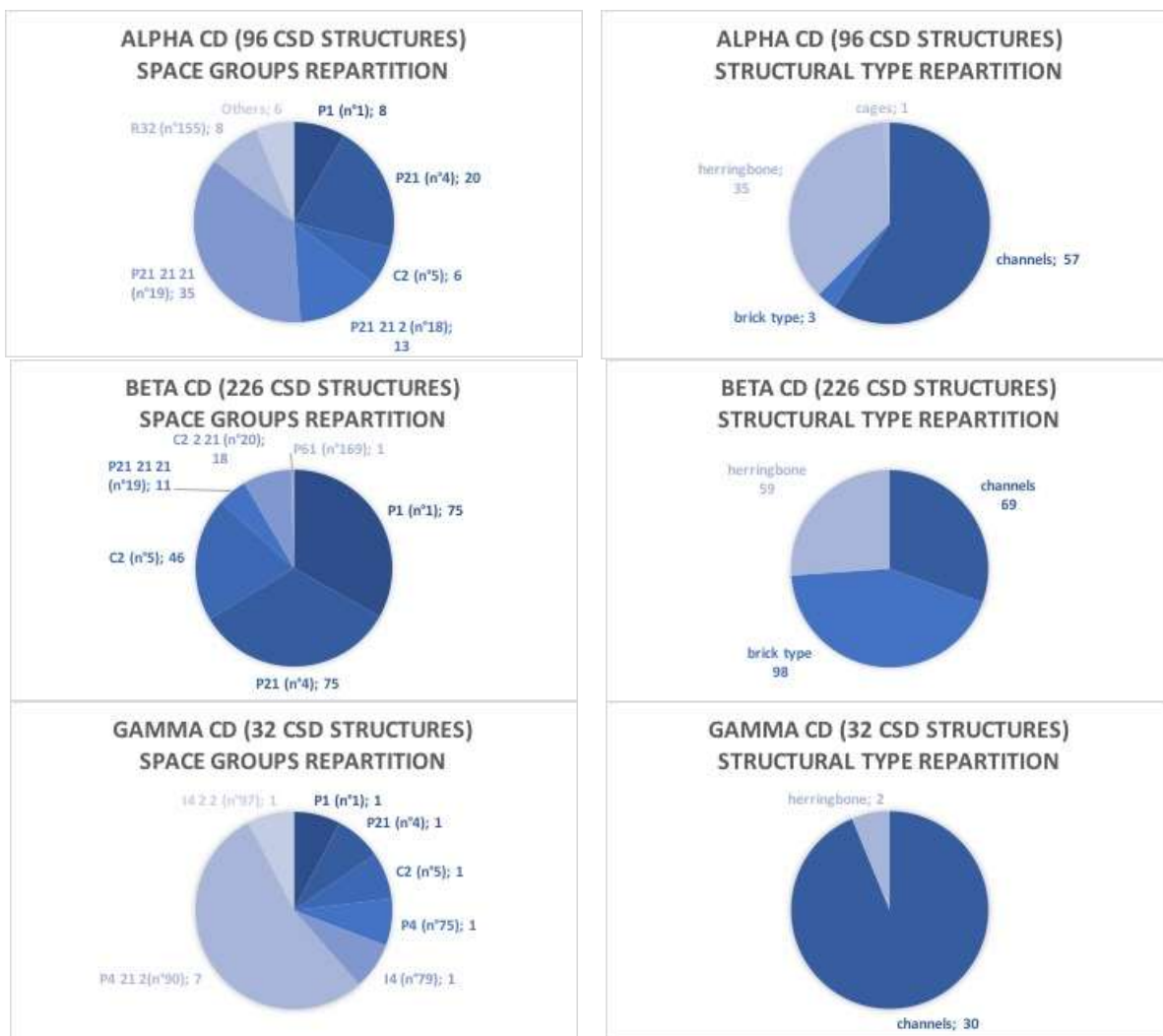


Figure 1.9. Repartition in term of space groups and structural types of the structures involving α CD, β CD and γ CD available in the CSD version 5.39 update 3 (May 2018).

Only 2 structures involving CDs and polycyclic aromatic hydrocarbon compounds are available in the CSD. They consist in the complexation of pyrene by β CD in presence of cyclohexanol or octanol. (CSD REF CODE PUKPOA and PUKPIU²). Both structures adopt a channel head to head structural type with a pyrene molecule inserted between the upper rim of two CD as represented on Figure 1.10 below.

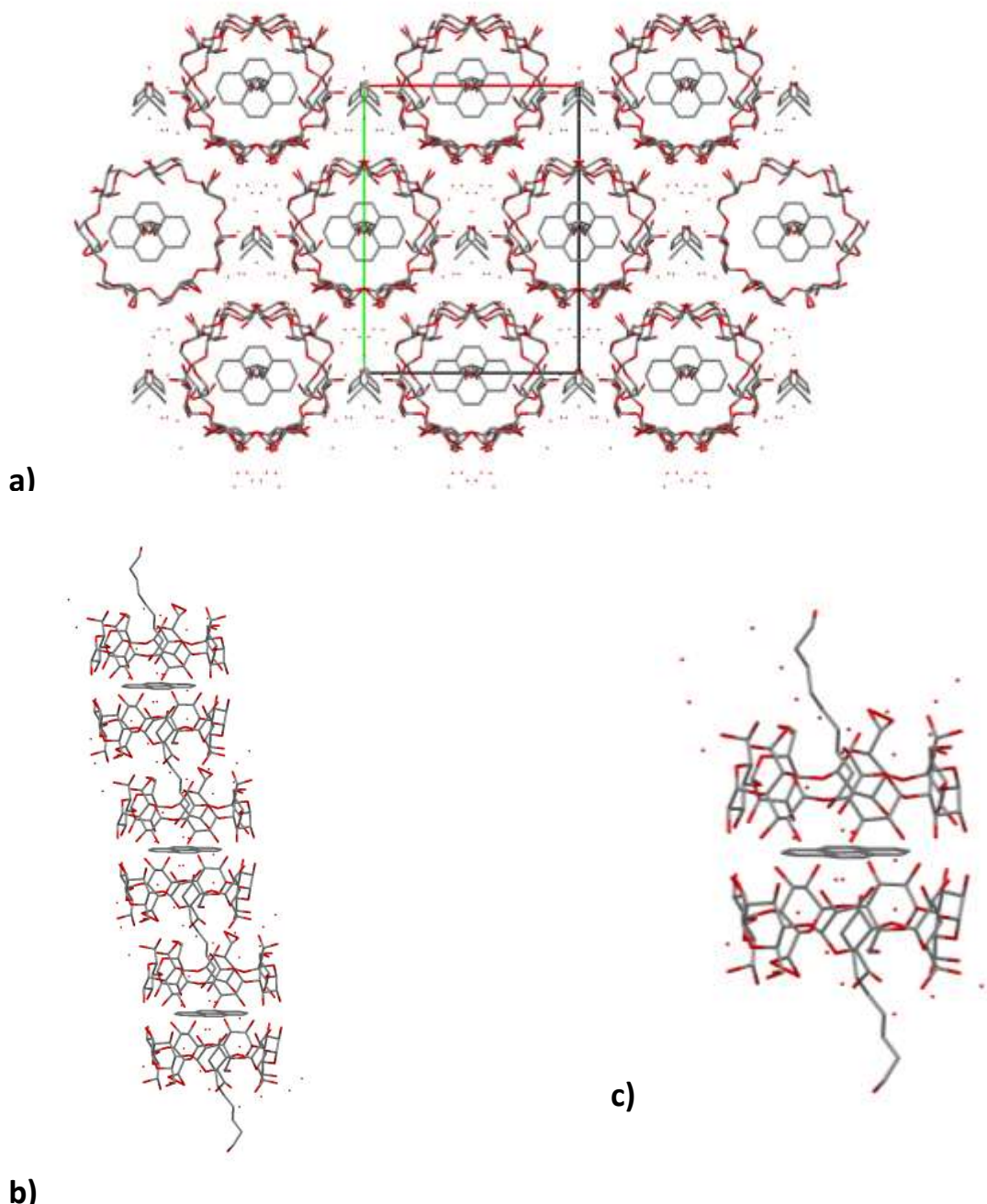


Figure 1.10 : a) View along c axis of the CSD REF CODE PUKPIU involving β CD, octanol and pyrene molecules. Octanol molecules are disordered and not totally resolved. b) View of a channel. c) Detail of the complexed unit involved in a channel. Hydrogen atoms are not represented, carbon atoms are represented in grey and oxygen atoms are represented in red.

Many different intermolecular forces are involved in the formation of CD inclusion complexes. These include Van der waals forces, hydrogen bonding and hydrophobic interactions.

Van der Waals^{105,106} forces are weak attractive forces (distance dependent) which occur from dipole dipole interactions. Moreover, hydrogen bonding involves interaction between a hydrogen atom and another strong electronegative atom resulting in comparatively strong dipole dipole interactions.

Hydrophobic interactions^{107,108}, which are relatively stronger, are contributing factors needed for both formation and stabilization of CD inclusion complexes in comparison to weaker van der Waal forces and hydrogen bonding.

The development of these interactions results due to the entropy change by the release of high energy water molecules from the CD cavity. The hydrophobic character of the guest molecule accounts for the stability of CD inclusion complexes. More is the apolar character of the included molecule; more is the stability of the system.

1.7 Molecular modelling of CDs and their inclusion complexes

Lipkowitz¹⁰⁹ has provided in 1998 an excellent review on the application of computational chemistry to the study of CDs updated in 2006 by Castro¹¹⁰. Two recently published reviews in 2017 by Zhao¹¹¹ and in 2018 by Quevedo¹¹², have clearly showed the specialised expertise and experience required to tackle the molecular modelling of such complex molecules and advanced level difficulties of host-guest interactions.

In order to get a better understanding of the binding events, many theoretical methods including Molecular Mechanics (MM), Molecular Dynamics (MD), and more recently, Quantum Mechanical (QM) methods such as ab initio and Density Functional Theory (DFT), have also been used to study the CD complexes. All these experimental and theoretical methods, when properly utilized in combination with each other, have proven to be extremely powerful in solving the structural, energetic, and dynamic problems associated with CDs and CD complexes.

New methods based upon DFT computations are now largely used due to the new efficiency of computers allowing quantum modelling of larger systems.

The inclusion of a hydrophobic guest molecule^{113,114}, compared to the polar bulk solvent in CDs is a consequence of an interaction based upon covalent forces. The internal cavity of CDs is able to accommodate solvent molecules, which means that the inclusion process requires the displacement of these solvent molecules. There is a great interest in the study of the structural and energetic properties driving the inclusion of guest molecules. Experimental techniques are somehow limited to provide information at a molecular level and performing experimental assays is expensive and time consuming. A wide range of molecular modelling methods are able to characterize the behaviour of such systems at molecular levels.

Scientific computing has evolved¹¹⁵ to a great extent in the past years and advances are available for the classical and quantum ways of modelling larger molecules and inclusion complex systems¹¹⁶⁻¹¹⁸. Thus, numerous publications were published recently concerning large scale molecular modeling simulation studies involving CDs systems.

The structural and energetic behavior associated with the inclusion of guest molecules in CDs have been described by means of molecular modeling methods, including molecular docking, molecular dynamics and free energy of binding analyses¹¹⁹⁻¹²⁸. More advanced research efforts include detailed quantum calculations to assess the binding of the guest molecule and the stability of complexes¹²⁹⁻¹³¹. Finding the best CD system for a specific guest molecule is also feasible by applying molecular modeling methods¹³². Moreover, molecular modeling techniques have been widely used to assess the chiral selection potential of CDs, which is of great pharmaceutical and industrial relevance¹³³⁻¹⁴⁰.

An important aspect that needs to be assessed while preparing CDs inclusion complexes is the corresponding stoichiometry. Although this experimental determination is very tedious, molecular modeling techniques are capable of assessing the number of guest molecules that

may be included in the CD hydrophobic cavity^{141,142}. It is well known that the structure of inclusion complexes with CDs may be considerably modified by the presence of co-solvent molecules and as such, it is relevant to anticipate its effect on the inclusion behavior. In this regard, Zhang et al. exhaustively modeled the effect of commonly used alcohol co-solvents on the inclusion properties of CDs^{143,144}.

Extensive reports have described the possibility of further enhancing the solubilization and complexation induced by CD through the addition of auxiliary agents able to efficiently interact with binary complexes and form ternary aggregates. To date, a wide range of chemicals have been reported as potential third compounds; among them, the most extensively studied are amino acids, polymers and hydroxyl agents¹⁴⁵. The presence of any third agent like co-solvent affects the binary complex, so the molecular modeling methods arise as a very powerful screening technique by selecting the most appropriate molecule by large scale experimental screening and overcoming the limitation of experimental testing for some molecules.

In recent years, a lot of interest has been shown in supramolecular systems in which multiple CDs units forms part of the supramolecular system as covalent or non-covalent moieties, making it possible to obtain sophisticated materials which able to comply with specific functions¹⁴⁶. In the simplest example of the simulation of systems containing multiple CD units, Zhang et al. applied molecular modeling techniques to model the dimerization behavior of β CD in different solvents¹⁴⁷⁻¹⁴⁹.

From the discussed research efforts, it can be seen that plenty of molecular modeling tools, including software, force fields and workflow designs are available. The details are summarized in Table 1.4. As can be seen, the selection of the method, calculation protocol and simulation workflow is highly dependent on the type of system under analysis and the kind of hypothesis under study. Clearly, the utilization of theoretical modeling tools is highly complementary with experimental techniques towards the possibility of describing CDs systems at an atomistic level.

Software	Methodology	Scoring function/forcefield	References
NAMD	MD	CHARMM27	150
Autodock Vina, GAUSSIAN09	Docking, QM	Autodock scoring	151
GAUSSIAN09, AMBER14	MD	GLYCAM-06j	152
AMBER10	MD	GLYCAM-04	153
CDOCKER, AMBER12	Docking, MD	GLYCAM-06	154
ROSETTA 5.98, AMBER12	Docking,	MD GLYCAM-06j	155
Sybyl 7.1, GAUSSIAN03, GOLD	Docking	Tripes FF, GoldScore	156
GAUSSIAN09, AMBER9	MD	GLYCAM-04	157
GAUSSIAN09, CDOCKER, AMBER12	Docking, MD	GLYCAM-06	121
FRED, AMBER12	Docking, MD	GLYCAM-06	124
PRESTO v.3	MD	GAFF	125
MacroModel v9.9	Docking	OPLS2005	126
AMBER12	MD	GAFF	158
GROMACS 4.5.3	MD	GROMOS 53a6	159
GAUSSIAN09	Manual docking	PM3	129
Schrödinger Small Molecule Drug Discovery Suite 2014- 1, GAUSSIAN 09, AMBER12	Docking, MD	FF99SB	131
NAMD	MD	GLYCAM-06	160
TINKER	Docking	MMFF94	132
Autodock 4.2, AMBER12	Docking, MD	Autodock scoring, GLYCAM-06	133
Discovery Studio, AMBER9	Docking, MD	GAFF	134
GAUSSIAN03, Autodock 4.2, Material Studio 6.0	Docking, MD	COMPASS	135
GAUSSIAN03, ArgusLab, DL_POLY 2.17	Docking, MD	DREIDING	136
Autodock 4.2, AMBER11	Docking, MD	Autodock scoring	161
HYPERCHEM 8.0	Docking	MM	142
GROMACS	MD	Q4md-CD	143
Maestro v8.5	Docking	Glide score	162

Glide v5.5	Docking	Glide score	163
Autodock 4.2	Docking	Autodock scoring	164
VLifeMDS 4.	Docking	MMFF94	165
GOLD 5.2	Docking	ChemPLP	166
FRED, AMBER14	Docking, MD, ChemGauss,	GLYCAM06	167
VLifeMDS 4.3	Docking	MMFF	168
YASARA	MD	AMBER03	169-171
GROMACS, AMBER10	MD	GAFF, GLYCAM06	147
GROMACS, AMBER10	MD	Q4md-CD	149
Tinker 4.2	MD	MMFF94	172
Insight/Discover 2000	MD	CVFF	173
GROMACS 4.5.5	MD	GROMOS96(53a6)	174,175
NAMD	MD	CHARMM27CSFF, CGenFF	176
LAMMPS	MD	PCFF	177
Autodock 4.2/GROMACS 4.6.2	Docking, MD	GROMOS96(53a6)	178

Table 1.4 : Compilation of the molecular modeling methods used in the study cases¹¹².

1.8 Different Methods to prepare the complexes

There are many different methods reported in the literature to prepare stable inclusion complexes. Mainly, the procedure for the preparation of CD guest complexes in water depends upon the guest properties^{9,179}. One of the most common procedure is to stir or shake vigorously an aqueous solution of CD (cold or warm) with the guest molecule or its solution. equilibrium is reached with intense stirring and slow cooling in few hours but there are different choices of the preparation method varies among researchers.

a) Solvent evaporation

In this method, the host and the guest are dissolved separately into two mutually miscible solvents, mixing of both solutions to get molecular dispersion and finally evaporating the solvent. The inclusion compounds crystallize out on slow cooling or evaporation¹⁸⁰⁻¹⁸².

b) Kneading

In this case the CD is not dissolved, it is kneaded with a small amount to make a slurry and then guest components added. On stirring in a mixer or mixing manually in mortar-pestle, the viscosity of the mixture increases, giving a paste which can be dried and powdered¹⁸³⁻¹⁸⁴.

c) Freeze drying and spray drying

To obtain fine particles of the complexes, these two methods are preferred. Equimolar quantities of the guest molecules are dissolved in a saturated solution of CDs. The guest molecules which are not soluble in water can be solubilised by adding a co-solvent. The solution is either freeze dried¹⁸⁵⁻¹⁸⁷ or spray dried¹⁸⁸⁻¹⁹⁰.

1.9 Different spectroscopic techniques to analyse inclusion complexes

The CD inclusion complexes prepared by different methods can be further studied and analysed by thermal and spectroscopic techniques. The typical thermal analytical techniques include thermal gravimetric analysis and differential scanning calorimetry. Spectral analyses include Fourier transform Infrared/Raman, Nuclear magnetic resonance and ultraviolet-visible spectroscopy. Other characterization techniques include powder x-ray diffraction and high performance liquid chromatography. Here, we have tried to give an introduction and briefly explained the techniques used in this thesis. All the techniques will be described in the following chapters.

1.9.1 Nuclear magnetic resonance Spectroscopic Analysis

Proton NMR is a robust technique that is regularly used to explore CD inclusion complexes. The first attempt of characterization to study inclusion complexes was made by Demar and Thakkar¹⁹¹ in 1970. They observed changes in the chemical shifts of the protons attached to the C3 and C5 positions of CD when various guest molecules were introduced. These protons are present inside the cavity of the CDs (as explained previously). This data was the first direct spectroscopic evidence for the formation of inclusion complexes where the guest molecule resides inside the CD cavity. Since then, NMR studies have been widely used to characterize inclusion complexes and determine stoichiometry. The method of continuous variation is used to determine the stoichiometry of the system. For example- The researchers¹⁹² have used this method to determine the stoichiometry of the β -sitosterol: β CD inclusion complexes. Briefly, it involves preparing a series of solutions containing both the host and the guest in varying proportions and the total concentration of the host and guest solutions are kept constant in all solutions. The observed parameter is a host or guest chemical shift that is sensitive to complex formation. The plot of $\Delta\delta \times [\beta\text{-CD}]$ against a mole fraction of $\beta\text{-CD}$, ($r=m/[m/n]$), where m and n represent the stoichiometric ratio of β CD and β -sitosterol. From this data, it was determined that due to the fact that the plot shows a maximum value at $r=0.5$, it could be concluded that the β -sitosterol: β CD complex exists in a 1:1 stoichiometric ratio.

1.9.2 Fourier Transform Raman spectroscopy

FT-Raman technique; very similar to FTIR, spectra show characteristic wavenumber frequencies in the stretching and bending of the key chemical bonds of a molecule. In the comparison between pure drug/any guest, pure CD, CD-drug physical mixture and CD-drug inclusion compound, the spectrum of the physical mixture is an overlay of each pure component spectra. However, in the inclusion compound, there are shifts in absorbance bands to a lower frequency, increases or decreases in intensity, and broadening of bands involved in the formation of hydrogen bonds due to the CD-drug interaction¹⁹³⁻¹⁹⁷.

1.9.3 Powder X-ray diffraction

XRD is a solid-state characterization technique used to identify phases of a crystalline compound and can provide information on the unit cell dimensions of a crystalline lattice.

Changes in the crystallinity will be observed if an inclusion complex is present, although it is important to consider polymorphic transformations which may occur in the drug molecules during the complex formation processing. The diffraction pattern of a physical mixture is typically a sum of each component's pattern, while diffractogram of inclusion compounds display a new pattern not seen in the pure components. Often in the diffraction pattern of an inclusion compound a smooth, broad peak is observed which indicates the presence of an amorphous compound devoid of crystallinity. This is generally taken as an indication of a true complex.

1.9.4 Differential Scanning Calorimetry

DSC can be used to determine the melting temperature of crystalline inclusion complexes. when a guest molecule is encapsulated in CD's cavity, the complex has a melting, boiling, or sublimation points that are generally different from the individual components. Pandit et al¹⁹⁸ studied pioglitazone/CD inclusion complexes prepared by spray drying and kneading methods. The DSC thermograms displayed endothermic peaks at 201.9° and 68.13° for pure pioglitazone and methylated-β-CD, respectively. The complexes prepared by different methods displayed one endothermic peak. the complex prepared by the kneading method showed a peak at 181.1°C, while those prepared by the spray-drying method showed a peak at 154.1°C. It was concluded that the disappearance of the pioglitazone's endothermic peak in these systems indicated the formation of a true inclusion complex. Other authors^{181,199,200} have also reported that CD inclusion complexes with a variety of guest drugs/molecules exhibit the disappearance of the characteristic endothermic peaks of the guest molecule.

1.10 Aromatic hydrocarbons (AHs)

Aromatic hydrocarbons are organic compounds consisting of only carbon and hydrogen. They are chemically composed of two or more fused aromatic rings like benzene. In simpler terms we can say, if the planar cyclic molecule containing certain number of π electrons, satisfies the Huckel's rule^{201,202} ($4n+2$, $n=1,2,\dots$) The arrangement of these rings could be linear, cluster or angular. They are classified into two categories – “small PAH's” and “large” PAH's. Small PAH's contain up to six aromatic rings arranged in different fashions whereas large PAH's have more than six aromatic rings. Single or double rings aromatic compounds like benzene and naphthalene and their derivatives such as toluene, fluorobenzene, β-naphthol respectively are not considered as PAH's. They are being considered as Monocyclic or bicyclic aromatic hydrocarbons.

PAH's are generally characterized by properties like high melting and boiling points, low vapour pressure and very low aqueous solubility (decreases with increasing molecular weight). Aqueous solubility of PAH's decreases with addition of a new aromatic ring. They are highly lipophilic that's why are very soluble in organic solvents. The other properties include light sensitivity, heat resistance, conductivity, emit resistance and corrosion resistance. The most common uses of PAH's are intermediaries in pharmaceuticals, agricultural products, thermosetting plastics, photographic products, lubricating materials and other chemical industries.

1.10.1 Sources of Aromatic hydrocarbons in the environment

The main sources of aromatic hydrocarbons such as benzene²⁰³⁻²⁰⁵ and naphthalene²⁰⁶⁻²⁰⁸ and other Polycyclic aromatic hydrocarbons^{209,210} (PAH's) are incomplete combustion of organic materials like coal, oil, wood or either by natural combustion sources like forest fires or man-made combustion sources like automobile emissions or cigarette smoke. The major sources of PAH's to the environment are of three different types namely: pyrogenic, petrogenic and biological.

- (a) **Pyrogenic PAHs**- formed when organic substances are exposed to high temperatures under low or no oxygen conditions. e.g- destructive distillation of coal, thermal cracking of petroleum, incomplete combustion of fuels in vehicles and incomplete burning of wood in the forest. They are generally found in urban areas with higher concentrations and locations near some industry or refinery.
- (b) **Petrogenic PAHs**- They are formed during crude oil maturation. The main sources are oceanic and fresh water oil spills, underground or above ground storage leakages. Petrogenic PAHs are common due to large scale use of transportation, use of crude oil and crude oil products.
- (c) **Biological production**- they are not very common but still synthesised by certain plants and bacteria or formed during degradation of vegetative matter. The mode of formation can be either natural or anthropogenic.

The few examples of natural sources are forest or brush fires, bacterial or algae synthesis, volcanic eruptions, petroleum seepage, etc. anthropogenic sources include automotive emissions, cigarette and cigar smoke, aircraft exhaust, petroleum product spills, sewage sledge etc.

1.10.2 Occurrence of PAH in the living environment

PAH's enter the food chain through terrestrial and aquatic environments. PAH's can be added to soils if fill materials contain PAHs. Once they are deposited onto the earth's surface, they can become mobile. The octanol-water partitioning coefficient determines the sorption of PAHs to soils as it is related to solubility of an organic compound in water²¹¹. Living beings especially mammals can absorb PAH's by various routes like inhalation, skin contact and ingestion whereas plants can get exposed to PAH's from soils through roots and can also translocate them to other plant parts. They are moderately persistent in the environment and can be bio-accumulated in aquatic plants and animals²¹²⁻²¹⁴.

PAHs are lipophilic in nature and are generally have a very poor aqueous solubility but they can accumulate in lipid tissues of plants and animals. Heavier PAH preferentially associate with particulate matter, when particulates fall out into surface water the adsorbed PAH finally end up in fresh water or marine sediments. The main route of human exposure to sedimentary PAHs is through marine lives which make up part of the human diet. PAH's contained in sediments and pore water are taken in by the benthic organisms^{215,216} such as lobsters, mussels and clams which are either consumed directly humans or are consumed by higher predators which are also a part of the human diet, such as fish, crabs, squid etc.

1.10.3 Effect on human health

PAHs are generally known for their carcinogenic²¹⁷, mutagenic²¹⁸ and teratogenic properties and therefore pose a serious threat to the health and wellbeing of humans. Due to these

reasons, PAHs are listed as the priority substances to be detected in the environment by the E.U. WFD²¹⁹ and by the United States Environment Protection Agency²²⁰. When a person is exposed to PAHs, the exposure will be to the whole group and never to single PAHs. Once the PAHs enter the organism they require a multistep metabolic activation by specific enzymes. Most metabolites of PAH are excreted in faeces and urine. Mixture of PAHs are known to cause short term effect like skin irritation and inflammation. Anthracene, benzo(a) pyrene and naphthalene are direct skin irritants. The frequent exposure can cause long term health effects such as decreased immune function, cataracts, kidney and liver damage, breathing problems and lung function abnormalities. Metabolites like epoxides²²¹ and dihydrodiols²²² of some PAH's can bind to cellular proteins and DNA. Occupational studies²²³ of workers provide the evidence of carcinogenic nature of PAHs to humans.

1.10.4 Detection of Aromatic hydrocarbons in the environment

There are many different analytical methods to detect the presence of aromatic hydrocarbons in the environmental samples. In 1976, a group of researchers²²⁴ published an article providing details about determination of PAHs in atmospheric particulate matter by high pressure liquid chromatography (HPLC) coupled with online fluorescence detection followed by another group²²⁵ that used reversed phase liquid chromatography(LC). For soil samples, the researchers²²⁶ have used the techniques like high resolution gas chromatography-mass spectroscopy (HRGC-MS) and liquid chromatography fluorescence detection (LC-FD). The water samples were treated by ultrasound-assisted emulsification microextraction (USAEME) method²²⁷ by dispersive liquid-liquid microextraction (DLLME)²²⁸, gas chromatography-mass spectrometry²²⁹ and also by analytical methods explained by Manoli *et al.*²³⁰

After considering the literature for detection and determination of aromatic hydrocarbons in the environment, we can conclude that despite the benefits in sensitivity and reliability of these techniques they are not applicable for real-time monitoring of the chemical pollution. As a consequence, there is a great interest in developing alternative analytical methods such as chemical and biochemical sensors, noting that later approach of sensing tools could be applied for on-site and in-situ monitoring of environmental quality.

1.11 References

1. Tijunelyte, I., Dupont, N., Milosevic, I., Barbey, C., Rinnert, E., Lidgi-Guigui, N., Guenin, E. and de la Chapelle, M.L., 2017. Investigation of aromatic hydrocarbon inclusion into cyclodextrins by raman spectroscopy and thermal analysis. *Environmental Science And Pollution Research*, 24(35), pp.27077-27089.
2. Udachin, K.A. and Ripmeester, J.A., 1998. A novel mode of inclusion for pyrene in β -cyclodextrin compounds: The crystal structures of β -cyclodextrin with cyclohexanol and pyrene, and with n-octanol and pyrene. *Journal of the American Chemical Society*, 120(5), pp.1080-1081.
3. Groom, C.R., Bruno, I.J., Lightfoot, M.P. and Ward, S.C., 2016. The Cambridge structural database. *Acta Crystallographica Section B: Structural Science, Crystal Engineering and Materials*, 72(2), pp.171-179.
4. Raymo, F.M. and Stoddart, J.F., 1999. Interlocked macromolecules. *Chemical reviews*, 99(7), pp.1643-1664.
5. Nepogodiev, S.A. and Stoddart, J.F., 1998. Cyclodextrin-based catenanes and rotaxanes. *Chemical reviews*, 98(5), pp.1959-1976.
6. Powell, H.M., 1948. 15. The structure of molecular compounds. Part IV. Clathrate compounds. *Journal of the Chemical Society (Resumed)*, pp.61-73.
7. Cram, D.J., 1986. Preorganization—from solvents to spherands. *Angewandte Chemie International Edition in English*, 25(12), pp.1039-1057.
8. Szejtli, J., 1998. Introduction and general overview of cyclodextrin chemistry. *Chemical reviews*, 98(5), pp.1743-1754.
9. Saenger, W., 1980. Cyclodextrin inclusion compounds in research and industry. *Angewandte Chemie International Edition in English*, 19(5), pp.344-362.
10. Szejtli, J., 1997. Utilization of cyclodextrins in industrial products and processes. *Journal of Materials Chemistry*, 7(4), pp.575-587.
11. SZEJTLI, J., ATWOOD, J. L., & LEHN, J.-M. (1996). *Comprehensive supramolecular chemistry. Volume 3, Volume 3*. New York, Pergamon.
12. Loftsson, T. and Duchêne, D., 2007. Cyclodextrins and their pharmaceutical applications. *International journal of pharmaceutics*, 329(1-2), pp.1-11.
13. Szejtli, J., 1988. Cyclodextrins in pharmaceuticals. In *Cyclodextrin Technology* (pp. 186-306). Springer, Dordrecht.
14. Loftsson, T. and Brewster, M.E., 1996. Pharmaceutical applications of cyclodextrins. 1. Drug solubilization and stabilization. *Journal of pharmaceutical sciences*, 85(10), pp.1017-1025.
15. Jug, M. and Bećirević-Laćan, M., 2008. Cyclodextrin-based pharmaceutical. *Rad Hrvatske akademije znanosti i umjetnosti: Medicinske znanosti*, (499= 32), pp.9-26..
16. Szente, L. and Szejtli, J., 2004. Cyclodextrins as food ingredients. *Trends in Food Science & Technology*, 15(3-4), pp.137-142.
17. Fenyvesi, E., Vikmon, M.A. and Szente, L., 2016. Cyclodextrins in food technology and human nutrition: benefits and limitations. *Critical reviews in food science and nutrition*, 56(12), pp.1981-2004.
18. Astray, G., Gonzalez-Barreiro, C., Mejuto, J.C., Rial-Otero, R. and Simal-Gándara, J., 2009. A review on the use of cyclodextrins in foods. *Food Hydrocolloids*, 23(7), pp.1631-1640.

19. Szejtli, J., 1982. Cyclodextrins in food, cosmetics and toiletries. *Starch-Stärke*, 34(11), pp.379-385.
20. Buschmann, H.J. and Schollmeyer, E., 2002. Applications of cyclodextrins in cosmetic products: a review. *Journal of cosmetic science*, 53(3), pp.185-192.
21. Tarimci, N., 2011. Cyclodextrins in the cosmetic field. *Cyclodextrins in Pharmaceuticals, Cosmetics, and Biomedicine: Current and Future Industrial Applications*, pp.131-144.
22. Dodziuk, H. ed., 2006. *Cyclodextrins and their complexes: chemistry, analytical methods, applications*. John Wiley & Sons.
23. Harata, K., Uekama, K., Otagiri, M., Hirayama, F. and Ohtani, Y., 1985. The Structure of the Cyclodextrin Complex. XVIII. Crystal Structure of β -Cyclodextrin–Benzyl Alcohol (1: 1) Complex Pentahydrate. *Bulletin of the Chemical Society of Japan*, 58(4), pp.1234-1238.
24. Szejtli, J., 1990. The cyclodextrins and their applications in biotechnology. *Carbohydrate Polymers*, 12(4), pp.375-392.
25. Bar, R., 1996. Application of cyclodextrins in biotechnology. In *Proceedings of the Eighth International Symposium on Cyclodextrins* (pp. 521-526). Springer, Dordrecht.
26. Bhaskara-Amrit, U.R., Agrawal, P.B. and Warmoeskerken, M.M.C.G., 2011. Applications of β -cyclodextrins in textiles. *AUTEX research journal*, 11(4), pp.94-101.
27. Buschmann, H.J., Knittel, D. and Schollmeyer, E., 2001. New textile applications of cyclodextrins. *Journal of inclusion phenomena and macrocyclic chemistry*, 40(3), pp.169-172.
28. Szejtli, J., 2003. Cyclodextrins in the textile industry. *Starch-Stärke*, 55(5), pp.191-196.
29. PRINGSHEIM, H., & ABBE, C. (1932). *The chemistry of the monosaccharides and of the polysaccharides*. New York, McGraw-Hill Book Company, Inc.
30. Crini, G., 2014. A history of cyclodextrins. *Chemical reviews*, 114(21), pp.10940-10975.
31. Del Valle, E.M., 2004. Cyclodextrins and their uses: a review. *Process biochemistry*, 39(9), pp.1033-1046.
32. López-Nicolás, J.M., Rodríguez-Bonilla, P. and García-Carmona, F., 2014. Cyclodextrins and antioxidants. *Critical reviews in food science and nutrition*, 54(2), pp.251-276.
33. Zhang, J. and Ma, P.X., 2013. Cyclodextrin-based supramolecular systems for drug delivery: recent progress and future perspective. *Advanced drug delivery reviews*, 65(9), pp.1215-1233.
34. Belikov, V.G., Kompantseva, E.V. and Botezat-Belyi, Y.K., 1986. Cyclodextrins and their inclusion compounds with drugs. *Pharmaceutical Chemistry Journal*, 20(5), pp.299-306.
35. Eastburn, S.D. and Tao, B.Y., 1994. Applications of modified cyclodextrins. *Biotechnology advances*, 12(2), pp.325-339.
36. Tang, W., Ng, S.C. and Sun, D., 2013. *Modified cyclodextrins for chiral separation* (pp. 209-216). Berlin: Springer.
37. Wyrwalski, F., Léger, B., Lancelot, C., Roucoux, A., Monflier, E. and Ponchel, A., 2011. Chemically modified cyclodextrins as supramolecular tools to generate carbon-supported ruthenium nanoparticles: An application towards gas phase hydrogenation. *Applied Catalysis A: General*, 391(1-2), pp.334-341.
38. Stella, V.J. and Rajewski, R.A., 1997. Cyclodextrins: their future in drug formulation and delivery. *Pharmaceutical research*, 14(5), pp.556-567.

39. Culha, M., Lavrik, N.V., Schell, F.M., Tipple, C.A. and Sepaniak, M.J., 2003. Characterization of volatile, hydrophobic cyclodextrin derivatives as thin films for sensor applications. *Sensors and Actuators B: Chemical*, 92(1-2), pp.171-180.
40. Ogoshi, T. and Harada, A., 2008. Chemical sensors based on cyclodextrin derivatives. *Sensors*, 8(8), pp.4961-4982.
41. Cutrone, G., Casas-Solvas, J.M. and Vargas-Berenguel, A., 2017. Cyclodextrin-modified inorganic materials for the construction of nanocarriers. *International journal of pharmaceutics*, 531(2), pp.621-639.
42. Varan, G., Varan, C., Erdoğar, N., Hincal, A.A. and Bilensoy, E., 2017. Amphiphilic cyclodextrin nanoparticles. *International journal of pharmaceutics*, 531(2), pp.457-469.
43. Fathi, M., Martin, A. and McClements, D.J., 2014. Nanoencapsulation of food ingredients using carbohydrate based delivery systems. *Trends in food science & technology*, 39(1), pp.18-39.
44. Jansook, P., Ogawa, N. and Loftsson, T., 2018. Cyclodextrins: structure, physicochemical properties and pharmaceutical applications. *International journal of pharmaceutics*, 535(1-2), pp.272-284.
45. Miyazawa, I., Ueda, H., Nagase, H., Endo, T., Kobayashi, S. and Nagai, T., 1995. Physicochemical properties and inclusion complex formation of δ -cyclodextrin. *European journal of pharmaceutical sciences*, 3(3), pp.153-162..
46. Wistuba, D., Bogdanski, A., Larsen, K.L. and Schurig, V., 2006. δ -Cyclodextrin as novel chiral probe for enantiomeric separation by electromigration methods. *Electrophoresis*, 27(21), pp.4359-4363.
47. Akasaka, H., Endo, T., Nagase, H., UEDA, H. and KOBAYASHI, S., 2000. Complex formation of cyclomaltononaose δ -cyclodextrin (δ -CD) with macrocyclic compounds. *Chemical and pharmaceutical bulletin*, 48(12), pp.1986-1989.
48. Furuishi, T., Endo, T., Nagase, H., Ueda, H. and Nagai, T., 1998. Solubilization of C70 into water by complexation with δ -cyclodextrin. *Chemical and pharmaceutical bulletin*, 46(10), pp.1658-1659.
49. Bekers, O., Uijtendaal, E.V., Beijnen, J.H., Bult, A. and Underberg, W.J.M., 1991. Cyclodextrins in the pharmaceutical field. *Drug development and industrial pharmacy*, 17(11), pp.1503-1549.
50. Miranda, J.C.D., Martins, T.E.A., Veiga, F. and Ferraz, H.G., 2011. Cyclodextrins and ternary complexes: technology to improve solubility of poorly soluble drugs. *Brazilian journal of pharmaceutical sciences*, 47(4), pp.665-681.
51. Saenger, W. and Steiner, T., 1998. Cyclodextrin Inclusion Complexes: Host–Guest Interactions and Hydrogen-Bonding Networks. *Acta Crystallographica Section A*, 54(6-1), pp.798-805.
52. Bender, M.L. and Komiyama, M., 2012. *Cyclodextrin chemistry*(Vol. 6). Springer Science & Business Media.
53. Yoshii, H., Furuta, T., Okita, E., Toyomi, A., Linko, Y.Y. and Linko, P., 1998. The increased effect of kneading on the formation of inclusion complexes between d-limonene and β -cyclodextrin at low water content. *Bioscience, biotechnology, and biochemistry*, 62(3), pp.464-468.

54. Szente, L. and Szejtli, J., 1999. Highly soluble cyclodextrin derivatives: chemistry, properties, and trends in development. *Advanced drug delivery reviews*, 36(1), pp.17-28.
55. Matsuda, H. and Arima, H., 1999. Cyclodextrins in transdermal and rectal delivery. *Advanced drug delivery reviews*, 36(1), pp.81-99.
56. Rekharsky, M.V. and Inoue, Y., 1998. Complexation thermodynamics of cyclodextrins. *Chemical reviews*, 98(5), pp.1875-1918.
57. Tablet, C., Matei, I. and Hillebrand, M., 2012. The determination of the stoichiometry of cyclodextrin inclusion complexes by spectral methods: possibilities and limitations. In *Stoichiometry and Research-The Importance of Quantity in Biomedicine*. InTech.
58. Kondo, H., Nakatani, H. and Hiromi, K., 1976. Interaction of cyclodextrins with fluorescent probes and its application to kinetic studies of amylase. *The Journal of Biochemistry*, 79(2), pp.393-405.
59. Bruno, I.J., Cole, J.C., Edgington, P.R., Kessler, M., Macrae, C.F., McCabe, P., Pearson, J. and Taylor, R., 2002. New software for searching the Cambridge Structural Database and visualizing crystal structures. *Acta Crystallographica Section B*, 58(3-1), pp.389-397.
60. Mercury CSD 2.0 - New Features for the Visualization and Investigation of Crystal Structures C. F. Macrae, I. J. Bruno, J. A. Chisholm, P. R. Edgington, P. McCabe, E. Pidcock, L. Rodriguez-Monge, R. Taylor, J. van de Streek and P. A. Wood, *J. Appl. Cryst.*, 41, 466-470, 2008.
61. Aree, T. and Chaichit, N., 2003. A new crystal form of β -cyclodextrin-ethanol inclusion complex: channel-type structure without long guest molecules. *Carbohydrate research*, 338(15), pp.1581-1589.
62. Huang, L., Allen, E. and Tonelli, A.E., 1999. Inclusion compounds formed between cyclodextrins and nylon 6. *Polymer*, 40(11), pp.3211-3221.
63. Tsai, C.C., Leng, S., Jeong, K.U., Van Horn, R.M., Wang, C.L., Zhang, W.B., Graham, M.J., Huang, J., Ho, R.M., Chen, Y. and Lotz, B., 2010. Supramolecular structure of β -cyclodextrin and poly (ethylene oxide)-block-poly (propylene oxide)-block-poly (ethylene oxide) inclusion complexes. *Macromolecules*, 43(22), pp.9454-9461.
64. Harata, K., Takenaka, Y. and Yoshida, N., 2001. Crystal structures of 6-deoxy-6-monosubstituted β -cyclodextrins. Substituent-regulated one-dimensional arrays of macrocycles. *Journal of the Chemical Society, Perkin Transactions 2*, (9), pp.1667-1673.
65. Ogawa, N., Nagase, H., Loftsson, T., Endo, T., Takahashi, C., Kawashima, Y., Ueda, H. and Yamamoto, H., 2017. Crystallographic and theoretical studies of an inclusion complex of β -cyclodextrin with fentanyl. *International journal of pharmaceuticals*, 531(2), pp.588-594.
66. Christoforides, E., Papaioannou, A. and Bethanis, K., 2018. Crystal structure of the inclusion complex of cholesterol in β -cyclodextrin and molecular dynamics studies. *Beilstein journal of organic chemistry*, 14, p.838.
67. Ceborska, M., Asztemborska, M. and Lipkowski, J., 2012. Rare 'head-to-tail' arrangement of guest molecules in the inclusion complexes of (+)- and (-)-menthol with β -cyclodextrin. *Chemical Physics Letters*, 553, pp.64-67.
68. Prochowicz, D., Kornowicz, A., Justyniak, I. and Lewiński, J., 2016. Metal complexes based on native cyclodextrins: synthesis and structural diversity. *Coordination Chemistry Reviews*, 306, pp.331-345.

69. Lindner, K. and Saenger, W., 1982. Crystal and molecular structure of cyclohepta-amylose dodecahydrate. *Carbohydrate Research*, 99(2), pp.103-115.
70. Maclennan, J.M. and Stezowski, J.J., 1980. The crystal structure of uncomplexed-hydrated cyclooctaamylose. *Biochemical and biophysical research communications*, 92(3), pp.926-932.
71. Pop, M.M., Goubitz, K., Borodi, G., Bogdan, M., De Ridder, D.J., Peschar, R. and Schenk, H., 2002. Crystal structure of the inclusion complex of β -cyclodextrin with mefenamic acid from high-resolution synchrotron powder-diffraction data in combination with molecular-mechanics calculations. *Acta Crystallographica Section B: Structural Science*, 58(6), pp.1036-1043.
72. Aree, T., Schulz, B. and Reck, G., 2003. Crystal structures of β -cyclodextrin complexes with formic acid and acetic acid. *Journal of inclusion phenomena and macrocyclic chemistry*, 47(1-2), pp.39-45.
73. Fourtaka, K., Christoforides, E., Mentzafos, D. and Bethanis, K., 2018. Crystal structures and molecular dynamics studies of the inclusion compounds of β -citronellol in β -cyclodextrin, heptakis (2, 6-di-O-methyl)- β -cyclodextrin and heptakis (2, 3, 6-tri-O-methyl)- β -cyclodextrin. *Journal of Molecular Structure*, 1161, pp.1-8.
74. Seidel, R.W. and Koleva, B.B., 2009. β -Cyclodextrin 10.41-hydrate. *Acta Crystallographica Section E: Structure Reports Online*, 65(12), pp.o3162-o3163.
75. Harata, K., Rao, C.T. and Pitha, J., 1993. Crystal structure of 6-O-[(R)-2-hydroxypropyl] cyclomaltoheptaose and 6-O-[(S)-2-hydroxypropyl] cyclomaltoheptaose. *Carbohydrate research*, 247, pp.83-98.
76. Gessler, K., Steiner, T., Koellner, G. and Saenger, W., 1993. Crystal structures of cyclomaltoheptaose (beta-cyclodextrin) complexed with ethylene glycol. 8.0 H₂O and glycerol. 7.2 H₂O. *Carbohydrate research*, 249(2), pp.327-344.
77. Steiner, T., Koellner, G. and Saenger, W., 1992. A vibrating flexible chain in a molecular cage: Crystal structure of the complex cyclomaltoheptaose (β -cyclodextrin)-1, 4-butanediol· 6.25 H₂O. *Carbohydrate research*, 228(2), pp.321-332.
78. Zhao, Y.L., Benítez, D., Yoon, I. and Stoddart, J.F., 2009. Inclusion Behavior of β -Cyclodextrin with Bipyridine Molecules: Factors Governing Host-Guest Inclusion Geometries. *Chemistry—An Asian Journal*, 4(3), pp.446-456.
79. Harata, K., 1978. The Structure of the Cyclodextrin Complex. VII. The Crystal Structure of the α -Cyclodextrin–DMSO–Methanol (1: 1: 2) Dihydrate Complex A Simultaneous Inclusion of DMSO and Methanol. *Bulletin of the Chemical Society of Japan*, 51(6), pp.1644-1648.
80. Onagi, H., Carrozzini, B., Cascarano, G.L., Easton, C.J., Edwards, A.J., Lincoln, S.F. and Rae, A.D., 2003. Separated and Aligned Molecular Fibres in Solid State Self-Assemblies of Cyclodextrin [2] Rotaxanes. *Chemistry—A European Journal*, 9(24), pp.5971-5977.
81. Hingerty, B. and Saenger, W., 1976. Topography of cyclodextrin inclusion complexes. 8. Crystal and molecular structure of the. alpha.-cyclodextrin-methanol-pentahydrate complex. Disorder in a hydrophobic cage. *Journal of the American Chemical Society*, 98(11), pp.3357-3365.
82. Eliadou, K., Yannakopoulou, K., Rontoyianni, A. and Mavridis, I.M., 1999. NMR Detection of Simultaneous Formation of [2]-and [3] Pseudorotaxanes in Aqueous Solution between α -Cyclodextrin and Linear Aliphatic α , ω -Amino acids, an α , ω -

- Diamine and an α , ω -Diacid of Similar Length, and Comparison with the Solid-State Structures. *The Journal of Organic Chemistry*, 64(17), pp.6217-6226.
83. Gallois-Montbrun, D., Le Bas, G., Mason, S.A., Prange, T. and Lesieur, S., 2013. A highly hydrated α -cyclodextrin/1-undecanol inclusion complex: crystal structure and hydrogen-bond network from high-resolution neutron diffraction at 20 K. *Acta Crystallographica Section B: Structural Science, Crystal Engineering and Materials*, 69(2), pp.214-227.
 84. Lindner, K. and Saenger, W., 1982. Crystal and molecular structures of cyclomaltoheptaose inclusion complexes with HI and with methanol. *Carbohydrate Research*, 107(1), pp.7-16.
 85. Wang, J.L., Miao, F.M., Zhou, W.H. and Ma, S.K., 2002. Synthesis and Structure of Inclusion Complex of Cyclomaltoheptaose (β -Cyclodextrin) with m-Aminophenol. *Chinese Journal of Chemistry*, 20(4), pp.358-361.
 86. Makedonopoulou, S., Tulinsky, A. and Mavridis, I.M., 1999. The Dimeric Complex of Beta-Cyclodextrin with 1, 13-tridecanedioic acid. *Supramolecular Chemistry*, 11(1), pp.73-81.
 87. Makedonopoulou, S. and Mavridis, I.M., 2000. Structure of the inclusion complex of β -cyclodextrin with 1, 12-dodecanedioic acid using synchrotron radiation data; a detailed dimeric β -cyclodextrin structure. *Acta crystallographica Section B*, 56(2), pp.322-331.
 88. Makedonopoulou, S. and Mavridis, I.M., 2001. The dimeric complex of cyclomaltoheptaose with 1, 14-tetradecanedioic acid. Comparison with related complexes. *Carbohydrate research*, 335(3), pp.213-220.
 89. WANG, E., CHEN, G. and HAN, C., 2009. A Novel Inclusion Complex of 8-Hydroxyquinoline Sandwiched Between Two β -Cyclodextrins.
 90. Paulidou, A., Maffeo, D., Yannakopoulou, K. and Mavridis, I.M., 2010. Similar modes of inclusion in complexes of β -cyclodextrin with sulfonylurea hypoglycemic drugs. *CrystEngComm*, 12(2), pp.517-525.
 91. Hadjoudis, E., Yannakopoulou, K., Chatziefthimiou, S.D., Paulidou, A. and Mavridis, I.M., 2011. Supramolecular control of photochromism in a β -cyclodextrin/Schiff base system. *Journal of Photochemistry and Photobiology A: Chemistry*, 217(2), pp.293-298.
 92. Aree, T. and Chaichit, N., 2003. Crystal structure of β -cyclodextrin-benzoic acid inclusion complex. *Carbohydrate research*, 338(5), pp.439-446.
 93. Aree, T. and Chaichit, N., 2008. Crystal form III of β -cyclodextrin-ethanol inclusion complex: layer-type structure with dimeric motif. *Carbohydrate research*, 343(13), pp.2285-2291.
 94. Aree, T. and Jongrungruangchok, S., 2016. Crystallographic evidence for β -cyclodextrin inclusion complexation facilitating the improvement of antioxidant activity of tea (+)-catechin and (-)-epicatechin. *Carbohydrate polymers*, 140, pp.362-373.
 95. Wang, E.J., Yan, Z. and Cai, J., 2007. Crystal structure of a cyclomaltoheptaose-4-hydroxybiphenyl inclusion complex. *Carbohydrate research*, 342(11), pp.1530-1534.
 96. Paulidou, A., Maffeo, D., Yannakopoulou, K. and Mavridis, I.M., 2008. Crystal structure of the inclusion complex of the antibacterial agent triclosan with cyclomaltoheptaose and NMR study of its molecular encapsulation in positively and negatively charged cyclomaltoheptaose derivatives. *Carbohydrate research*, 343(15), pp.2634-2640.
 97. Mentzafos, D., Mavridis, I.M. and Hursthouse, M.B., 1996. β -Cyclodextrin (Z)-9-Dodecen-1-ol 2: 1 Complex. *Acta Crystallographica Section C*, 52(5), pp.1220-1223.

98. Aree, T., Chaichit, N. and Engkakul, C., 2008. Polymorphism in β -cyclodextrin–benzoic acid inclusion complex: a kinetically controlled crystal growth according to the Ostwald's rule. *Carbohydrate research*, 343(14), pp.2451-2458.
99. Aree, T. and Jongrungruangchok, S., 2016. Enhancement of antioxidant activity of green tea epicatechins in β -cyclodextrin cavity: Single-crystal X-ray analysis, DFT calculation and DPPH assay. *Carbohydrate polymers*, 151, pp.1139-1151.
100. Aree, T. and Jongrungruangchok, S., 2018. β -Cyclodextrin encapsulation elevates antioxidant capacity of tea: A closing chapter on non-epicatechins, atomistic insights from X-ray analysis, DFT calculation and DPPH assay. *Carbohydrate polymers*, 194, pp.24-33.
101. Forgan, R.S., Smaldone, R.A., Gassensmith, J.J., Furukawa, H., Cordes, D.B., Li, Q., Wilmer, C.E., Botros, Y.Y., Snurr, R.Q., Slawin, A.M. and Stoddart, J.F., 2011. Nanoporous carbohydrate metal–organic frameworks. *Journal of the American Chemical Society*, 134(1), pp.406-417.
102. Steiner, T. and Saenger, W., 1998. Channel-Type Crystal Packing in the Very Rare Space Group P4212 with $Z'=3/4$: Crystal Structure of the Complex γ -Cyclodextrin–Methanol–n-Hydrate. *Acta Crystallographica Section B*, 54(4), pp.450-455.
103. Lindner, K. and Saenger, W., 1980. Crystal structure of the γ -cyclodextrin n-propanol inclusion complex; Correlation of α -, β -, γ -cyclodextrin geometries. *Biochemical and biophysical research communications*, 92(3), pp.933-938.
104. Ding, J.I.A.N.P.I.N.G., Steiner, T.H.O.M.A.S. and Saenger, W.O.L.F.R.A.M., 1991. Structure of the γ -cyclodextrin–1-propanol–17H₂O inclusion complex. *Acta Crystallographica Section B*, 47(5), pp.731-738.
105. Israelachvili, J.N., 1974. The nature of van der Waals forces. *Contemporary Physics*, 15(2), pp.159-178.
106. Berland, K., Cooper, V.R., Lee, K., Schröder, E., Thonhauser, T., Hyldgaard, P. and Lundqvist, B.I., 2015. van der Waals forces in density functional theory: a review of the vdW-DF method. *Reports on Progress in Physics*, 78(6), p.066501.
107. Hummer, G., Garde, S., Garcia, A.E., Pohorille, A. and Pratt, L.R., 1996. An information theory model of hydrophobic interactions. *Proceedings of the National Academy of Sciences*, 93(17), pp.8951-8955.
108. Meyer, E.E., Rosenberg, K.J. and Israelachvili, J., 2006. Recent progress in understanding hydrophobic interactions. *Proceedings of the National Academy of Sciences*, 103(43), pp.15739-15746.
109. Lipkowitz, K.B., 1998. Applications of computational chemistry to the study of cyclodextrins. *Chemical reviews*, 98(5), pp.1829-1874.
110. Castro, E.A. and Barbiric, D.A.J., 2006. Molecular modeling and cyclodextrins: a relationship strengthened by complexes. *Current Organic Chemistry*, 10(7), pp.715-729.
111. Zhao, Q., Zhang, W., Wang, R., Wang, Y. and Ouyang, D., 2017. Research advances in molecular modeling in cyclodextrins. *Current pharmaceutical design*, 23(3), pp.522-531.
112. Quevedo, M.A. and Zoppi, A., 2018. Current trends in molecular modeling methods applied to the study of cyclodextrin complexes. *Journal of Inclusion Phenomena and Macrocyclic Chemistry*, pp.1-14.
113. Atwood, J.L., 2017. *Comprehensive Supramolecular Chemistry II*. Elsevier.

114. Atwood, J.L., Davies, J.E.D., Mac-Nicol, D.D., Vogtle, F., Lehn, J.M. and König, B., 1997. Comprehensive supramolecular chemistry. *Angewandte Chemie-English Edition*, 36(5), pp.530-530.
115. Amharar, Y., Grandeury, A., Sanselme, M., Petit, S. and Coquerel, G., 2012. A hybrid mechanism in chiral discrimination induced by crystallization of supramolecular compounds. *The Journal of Physical Chemistry B*, 116(20), pp.6027-6040.
116. Snir, M., 2014, June. The future of supercomputing. In *Proceedings of the 28th ACM international conference on Supercomputing* (pp. 261-262). ACM.
117. Xie, X., Fang, X., Hu, S. and Wu, D., 2010. Evolution of supercomputers. *Frontiers of Computer Science in China*, 4(4), pp.428-436.
118. Maximova, T., Moffatt, R., Ma, B., Nussinov, R. and Shehu, A., 2016. Principles and overview of sampling methods for modeling macromolecular structure and dynamics. *PLoS computational biology*, 12(4), p.e1004619.
119. Wang, R., Zhou, H., Siu, S.W., Gan, Y., Wang, Y. and Ouyang, D., 2015. Comparison of three molecular simulation approaches for cyclodextrin-ibuprofen complexation. *Journal of Nanomaterials*, 16(1), p.267.
120. Sheng Cai, W., Wang, T., Zhe Liu, Y., Liu, P., Chipot, C. and Guang Shao, X., 2011. Free energy calculations for cyclodextrin inclusion complexes. *Current Organic Chemistry*, 15(6), pp.839-847.
121. Sangpheak, W., Khuntawee, W., Wolschann, P., Pongsawasdi, P. and Rungrotmongkol, T., 2014. Enhanced stability of a naringenin/2, 6-dimethyl β -cyclodextrin inclusion complex: Molecular dynamics and free energy calculations based on MM- and QM-PBSA/GBSA. *Journal of Molecular Graphics and Modelling*, 50, pp.10-15.
122. Rutenberg, R., Leitius, G., Fallik, E. and Poverenov, E., 2016. Discovery of a non classic host guest complexation mode in a β -cyclodextrin/propionic acid model. *Chemical Communications*, 52(12), pp.2565-2568.
123. Rahim, M., Madi, F., Nouar, L., Haiahem, S., Fateh, D. and Khatmi, D., 2014. β -Cyclodextrin Interaction with Edaravone: Molecular Modeling Study. In *Advances in Quantum Chemistry* (Vol. 68, pp. 269-278). Academic Press.
124. Onnainty, R., Schenfeld, E.M., Quevedo, M.A., Fernández, M.A., Longhi, M.R. and Granero, G.E., 2012. Characterization of the hydrochlorothiazide: β -cyclodextrin inclusion complex. Experimental and theoretical methods. *The Journal of Physical Chemistry B*, 117(1), pp.206-217.
125. Oda, M. and Kuroda, M., 2016. Molecular dynamics simulations of inclusion complexation of glycyrrhizic acid and cyclodextrins (1: 1) in water. *Journal of Inclusion Phenomena and Macrocyclic Chemistry*, 85(3-4), pp.271-279.
126. Nociari, M.M., Lehmann, G.L., Bay, A.E.P., Radu, R.A., Jiang, Z., Goicochea, S., Schreiner, R., Warren, J.D., Shan, J., de Beaumais, S.A. and Ménand, M., 2014. Beta cyclodextrins bind, stabilize, and remove lipofuscin bisretinoids from retinal pigment epithelium. *Proceedings of the National Academy of Sciences*, p.201400530.
127. Kogawa, A.C., Zoppi, A., Quevedo, M.A., Longhi, M.R. and Nunes Salgado, H.R., 2014. Complexation between darunavir and β -Cyclodextrin. Experimental and theoretical studies.
128. Al-Rawashdeh, N.A., Al-Sadeh, K.S. and Al-Bitar, M.B., 2013. Inclusion complexes of sunscreen agents with β -cyclodextrin: spectroscopic and molecular modeling studies. *Journal of Spectroscopy*, 2013.

129. Sahra, K., Dinar, K., Seridi, A. and Kadri, M., 2015. Investigation on the inclusion of diclofenac with β -cyclodextrin: a molecular modeling approach. *Structural Chemistry*, 26(1), pp.61-69.
130. Angelova, S., Nikolova, V., Molla, N. and Dudev, T., 2017. Factors Governing the host-guest interactions between IIA/IIB group metal cations and α -cyclodextrin: a DFT/CDM study. *Inorganic chemistry*, 56(4), pp.1981-1987.
131. Ateba, B.A., Lissouck, D., Azébazé, A., Ebelle, C.T., Nassi, A., Ngameni, E., Duportail, G., Mbazé, L. and Kenfack, C.A., 2016. Characterization of Mamea A/AA in solution and in interaction with β -cyclodextrin: UV-visible spectroscopy, cyclic voltammetry and DFT-TDDFT/MD study. *Journal of Molecular Liquids*, 213, pp.294-303.
132. Tóth, G., Mohácsi, R., Rácz, Á., Rusu, A., Horváth, P., Szente, L., Béni, S. and Noszál, B., 2013. Equilibrium and structural characterization of ofloxacin-cyclodextrin complexation. *Journal of Inclusion Phenomena and Macrocyclic Chemistry*, 77(1-4), pp.291-300.
133. Shi, M., Zhang, C., Xie, Y. and Xu, D., 2015. Stereoselective inclusion mechanism of ketoprofen into β -cyclodextrin: insights from molecular dynamics simulations and free energy calculations. In *Guosen Yan* (pp. 29-40). Springer, Berlin, Heidelberg.
134. Melani, F., Pasquini, B., Caprini, C., Gotti, R., Orlandini, S. and Furlanetto, S., 2015. Combination of capillary electrophoresis, molecular modeling and NMR to study the enantioselective complexation of sulpiride with double cyclodextrin systems. *Journal of pharmaceutical and biomedical analysis*, 114, pp.265-271.
135. Li, L., Li, X., Luo, Q. and You, T., 2015. A comprehensive study of the enantioseparation of chiral drugs by cyclodextrin using capillary electrophoresis combined with theoretical approaches. *Talanta*, 142, pp.28-34.
136. Ghatee, M.H. and Sedghamiz, T., 2014. Chiral recognition of propranolol enantiomers by β -cyclodextrin: quantum chemical calculation and molecular dynamics simulation studies. *Chemical Physics*, 445, pp.5-13.
137. Alvira, E., 2013. Molecular dynamics study of the influence of solvents on the chiral discrimination of alanine enantiomers by β -cyclodextrin. *Tetrahedron: Asymmetry*, 24(19), pp.1198-1206.
138. Alvira, E., 2013. Influence of molecular stereochemistry on the continuum model for van der waals interaction between β -cyclodextrin and linear molecules. *Current Physical Chemistry*, 3(3), pp.357-365.
139. Alvira, E., 2015. Theoretical study of the separation of valine enantiomers by β -cyclodextrin with different solvents: a molecular mechanics and dynamics simulation. *Tetrahedron: Asymmetry*, 26(15-16), pp.853-860.
140. Abou-Zeid, L.A. and Hefnawy, M., 2015. Molecular Modeling study of the Chiral Recognition of Celiprolol Enantiomers by a β -Cyclodextrin. *Pharmaceut. Chem. J*, 2(3), pp.16-23.
141. Periasamy, R., Kothainayaki, S. and Sivakumar, K., 2016. Encapsulation of dicinnamalacetone in β -cyclodextrin: A physicochemical evaluation and molecular modeling approach on 1: 2 inclusion complex. *Journal of Macromolecular Science, Part A*, 53(9), pp.546-556.
142. Terekhova, I., Kumeev, R., Alper, G., Chakraborty, S., Pérez-Sánchez, H. and Núñez-Delicado, E., 2016. Molecular recognition of aromatic carboxylic acids by

- hydroxypropyl- γ -cyclodextrin: experimental and theoretical evidence. *RSC Advances*, 6(55), pp.49567-49577.
143. Zhang, H., Ge, C., van der Spoel, D., Feng, W. and Tan, T., 2012. Insight into the structural deformations of beta-cyclodextrin caused by alcohol cosolvents and guest molecules. *The Journal of Physical Chemistry B*, 116(12), pp.3880-3889.
 144. Zhang, H., Feng, W., Li, C., Lv, Y. and Tan, T., 2012. A model for the shuttle motions of puerarin and daidzin inside the cavity of β -cyclodextrin in aqueous acetic acid: insights from molecular dynamics simulations. *Journal of molecular modeling*, 18(1), pp.221-227.
 145. Figueiras, A., Sarraguça, J.M., Pais, A.A., Carvalho, R.A. and Veiga, J.F., 2010. The role of l-arginine in inclusion complexes of omeprazole with cyclodextrins. *AAPS PharmSciTech*, 11(1), pp.233-240.
 146. Harada, A., Takashima, Y. and Yamaguchi, H., 2009. Cyclodextrin-based supramolecular polymers. *Chemical Society Reviews*, 38(4), pp.875-882.
 147. Zhang, H., Tan, T., Feng, W. and Van Der Spoel, D., 2012. Molecular recognition in different environments: β -cyclodextrin dimer formation in organic solvents. *The Journal of Physical Chemistry B*, 116(42), pp.12684-12693.
 148. Zhang, H., Tan, T., Hetényi, C. and Van Der Spoel, D., 2013. Quantification of solvent contribution to the stability of noncovalent complexes. *Journal of chemical theory and computation*, 9(10), pp.4542-4551.
 149. Zhang, H., Tan, T., Hetényi, C., Lv, Y. and Van Der Spoel, D., 2014. Cooperative binding of cyclodextrin dimers to isoflavone analogues elucidated by free energy calculations. *The Journal of Physical Chemistry C*, 118(13), pp.7163-7173.
 150. Ren, B., Zhang, M., Gao, H., Zheng, J. and Jia, L., 2016. Atomic elucidation of the cyclodextrin effects on DDT solubility and biodegradation. *Physical Chemistry Chemical Physics*, 18(26), pp.17380-17388.
 151. Ceron-Carrasco, J.P., den-Haan, H., Peña-García, J., Contreras-García, J. and Perez-Sanchez, H., 2016. Exploiting the cyclodextrins ability for antioxidants encapsulation: A computational approach to carnosol and carnosic acid embedding. *Computational and Theoretical Chemistry*, 1077, pp.65-73.
 152. Suárez, D. and Díaz, N., 2017. Conformational and entropy analyses of extended molecular dynamics simulations of α -, β - and γ -cyclodextrins and of the β -cyclodextrin/nabumetone complex. *Physical Chemistry Chemical Physics*, 19(2), pp.1431-1440.
 153. Ivanov, P., 2014. Further studies on the conformations of large-ring cyclodextrins. *Bulgarian Chemical Communications 46 Special Issue A*, pp.238-245.
 154. Khuntawee, W., Rungrotmongkol, T., Wolschann, P., Pongsawasdi, P., Kungwan, N., Okumura, H. and Hannongbua, S., 2016. Conformation study of ϵ -cyclodextrin: Replica exchange molecular dynamics simulations. *Carbohydrate polymers*, 141, pp.99-105.
 155. Shityakov, S., Salmas, R.E., Durdagi, S., Salvador, E., Pápai, K., Yáñez-Gascón, M.J., Pérez-Sánchez, H., Puskás, I., Roewer, N., Förster, C. and Broscheit, J.A., 2016. Characterization, in vivo evaluation, and molecular modeling of different propofol-cyclodextrin complexes to assess their drug delivery potential at the blood-brain barrier level. *Journal of chemical information and modeling*, 56(10), pp.1914-1922.
 156. Devasari, N., Dora, C.P., Singh, C., Paidi, S.R., Kumar, V., Sobhia, M.E. and Suresh, S., 2015. Inclusion complex of erlotinib with sulfobutyl ether- β -cyclodextrin: Preparation,

- characterization, in silico, in vitro and in vivo evaluation. *Carbohydrate polymers*, 134, pp.547-556.
157. Altarsha, M., Ingrosso, F. and Ruiz-López, M.F., 2012. Cavity closure dynamics of peracetylated β -cyclodextrins in supercritical carbon dioxide. *The Journal of Physical Chemistry B*, 116(13), pp.3982-3990.
 158. Sugita, M. and Hirata, F., 2016. Predicting the binding free energy of the inclusion process of 2-hydroxypropyl- β -cyclodextrin and small molecules by means of the MM/3D-RISM method. *Journal of Physics: Condensed Matter*, 28(38), p.384002.
 159. Sancho, M.I., Andujar, S., Porasso, R.D. and Enriz, R.D., 2016. Theoretical and experimental study of inclusion complexes of β -cyclodextrins with chalcone and 2', 4'-dihydroxychalcone. *The Journal of Physical Chemistry B*, 120(12), pp.3000-3011.
 160. Cao, R. and Wu, S., 2015. In silico properties characterization of water-soluble γ -cyclodextrin bi-capped C60 complex: Free energy and geometrical insights for stability and solubility. *Carbohydrate polymers*, 124, pp.188-195.
 161. Suliman, F.O. and Elbashir, A.A., 2012. Enantiodifferentiation of chiral baclofen by β -cyclodextrin using capillary electrophoresis: a molecular modeling approach. *Journal of Molecular Structure*, 1019, pp.43-49.
 162. Chandrasekaran, S., Sudha, N., Premnath, D. and Enoch, I.V., 2015. Binding of a chromen-4-one Schiff's base with bovine serum albumin: capping with β -cyclodextrin influences the binding. *Journal of Biomolecular Structure and Dynamics*, 33(9), pp.1945-1956.
 163. Sameena, Y., Sudha, N., Chandrasekaran, S. and Enoch, I.V., 2014. The role of encapsulation by β -cyclodextrin in the interaction of raloxifene with macromolecular targets: a study by spectroscopy and molecular modeling. *Journal of biological physics*, 40(4), pp.347-367.
 164. Yan, J., Wu, D., Ma, X., Wang, L., Xu, K. and Li, H., 2015. Spectral and molecular modeling studies on the influence of β -cyclodextrin and its derivatives on aripiprazole-human serum albumin binding. *Carbohydrate polymers*, 131, pp.65-74.
 165. Sapte, S. and Pore, Y., 2016. Inclusion complexes of cefuroxime axetil with β -cyclodextrin: Physicochemical characterization, molecular modeling and effect of L-Arginine on complexation. *Journal of pharmaceutical analysis*, 6(5), pp.300-306.
 166. Suvarna, V., Kajwe, A., Murahari, M., Pujar, G.V., Inturi, B.K. and Sherje, A.P., 2017. Inclusion complexes of nateglinide with HP- β -CD and L-arginine for solubility and dissolution enhancement: preparation, characterization, and molecular docking study. *Journal of Pharmaceutical Innovation*, 12(2), pp.168-181.
 167. Méndez, S.G., Espinar, F.J.O., Alvarez, A.L., Longhi, M.R., Quevedo, M.A. and Zoppi, A., 2016. Ternary complexation of benzoic acid with β -cyclodextrin and aminoacids. Experimental and theoretical studies. *Journal of Inclusion Phenomena and Macrocyclic Chemistry*, 85(1-2), pp.33-48.
 168. Jadhav, P., Petkar, B., Pore, Y., Kulkarni, A. and Burade, K., 2013. Physicochemical and molecular modeling studies of cefixime-L-arginine-cyclodextrin ternary inclusion compounds. *Carbohydrate polymers*, 98(2), pp.1317-1325.
 169. Swiech, O., Mieczkowska, A., Chmurski, K. and Bilewicz, R., 2012. Intermolecular interactions between doxorubicin and β -cyclodextrin 4-methoxyphenol conjugates. *The Journal of Physical Chemistry B*, 116(6), pp.1765-1771.

170. Swiech, O., Majdecki, M., Debinski, A., Krzak, A., Stępkowski, T.M., Wójciuk, G., Kruszewski, M. and Bilewicz, R., 2016. Competition between self-inclusion and drug binding explains the pH dependence of the cyclodextrin drug carrier–molecular modelling and electrochemistry studies. *Nanoscale*, 8(37), pp.16733-16742.
171. Swiech, O., Dutkiewicz, P., Wójciuk, K., Chmurski, K., Kruszewski, M. and Bilewicz, R., 2013. Cyclodextrin derivatives conjugated with aromatic moieties as pH-responsive drug carriers for anthracycline. *The Journal of Physical Chemistry B*, 117(43), pp.13444-13450.
172. Staelens, N., Leherte, L. and Vercauteren, D.P., 2015. Formation and structural, energetic and dynamic properties of cyclodextrin host tubes and included guest molecules. *Supramolecular Chemistry*, 27(1-2), pp.90-109.
173. Raffaini, G. and Ganazzoli, F., 2013. A molecular modeling study of complex formation and self-aggregation behavior of a porphyrin– β -cyclodextrin conjugate. *Journal of Inclusion Phenomena and Macrocyclic Chemistry*, 76(1-2), pp.213-221.
174. Mixcoha, E., Campos-Terán, J. and Piñeiro, A., 2014. Surface adsorption and bulk aggregation of cyclodextrins by computational molecular dynamics simulations as a function of temperature: α -CD vs β -CD. *The Journal of Physical Chemistry B*, 118(25), pp.6999-7011.
175. Khuntawee, W., Wolschann, P., Rungrotmongkol, T., Wong-ekkabut, J. and Hannongbua, S., 2015. Molecular dynamics simulations of the interaction of beta cyclodextrin with a lipid bilayer. *Journal of chemical information and modeling*, 55(9), pp.1894-1902.
176. Singharoy, A. and Chipot, C., 2016. Methodology for the simulation of molecular motors at different scales. *The Journal of Physical Chemistry B*, 121(15), pp.3502-3514.
177. Tallury, S.S., Smyth, M.B., Cakmak, E. and Pasquinelli, M.A., 2012. Molecular dynamics simulations of interactions between polyanilines in their inclusion complexes with β -cyclodextrins. *The Journal of Physical Chemistry B*, 116(7), pp.2023-2030.
178. Muhammad, E.F., Adnan, R., Latif, M.A.M. and Rahman, M.B.A., 2016. Theoretical investigation on insulin dimer– β -cyclodextrin interactions using docking and molecular dynamics simulation. *Journal of Inclusion Phenomena and Macrocyclic Chemistry*, 84(1-2), pp.1-10.
179. Szejtli, J., 1982. Cyclodextrins and their inclusion complexes. *Akademiai Kiado*, 25.
180. Ghosh, A., Biswas, S. and Ghosh, T., 2011. Preparation and evaluation of silymarin β -cyclodextrin molecular inclusion complexes. *Journal of young pharmacists: JYP*, 3(3), p.205.
181. Wang, J., Cao, Y., Sun, B. and Wang, C., 2011. Physicochemical and release characterisation of garlic oil– β -cyclodextrin inclusion complexes. *Food chemistry*, 127(4), pp.1680-1685.
182. Mangolim, C.S., Moriwaki, C., Nogueira, A.C., Sato, F., Baesso, M.L., Neto, A.M. and Matioli, G., 2014. Curcumin– β -cyclodextrin inclusion complex: stability, solubility, characterisation by FT-IR, FT-Raman, X-ray diffraction and photoacoustic spectroscopy, and food application. *Food chemistry*, 153, pp.361-370.
183. Sapkal, N.P., Kilor, V.A., Bhursari, K.P. and Daud, A.S., 2007. Evaluation of some methods for preparing gliclazide– β -cyclodextrin inclusion complexes. *Tropical journal of pharmaceutical research*, 6(4), pp.833-840.

184. Figueiras, A., Carvalho, R.A., Ribeiro, L., Torres-Labandeira, J.J. and Veiga, F.J., 2007. Solid-state characterization and dissolution profiles of the inclusion complexes of omeprazole with native and chemically modified β -cyclodextrin. *European Journal of Pharmaceutics and Biopharmaceutics*, 67(2), pp.531-539.
185. Syukri, Y., Fernanda, L., Utami, F.R., Qiftayati, I., Kusuma, A.P. and Istikaharah, R., 2015. Preparation And Characterization Of β -Cyclodextrin Inclusion Complexes Oral Tablets Containing Poorly Water Soluble Glimipiride Using Freeze Drying Method. *INDONESIAN JOURNAL OF PHARMACY*, 26(2), p.71.
186. Agrawal, G.P. and Bhargava, S., 2008. Preparation & characterization of solid inclusion complex of cefpodoxime proxetil with β -cyclodextrin. *Current drug delivery*, 5(1), pp.1-6.
187. Cheirsilp, B. and Rakmai, J., 2016. Inclusion complex formation of cyclodextrin with its guest and their applications. *Biol Eng Med*, 2, pp.1-6.
188. Sinha, V.R., Anitha, R., Ghosh, S., Nanda, A. and Kumria, R., 2005. Complexation of celecoxib with β -cyclodextrin: Characterization of the interaction in solution and in solid state. *Journal of pharmaceutical sciences*, 94(3), pp.676-687.
189. Szejtli, J. and Szenté, L., 2005. Elimination of bitter, disgusting tastes of drugs and foods by cyclodextrins. *European journal of pharmaceutics and biopharmaceutics*, 61(3), pp.115-125.
190. Shan-Yang, L. and Yuh-Horng, K., 1989. Solid particulates of drug- β -cyclodextrin inclusion complexes directly prepared by a spray-drying technique. *International journal of pharmaceutics*, 56(3), pp.249-259.
191. Demarco, P.V. and Thakkar, A.L., 1970. Cyclohepta-amylose inclusion complexes. A proton magnetic resonance study. *Journal of the Chemical Society D: Chemical Communications*, (1), pp.2-4.
192. Cowins, J., Abimbola, O., Ananaba, G., Wang, X.Q. and Khan, I., 2015. Preparation and characterization of β -sitosterol/ β -cyclodextrin crystalline inclusion complexes. *Journal of Inclusion Phenomena and Macrocyclic Chemistry*, 83(1-2), pp.141-148.
193. Bertoluzza, A., Rossi, M., Taddei, P., Redenti, E., Zanol, M. and Ventura, P., 1999. FT-Raman and FT-IR studies of 1: 2.5 piroxicam: β -cyclodextrin inclusion compound. *Journal of molecular structure*, 480, pp.535-539.
194. Mohan, P.K., Sreelakshmi, G., Muraleedharan, C.V. and Joseph, R., 2012. Water soluble complexes of curcumin with cyclodextrins: Characterization by FT-Raman spectroscopy. *Vibrational Spectroscopy*, 62, pp.77-84.
195. Veiga, F., Teixeira-Dias, J.J.C., Kedzierewicz, F., Sousa, A. and Maincent, P., 1996. Inclusion complexation of tolbutamide with β -cyclodextrin and hydroxypropyl- β -cyclodextrin. *International journal of pharmaceutics*, 129(1-2), pp.63-71.
196. de Oliveira, V.E., Almeida, E.W., Castro, H.V., Edwards, H.G., Dos Santos, H.F. and de Oliveira, L.F.C., 2011. Carotenoids and β -cyclodextrin inclusion complexes: Raman spectroscopy and theoretical investigation. *The Journal of Physical Chemistry A*, 115(30), pp.8511-8519.
197. Iliescu, T., Baia, M. and Miclăuş, V., 2004. A Raman spectroscopic study of the diclofenac sodium- β -cyclodextrin interaction. *European journal of pharmaceutical sciences*, 22(5), pp.487-495.

198. Pandit, V., Gorantla, R., Devi, K., Pai, R.S. and Sarasija, S., 2011. Preparation and characterization of pioglitazone cyclodextrin inclusion complexes. *Journal of young pharmacists: JYP*, 3(4), p.267.
199. Ficarra, R., Tommasini, S., Raneri, D., Calabro, M.L., Di Bella, M.R., Rustichelli, C., Gamberini, M.C. and Ficarra, P., 2002. Study of flavonoids/ β -cyclodextrins inclusion complexes by NMR, FT-IR, DSC, X-ray investigation. *Journal of pharmaceutical and biomedical analysis*, 29(6), pp.1005-1014.
200. Badr-Eldin, S.M., Elkheshen, S.A. and Ghorab, M.M., 2008. Inclusion complexes of tadalafil with natural and chemically modified β -cyclodextrins. I: Preparation and in-vitro evaluation. *European Journal of Pharmaceutics and Biopharmaceutics*, 70(3), pp.819-827.
201. Gutman, I. and Bosanac, S., 1977. Quantitative approach to hückel rule the relations between the cycles of a molecular graph and the thermodynamic stability of a conjugated molecule. *Tetrahedron*, 33(14), pp.1809-1812.
202. Feixas, F., Matito, E., Sola, M. and Poater, J., 2008. Analysis of Hückel's [4n+2] Rule through Electronic Delocalization Measures. *The Journal of Physical Chemistry A*, 112(50), pp.13231-13238.
203. JS, P., Kadam, D.V., Marapur, S.C. and Kamalapur, M.V., INCLUSION COMPLEX SYSTEM; A NOVEL TECHNIQUE TO IMPROVE THE SOLUBILITY AND BIOAVAILABILITY OF POORLY SOLUBLE DRUGS: A REVIEW.
204. Wallace, L.A., 1989. Major sources of benzene exposure. *Environmental Health Perspectives*, 82, p.165.
205. Birkett, D., Maggs, C.A. and Dring, M.J., 1998. Maerl (volume V). *An overview of dynamic and sensitivity characteristics for conservation management of marine SACs. Scottish Association for Marine Science (UK Marine SACs Project)*.
206. Jia, C. and Batterman, S., 2010. A critical review of naphthalene sources and exposures relevant to indoor and outdoor air. *International journal of environmental research and public health*, 7(7), pp.2903-2939.
207. El-Masri, H., 2005. *Toxicological Profile for Naphthalene, 1-methylnaphthalene, and 2-methylnaphthalene*. Agency for Toxic Substances and Disease Registry.
208. Irwin, R.J., Mouwerik, M.V., Stevens, L.Y.N.E.T.T.E., Seese, M.D. and Basham, W.E.N.D.Y., 1997. Environmental contaminants encyclopedia, naphthalene entry. *National Park Service*, pp.1-80.
209. Manzetti, S., 2013. Polycyclic aromatic hydrocarbons in the environment: environmental fate and transformation. *Polycyclic Aromatic Compounds*, 33(4), pp.311-330.
210. Ravindra, K., Sokhi, R. and Van Grieken, R., 2008. Atmospheric polycyclic aromatic hydrocarbons: source attribution, emission factors and regulation. *Atmospheric Environment*, 42(13), pp.2895-2921.
211. Means, J.C., Wood, S.G., Hassett, J.J. and Banwart, W.L., 1980. Sorption of polynuclear aromatic hydrocarbons by sediments and soils. *Environmental Science & Technology*, 14(12), pp.1524-1528.
212. Bai, Y., Meng, W., Xu, J., Zhang, Y., Guo, C., Lv, J. and Wan, J., 2014. Occurrence, distribution, environmental risk assessment and source apportionment of polycyclic aromatic hydrocarbons (PAHs) in water and sediments of the Liaohe River Basin, China. *Bulletin of environmental contamination and toxicology*, 93(6), pp.744-751.

213. Alegbeleye, O.O., Opeolu, B.O. and Jackson, V.A., 2017. Polycyclic aromatic hydrocarbons: a critical review of environmental occurrence and bioremediation. *Environmental management*, 60(4), pp.758-783.
214. Kayal, S.I. and Connell, D.W., 1989. Occurrence and distribution of polycyclic aromatic hydrocarbons in surface sediments and water from the Brisbane River estuary, Australia. *Estuarine, Coastal and Shelf Science*, 29(5), pp.473-487.
215. Balcioğlu, E.B., 2016. Potential effects of polycyclic aromatic hydrocarbons (PAHs) in marine foods on human health: a critical review. *Toxin Reviews*, 35(3-4), pp.98-105.
216. Tongo, I., Ogbeide, O. and Ezemonye, L., 2017. Human health risk assessment of polycyclic aromatic hydrocarbons (PAHs) in smoked fish species from markets in Southern Nigeria. *Toxicology reports*, 4, pp.55-61.
217. Luch, A., 2005. The carcinogenic effects of polycyclic aromatic hydrocarbons.
218. Farmer, P.B., Singh, R., Kaur, B., Sram, R.J., Binkova, B., Kalina, I., Popov, T.A., Garte, S., Taioli, E., Gabelova, A. and Cebulska-Wasilewska, A., 2003. Molecular epidemiology studies of carcinogenic environmental pollutants: effects of polycyclic aromatic hydrocarbons (PAHs) in environmental pollution on exogenous and oxidative DNA damage. *Mutation Research/Reviews in Mutation Research*, 544(2), pp.397-402.
219. Wenzl, T., Simon, R., Anklam, E. and Kleiner, J., 2006. Analytical methods for polycyclic aromatic hydrocarbons (PAHs) in food and the environment needed for new food legislation in the European Union. *TrAC Trends in Analytical Chemistry*, 25(7), pp.716-725.
220. United States. Environmental Protection Agency. Environmental Criteria, Assessment Office (Cincinnati and Ohio), 1993. *Provisional guidance for quantitative risk assessment of polycyclic aromatic hydrocarbons*. Environmental Criteria and Assessment Office, Office of Health and Environmental Assessment, US Environmental Protection Agency.
221. Baird, W.M., Hooven, L.A. and Mahadevan, B., 2005. Carcinogenic polycyclic aromatic hydrocarbon-DNA adducts and mechanism of action. *Environmental and molecular mutagenesis*, 45(2-3), pp.106-114.
222. Harvey, R.G., 1991. *Polycyclic aromatic hydrocarbons: chemistry and carcinogenicity*. CUP Archive.
223. Mastrangelo, G., Fadda, E. and Marzia, V., 1996. Polycyclic aromatic hydrocarbons and cancer in man. *Environmental health perspectives*, 104(11), p.1166.
224. Fox, M.A. and Staley, S.W., 1976. Determination of polycyclic aromatic hydrocarbons in atmospheric particulate matter by high pressure liquid chromatography coupled with fluorescence techniques. *Analytical chemistry*, 48(7), pp.992-998.
225. May, W.E. and Wise, S.A., 1984. Liquid chromatographic determination of polycyclic aromatic hydrocarbons in air particulate extracts. *Analytical Chemistry*, 56(2), pp.225-232.
226. Berset, J.D., Ejem, M., Holzer, R. and Lischer, P., 1999. Comparison of different drying, extraction and detection techniques for the determination of priority polycyclic aromatic hydrocarbons in background contaminated soil samples. *Analytica chimica acta*, 383(3), pp.263-275.
227. Saleh, A., Yamini, Y., Faraji, M., Rezaee, M. and Ghambarian, M., 2009. Ultrasound-assisted emulsification microextraction method based on applying low density organic solvents followed by gas chromatography analysis for the determination of polycyclic

- aromatic hydrocarbons in water samples. *Journal of Chromatography A*, 1216(39), pp.6673-6679.
228. Rezaee, M., Assadi, Y., Hosseini, M.R.M., Aghaee, E., Ahmadi, F. and Berijani, S., 2006. Determination of organic compounds in water using dispersive liquid–liquid microextraction. *Journal of Chromatography A*, 1116(1-2), pp.1-9.
229. El-Beqqali, A., Kusak, A. and Abdel-Rehim, M., 2006. Fast and sensitive environmental analysis utilizing microextraction in packed syringe online with gas chromatography–mass spectrometry: Determination of polycyclic aromatic hydrocarbons in water. *Journal of Chromatography A*, 1114(2), pp.234-238.
230. Manoli, E. and Samara, C., 1999. Polycyclic aromatic hydrocarbons in natural waters: sources, occurrence and analysis. *TrAC Trends in Analytical Chemistry*, 18(6), pp.417-428.

Chapter-2 Materials and Methods

2.1 Introduction

In this part of the thesis we have explained step by step the descriptions of the methods used for the preparation and analysis of the inclusion complexes between β CD and guest molecules. The first step was to study the interaction between β CD and linear alcohols followed by β CD aromatic molecule studies. The methods chosen here are appropriate, effective and widely used and are available in the laboratory. We have carried out the studies in liquid (solutions) as well as in the solid states (powders). In solutions, the formation of the complexes was studied using ^1H NMR. The results obtained have allowed us to determine the stoichiometry of the complex in solutions by Job's method. The complexation results are considered as the basis of complexation in condensed matter. After obtaining convincing results in liquid state, in the next step we prepared fine crystalline powder in the solid state and analysed them using Thermal analysis (DSC) and powder X-ray diffraction. The main reason to use these methods was to quickly check the formation of an inclusion complex. Another approach taken to analyse the solid samples is by Raman Spectroscopy. In order to understand the behaviour of molecules in the system lastly, we performed molecular modelling studies with two main objectives: firstly, we simulated Raman Spectra in order to help normal mode attributions and secondly, we applied semi empirical methods to check the stability of the complexes in comparison with the experimental results.

To carry out this thesis, the prime step was to understand the role of each component taking part in complexation. For that, we prepared different solutions namely β CD in D_2O to know the NMR spectrum, Linear alcohols in D_2O , Mixture of β CD and linear alcohols solutions prepared in D_2O separately to check the inclusion of their hydrophobic part inside the β CD cavity, mixture of β CD and aromatic compounds solutions prepared in D_2O separately and also in ethanolic aqueous mixture (to interpret the solubility issues of aromatic hydrocarbons). Aromatic hydrocarbons are non-polar compounds whereas water is highly polar in nature. Therefore, the solubility issues came into our notice. As we know, **Like dissolves like**, the idea of adding linear alcohols to the aqueous solution resolved the solubility issue to some extent.

β CD (Cyclolab R&D.Ltd., Budapest, Hungary MW 1135.0) was used as received. Higher linear alcohols (>4C) were obtained from Aldrich (Pentanol $\geq 99\%$, heptanol-98%, Nonanol-98%, Decanol- 99%, undecanol 99%) Merck (Methanol, Ethanol, Propanol, Butanol and Octanol). D_2O (99.9 %) for NMR studies was purchased from euriso-top). All the chemicals were used as received.

P.S – β CD was used as received to carry out all characterization studies.

2.2 Liquid state studies: ^1H NMR analysis of the Stoichiometry of the Host and guest complexes

2.2.1 Introduction and Principles of Nuclear Magnetic Resonance

Nuclear magnetic resonance commonly referred as NMR was first observed in 1937 by Nobel prize winner physicist Isidor Issac Rabi. Since the day this technique was first introduced in the field of chemistry, its use has grown and become essential to study the structures, dynamics and chemical environment of molecules. This non-destructive technique exploits the magnetic properties of certain nuclei to study chemical, physical and biological properties of matter. For our studies, this technique has proved to be most important for structural elucidation of the systems in solution state. Also, another important motive to use this technique is to understand the driving forces and binding modes in the non-covalent associations followed by the ideal use of these factors for new applications. This structural depiction is essential for supramolecular host-guest systems for better understanding of their applications in different fields of medicine¹⁻⁴, cosmetics, Food chemistry⁵⁻⁷, Pharmacy⁸⁻¹⁴, catalysis¹⁵, encapsulation of organic pollutants^{16,17} etc.

In the previous chapter, we have given a quick overview on CDs and about the objective of this thesis. This section will be devoted to the first step analysis i.e evidence of inclusion complex formation in the liquid state by ^1H NMR. Nuclear Magnetic Resonance (NMR) is the technique used to study the chemistry between the β -CD and the other guest molecules and would give us a brief idea about the stoichiometry of the complexes under observation. Previously, not many researchers tried to carry out this type of study with longer alcohols but few were able to publish results with shorter alcohols chains¹⁸. The studies with different kinds of alcohols have also been reported that were carried out with different objectives¹⁹⁻²³. The advancements in the technique would help in better understanding of the ternary system.

2.2.1.1 Principle of NMR

The principle of NMR technique is based on the magnetic properties of the nuclei of atoms which can be utilized to yield chemical information. The subatomic particles like protons, neutrons and electrons have spin. In some atoms, e.g- ^{12}C , ^{16}O , ^{32}S the spins are paired and cancel each other out such that the nucleus of the atom has no overall spin. However, in many atoms like – ^1H , ^{13}C , ^{31}P , ^{15}N , and ^{19}F . The nucleus does possess an overall spin. In order to determine the spin of a given nucleus the following rules can be followed:

If the number of neutrons and the number of protons are both even, the nucleus has no spin. Nuclei having both charge and mass number even (no. proton=no. of neutrons= $2n$, $n=1,2,3$ etc.) have zero spin quantum number. Nuclei having odd charge number and even mass number have integral spin quantum number. Nuclei with odd mass number have half integral spin.

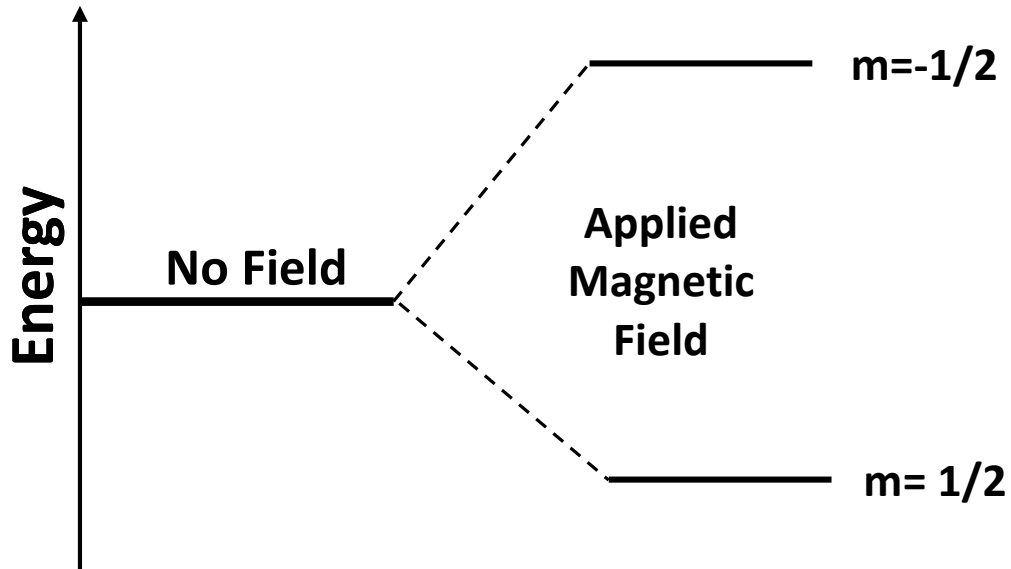


Figure 2.1 : Energy levels of a nucleus with spin quantum number.

In quantum mechanical terms, in presence of external magnetic field of strength B_0 , the nuclear magnetic moment of a nucleus will align either with or against the applied magnetic field B_0 . In other words, we can say that a nucleus of spin I (overall spin) will have $2I+1$ possible orientation. A nucleus with spin $1/2$ will have two possible orientations. In the absence of an external magnetic field, these orientations are degenerate i.e they possess equal energy. On applying the magnetic field, these energy levels will split into two, with $m= - 1/2$ and $m= 1/2$ (Figure 2.1). Negative value of m corresponds to the orientation of the nuclei in the direction of magnetic field applied and for positive value vice versa.

If a magnetic field is applied, then the energy levels split. Each level is given a magnetic quantum number, m .

The spinning of a nucleus is equivalent to the circulation of a positive charge around the axis of spinning. This, in turn produces a tiny magnet placed along the spin axis resulting in generation of small magnetic field. The nucleus therefore is comprised of a magnetic moment, μ , which is proportional to its spin I .

The relationship between μ and I can be expressed as:

$$\mu = \frac{\gamma I h}{2\pi} \quad (1)$$

Where,

$\gamma = \text{gyromagnetic ratio}$

$h = \text{Planck's constant}$

The constant, γ , is called gyromagnetic ratio and is a fundamental nuclear constant which has different value for every nucleus.

The energy of a nucleus placed in a magnetic field B_0 is given by the relation

$$E = -\frac{\gamma h m B_0}{2\pi} \quad (2)$$

The energy difference between the two nuclear levels can be expressed as:

$$\Delta E = \frac{\gamma h B_0}{2\pi} \quad (3)$$

The above relation implies that ΔE and B_0 are directly proportional to each other. It also means that if a nucleus has a relatively large gyromagnetic ratio, then ΔE is also correspondingly large (Figure 2.2).

When placed in the magnetic field, the charged particle will precess (change in the orientation of the rotational axis of a rotating body) about the magnetic field. In NMR, the charged nucleus, will then exhibit precessional (Figure 2.3) motion at a characteristic frequency known as the Larmor Frequency, which is identical to the transition frequency. The Larmor frequency is specific to each nucleus.

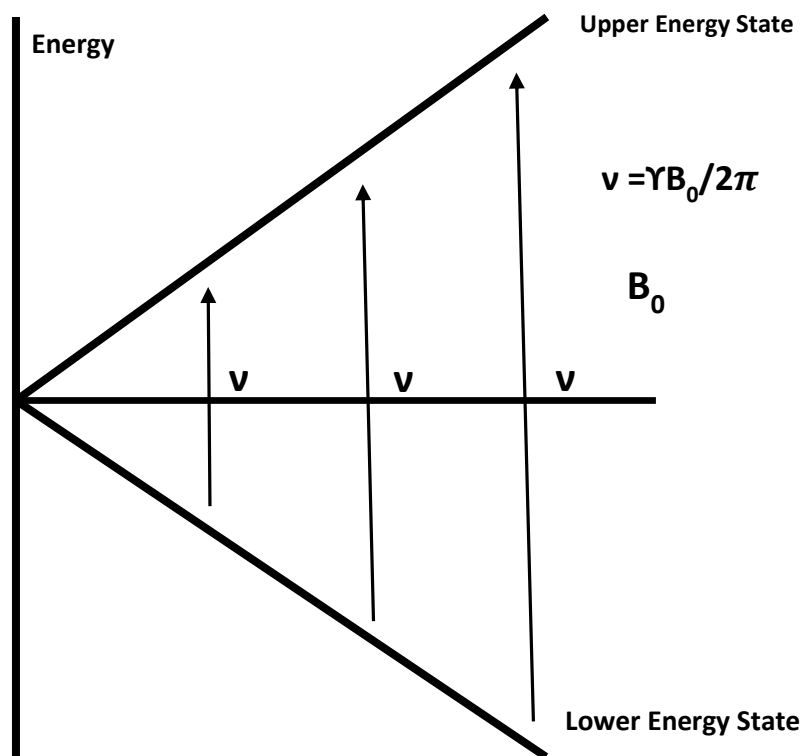


Figure 2.2 : Effect of magnetic field on the energy gap between two possible states adopted by a spinning nucleus.

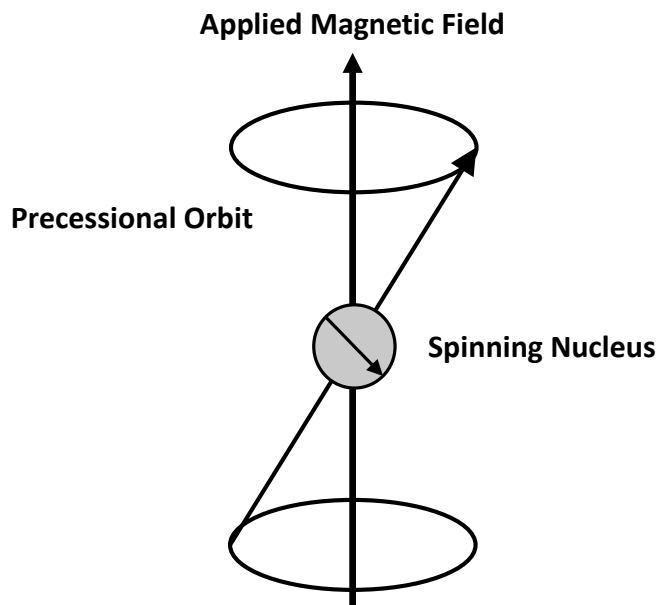


Figure 2.3 : Spinning motion of a nucleus on its axis.

The potential energy of the precessing nucleus can be written as:

$$E = -\mu B \cos \vartheta$$

Where θ = angle between the direction of the applied magnetic field and the axis of the nuclear rotation.

If the nucleus absorbs some energy, then the angle of precession, θ , will change. For a nuclear spin of 1/2, absorption of radiation 'switch' the magnetic moment (it goes to higher energy state) so that it opposes the applied field (Figure 2.4).

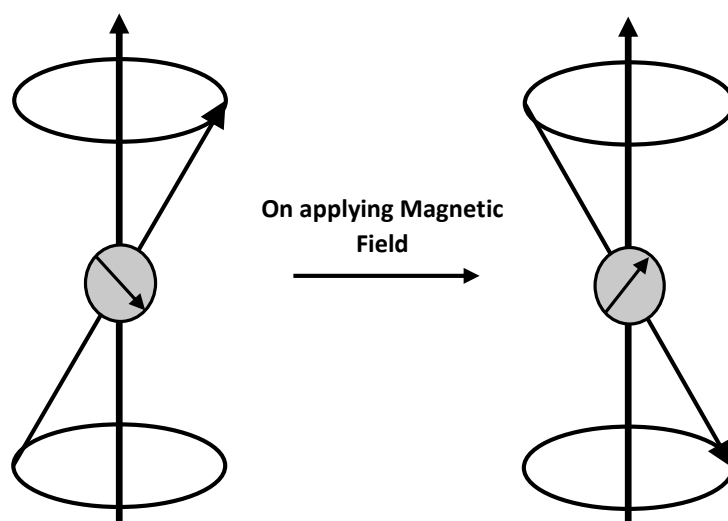


Figure 2.4 : Flipping of the magnetic moment on absorption of energy.

Transition from one level to another can take place in either directions, i.e the nucleus can be promoted from the lower energy level to the upper one (upward transition) with the

absorption of radiation and also it can come back from the upper level to the lower level (downward transition) with emission of radiation. It can be expected statistically, that the rate at which transitions from a level takes place depends on the population of the level. There occurs a net absorption if one type of transition is more than the other.

The widest application of NMR is in the field of organic chemistry where it has been employed for the structural elucidation of organic compounds. The only widely distributed magnetic active nucleus in organic compound is the hydrogen atom whereas the other atoms like ^{12}C and ^{16}O are the magnetic inactive atoms and do not exhibit any NMR signals.

The structure elucidation of organic compounds is based on two principles. These are the Chemical Shift and the spin-spin Interaction.

2.2.1.2 Chemical Shift

When we talk about supramolecular entities, the nuclei are not present as single nuclei but are associated with electronic clouds.

The different types of nuclei (^1H , ^{13}C , ^{19}F , ^{31}P) absorb radiation of suitable wavelength when exposed to external magnetic field (B_0), where the electrons of the atom circulate about the direction of the applied magnetic field. Also, this circulation causes a small magnetic field at the nucleus which opposes the externally applied field. So, the magnetic field experienced at the nucleus is less than the applied field by a fraction σ

$$B = B_0(1 - \sigma)$$

Where,

B_0 = external magnetic field

B = observed magnetic field

σ = Shielding Constant

In practice, we define chemical shift of a sample as

$$\delta = \frac{B_{\text{sample}} - B_{\text{ref}}}{B_0} * 10^6 \text{ ppm}$$

Since $B \propto \nu$ ($E = h\nu = \frac{\gamma h m B}{2\pi}$)

hence

$$\delta = \frac{\nu_{\text{sample}} - \nu_{\text{TMS}}}{\nu_0} * 10^6 \text{ ppm}$$

Where the reference compound commonly used is Tetramethylsilane (TMS). TMS contains 12 protons which are all equivalent and 4 carbons which are also equivalent. This means that it gives a single, strong signal in the spectrum, which turns out to be outside the range of most other signals, especially from organic compounds. For the analysis, the chemical shift scales are allocated zero value at the TMS peak, but now residual solvent peaks are used for calibrations of most of the spectra. For our results, deuterated solvent D_2O (99.9%) is used which produces a peak in proton NMR.

2.2.1.3 Spin-Spin Interaction for ¹H NMR spectroscopy

The interaction between the spins of neighbouring nuclei in a molecule may cause the splitting of NMR spectrum. This phenomenon is known as spin-spin interaction. The splitting pattern is related to the number of equivalent hydrogen atom at the nearby nuclei.

The magnitude of the splitting between the lines of a given multiplet is given by the spin-spin coupling constant J . The scalar coupling J is a thorough bond interaction, in which the spin of one nucleus polarizes the spins of the intervening electrons and the polarized electrons distresses the energy levels of the magnetic nuclei in the close proximity. This leads to a lowering of the energy of the neighbouring nucleus when the perturbing nucleus has one spin and increase in energy when it has the other spin. The J coupling (in Hertz) is always constant at different external magnetic field strength and is mutual ($J_{AB}=J_{BA}$) for nuclei A and B with a non-zero spin. The magnitude of J decreases rapidly as the number of intervening bond increases as the effect is usually transmitted through the bonding electrons.

Spin-spin coupling constants can be affected by a number of factors like hybridization of the atoms involved in the coupling, the bond angles, the dihedral angles, the C-C bond lengths and substituent effects (electronegativity, neighbouring bond and lone pair effects). The signs of coupling constants show some consistency.

- $^1J_{C-H}$ and many other one-bond couplings are positive.
- $^2J_{H-H}$ in sp^3 CH_2 groups are negative, some others are positive.
- $^3J_{H-H}$ is always positive.

The multiplicity of the peaks of a group of equivalent protons is determined by the neighbouring protons. In general, if n equivalent protons interact or couple with the protons on an adjacent carbon atom, the resonance peak splits into $n+1$ peaks or signals. Also, protons of the same group do not interact among themselves to cause observable splitting.

The proton-NMR spectrum of a molecule thus gives information about

- a) The number of peaks which enables us to know about the kinds of protons present in a molecule.
- b) The positions of the peaks which tells us about the electronic environment of each kind of proton.
- c) The intensities of the peaks which tell us about the number of protons of each kind that are present and
- d) The splitting of the peak into several peaks which tells us about the environment of each kind of a proton with respect to other nearby protons in the molecule.

2.2.2 Experimental Set Up

In NMR spectrometers (Figure 2.5), the rotating secondary magnetic field is produced by sending the output of a radiofrequency oscillator through a helical coil (solenoid) of wire whose axis is perpendicular to the direction of the main magnetic field. The latter is generated with the help of an electromagnet. The sample under study is placed in a glass tube positioned along the axis of the coil. An electric current passing through such a coil produces magnetic field on its centre and directed along the axis. This magnetic field reverses its direction with

the same frequency as the current from the oscillator. This alternating magnetic field is equivalent to two rotating magnetic fields which are operating in opposite directions with the same frequency. One of these directions is the same as that of the precessional motion of the nucleus and this rotating field acts as a secondary magnetic field. When the frequency of the alternating current supplied to the coil and the magnetic field experienced by the nucleus have values equal to the frequency of separation between the two levels, a condition of resonance exists and thereby the nucleus can either absorb or emit energy from the secondary magnetic field. As stated earlier, there will be a net absorption of energy as the ground level is more populated than the excited level.

The above resonance phenomenon can be achieved by either of the following types:

1. By varying the frequency of the oscillator keeping the external magnetic field constant.
2. By varying the external magnetic field keeping the frequency of the oscillator constant.

In the former, the Larmor frequency to be kept at a constant value and varying the external circulating magnetic field till it becomes equal to the Larmor precessional frequency. However, in the latter, the frequency of the external circulating magnetic field to be kept constant and to vary the Larmor frequency till it becomes equal to the frequency of the external circulating magnetic field.

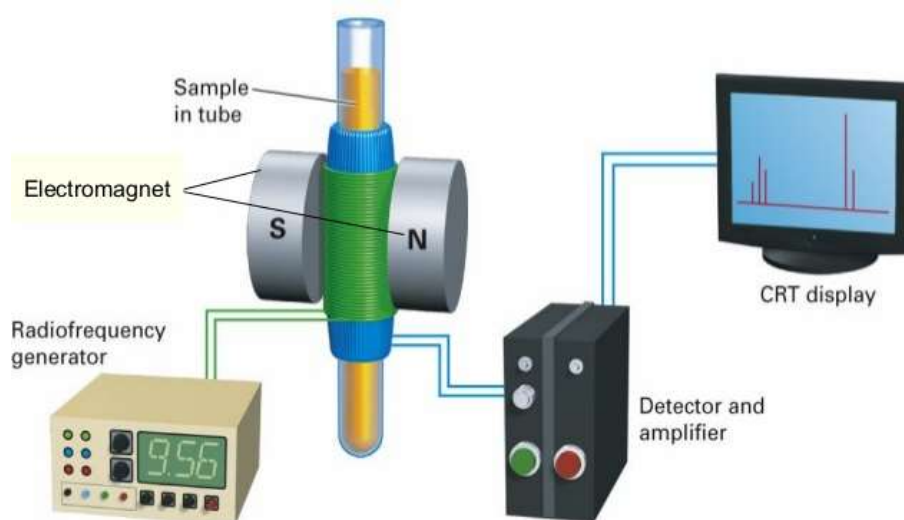


Figure 2.5 : Experimental setup for NMR.

^1H NMR spectra were recorded with Bruker Ultra ShieldTM plus 400 MHz instrument at 298 K temperature in a deuterium oxide (D_2O) solution (99.9%, Eurisotop). Tetramethylsilane (TMS) was used as reference for all βCD : alcohols and βCD : aromatics spectra registered. For the analysis, the chemical shift scales are allocated zero value at the TMS peak, but the residual D_2O deuterated solvent water peaks are used for calibrations of most of the spectra.

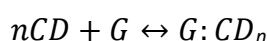
2.2.3 Method of Continuous Variation (Job's method)

2.2.3.1 Principle of the Job's method

In this method, we keep the total number of moles of reactants constant throughout a series of mixtures and reactants, but varies the mole fraction of each reactant from mixture to mixture. This method can be applied theoretically as well as experimentally to show classification of inclusion complexes²⁴. Many researchers have used this method to confirm the stoichiometry of the inclusion complexes formed by β CD with different guests by U.V spectroscopic studies, NMR studies or fluorescence studies^{11,25-35}. In the recent times, researchers have also developed modified Job plot methodology for the host-guest stoichiometry determination and one such method is called MacCarthy method^{36,37}. This method provides fast and easy means to determine host-guest stoichiometry or in other words we can say – this method uses ‘shortcuts’ in the method of continuous variation. There are certain limitations of job’s method³⁸ like – it fails when more than one compounds are formed in the system yet it is still primarily used. The method has also been used to study the molecular formulas determination in case of ionic species³⁹ or other complex formations^{40,41}.

The stoichiometry of the complexes formed with higher linear alcohols (6 C to 11 C) were determined by method of continuous variation or job’s method⁴².

For the study of a reaction:



The association constant of the inclusion complex can be written as:

$$k = \frac{[G:CD_n]}{[G][CD]^n} \quad (1)$$

Where,

[G:CD_n] = complex concentration

[G] and [CD] = concentration of free G and CD in the mixture

Let [G]_t and [CD]_t be the total concentration of G and CD in the sample, we can further write,

$$[G] = [G]_t - [G:CD_n] \quad (2)$$

$$[CD] = [CD]_t - n[G:CD_n] \quad (3)$$

The method of continuous variation imposes two conditions,

- a) The initial concentration of the solutions to be identical, and
- b) Solutions should be mixed by keeping the total volume constant

This results in:

$$[G]_t + [CD]_t = M \quad (4)$$

Where M is the total concentration of the mixture

$$r = [G]_t / ([G]_t + [CD]_t) \quad (5)$$

where r = the molar proportion of the guest molecule (0 < r < 1)

the concentrations of free species then can be deduced from the following relationships:

$$[G] = rM - [G : CD_n] \quad (6)$$

$$[CD] = M(1 - r) - n [G : CD_n] \quad (7)$$

The complex concentration $[G : CD_n]$ is therefore a function of r and it passes through a maximum when the derivative $d[G : CD_n]/dr$ is zero. The derivation of equations (1), (6) and (7) with respect to r leads to the following relations.

$$[CD] \cdot d[G]/dr + n \cdot [G] \cdot d[CD]/dr = 0 \quad (8)$$

$$d[G]/dr = M \quad (9)$$

$$d[CD] = -M \quad (10)$$

these three equations can be combined into one:

$$[CD] = n[G] \quad (11)$$

Using equations (6), (7) and (11), we obtain, a unique solution and the maximum complex concentration is obtained for $r = 1/(1+n)$

This relationship does not depend on the association constant K_a or the value of the concentration M .

For the study of inclusion complexes, we are in rapid exchange with respect to the observation time. We can write the following relation.

$$P(G)_{obs} \cdot [G]_t = P(G)_c \cdot [G : CD_n] + P(G)_f \cdot [G] \quad (12)$$

Where $P(G)_{obs}$, $P(G)_f$ and $P(G)_c$ represent respectively, the value for the observed parameter and its value in the free state and in the pure complex. In all of the following studies, we will only consider parameter variations observed with the following conventions

$$\Delta P_{obs} = P_{obs} - P_f$$

$$\Delta P_c = P_c - P_f$$

Equation (12) becomes

$$\Delta P(G)_c \cdot [G : CD_n] = \Delta P(G)_{obs} \cdot [G]_t$$

$\Delta P(G)_{obs}$, being proportional to $[G : CD_n]$, so it is a function of r . The plot of the function $f(r) = \Delta P(G)_{obs} \cdot [G]_t$ must then pass through a maximum of $r = 1/(1 + n)$ and make it possible to determine n . The same procedure can be followed for the compound $[CD]$ and thus confirm the stoichiometry.

This method is applied in UV, in fluorescence, in NMR, where the parameter P is the absorbance, fluorescence intensity or the chemical shift variation. In NMR, the determination of n is done by recording a series of 1H spectra in 1D and then we follow the variations of the chemical shifts of the CD protons or the guest molecule that have to move with the change of the CD concentration and the G.

Are:

δ_l = the chemical shift of a proton of the guest molecule or (CD) free

δ_c = the chemical shift of the same proton in the mixture G:CD

$$\Delta\delta_{\text{obs}} = \delta_l - \delta_c$$

Then, by comparing $\Delta\delta_{\text{obs}} \times [G]_0$ (or $[CD]_0$) as a function of r , we obtain a bell-shaped curve centered on a r_{max} value.

With:

$[G]_0$ = initial concentration of the molecule included

$[CD]_0$ = initial concentration of the cyclodextrin

From r_{max} , we can determine n

For example, if $r_{\text{max}} = 0.5$

$$r_{\text{max}} = 1/(1+n) = 0.5$$

if, $n=1$

so, we can say that there is formation of type 1:1 of inclusion complex

The maximum point of the curve obtained shows the stoichiometry of the complex when the concentrations are high. For our studies, we have taken 10mM concentration of both the solutions which were mixed together in different volume ratios by keeping the total volume in the tube constant in all the cases. The typical shape of the job's plot can be seen in the following Figure 2.6 for 1:1, 1:2 and 2:1 stoichiometry.

The peaks obtained for β CD in D_2O are taken as reference for job's plot calculations. All the solutions prepared for different volume ratios of β CD and guest molecule mixture are compared to the reference peaks and chemical shift is calculated. The chemical shift values are then plotted against mole fraction of β CD.

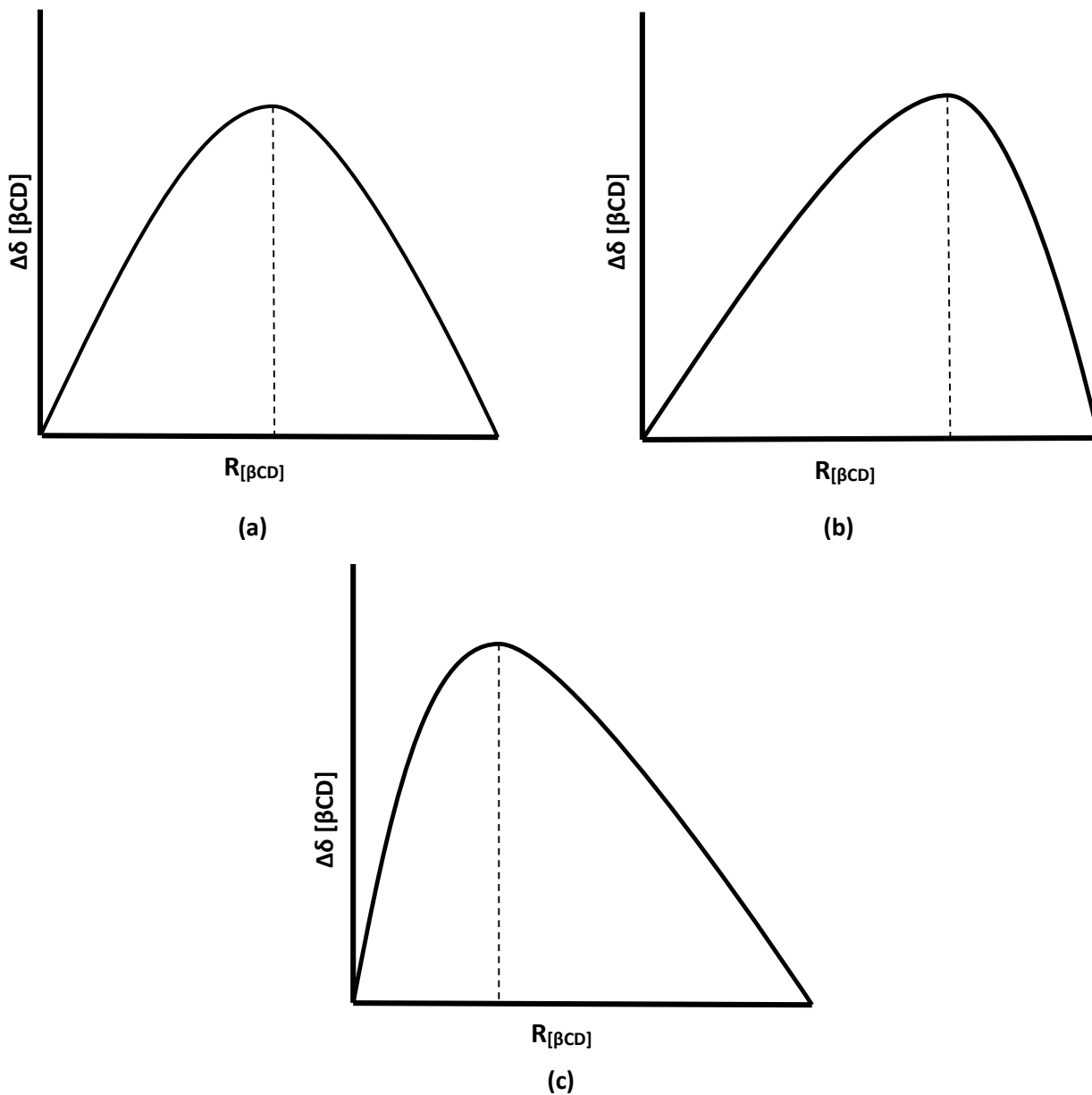


Figure 2.6 : Graphical representation of job's plot showing (a)1:1 (b) 2:1 and (c) 1:2 complexations respectively.

2.2.3.2 Sample preparation for NMR studies (β CD:Alcohols)

10 mM solutions of β CD and alcohols were prepared separately in D_2O . The two solutions were mixed with different volume ratios (Table 2.1) keeping the final volume of the solution to 500 μ l for each sample.

No. of sample	Volume of 10mM β CD solution (μ l)	Volume of 10mM alcohol solution (μ l)	Volumetric fraction of β CD ($R_{\beta CD}$)	Volumetric fraction of alcohol ($R_{alc.}$)
1	450	50	0.9	0.1
2	400	100	0.8	0.2
3	350	150	0.7	0.3
4	300	200	0.6	0.4
5	250	250	0.5	0.5
6	200	300	0.4	0.6
7	150	350	0.3	0.7
8	100	400	0.2	0.8
9	50	450	0.1	0.9

Table 2.1 : The different mixtures of solution prepared for β CD and linear alcohols.

2.2.3.3 Sample preparation for NMR studies (β CD:Aromatics)

10mM solutions of β CD and Alcohols were prepared separately in D_2O and 30%ethanolic D_2O respectively. The two solutions were mixed with different volume ratios keeping the final volume of the solution to 500 μ l for each sample (Table 2.2).

No. of sample	Volume of 10mM β CD solution (μ l)	Volume of 10mM aromatic solution (μ l)	Volumetric fraction of β CD ($R_{\beta CD}$)	Volumetric fraction of aromatic ($R_{arom.}$)
1	450	50	0.9	0.1
2	400	100	0.8	0.2
3	350	150	0.7	0.3
4	300	200	0.6	0.4
5	250	250	0.5	0.5
6	200	300	0.4	0.6
7	150	350	0.3	0.7
8	100	400	0.2	0.8
9	50	450	0.1	0.9

Table 2.2 : The different mixtures of solution prepared for β CD and Aromatic hydrocarbons.

2.2.4 1H NMR in structural analysis of CDs and their inclusion complexes

NMR is one of the major technique used for studying the structural and molecular interactions of biomolecules. Before studying the CD interactions, the assignment of NMR signals of the molecules must be achieved. The assignment of 1H resonances to their corresponding protons atoms is usually achieved by using different 1D or 2D NMR experiments. There are many hydroxyl protons in CDs and they are potentially important for conformational studies since they can be involved in intra- and inter molecular hydrogen bond interactions. Most of the structural studies of CD by NMR studies are done in D_2O solutions. In this solvent, the hydroxyl

protons are not observed in ^1H NMR spectra due to exchange with deuterium. The glucopyranose unit is presented in the Figure 2.7.

Chemical shift is one of the parameter of protons which is used to investigate conformation of CDs. It provides information on the grade of shielding and deshielding. Upfield shifts are indicative of reduced hydration while downfield shifts are observed for hydrogens in proximity of ring oxygen or other hydroxyls. The observed chemical shift is the combined effect of hydrogen bonding that will give a downfield shift and reduced hydration that gives an uplift shift.

H3 and H5 protons are located in the interior of the CDs cavity (Figure 2.8) and it is therefore likely that the interaction of the host with the β CD inside the cavity will affect the chemical shifts for H3 and H5 protons. This, in turn, can provide a rational for inclusion processes.

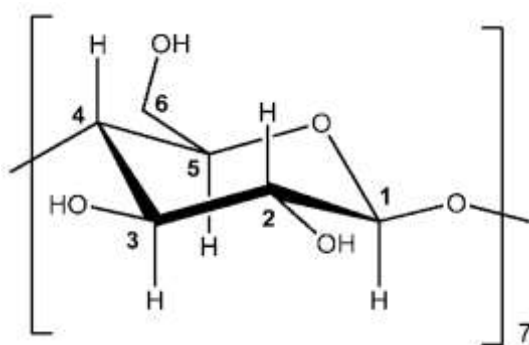


Figure 2.7 : Glucopyranose unit with atoms numbering.

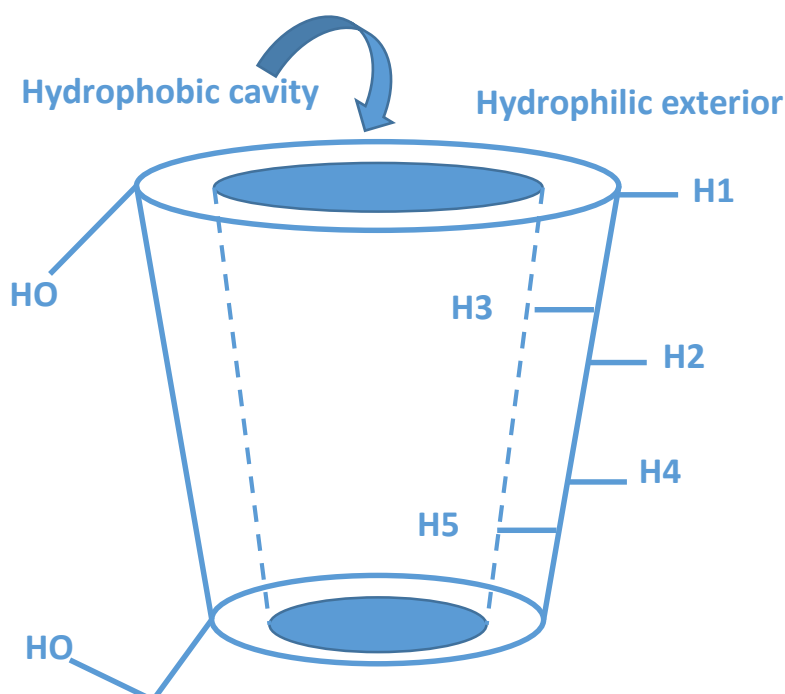


Figure 2.8 : Positions of different Hydrogens in a CD molecule.

The technique is so much useful for structural determination that it has been used as one of the fundamental technique to study CD inclusion complexes

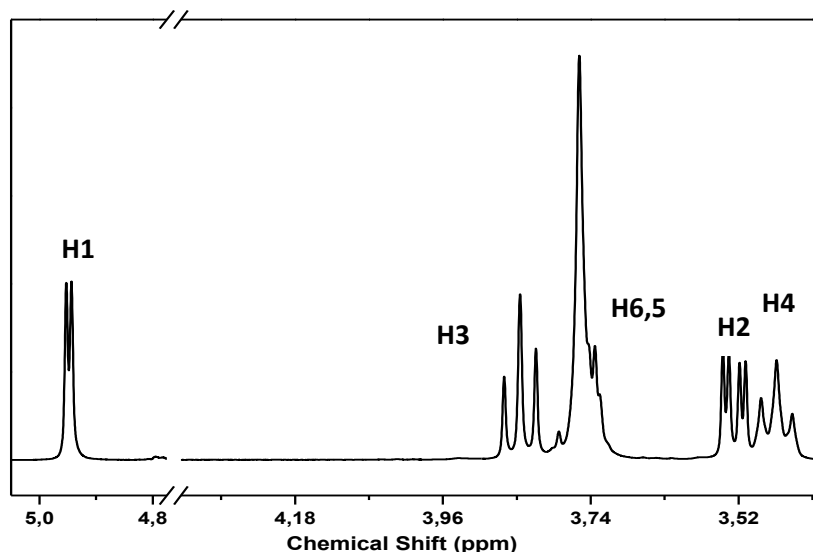


Figure 2.9 : ^1H NMR experimental spectrum of βCD (10mM) solution in D_2O .

The proton NMR studies of βCD s inclusion complexes were first successfully studied in 1970 by Demarko and Thakkar²⁵. This study considered as the fundamental for the NMR spectroscopy analysis. Scientists and Researchers are using this technique till date and explaining inclusion complex phenomena in different fields. A complete analysis of the NMR studies of cyclodextrins and cyclodextrin complexes by Schneider et al. is also available⁴³.

By following the previous results about the C_1 shape of the glucose units (Figure 2.7), they explained the effect of inclusion for all different types of protons βCD s contain. There are six types of protons present in an un-complexed βCD . The H-3 and H-5 protons are present towards the interior of the molecule and H-1, H-2 and H-4 located on its exterior. If the inclusion occurs, protons located inside the cavity or near will be highly affected or becomes strongly shielded. On the other hand, if the binding of the guest molecules takes place at the periphery or at the exterior of the molecule the protons present there will be strongly affected. The phenomenon of inclusion can be seen by shifting in the peaks positions of the respective protons.

The 1D NMR experiment was recorded for βCD 10mM solution in D_2O (Figure 2.9). In the 1H-NMR spectra we can see isolated peaks for H1, H2, H3 and H4 while H5 and H6 are overlapped. The peaks corresponding to the OH groups are not present due to the fast exchange between the displacing hydrogens and the deuterium atoms from D_2O .

This spectrum shows the most shielded (H4) and the deshielded (H1) protons. The surface area of the absorption peak is proportional to the number of protons involved. The chemical shifts corresponding to all the protons for αCD , βCD and γCD were observed experimentally and are listed in the Table 2.3.

	H1	H2	H3	H4	H5	H6
α – CD	4.94	3.51	3.87	3.46	3.73	3.80
β – CD	4.94	3.52	3.84	3.46	3.73	3.75
γ – CD	4.99	3.54	3.82	3.47	3.73	3.76

Table 2.3 : Experimentally Observed $^1\text{H-NMR}$ chemical shifts, (δ ppm), of C-H protons in unsubstituted CDs in D_2O .

In the first step of our research, the focus was on the insertion of linear hydrophobic chain of alcohols inside the CD's cavity. This fundamental part was done to observe the behaviour of complexation, stoichiometry, host-guest size selectivity and dependency. The homologues series of linear aliphatic alcohols have been tried to make complexes with βCD . Similar method has been carried out with all the alcohols starting from methanol (1C) to Undecanol (11C). While doing the experiments with smaller alcohols (till 4C), no significant shifts in the position of hydrogen (H3 and H5) which are present inside the cavity have been noticed. This concludes that the smaller alcohol molecules act as solvent molecules. Their presence can be observed anywhere around or inside the cavity. No real inclusion complexation is thus observed. In the case of higher alcohols ($\geq 5\text{C}$ till 11C), we have observed notable changes in the peak positions of internal hydrogens which means the alkyl chain, that has entered the cavity is long enough to disturb the internal orientation where some new non-covalent bonds are in the making as well as breaking from the uncomplexed CD.

2.2.5 Proton NMR Spectrum of alcohols

The spectrum of a linear alcohol (e.g for hexanol, Figure 2.10) contains different types of protons (in different chemical environments) such as hydroxyl (OH), methylene (CH_2) and methyl (CH_3) groups. The number of peaks and chemical shift changes with addition of new carbon and hydrogens as we go higher in the series.

In general, liquid alcohols consist of hydrogen bonded chains of molecules. The results have been experimentally tested with X-ray technique by a group of researchers⁴⁴. While forming an inclusion complex, the peaks observed around 3.5 ppm are superimposed with H2 and H4 peaks of the βCD entity. Furthermore, the peaks around 1.5 ppm are related to the aliphatic part of the linear alcohol are specific to these compounds. Table 2.4 lists the position and multiplicity of the proton NMR peak in all higher alcohols studied.

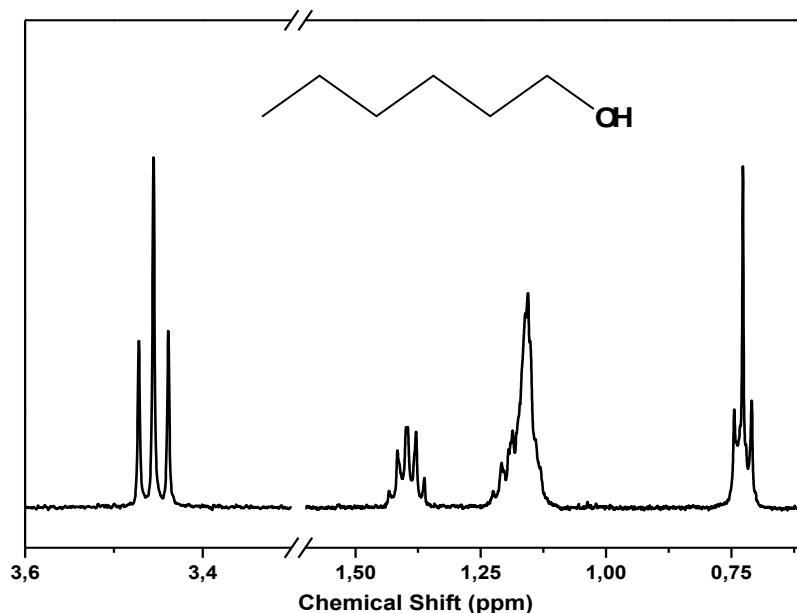


Figure 2.10 : Observed proton NMR spectrum of Hexanol.

Alcohol	Chemical shift (ppm)	Multiplicity
Methanol	3.22	Singlet
Ethanol	3.53	Quartet
	1.05	Triplet
Propanol	3.43	Triplet
	1.43	Sextet
	0.77	Triplet
Butanol	3.48	Triplet
	1.40	Quintet
	1.23	Sextet
	0.77	Triplet
Pentanol	3.46	Triplet
	1.42	Quintet
	1.19	Multiplet
	0.76	Triplet
Hexanol	3.45	Triplet
	1.39	Quintet
	1.18	Multiplet
	0.72	Triplet
Heptanol	3.45	Triplet
	1.40	Quintet
	1.16	Multiplet
	0.72	Triplet
Octanol	3.45	Triplet
	1.40	Quintet
	1.16	Multiplet
	0.72	Triplet
Nonanol	3.45	Triplet
	1.40	Quintet

	1.16 0.72	Multiplet Triplet
Decanol	3.45 1.40 1.16 0.76	Triplet Quintet Multiplet Triplet
Undecanol	3.45 1.40 1.16 0.83	Triplet Quintet Multiplet Triplet

Table 2.4. The position and multiplicity of the proton NMR peak in all alcohols studied.

2.3. Sample preparation by Co-precipitation for solid state characterization

2.3.1 β CD:alcohol powders

The solutions of different stoichiometry (1:1, 1:2) were prepared.

The β CD was dissolved in double distilled water by constant stirring on agitator (15 min) followed by sonication (10-12 min) to dissolve completely. The solutions were kept at 40°C in a thermostat for about 10 min. The next step was heating the solution at 85°C for about 15 min in a water bath with shaking at regular intervals. The solution was cooled down to 60°C and preheated alcohol was added. The solution was again heated for 10 min with shaking. The final solution was kept at different temperatures for gradual cooling (60°C, 45°C, RT and 2-3°C). The solution was cooled in fridge for 48 hours at least.

After cooling, White coloured solid product was obtained in all the cases. The samples were then transferred to centrifuge tube, were shaken vigorously and were washed with distilled water and ethanol separately. The solid product obtained was put in the desiccator overnight to remove the moisture. The dried powder obtained was further stored at 40°C (2h) to dry completely. Once the samples were dried; different characterizations were performed.

2.3.2 β CD:Alcohol:Aromatic compound

The solutions of different stoichiometry were prepared (1:1:1, 1:2:1, 1:1:2)

The β CD was dissolved in 30% ethanolic double distilled water by constant stirring on agitator (15 min) followed by sonication (10-12 min) to dissolve completely. The solutions were kept at 40°C in a thermostat for about 10 min. The next step was heating the solution at 85°C for about 15 min in a water bath with shaking at regular intervals. the solution was cooled down to 60°C and preheated alcohol was added. The solution was again heated for 10 min with shaking. Again after cooling to 60°C, aromatic compound was added to the solution and was heated again at 85°C for 10 min.

The final solution was kept at different temperatures for gradual cooling (60°C, 45°C, RT and 2-3°C). The solution was cooled in fridge for 48 hours at least.

After cooling, white coloured solid product was obtained in all the cases. The samples were then transferred to centrifuge tube, were shaken vigorously and was washed with distilled water and ethanol separately. The solid product obtained was put in the desiccator overnight

to remove the moisture. The dried powder obtained was further stored at 40°C (2h) to dry completely. One the samples were dried; different characterizations were performed.

2.3.3 Crystallisation Assays

All solutions have been prepared by the same general protocol^{45,46}: 10 mM of aromatic guest dissolved in alcohol has been added slowly along the side of the test tube to the aq. solution of β CD of same molar concentration to obtain an **interface** between the two solutions. Crystals were obtained by liquid diffusion after several weeks at room temperature by keeping the test tube undisturbed (Figure 2.11). The crystals obtained at the bottom of the test tube were quite large in size and were suitable for single Crystal X-ray diffraction studies.

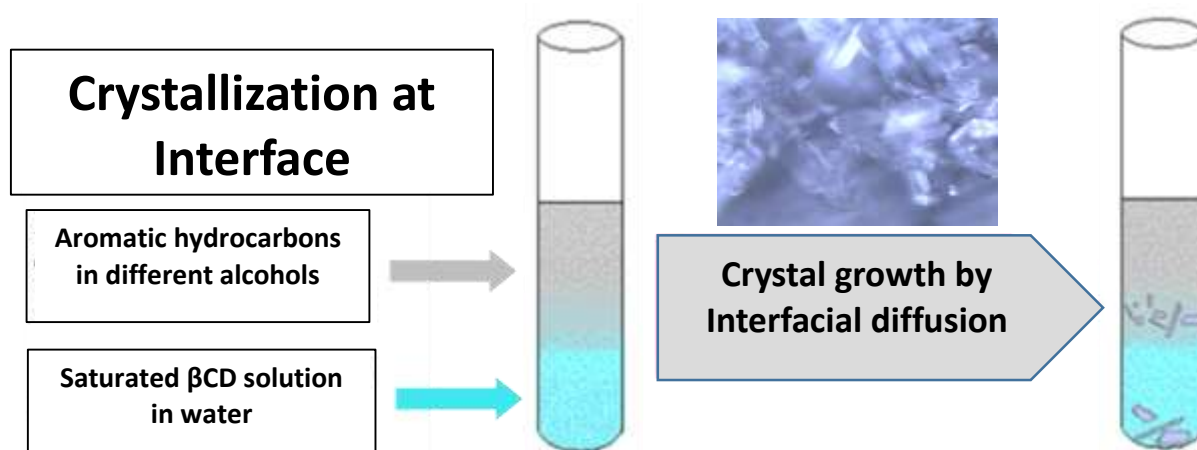


Figure 2.11 : Schematic of crystal formation at liquid-liquid interface.

2.4 Solid State studies: Part 1: Thermal Characterization of the complexes

Thermogravimetric analysis (TGA) and Differential Scanning Colorimetry (DSC) have proved as remarkable techniques to investigate quantitative and qualitative information about physical and chemical changes that involve endothermic or exothermic processes or changes in the heat capacity of the sample. For our studies, the samples prepared were characterized by DSC technique to carry out thermal studies.

DSC measurements were performed on SETARAM DSC 92 instrument, at the heating rate of 10K/min in the range 30-330°C. The powder samples were weighed (8-10 mg) and were set to measurements using aluminum crucibles. Each measurement has been done in doublet.

2.4.1 Principle of Power compensation DSC technique

The principle of power compensation DSC⁴⁷ is based on keeping the temperatures of the sample and reference as equal to each other while both temperatures are increased or decreased linearly. To carry out the measurement two independent heating units are employed. The power needed to maintain the sample temperature equal to the reference temperature is measured. The small heating units enable faster heating, cooling and equilibration rates. They are fixed to a large temperature-controlled heat sink. The platinum resistance thermometers acting as temperature sensors, which are present in sample and

reference holders to continuously monitor the temperature of the materials. Both sample and reference are kept at the programmed temperature by supplying power to the sample and reference heaters. The instrument records the power difference needed to maintain the sample and reference at the same temperature as a function of programmed temperatures (Figure 2.12). The response time is rapid for power compensated DSC in comparison to other forms of DSC instruments.

Whether more or less heat must flow to the sample depends on if the process is exothermic or endothermic. This technique also provides access to accurate thermodynamic data as well as information regarding reactivity and phase transformations.

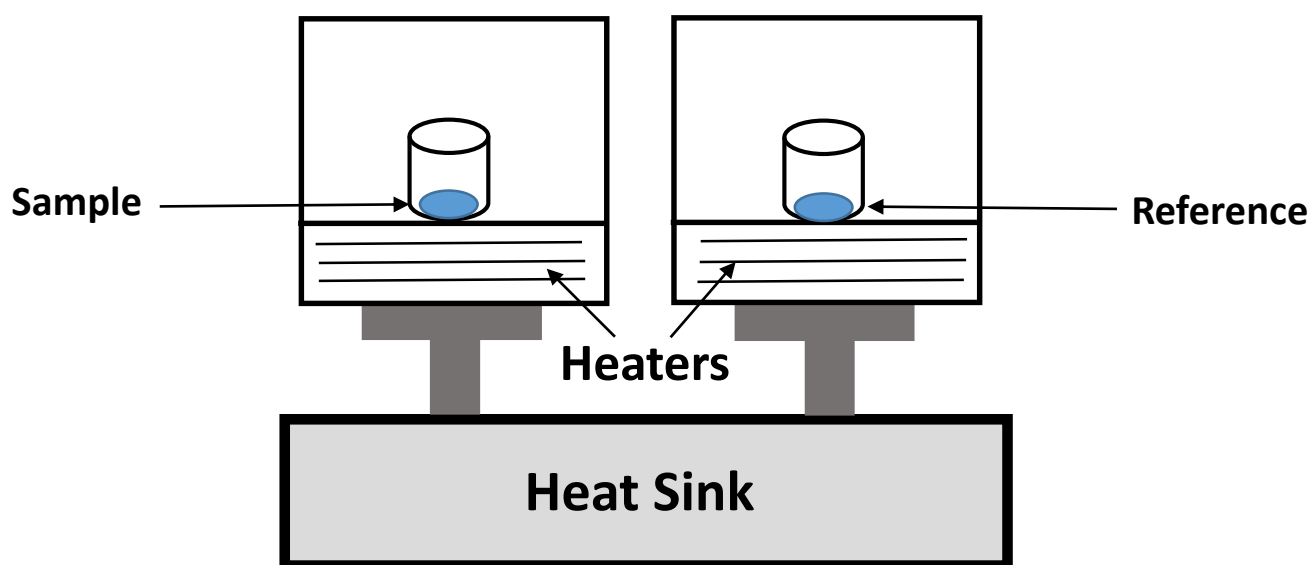


Figure 2.12 : Power Compensated DSC.

The appearance of endothermic curve occurs when heat flows into the sample as a result of different thermal processes like heat capacity (heating), glass transition, melting, evaporation or any other endothermic processes. On the other hand, exothermic curve occurs when heat flows out of the sample due to various reasons like heat capacity (cooling), crystallization, curing, oxidation or any other exothermic processes. The variation observed above the zero line (base) and below are termed as exothermic and endothermic transition respectively. The area under the peaks or the curves reveals to the amount of heat evolved and absorbed or in other words we can say that they are directly proportional. Also, the height of the curve corresponds to the rate of the reaction.

2.4.2 DSC analysis of β CD

These thermal methods are widely used to characterize CDs and their inclusion compounds. CDs generally formed hydrates (depending on the crystallization conditions). β CD exists either as undecahydrate or dodecahydrate where the difference is only of the distribution of these water molecules in the cavity. The native CDs are known to show similar thermal behaviour. Differences can be found in water content, onset temperatures of thermal degradation and the mass loss values at given temperatures. β CD is by far the most widely used, among the other types available. The observed thermogram of native β CD is shown in the Figure 2.13.

The thermoanalytical profile have been studied by many researchers^{48,49} can be divided into three different parts:

1. Water loss from ambient temperature upto 120°C (temperature is shifted on the higher side as high energy is needed to remove the tightly bound water molecules inside the cavity).
2. Above 250°C thermal degradation followed by oxidation in air, in solid state at first and continuing in liquid state (300°C).
3. Lastly, ignition takes place in air above 300°C.

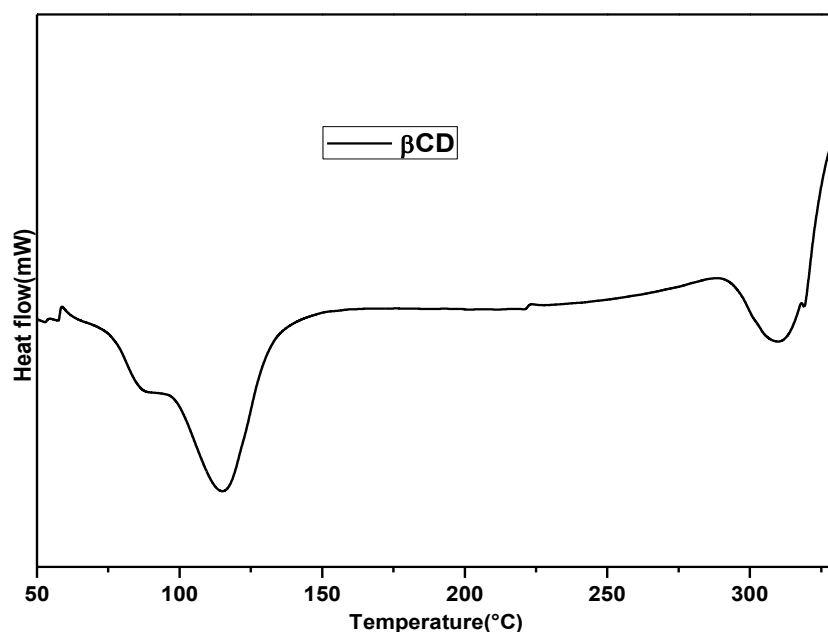


Figure 2.13 : Observed DSC thermogram of β CD.

2.4.3 Thermal characterization of Inclusion compounds

DSC technique is useful to determine the encapsulation of guest molecule by the β CD cavity or if the inclusion complex has formed. According to the principle of the technique, thermal transitions like melting point (MP) or boiling point (BP) of the guests would be observed indicating uncomplexed guest molecules in the solid complex. If no guests melting peaks are observed in the DSC scans for any of the guest in the sample suggests successful inclusion of guest molecule in the β CD.

For multicomponent system such as inclusion compounds, thermal characterization methods are the prime consideration. This type of analysis is frequently used as standard method for quick initial stage investigation. The method of carrying out thermal studies of inclusion complexes is generally similar: comparison of thermal behaviours of single components, their physical mixture and the complexes prepared by following a standard procedure.

For the study of CDs, DSC is often used to study the formation of inclusion complex. The CD: guest thermogram generally consists of endothermic effects at the melting/boiling temperatures of the guest molecules. If the melting temperature appears to be same as the

melting temperature of the guest molecule, then one can confirm the presence of guest in the solid state but it does not indicate the inclusion. If a new curve is observed at a new temperature, then it might be due to inclusion complex formation.

For CD:guest inclusion complexes thermal investigations, this technique has been again used by different researchers for determining the behaviour in various fields of applications^{50,51-67}.

2.5 Solid State studies: Part 2: X-ray diffraction analysis of CDs

Among the numerous techniques available for solid state characterization, X-ray diffraction technique plays an important role due to non-destructive nature and its ability to produce a unique pattern for any given crystalline phase. The diffraction pattern obtained can be viewed as 'fingerprint' of the phase under observation.

XRD analysis of the powders obtained after co-precipitation in solution and under vacuum drying were carried out at ambient temperature using $\theta/2\theta$ RIGAKU MINIFLEX diffractometer with $\text{CuK}\alpha$ radiation (1.5405 Å). Data were systematically collected from 14° to 4° in 2θ with a scan speed of 2°/ min in 2θ and a step size of 0.02°. Each analysis has been done in triplicate.

2.5.1 Principle

X-ray diffraction is based on constructive interference of monochromatic x-rays to determine the arrangements of atoms in a crystalline sample. Cathode ray tube are used to generate x-rays followed by filtration of rays to produce monochromatic radiation. This radiation is further parallelized to concentrate and directed towards the sample. The rays reflected from the sample have the maximum intensity when Bragg's law (Figure 2.14) is obeyed.

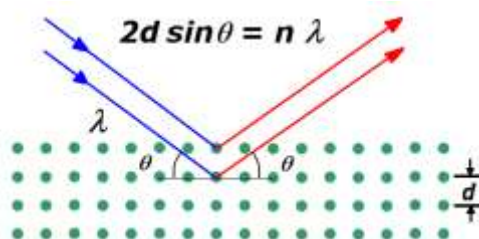


Figure 2.14 : Bragg's Law reflection.

Where, n is an integer, λ is the wavelength of the incident light, d is the inter planar distance and θ is the angle of diffraction. The x-ray crystallographic pattern between twice the angles of diffraction (2θ) against intensity of diffraction is very useful for the analysis.

For our systems, we have obtained final results in the form of powders so they may be composed of many small and finely ground crystals, known as crystallites. The orientation of these crystallites are presumed to be random. If X-ray analysis would be carried out on these crystallites, diffraction would occur from those oriented at the right angles (Bragg's law). The diffracted beams make an angle of 2θ with the incident beam.

The diffraction pattern obtained provides information like:

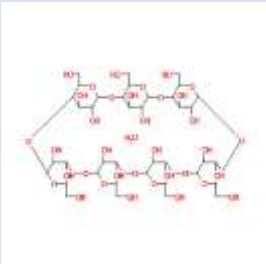
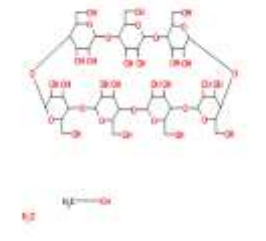
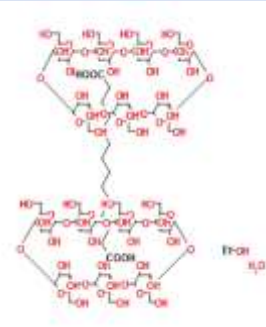
1. Peak positions determined by size and symmetry of the unit cell- the lattice.
2. Peak intensities determined by the positions of the atoms in the unit cell- the motif.

3. Peak widths influenced by size/strains of crystallites- the texture.

2.5.2 Reference CSD structures of β CD inclusion complexes available in the Cambridge Structural Database⁶⁸ and their simulated diffraction patterns

With its establishment in 1965, the CSD is one of the largest storehouse for crystal structures where small organic and metal organic crystals structure are being submitted each day. So far, only 226 organic structures involving β CD molecules and their derivatives are available out of 900000 entries already deposited. As already explained in the state of the art chapter 1, those structures can be classified in two major structural types: channels and herringbone or dimer brick cages⁶⁹. Those structures are very similar with the repartitions in term of space groups, volumes and parameters as exposed in chapter 1.

On comparing the positions of the principal diffraction peaks, we are able to assign the structural type for the phases (in good probability) constituting the powders analysed. Some structures referenced in CSD with a reference code (REFCODE) are taken as references for the following study. Their principal characteristics are given in Table 2.5.

CSD REFCOD chemical diagram	Crystallographic parameters Spacegroup Cell parameters (Å)	Structure type
BCDEXD10⁷⁰ 	P 2 ₁ a=21.29, b= 10.33, c=15.1 ($\alpha=90^\circ$, $\beta=112.3^\circ$, $\gamma=90^\circ$) 3072.509	Herringbone dual channels along b axis
BOBPIR⁷¹ 	P 2 ₁ a=21.03 ,b= 10.11, c=15.33 ($\alpha=90^\circ$, $\beta=111.02^\circ$, $\gamma=90^\circ$) 3042.469	Herringbone dual channels along b axis Ethanol molecules are distributed anywhere in the structure.
CACPOM⁷² 	P 1 a=18.2423, b= 15.4915, c=15.4362 ($\alpha=102.755^\circ$, $\beta=113.0096^\circ$, $\gamma=99.78^\circ$) 3753.311	Dimer Brick type dual channels along a axis Guest molecules are inserted in the channels

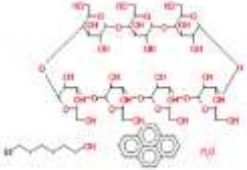
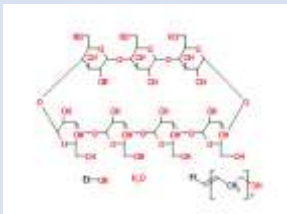
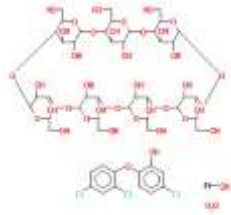
<p>PUKPIU⁷³</p> 	<p>C 2</p> <p>a=19.3267 ,b= 24.4409, c=15.9220 ($\alpha=90^\circ$, $\beta=109.0^\circ$, $\gamma=90^\circ$)</p> <p>7111.27</p>	<p>Channels along c axis</p> <p>Disordered octanol molecules are inserted in the channel.</p> <p>Pyrene guest molecules are inserted between two cyclodextrin molecules in the channel</p>
<p>ZUZXOH⁷⁴</p> 	<p>C 2</p> <p>a=19.238 ,b= 24.477, c=15.79 ($\alpha=90^\circ$, $\beta=109.52^\circ$, $\gamma=90^\circ$)</p> <p>7007.984</p>	<p>Channels (tilted molecules) along c axis</p> <p>Ethanol molecules are anywhere in the structure.</p> <p>Guest molecules are inserted in the channel</p>
<p>POHXUG⁷⁵</p> 	<p>P 1</p> <p>A=15.189, b =15.230, c= 16.293 ($\alpha=91.07^\circ$, $\beta= 91.05^\circ$, $\gamma= 100.71^\circ$)</p> <p>3701.822</p>	<p>channels along c axis</p> <p>Ethanol molecules are anywhere in the structure.</p> <p>Guest molecules are inserted in the channel</p>

Table 2.5 : Principal structural characteristics of the CSD structures used further as references.

Simulated patterns are calculated for 4° to 14° in 2 theta with the help of the CSD Mercury software and are represented in Figure 2.15. By default, the FWHM parameter has been set to 0,1 and the lambda value to 1.5405 \AA . Tables 2.6 to 2.10 give the principles features and peaks in the simulated diffractograms.

Peak positions are relative to the cell parameters although intensity is related to the composition of the motif and width to the crystallinity of the sample. For example, in the case of BOBPIR and BCDEXD10, the cell parameters, the CD's tridimensional packing are very similar and the only difference is the presence of some methanol molecules instead of water molecules in BOBPIR. The two patterns are very similar with only some small differences between some corresponding peak intensities.

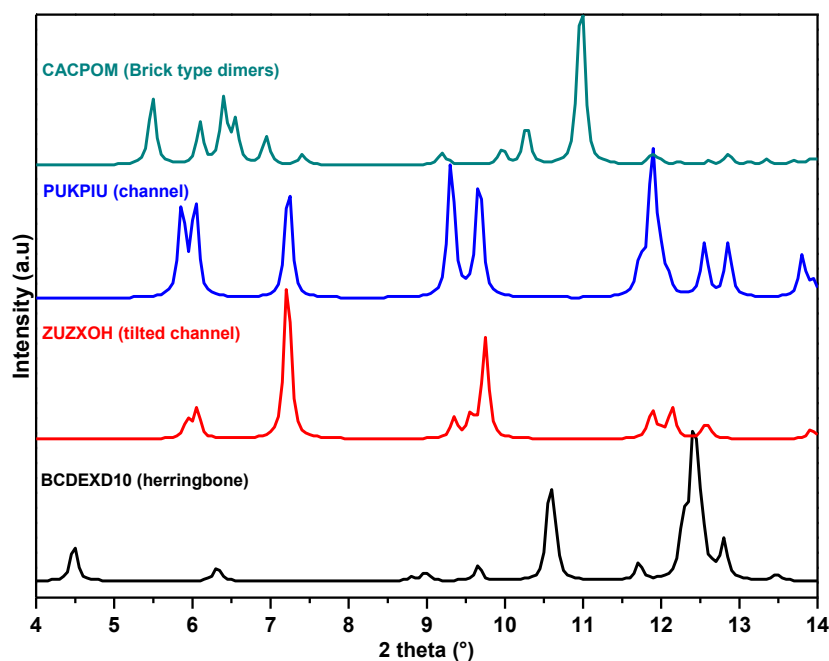


Figure 2.15 : Types of diffraction patterns obtained by different style arrangements of β CD while forming an inclusion complex. Simulation done with the Mercury software ($\lambda_{Cu}=1.5405 \text{ \AA}$, FWHM = 0.1).

2theta	Relative intensity	d-spacing (\AA)	h	k	l
4,5	22	19,6977	1	0	0
6,3	8	13,9707	0	0	1
8,8	3	10,0416	2	0	-1
9,0	5	9,84886	2	0	0
		9,77831	1	0	1
9,7	10	9,14832	1	1	0
10,6	61	8,35824	1	1	-1
		8,30604	0	1	1
11,7	12	7,54728	1	0	-2
12,3	50	7,2003	2	1	-1
12,4	100	7,12822	2	1	0
		7,10134	1	1	1
		7,06294	3	0	-1
12,7	29	6,98533	0	0	2
		6,90916	2	0	1
13,5	4	6,5659	3	0	0

Table 2.6 : Simulated X-ray pattern of CSD refcode BCDEXD10⁷⁰ for $4^\circ < 2\theta < 14^\circ$: Dual channel Herringbone structural type. ($\lambda_{Cu}=1.5405 \text{ \AA}$, FWHM = 0.1).

Dual channel herringbone type simulated patterns, like those of BCDEXD10, are characterized by the presence of a peak at a low 2 theta angle around 4.5° and at least two intensive peak around 10.6° and 12.4° in 2theta.

2theta	Relative intensity	d-spacing (Å)	h	k	l
5,5	44	16,0928	1	0	0
6,1	29	14,481	0	1	0
6,4	46	13,7923	1	0	-1
6,5	32	13,4772	0	0	1
6,9	19	12,7194	1	-1	0
7,4	7	11,927	0	1	-1
8,5	0	10,4088	1	1	-1
9,2	8	9,6131	1	-1	-1
		9,50059	1	1	0
9,9	10	8,92566	1	-1	1
		8,86284	2	0	-1
10,3	23	8,614	1	0	1
		8,60065	0	1	1
10,9	100	8,08026	2	-1	0
		8,04641	2	0	0
		7,94399	2	-1	-1
11,8	7	7,52423	1	0	-2
		7,44564	1	-2	0
		7,43471	0	2	-1
		7,37368	1	1	-2
12,2	5	7,24051	0	2	0
		7,22576	2	1	-1
12,6	2	7,01829	0	1	-2
12,8	7	6,89616	2	0	-2
		6,87372	1	-2	1
13,1	3	6,73859	0	0	2
		6,63131	1	2	-1
13,7	2	6,46318	1	1	1
		6,42759	2	1	-2
13,9	2	6,35971	2	-2	0
		6,31045	2	1	0

Table 2.7: Simulated X-ray pattern of CSD refcode CACPOM⁷² for 4° < 2theta < 14° : dual channels made with dimer brick structural type. ($\lambda_{Cu}=1.5405 \text{ \AA}$, FWHM = 0.1).

Dual channel made with dimer brick structural type simulated patterns, like those of CACPOM, are characterized by the presence of a broad non intensive doublet at a low 2 theta angle around 5.5° and 6.1° and at least one intensive peak around 10.9° in 2theta.

2theta	Relative intensity	d-spacing (Å)	h	k	l
5,9	61	15,0545	0	0	1
6,0	63	14,6353	1	1	0
7,2	68	12,2204	0	2	0
		12,2041	1	1	-1
9,3	89	9,48797	0	2	1
		9,34626	1	1	1
		9,262	2	0	-1
9,7	73	9,13688	2	0	0
11,7	34	7,54119	1	1	-2
		7,52727	0	0	2
11,9	100	7,44096	1	3	0
		7,38148	2	2	-1
		7,31767	2	2	0
12,5	37	7,05233	1	3	-1
		7,04291	2	0	-2
12,9	37	6,88027	2	0	1
13,8	29	6,40903	0	2	2
		6,34487	1	3	1

Table 2.8 : Simulated X-ray pattern of CSD refcode PUKPIU⁷³ for 4°<2theta<14° : Channel structural type. ($\lambda_{Cu}=1,5406$. Å m, FWHM = 0.1).

Channel structural type simulated patterns, like those of PUKPIU, are characterized by the presence of broad medium intensive peaks at 2theta angle around 6°, 7.2°, 9.7° and 12° and a doublet around 12.5° and 13° in 2 theta.

2 theta (°)	Relative intensity	d-spacing (Å)	h	k	l
5,4	11	16,2861	0	0	1
5,9	7	14,9609	0	1	0
		14,9207	1	0	0
7,5	6	11,7115	1	-1	0
7,9	34	11,1432	0	1	-1
		11,1253	1	0	-1
8,1	100	10,8964	0	1	1
		10,8821	1	0	1
9,1	10	9,7	1	1	0
9,3	11	9,5091	1	-1	1
		9,50748	1	-1	-1
10,5	2	8,44213	1	1	-1
10,8	29	8,22958	1	1	1
		8,14307	0	0	2

11,8	4	7,48046	0	2	0
		7,46037	2	0	0
12,2	19	7,24994	1	-2	0
		7,23621	2	-1	0
		7,22074	0	1	-2
		7,2155	1	0	-2
12,5	2	7,08571	0	1	2
		7,0821	1	0	2
12,9	2	6,85639	0	2	-1
		6,84031	2	0	-1
13,1	8	6,74048	0	2	1
		6,72634	2	0	1
		6,68633	1	-1	2
		6,68521	1	-1	-2
13,3	34	6,65056	1	-2	1
		6,63913	2	-1	-1
		6,59641	1	-2	-1
		6,58687	2	-1	1

Table 2.9 : Simulated X-ray pattern of CSD refcode POHXUG⁷⁵ for $4^\circ < 2\theta < 14^\circ$: Channel structural type. ($\lambda_{Cu} = 1.5405 \text{ \AA}$, FWHM = 0.1).

Channel structural type simulated patterns, like those of POHXUG, are characterized by the presence of an intensive peak at 2 theta angle around 8° .

2theta (°)	Relative intensity	d-spacing (Å)	h	k	l
5,9	14	14,8825	0	0	1
6,1	21	14,57	1	1	0
7,2	100	12,2385	0	2	0
		12,1724	1	1	-1
9,3	15	9,45277	0	2	1
9,6	18	9,24421	1	1	1
		9,23386	2	0	-1
9,7	68	9,06615	2	0	0
11,8	19	7,49164	1	1	-2
		7,44123	0	0	2
		7,44045	1	3	0
		7,37116	2	2	-1
12,1	21	7,285	2	2	0
12,5	9	7,05311	1	3	-1
		7,01514	2	0	-2
13,0	0	6,7988	2	0	1
13,9	5	6,3582	0	2	2
		6,31763	1	3	1

Table 2.10 : Simulated X-ray pattern of CSD refcode ZUZXOH⁷⁴ for 4°<2theta<14°: Channel structural type. (λ_{Cu} =1.5405 Å , FWHM = 0.1).

Channel structural type made with slightly tilted CD molecules simulated patterns, like those of ZUZXOH, are characterized by the presence of an intensive peak at 2 theta angle around 7.2° and a less intensive peak around 9.7° in 2 theta.

2.5.3 Structural characterization of β CD powder (as received)

In Figure 2.16 are superposed the experimental pattern for β CD powder as received and the simulated pattern of BCDEXD10 consisting in the crystal structure of a cyclohepta-amylose dodecahydrate clathrate. Crystals presenting a herringbone structure type must be in majority present in the powder while a small amount of crystals presenting a channel structure, like those of ZUZXOH, in relation with the presence of a supplementary small peak around 7,2° must be also present in the sample. Table 2.11 gives the principal features for the experimental pattern of β CD powder (as received).

2theta (°)	Relative intensity	Assignment
4.5	100	BCDEXD10
6.1	11	BCDEXD10 +ZUZXOH
7.2	12	ZUZXOH
9	85	BCDEXD10 +ZUZXOH
9.8	20	BCDEXD10 +ZUZXOH
10	13	BCDEXD10
10.7	50	BCDEXD10
11.6	15	BCDEXD10
12	70	ZUZXOH
12.5	68	BCDEXD10
12.7	30	BCDEXD10 +ZUZXOH
13.4	6	BCDEXD10
13.6	9	BCDEXD10

Table 2.11 : Experimental X-ray pattern of β CD (as received) and CSD refcode reference assignment.

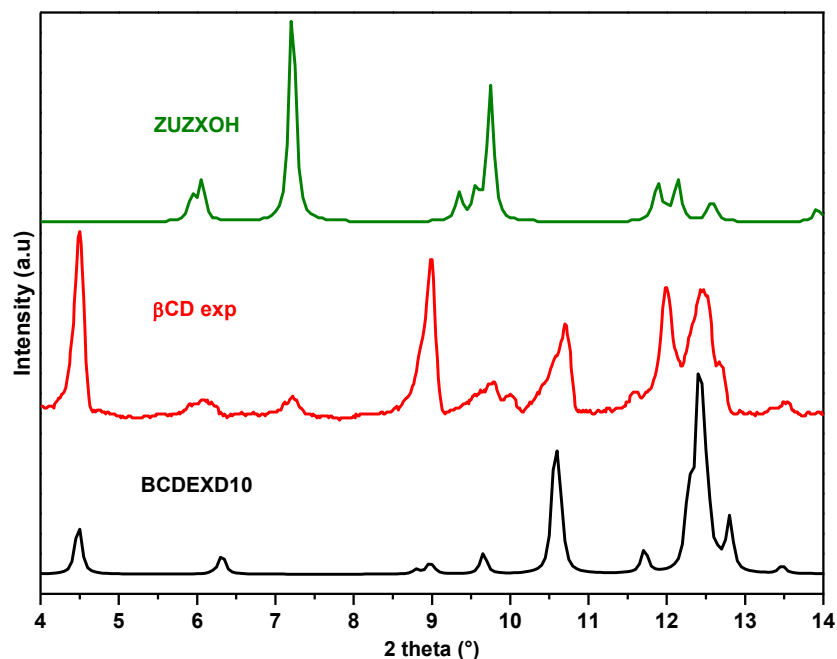


Figure 2.16 comparison of diffraction patterns of experimentally observed and simulated herringbone structure (BCDEXD10) from literature of β CD. The CSD reference are BCDEXD10 and ZUZXOH. The experimentally observed β CD pattern can be seen to show peaks corresponding to both these structures.

2.5.4 Structural characterization of Inclusion compounds

X-ray diffraction method is a very useful technique for the detection of CD complexation in powder or microcrystalline states. Moreover, it is also used to measure the crystallinity of the formed complexes. The diffraction pattern obtained of the inclusion complex is expected to be different from that of each component if a true inclusion complex is formed⁷⁶⁻⁹⁹.

Generally, CD aggregates can possess two types of crystal structures: cages and channels (explained in the first chapter). Depending on the nature and size of the guest molecule, different crystal structures can be formed. For example- when the guest molecules are small like water or methanol, cage like structures are usually formed by CD molecules i.e both the opening of CDs are blocked by adjacent CD molecules present, leading to entrapping of the guest molecule in cage like fashion. On the other hand, if longer (Octanol) or bulkier molecules enter the cavity, the alignment of CDs can be in the fashion of channels (head to tail or head to head fashion). Therefore, the crystal structure can modify the solid state arrangement.

We have carried out the X-ray studies on the samples prepared to characterized the type of crystal structures they have formed for the ternary systems. The main expectation from this type of studies is to confirm whether the solid crystals obtained show channel type arrangement in a unit cell i.e they show the diffraction pattern with the peaks similar to that of channel type arrangements. Inclusion complex formation generally results in changes in the characteristic peaks of the β CD which can disappear and new peaks can appear. Also, effective drying of the samples can eliminate the water molecules resulting in decreased intensity of reflections and results finally in an amorphous structure.

CD inclusion complexes represent a multicomponent system for which PXRD approach is a crucial technique. Each crystalline phase exhibits a unique diffraction pattern, a mixture of two or more crystalline phases is sum of the individual patterns. The CSD reference are BCDEXD10 and ZUZXOH. The experimentally observed β CD pattern can be seen to show peaks corresponding to both these structures.

For a herringbone type arrangement for β CD (CSD BCDEXD10), the diffraction pattern show major peaks at 4.5°, 6.3°, 8.9°, 9.6°, 10.6°, 11.7°, 12.4° and 12.7° from 4° to 14° in 2 theta. These mentioned peaks are in accordance with our result obtained for β CD. The important peaks can be seen at the positions- 4.5°, 7.2°, 8.9°, 10.7°, 11.9° and 12.4°.

In case of channel type arrangement (CSD PUKPIU), the pattern shows peaks at: 5.8°, 6.0°, 7.2°, 9.3°, 9.6°, 11.9°, 12.5° and 12.8° and 13.8° from 4° to 14° in 2 theta. Table 2.12 lists the peak positions corresponding to these crystal structures and experimentally observed β CD.

Experimental patterns for less crystalline samples, as inclusion compounds based, show in general, larger peak corresponding to a bigger value of FWHM. In this case, for example, two peaks showing 2 theta values next to each other (close vicinity) appear like one broad peak. Experimental intensities can also be influenced by the preparation of the analysed sample, e.g. privileged orientation can increase some family planes intensities.

β CD herringbone type arrangement (Observed)	Herringbone (BCDEXD10)	ZUZXOH (tilted channel)	PUKPIU (channel)	CACPOM (Brick type dimers)
4.5°	4.5°	6.0	5.8	5.4
7.2°	6.3°	7.2	6.0	6.0
8.9°	8.9°	9.3	7.2	6.4
9.7°	9.6°	9.5	9.3	6.5
10.7°	10.6°	9.7	9.6	6.9
11.9°	11.7°	11.8	11.9	7.4
12.4°	12.4°	12.1	12.5	9.1
	12.7°	12.5	12.8	9.9
			13.8	10.2
				10.9

Table 2.12 : XRD peaks corresponding to different types of β CD Crystals.

The complexes prepared with octanol exhibited brick type dimers structural type. The comparison of the X ray patterns are plotted in Figure 2.17 for experimentally observed β CD: Octanol and simulated brick type dimers data (CACPOM⁷²) from literature.

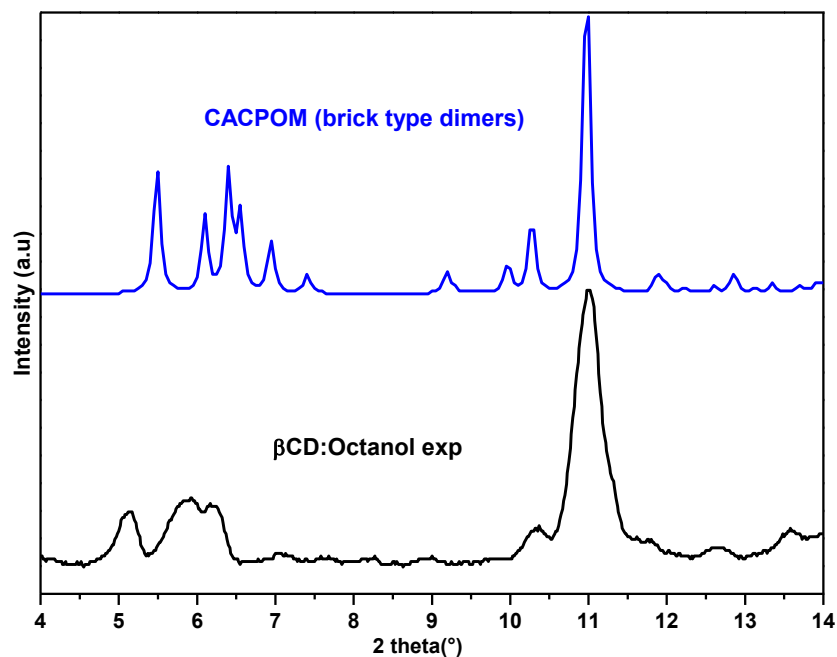


Figure 2.17 : Observed powder XRD pattern of β CD co-precipitated in presence of octanol in comparison with the powder xray simulated pattern from 4° to 14° in 2θ for CSD CACPOM exhibiting a brick type dimers structural type.

2.6 Solid state studies: Part-3. Raman Spectroscopy analysis of the inclusion complexes

Raman spectroscopy – one of the spectroscopic techniques that deals with the infrared region of the electromagnetic spectrum is used to provide information about different vibrational, rotational and other low-frequency modes in a system. Unlike other techniques, it deals with the *scattering of light* and not the absorption. Raman spectroscopy differentiates chemical structures, even if they contain the same atoms in different arrangements. Other positive aspects of the technique include non-contacting and non-destructive nature.

The objectives of this study were to verify the inclusion complexation and then to characterize the complexes and to use this methodology to identify and analyse the chemical effects occurred in the inclusion complexes prepared.

Raman spectra of all the precursors and the inclusion compounds obtained in the solid state were recorded using Xplora One (Horiba scientific) micro spectrometer. The wavelength of 680 nm and 780 nm for laser excitation was focused on the sample with 80x objective. Spectra were collected in the wavenumber ranges $200\text{-}3600\text{ cm}^{-1}$. Integration time for signal collection was set to 60s for all the measurements. Each spectrum obtained is the average of three repetitive measurements observed.

2.6.1 Principle

Let a beam of monochromatic light from the visible portion of the spectrum be chosen to such that it is not absorbed by the substance under study. If such a light is passed through the substance, nearly all of it is transmitted and a very small fraction of it is scattered in all directions. If the scattered light in a direction perpendicular to the incident beam is recorded, it is found not only to contain a line corresponding to the frequency of incident light, but also

a pattern of relatively weak lines on the low-frequency side of the incident light and a similar pattern of still more weak lines on the high frequency side. The line at the incident frequency is known as *Rayleigh line*. The other weak lines are called the Raman lines (after C.V Raman, discoverer of these lines). The difference between the frequencies of the Rayleigh line and a Raman line is known as the Raman shift.

In other words, we can explain as- when the molecule, excited to the higher unstable vibrational state, returns to the original vibrational state, we get Rayleigh scattering. If it returns to a different vibrational state, this gives rise to Raman scattering (Stokes and anti-Stokes) (Figure 2.18).

$$\Delta\nu = |\nu_0 - \nu_R|$$

where, the subscripts 0 and R stand for incident and Raman lines, respectively.

Raman spectra are comparable to infrared spectra, they have different regions that are helpful for functional groups detection and fingerprint regions that allow the identification of specific compounds. Raman spectra provide more information about certain types of organic compounds than do their infrared equivalents.

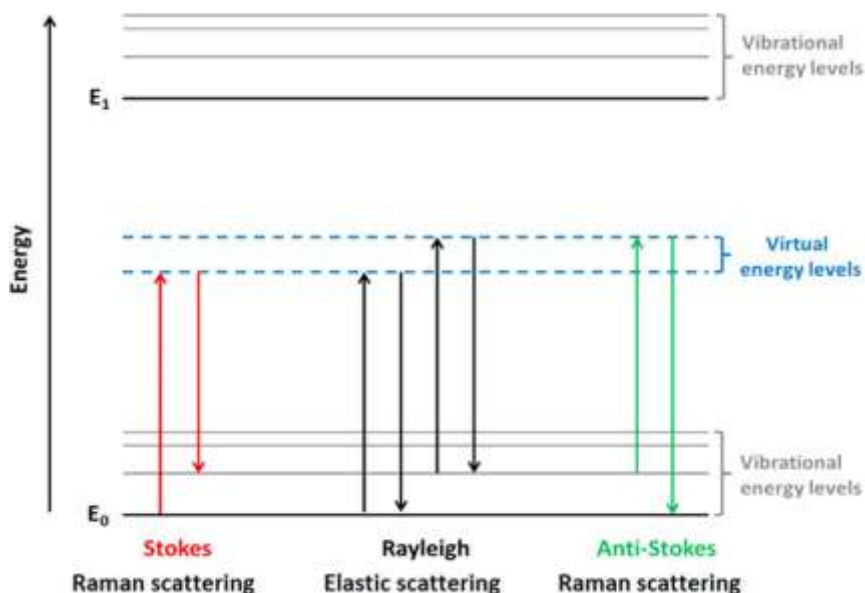


Figure 2.18 : "Jablonski" style diagram of energetic transitions involved in Raman scattering¹⁰⁰. Rayleigh scattering is elastic; the incident photon is of the same energy as the scattered photon. Raman scattering is inelastic; in Stokes scattering, the incident photon is of greater energy than the scattered photon, while in anti-Stokes scattering, the incident photon is of lower energy.

2.6.2 Theory

The Raman spectroscopy is observed only when a periodic change in the polarizability of molecule due to its vibrational and rotational oscillations.

When a molecule is placed in static electric field, it becomes polarized. Consequently, the molecule acquires an induced dipole moment that can be written as,

$$P_{ind} = \alpha E$$

where α is the polarizability of the molecule.

In the presence of a beam of radiation, the molecule also acquires an induced dipole moment due to the electrical component of the incident light. This electrical component is not static but varies as the sine (or cosine) wave according to the equation:

$$E = E_0 \sin(2\pi\nu t)$$

Where ν is the frequency of the radiation and t is the time. Therefore, the induced dipole moment also oscillates according to the equation

$$P_{ind} = \alpha E = \alpha E_0 \sin(2\pi\nu t)$$

According to the electromagnetic theory, an oscillating dipole emits radiation of its own frequency. This explains the occurrence of Rayleigh line in the light scattered by the substance. The presence of Raman lines is due to the periodic change in the value of α due to the internal vibrational or rotational motion.

According to the equation,

$$\alpha = \alpha_0 + \left(\frac{\partial\alpha}{\partial\varepsilon}\right) \varepsilon_0 \sin(2\pi\nu_i t)$$

where $\left(\frac{\partial\alpha}{\partial\varepsilon}\right)$ is the change in polarizability with displacement coordinate ε , ν_i the frequency of internal motion, and α_0 is the polarizability in the equilibrium position ε_0 .

The periodic change in the polarizability will also change periodically the induced dipole moment. When this periodic change is superimposed upon the periodic oscillation due to the electrical component of light, we get

$$\begin{aligned} P_{ind} &= \left\{ \alpha_0 + \left(\frac{\partial\alpha}{\partial\varepsilon}\right) (\varepsilon_0 \sin 2\pi\nu_i t) \right\} E_0 \sin(2\pi\nu t) \\ &= \alpha_0 E_0 \sin(2\pi\nu t) + \left(\frac{\partial\alpha}{\partial\varepsilon}\right) \varepsilon_0 E_0 \sin(2\pi\nu_i t) \sin(2\pi\nu t) \end{aligned}$$

Since,

$2 \sin \Phi \sin \Psi = \cos(\Phi - \Psi) - \cos(\Phi + \Psi)$, we get

$$P_{ind} = \alpha_0 E_0 \sin(2\pi\nu t) + \frac{1}{2} \left(\frac{\partial\alpha}{\partial\varepsilon}\right) (\varepsilon_0 E_0 \cos\{2\pi(\nu - \nu_i)t\} - \frac{1}{2} \left(\frac{\partial\alpha}{\partial\varepsilon}\right) (\varepsilon_0 E_0 \cos\{2\pi(\nu + \nu_i)t\})$$

That is, induced dipole moment of the molecule not only oscillates with frequency ν , but also with frequencies ν_i (Stokes) and ν_i (anti-Stokes) it is thus expected that besides the frequency, the oscillating dipole will also emit radiations of frequencies ν_i and ν_i these radiations appear as the Raman lines in the light scattered by the substance.

Conditions for observing Raman lines

1. The molecule must have a permanent dipole moment.
2. There should be a change in dipole moment during the vibrational motion

2.6.3 Molecular theory

When a photon interacts with a complex molecule, energy is either absorbed or emitted. This type of interaction leads to excitation of molecules to higher vibrational states. These vibrations are quantized and are called normal modes of vibrations of a molecule. The vibrational modes of a linear molecule are defined as $3N-5$ normal modes while a non-linear molecule has $3N-6$ normal modes (N = number of atoms). The motion characterized by normal modes could be:

1. Bending motion between three atoms connected by two bonds.
2. Stretching motion between two bonded atoms.
3. Out of plane deformation modes.

The observed vibrational spectrum of a compound or molecule contains different bands. The normal vibrations of the molecules are associated with appropriate Raman frequencies. The assignment of Raman spectra is generally based on the group frequency concept. By comparing the spectra of large number of different compounds, the presence of certain groups has been observed (C-H, C=O, O-H, C=C, C=N etc.) and can be correlated with repeated occurrence of the absorption bands in the vibrational spectra where the positions change slightly from going from one compound to another. The different atomic groups vibrate at their own frequencies and are independent of the other groups present in the same molecule. These frequencies are called as characteristic group frequencies. The group frequency studies are extremely useful in the interpretation of vibrational spectra. If certain vibrations possess the constant spectral positions, they can be considered as good group frequencies.

Frequency shifts can also occur due to mechanical or electronic effects. Mechanical effects come into picture when there is change in mass or coupling of the vibrations. In this case, the force constant of the bond remains unaffected. The electronic effects are generally transferred by chemical bonds. For example- inductive, conjugative etc; also alteration in the force constant can occur. There are many other factors that can influence the correct frequency of the molecular vibration. There could be a combination of different effects and it is impossible to isolate them. A molecular group is always under the influence of different electronic environments. There are some important factors like coupled interactions, Fermi resonance, hydrogen bonding, electronic structure etc. which are liable for shifting the vibrational frequencies of certain groups from their usual values.

The energy and also the wavelength of the absorption peak may be impacted by the other vibrations in the molecule. When the vibrations contain a common atom strong coupling occurs between stretching vibrations. Moreover, interactions between bending vibrations occur only when the common bond is present between the vibrating groups.

Hydrogen bonding exists in a system containing a proton donor (X) and proton acceptor (Y), if there occurs an effective overlap between the s orbital of the donor and p- or - orbital of the acceptor group. Carboxyl, hydroxyl, amine or amide group are common proton donors in organic compounds whereas the common proton acceptors are electron deficient atoms like oxygen, nitrogen and halogens.

The X-H stretching bands move to lower frequencies usually with increased intensity and band widening. On the contrary, X-H bending vibrations usually shift to higher frequencies or shorter wavelengths. The different types of hydrogen bonding namely intramolecular and intermolecular also affect the spectral features. The intermolecular hydrogen bonds (association of two or more molecules of same or different compounds, a dimer) give rise to sharp and well defined bands whereas intramolecular (interaction of proton donor and acceptor, mainly present in the single molecule) results in broad bands. The hydrogen bonding can also take place between the solvent and molecular entities of a reaction.

There could be other internal factors to influence vibrational frequencies which come into picture such as electronic structure of the carbonyl group. The nature of the substituent group X in carbonyl compounds of the formula $R-C=O-X$ may influence the frequency of $C=O$ stretching by inductive and mesomeric effects. Due to the electronegativity difference between the carbonyl carbon and the substituent group X in RCOX compounds, inductive effect arises. Also, this effect involves the sigma bond electrons. On the other hand, mesomeric effect which is opposite to inductive effect includes electrons in the pi and non-bonding orbitals. These two effects cannot be separated from each other instead their contribution can only be estimated approximately.

Organic compounds are made up of certain kinds of atoms connected by different types of bonds. Hence, the vibrational spectrum of organic compounds can be divided into different typical regions: The A-X stretching vibrations are located in the highest frequency region, between 3700 and 2500 cm^{-1} . The region between 2500 and 2000 cm^{-1} exhibits stretching vibrations of groups with triple bonds as well as the antisymmetric stretching vibrations of groups with accumulative double bonds, $A=B=C$ (atoms of typical organic molecules). On moving ahead in the region 2000 and 1500 cm^{-1} , corresponds to stretching vibrations of double bonded $A=B$ groups. A-X deformation vibrations are observed between 1500 and 100 cm^{-1} . The region between 1300 and 600 cm^{-1} shows stretching vibrations of single bonds of atoms. The next region shows bending vibrations of these groups and stretching vibrations of groups with heavier atoms. Lastly, between 200 and 20 cm^{-1} the lattice vibrations of crystalline molecules are found. This aspect sets these spectra apart from the spectra of aliphatic compounds, which possess bands of broader width. Table 2.13 lists all common characteristic frequencies of organic compounds.

The aromatic ring system are the class of hydrocarbons where the centre of discussion is **benzene** ring and the higher members of the groups can be explained on basis of the results obtained for the monocyclic member i.e benzene. The vibrational spectra of aromatic systems have been found to possess many needle-sharp bands. The reason behind the sharpness of the aromatic absorption bands arises from the fact that aromatic systems are rigid molecules having little possibility for rotational isomerism.

The different vibrational modes that could be present in aromatic systems could be:

1. Carbon-hydrogen stretching and bending vibrations.

The bending modes are further classified as:

- a) In-plane bending
 - b) Out-of-plane bending (where the plane of reference is the plane of the aromatic ring)
2. Carbon-carbon ring stretching and bending modes (in-plane and out-of plane)
3. The ring substituent C_6H_5-X (where the hydrogen of benzene has been replaced by $-X$) will introduce additional modes:
- a) C-X stretching
 - b) C-X bending (in-plane and out-of plane).
4. If the X- group is multiatomic, such as $-CH_3$, $-CN$, $-NO_2$, $-OH$ or $-COOH$, then the internal vibrations of $-X$ (including its group frequencies) will be present in the spectrum of that particular substance.

Region	Functional group/ vibration	Compound
480-510	SS stretch	Dialkyl disulphides
616-630	Ring deformation	Monosubstituted benzenes
650-660	CCI stretch	Primary choloalkanes
620-715	CS stretch	Dialkyl disulphides
585-740	CS stretch	Alkyl sulphides
820-825	C_3O skeletal stretch	Secondary alcohols
720-830	Ring vibration	Para-disubstituted benzenes
749-835	Skeletal stretch	Isopropyl group
877	OO stretch	Hydrogen peroxide
850-900	Symmetric CNC stretch	Secondary amines
837-905	CC skeletal stretch	n-alkanes
830-930	Symmetric COC stretch	Aliphatic ethers
990-1010	Trigonal ring breathing	Mono-substituted benzenes
990-1010	Trigonal ring breathing	Meta-substituted benzenes
1015-1030	In-plane CH deformation	Mono-substituted benzenes
1020-1060	Ring vibration	Ortho-disubstituted benzenes
950-1150	C-C stretches	n-alkanes
1188-1196	Symmetric SO_2 stretch	Alkyl sulphates
1205	C_6H_5-C vibrations	Alkyl benzenes
1200-1230	Ring-vibration	Para-disubstituted benzenes
1251-1270	In-plane CH deformation	Cis-dialkyl ethylenes
1295-1305	CH_2 in phase twist	n-alkanes
1175-1310	CH_2 twist and rock	n-alkanes
1290-1314	In-plane CH deformation	Trans di-alkyl ethylenes
1330-1350	CH deformation	Isopropyl group
1368-1385	CH_3 symmetric deformation	n-alkanes
1370-1390	Ring stretch	Napthalenes
1385-1415	Ring Stretch	Anthracenes

1465-1466	CH ₃ deformation	n-alkanes
1446-1473	CH ₃ , CH ₂ deformations	n-alkanes
1550-1630	Ring stretches (doublet)	Benzene derivatives
1590-1650	NH ₂ scissors	Primary amines
1649-1654	Symmetric C=O stretch	Carboxylic acids (cyclic dimer)
1700-1725	C=O stretch	Aliphatic ketons
1720-1740	C=O stretch	Aliphatic aldehydes
2100-2160	CC stretch	Alkyl acetylenes
2232-2251	CN stretch	Aliphatic nitriles
2231-2301	CC stretch	Dialkyl acetylenes
2560-2590	SH stretch	Thiols
2849-2861	Symmetric CH ₂ stretch	n-alkanes
2883-2884	Symmetric CH ₃ stretch	n-alkanes
2912-2929	Anti-symmetric CH ₂ stretch	n-alkanes
2965-2969	Anti-symmetric CH ₃ stretch	n-alkanes
3000-3100	Aromatic CH stretch	Benzene derivatives
3330-3400	Bonded antisymmetric NH ₂ stretch	Primary amines

Table 2.13 : Common characteristic frequencies of organic compounds¹⁰¹.

The Raman spectroscopy provides a fingerprint of a biological or chemical compound. The vibrations are highly related with the molecular structure and the frequencies of vibration depend on the mass of the atoms, on the nature and the strength of the chemical bonds. Raman spectra of α D glucose unit^{102,103} contains different bands corresponding to C-O-H group, number of modes of vibration for C-H, CH₂ and OH. Therefore, for studying Raman spectra of CDs, one has to look for the position of above mentioned bands.

2.6.4 Raman spectrum of β CD

β CD consists of 7 glucopyranose units which are joined together by glycosidic bonds. Raman spectra of CDs contain different regions full of bands that can be used as windows for monitoring relevant modes, such as the stretching vibration of double bonds (C=C, C=O etc) and of aromatic C-H bonds. The region of the spectrum below 1500 cm⁻¹ contains maximum of the information or the peaks due to complex vibrational modes. Since β -CD is a large molecule, many researchers have studied the normal modes based on the assignment obtained from the calculations done on the smaller analogous compounds such as α -D glucopyranose (monosaccharide) and amylose (polysaccharide). Many have also compared the spectra obtained from molecular modelling analysis and physical measurement.

The structure of crystalline α -anomer form of glucopyranose unit shows the presence of OH group below the ring plane. This information can be easily confirmed by Raman spectroscopy. Moreover, the bands assigned for the complex modes of the CH₂OH are 1335 and 1250 cm⁻¹. For specific anomeric band of C-1-H, 860 cm⁻¹ has been assigned for deformation coupled with other motions. The other lines at 1349, 1071, 1020 and 913 cm⁻¹ is due to bending of C-O-H

groups. CH₂ vibrations can be observed at 1457, 1337, 1219 and 1011 cm⁻¹ corresponding to different vibration modes bending, wagging, twisting and rocking modes respectively.

The other bands to specific vibrational modes for X-C1-H (X=C2, O1 or O5) are at 1360, 1250, 1076, 1047 and 913 cm⁻¹. The band at 836 cm⁻¹ has generally been considered typical of anomeric configurations having C-1-H equatorial position. Another band assigned to Y-C2-H related mode (Y=C3, C1 or O2). In the frequency range below 1300 cm⁻¹, additional contribution due to C-O and C-C stretching modes are expected.

βCD has 147 atoms and can produce 435 normal vibration modes. linked through 1, 4-glycosidic bonds. The Raman spectrum obtained for βCD shows different modes of vibrations. The scissoring of OH appears at 1408 cm⁻¹, the out of plane bending vibrations are observed at 649, 579, 531, 438 and 356 cm⁻¹. The stretching vibrations of CH₂ and CH can be observed at 2939, 2901 cm⁻¹. Its scissoring vibrations appears at 1450, 1386, 1334 and 1251 cm⁻¹. The asymmetric and symmetric stretching of C-O-C appears at 945 cm⁻¹. The C-C stretching vibration occurs at 1125 cm⁻¹. The c-o stretching vibration occurs at 1085 and 1046 cm⁻¹.

The in-plane and out-of-plane deformation vibrations of glucose can also be observed. The breadth vibration of glucose ring appears at 927 and 852 cm⁻¹. The in-plane deformation vibration of glucose ring appears at 753 and 711 cm⁻¹ in the Raman spectrum. The bending vibration of C-C-C links appears at 317 cm⁻¹ in the Raman spectrum (Figure 2.19).

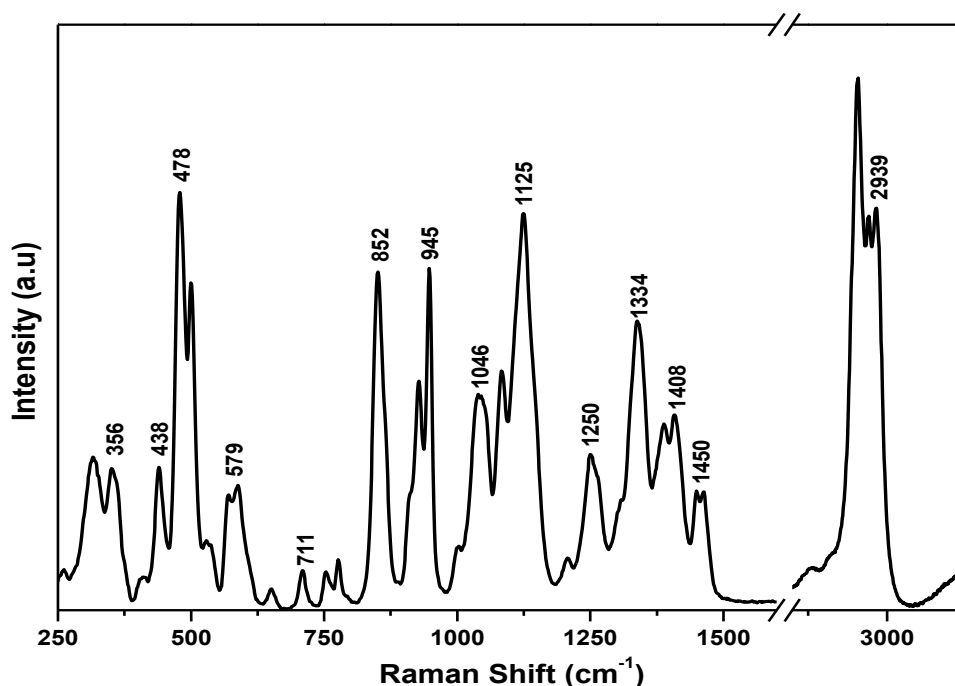


Figure 2.19 : Observed Raman Spectrum of βCD.

2.7 Molecular Modelling studies

Two methods of molecular modelling are used to obtain different level of result. These studies showed increased stability of the inclusion complex prepared with long chain aliphatic alcohols ($\geq 5C$). The first method - Simulation of RAMAN spectra and normal modes attribution by DFT calculations helped in band assignment in the Raman Spectra and the second method of manual docking was used to check the relative stability of 1:1 β CD: Alcohol complexes in aqueous solutions.

2.7.1 Simulation of RAMAN spectra and normal modes attribution by DFT calculations:

For solid state analysis, Raman^{104,105} spectroscopy is a used technique to gain important evidences on the complex formation, thanks to changing in the molecular vibrational modes (frequency and relative intensity) due to the molecular interaction between the host and the guest molecules. However, literature reveals, that complexes formed between CDs and non-polar aromatic compounds are still undergoing difficulties in spectroscopic based analysis¹⁰⁶, due to very weak molecular interactions.

It has already been observed that small shifts and variation in intensities for some bands in Raman spectra of guest molecules appear upon formation of inclusion complexes¹⁰⁷. The moieties of guest molecules that suffer from intermolecular interactions can be identified by assigning the shifted bands using DFT calculation. Starting from the nature of vibrations modified upon complexation, it becomes also possible to discuss the orientation of the guest molecules in the inclusion complexes. In experimental IR absorption spectra of inclusion complexes, bands due to CD are prominent¹⁰⁷, while it is not so obvious with Raman spectra. So, it becomes easier to observe Raman bands attributed to the guest molecules.

Quantum chemical computations predicting harmonic frequencies and spectral intensities are essential for interpretation of experimental spectra, particularly for large molecules¹⁰⁸. Accurate computation of IR and Raman intensities is difficult because of their dependence on dipole moment and polarizability derivatives. That's why it is invariably the relative, rather than absolute, band intensities that are used because experimental determination of absolute band intensities, especially for Raman bands, is difficult. Accordingly, the intensity of some bands is enhanced in experimental data in comparison with the calculated ones, especially for the more intensive ones, but the order of magnitude is kept on the whole spectra¹⁰⁹.

All calculations were carried out using the Gaussian09 suite of programs¹¹⁰. Following full geometry optimization of aromatic hydrocarbon with correct symmetry using the density functional three-parameter hybrid model B3LYP^{111,112} with the 6-311G(d,p) basis set, vibrational frequencies and Raman activities were calculated. The B3LYP method with the 6-311G(d,p) basis set is frequently used in predicting vibrational spectra of polyaromatic molecules. Raman intensities were computed from activities with GaussSum 3.0¹¹³ using an excitation wavelength of 785nm. The calculated harmonic frequencies of CH stretching vibrations were scaled by a factor and all the other frequencies by other scale f to allow a good agreement with observed ones for fluoranthene alone within almost 10 cm^{-1} on the whole spectra. Gaussview 5¹¹⁴ was used to visualize the participation and direction of atoms in vibrational normal modes in order to make bands assignments easier.

2.7.2 Manual docking of guest molecules in β CD by semi empirical PM3 method

Molecular modeling can help to characterize the binding behavior between CD as host and molecular guests. Our protocol is largely inspired by the publications of Sahra¹¹⁵ and of Zhang^{2,116}. The semi-empirical PM3 method has been shown to be a powerful tool in the study of CD complexes and combines high computational efficiency in calculating CD systems^{117,118}.

The starting geometries of the guests were constructed with the help of Chem3D Ultra (version 10, Cambridge soft com.) and were fully optimized with the PM3 method before inclusion into the CD cavity using Gaussian09 quantum mechanical package¹¹⁰.

The β CD structure was obtained from the crystallographic parameters provided from the Cambridge structural database (CSD). The optimization of the host molecule was performed using semi-empirical PM3 level of the theory without imposing any restrictions.

The coordinate system used to define the inclusion process of a guest in β CD is based on placing the glycosidic oxygen atoms of the CD onto the XY plane, and their center of mass was defined as the origin of the coordination system. Hydroxyl atoms from the lower (smaller, less open) rim containing in particular the CH₂-OH function are considered as positive while hydroxyl atoms from the upper rim (larger, more open) are considered as negative for the Z coordinates. The distance with the center of the host molecule is considered from the mass center of the guest molecule. We consider two possible orientations in the case of alcohol inclusion from approaching direction starting from a positive distance: (1) hydroxyl oriented to the center of CD cavity, namely A orientation and (2) aliphatic chain oriented to the center of CD cavity, namely B orientation.

The docking was emulated by keeping β CD at a fixed position (center) and approaching the guest along the Z-axis from at least +8 Å to -8 Å at 0.5 Å intervals by steps (Figure 2.20). Each resulting geometry guest/ β CD complex obtained was further optimized by PM3 method optimization. Avogadro software has been used for the complex structures construction¹¹⁹.

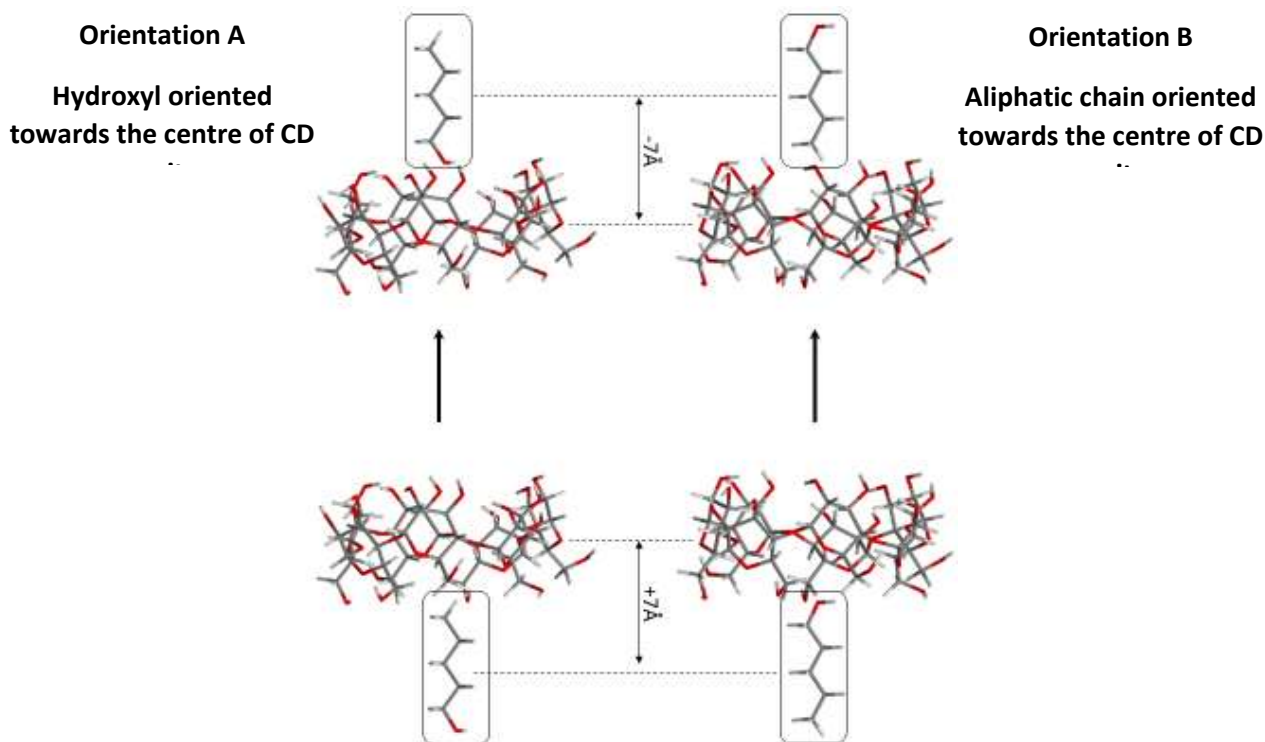


Figure 2.20 : Manual docking procedure of a guest (herein a pentanol molecule) in β CD with the two orientations A and B. Carbon, oxygen and hydrogen atoms are respectively represented in grey, red and white.

In order to investigate the binding energy changes upon complexation between the guest and β CD, calculation for the minimum energy structures is defined in Eq. (1) respectively¹²⁰

$$\Delta E_{\text{bind}} = \Delta E(\text{complex})^{\text{opt}} - [\Delta E(\text{host})^{\text{opt}} + \Delta E(\text{guest})^{\text{opt}}] \quad (1)$$

where $\Delta E(\text{complex})^{\text{opt}}$, $\Delta E(\text{host})^{\text{opt}}$ and $\Delta E(\text{guest})^{\text{opt}}$ represent the total optimized energy of the complex, the free host and the free guest, respectively.

Enthalpy changes (ΔH), Gibbs energy changes (ΔG) and entropy changes (ΔS) are computed with the following equations :

$$\Delta H = \Delta H(\text{complex})^{\text{opt}} - [\Delta H(\text{host})^{\text{opt}} + \Delta H(\text{guest})^{\text{opt}}] \quad (2)$$

where $\Delta H(\text{complex})^{\text{opt}}$, $\Delta H(\text{host})^{\text{opt}}$ and $\Delta H(\text{guest})^{\text{opt}}$ represent the enthalpy changes of the complex, the free host and the free guest, respectively.

$$\Delta G = \Delta G(\text{complex})^{\text{opt}} - [\Delta G(\text{host})^{\text{opt}} + \Delta G(\text{guest})^{\text{opt}}] \quad (3)$$

where $\Delta G(\text{complex})^{\text{opt}}$, $\Delta G(\text{host})^{\text{opt}}$ and $\Delta G(\text{guest})^{\text{opt}}$ represent the Gibbs energy changes of the complex, the free host and the free guest, respectively.

$$\Delta S = \Delta S(\text{complex})^{\text{opt}} - [\Delta S(\text{host})^{\text{opt}} + \Delta S(\text{guest})^{\text{opt}}] \quad (4)$$

where $\Delta S(\text{complex})^{\text{opt}}$, $\Delta S(\text{host})^{\text{opt}}$ and $\Delta S(\text{guest})^{\text{opt}}$ represent the entropy changes of the complex, the free host and the free guest, respectively.

The thermodynamic analysis was performed using water ($\epsilon = 78.39$) with the polarizable continuum implicit solvent model IEFPCM as implemented in GAUSSIAN09¹²¹.

The more negative binding energy change ΔE_{bind} is the more thermodynamically favorable in the inclusion complexation. The thermodynamic parameters such as enthalpy change (ΔH), entropy change (ΔS), and Gibbs free energy change (ΔG) of the complexation reaction were studied at 1 atm and 298.15 K. Enthalpy driven in nature exothermic processes are justified by a negative enthalpy change (ΔH). Furthermore, a more negative enthalpy change indicates the most thermodynamically favorable conformation. Negative values for the standard Gibbs energy changes ΔG indicate that inclusion reactions are spontaneous.

On the contrary, positive values for ΔH and ΔG indicate that the formation of the complexes are endothermic and non-spontaneous processes.

However, since the inclusion reaction happened in aqueous solution, the influence of water molecules on the inclusion process is be very important, and the effect of H₂O molecules mainly concentrates on ΔS by our calculation. A negative entropy effect can be the result of the combination of the host-guest reaction and the release of water molecules from the cavity. It has been shown that inclusion complexation process is enthalpy-entropy synergistically driven.

In basic molecular orbital theory approach, The LUMO as an electron acceptor represents the ability to receive an electron while HOMO represents the ability to give an electron¹²². So, the HOMO energy (E_{HOMO}) is related to the IP by Koopmann's theorem and the LUMO energy (E_{LUMO}) as electron affinity (EA)¹²³ is used for calculating the electronic chemical potential (μ), which is half the sum of energies of the HOMO and LUMO:

$$\mu = (E_{\text{HOMO}} + E_{\text{LUMO}})/2 \quad (5)$$

A negative chemical potential (μ) indicates a spontaneous inclusion process.

The gap energy (G) is the difference between the HOMO and LUMO; the hardness (η) is half of the energy gap between LUMO and HOMO.

$$G = E_{\text{HOMO}} - E_{\text{LUMO}} \quad (6)$$

$$\eta = (E_{\text{HOMO}} - E_{\text{LUMO}})/2 \quad (7)$$

Chemicals with large gap energy (G) value tend to have higher stability¹²⁴

The electrophilicity (ω) of molecules and their complexes is calculated using the following equation

$$\omega = \mu^2/2\eta \quad (8)$$

Large values of electrophilicity (ω) are the characteristics of the most electrophilic systems.

2.8 Conclusion

The chapter comprises of the materials used to prepare the samples and different methods used to characterize the complexes in solid as well as in the liquid state. The different principles of the respective techniques enable us to understand the basic idea behind the results obtained.

The solution studies obtained us the NMR spectrum of native β CD dissolved in D_2O . On inclusion complex formation, the shifting of H3 and H5 peaks indicated interaction between the host and guest molecules. The stoichiometry of the complex was calculated by job's plot method.

For characterization in solid state, different techniques have been used. The DSC curve of β CD showed the thermal characteristics of the system. The removal of tightly bound water molecules and decomposition at higher temperature are classical features of the curve.

Distinctive Powder XRD pattern of β CD indicates the type of crystal structure possessed when small molecules like water are present inside the cavity. β CD tend to form cage like crystals when complexed with smaller guest molecules.

Raman Spectroscopy provided details about the particular vibrational modes which occur when the cavity is occupied only by water molecules.

Any changes in these standard results of β CD obtained by using different techniques would indicate complexation.

2.9 References

1. Jullian, C., Miranda, S., Zapata-Torres, G., Mendizábal, F. and Olea-Azar, C., 2007. Studies of inclusion complexes of natural and modified cyclodextrin with (+) catechin by NMR and molecular modeling. *Bioorganic & medicinal chemistry*, 15(9), pp.3217-3224.
2. Zhang, J.Q., Wu, D., Jiang, K.M., Zhang, D., Zheng, X., Wan, C.P., Zhu, H.Y., Xie, X.G., Jin, Y. and Lin, J., 2015. Preparation, spectroscopy and molecular modelling studies of the inclusion complex of cordycepin with cyclodextrins. *Carbohydrate research*, 406, pp.55-64.
3. Rajendiran, N., Sankaranarayanan, R.K. and Saravanan, J., 2014. A study of supramolecular host-guest interaction of dothiepin and doxepin drugs with cyclodextrin macrocycles. *Journal of Molecular Structure*, 1067, pp.252-260.
4. Danel, C., Duval, C., Azaroual, N., Vaccher, C., Bonte, J.P., Bailly, C., Landy, D. and Goossens, J.F., 2011. Complexation of triptolide and its succinate derivative with cyclodextrins: Affinity capillary electrophoresis, isothermal titration calorimetry and 1H NMR studies. *Journal of Chromatography A*, 1218(48), pp.8708-8714.
5. Liu, B., Zeng, J., Chen, C., Liu, Y., Ma, H., Mo, H. and Liang, G., 2016. Interaction of cinnamic acid derivatives with β -cyclodextrin in water: Experimental and molecular modeling studies. *Food chemistry*, 194, pp.1156-1163.
6. Aksamija, A., Polidori, A., Plasson, R., Dangles, O. and Tomao, V., 2016. The inclusion complex of rosmarinic acid into beta-cyclodextrin: A thermodynamic and structural analysis by NMR and capillary electrophoresis. *Food chemistry*, 208, pp.258-263.

7. Kfoury, M., Auezova, L., Greige-Gerges, H., Ruellan, S. and Fourmentin, S., 2014. Cyclodextrin, an efficient tool for trans-anethole encapsulation: Chromatographic, spectroscopic, thermal and structural studies. *Food chemistry*, 164, pp.454-461.
8. Lula, I., De Sousa, F.B., Denadai, Â.M., de Lima, G.F., Duarte, H.A., dos Mares Guia, T.R., Faljoni-Alario, A., Santoro, M.M., de Camargo, A.C., dos Santos, R.A. and Sinisterra, R.D., 2012. Interaction between bradykinin potentiating nonapeptide (BPP9a) and β -cyclodextrin: A structural and thermodynamic study. *Materials Science and Engineering: C*, 32(2), pp.244-253.
9. Lula, I., Denadai, Â.L., Resende, J.M., de Sousa, F.B., de Lima, G.F., Pilo-Veloso, D., Heine, T., Duarte, H.A., Santos, R.A. and Sinisterra, R.D., 2007. Study of angiotensin-(1–7) vasoactive peptide and its β -cyclodextrin inclusion complexes: complete sequence-specific NMR assignments and structural studies. *peptides*, 28(11), pp.2199-2210.
10. Terekhova, I.V., Chislov, M.V., Brusnikina, M.A., Chibunova, E.S., Volkova, T.V., Zvereva, I.A. and Proshin, A.N., 2017. Thermodynamics and binding mode of novel structurally related 1, 2, 4-thiadiazole derivatives with native and modified cyclodextrins. *Chemical Physics Letters*, 671, pp.28-36.
11. Bernini, A., Spiga, O., Ciutti, A., Scarselli, M., Bottoni, G., Mascagni, P. and Niccolai, N., 2004. NMR studies of the inclusion complex between β -cyclodextrin and paroxetine. *European journal of pharmaceutical sciences*, 22(5), pp.445-450.
12. Danel, C., Azaroual, N., Brunel, A., Lannoy, D., Vermeersch, G., Odou, P. and Vaccher, C., 2008. Study of the complexation of risperidone and 9-hydroxyrisperidone with cyclodextrin hosts using affinity capillary electrophoresis and ^1H NMR spectroscopy. *Journal of Chromatography A*, 1215(1-2), pp.185-193.
13. Roy, M.N., Roy, A. and Saha, S., 2016. Probing inclusion complexes of cyclodextrins with amino acids by physicochemical approach. *Carbohydrate polymers*, 151, pp.458-466.
14. Rogez-Florent, T., Azaroual, N., Goossens, L., Goossens, J.F. and Danel, C., 2015. NMR investigation of the complexation and chiral discrimination of pyrazole sulfonamide derivatives with cyclodextrins. *Carbohydrate polymers*, 115, pp.598-604.
15. Cabaleiro-Lago, C., Nilsson, M., Valente, A.J., Bonini, M. and Söderman, O., 2006. NMR diffusometry and conductometry study of the host–guest association between β -cyclodextrin and dodecane 1, 12-bis (trimethylammonium bromide). *Journal of colloid and interface science*, 300(2), pp.782-787.
16. Seridi, L. and Boufelfel, A., 2013. Wogonin hosted@ β -cyclodextrin: structural, electronic and nuclear studies. *Journal of Molecular Liquids*, 188, pp.13-21.
17. Srinivasan, K., Stalin, T., Shanmugapriya, A. and Sivakumar, K., 2013. Spectroscopic and electrochemical studies on the interaction of an inclusion complex of β -cyclodextrin with 2, 6-dinitrophenol in aqueous and solid phases. *Journal of Molecular Structure*, 1036, pp.494-504.
18. Evans, C.H., Partyka, M. and Van Stam, J., 2000. Naphthalene complexation by β -cyclodextrin: influence of added short chain branched and linear alcohols. *Journal of inclusion phenomena and macrocyclic chemistry*, 38(1-4), pp.381-396.
19. Sasaki, K.J., Christian, S.D. and Tucker, E.E., 1989. Study of the stability of 1: 1 complexes between aliphatic alcohols and β -cyclodextrins in aqueous solution. *Fluid Phase Equilibria*, 49, pp.281-289.

20. Rekharsky, M.V., Mayhew, M.P., Goldberg, R.N., Ross, P.D., Yamashoji, Y. and Inoue, Y., 1997. Thermodynamic and nuclear magnetic resonance study of the reactions of α - and β -cyclodextrin with acids, aliphatic amines, and cyclic alcohols. *The Journal of Physical Chemistry B*, 101(1), pp.87-100.
21. Guernelli, S., Laganà, M.F., Mezzina, E., Ferroni, F., Siani, G. and Spinelli, D., 2003. Supramolecular Complex Formation: A Study of the Interactions between β -Cyclodextrin and Some Different Classes of Organic Compounds by ESI-MS, Surface Tension Measurements, and UV/Vis and ¹H NMR Spectroscopy. *European Journal of Organic Chemistry*, 2003(24), pp.4765-4776.
22. Baruah, K., Sinha, S., Hazarika, S. and Bhattacharyya, P.K., 2015. QM/MM Studies on Cyclodextrin-Alcohol Interaction. *Journal of Macromolecular Science, Part A*, 52(1), pp.64-68.
23. Liu, Y., Zhao, Y.L., Zhang, H.Y., Fan, Z., Wen, G.D. and Ding, F., 2004. Spectrophotometric study of inclusion complexation of aliphatic alcohols by β -cyclodextrins with azobenzene tether. *The Journal of Physical Chemistry B*, 108(26), pp.8836-8843.
24. Klausen, K.S. and Langmyhr, F.J., 1963. The use of the method of continuous variation for the classification of complexes with mole ratio 1: 1. *Analytica Chimica Acta*, 28, pp.335-340.
25. Demarco, P.V. and Thakkar, A.L., 1970. Cyclohepta-amylose inclusion complexes. A proton magnetic resonance study. *Journal of the Chemical Society D: Chemical Communications*, (1), pp.2-4.
26. Gibaud, S., Zirar, S.B., Mutzenhardt, P., Fries, I. and Astier, A., 2005. Melarsoprol-cyclodextrins inclusion complexes. *International journal of pharmaceutics*, 306(1-2), pp.107-121.
27. Jadhav, G.S. and Vavia, P.R., 2008. Physicochemical, in silico and in vivo evaluation of a danazol- β -cyclodextrin complex. *International journal of pharmaceutics*, 352(1-2), pp.5-16.
28. LOUKAS, Y.L., 1997. Measurement of molecular association in drug: cyclodextrin inclusion complexes with improved ¹H NMR studies. *Journal of pharmacy and pharmacology*, 49(10), pp.944-948.
29. Upadhyay, S.K. and Kumar, G., 2009. NMR and molecular modelling studies on the interaction of fluconazole with β -cyclodextrin. *Chemistry Central Journal*, 3(1), p.9.
30. Tablet, C., Matei, I. and Hillebrand, M., 2012. The determination of the stoichiometry of cyclodextrin inclusion complexes by spectral methods: possibilities and limitations. In *Stoichiometry and Research-The Importance of Quantity in Biomedicine*. InTech..
31. Darcsi, A., Szakács, Z., Zsila, F., Tóth, G., Rácz, Á. and Béni, S., 2016. NMR, CD and UV spectroscopic studies reveal uncommon binding modes of dapoxetine to native cyclodextrins. *RSC Advances*, 6(104), pp.102315-102328.
32. Brun, H., Paul, M., Razzouq, N., Binhas, M., Gibaud, S. and Astier, A., 2006. Cyclodextrin inclusion complexes of the central analgesic drug nefopam. *Drug development and industrial pharmacy*, 32(10), pp.1123-1134.
33. Zhao, R., Tan, T. and Sandström, C., 2011. NMR studies on puerarin and its interaction with beta-cyclodextrin. *Journal of biological physics*, 37(4), pp.387-400.
34. Hirose, K., 2001. A practical guide for the determination of binding constants. *Journal of inclusion phenomena and macrocyclic chemistry*, 39(3-4), pp.193-209.

35. Saha, S., Roy, A., Roy, K. and Roy, M.N., 2016. Study to explore the mechanism to form inclusion complexes of β -cyclodextrin with vitamin molecules. *Scientific reports*, 6, p.35764.
36. Long, B.M. and Pfeffer, F.M., 2015. On the use of 'shortcuts' in the method of continuous variation (Job's method). *Supramolecular Chemistry*, 27(1-2), pp.136-140.
37. MacCarthy, P., 1978. Simplified experimental route for obtaining Job's curves. *Analytical Chemistry*, 50(14), pp.2165-2165.
38. Gil, V.M. and Oliveira, N.C., 1990. On the use of the method of continuous variations. *Journal of Chemical Education*, 67(6), p.473.
39. Furlong, W.R., Rubinski, M.A. and Indralingam, R., 2013. The method of continuous variation: a laboratory investigation of the formula of a precipitate. *Journal of Chemical Education*, 90(7), pp.937-940.
40. Olson, E.J. and Bühlmann, P., 2011. Getting more out of a Job plot: determination of reactant to product stoichiometry in cases of displacement reactions and n: n complex formation. *The Journal of organic chemistry*, 76(20), pp.8406-8412.
41. Renny, J.S., Tomasevich, L.L., Tallmadge, E.H. and Collum, D.B., 2013. Method of continuous variations: applications of job plots to the study of molecular associations in organometallic chemistry. *Angewandte Chemie International Edition*, 52(46), pp.11998-12013.
42. Anigbogu, V.C., Munoz de la Pena, A., Ndou, T. and Warner, I.M., 1992. Determination of formation constants for. beta.-cyclodextrin complexes of anthracene and pyrene using reversed-phase liquid chromatography. *Analytical Chemistry*, 64(5), pp.484-489.
43. Schneider, H.J., Hacket, F., Rüdiger, V. and Ikeda, H., 1998. NMR studies of cyclodextrins and cyclodextrin complexes. *Chemical Reviews*, 98(5), pp.1755-1786.
44. Lehtola, J., Hakala, M. and Hamalainen, K., 2010. Structure of liquid linear alcohols. *The Journal of Physical Chemistry B*, 114(19), pp.6426-6436.
45. Mathapa, B.G. and Paunov, V.N., 2013. Self-assembly of cyclodextrin–oil inclusion complexes at the oil–water interface: a route to surfactant-free emulsions. *Journal of Materials Chemistry A*, 1(36), pp.10836-10846.
46. SHIMADA, K.A., KAWANO, K.I., ISHII, J.U. and NAKAMURA, T.A., 1992. Structure of inclusion complexes of cyclodextrins with triglyceride at vegetable oil/water interface. *Journal of food science*, 57(3), pp.655-656.
47. Tanaka, S., 1992. Theory of power-compensated DSC. *Thermochimica acta*, 210, pp.67-76.
48. Giordano, F., Novak, C. and Moyano, J.R., 2001. Thermal analysis of cyclodextrins and their inclusion compounds. *Thermochimica Acta*, 380(2), pp.123-151.
49. Bettinetti, G., Novák, C. and Sorrenti, M., 2002. Thermal and structural characterization of commercial α -, β -, and γ -cyclodextrins. *Journal of thermal analysis and calorimetry*, 68(2), pp.517-529.
50. Mura, P., Maestrelli, F., Cirri, M., Furlanetto, S. and Pinzauti, S., 2003. Differential scanning calorimetry as an analytical tool in the study of drug-cyclodextrin interactions. *Journal of Thermal Analysis and Calorimetry*, 73(2), pp.635-646.
51. Li, N. and Xu, L., 2010. Thermal analysis of β -cyclodextrin/Berberine chloride inclusion compounds. *Thermochimica Acta*, 499(1-2), pp.166-170.
52. Figueiras, A., Ribeiro, L., Torres-Labandeira, J.J. and Veiga, F.J., 2007. Evaluation of host-guest complex formation between a benzimidazolic derivative and cyclodextrins

- by UV-VIS spectrophotometry and differential scanning calorimetry. *Journal of Inclusion Phenomena and Macrocyclic Chemistry*, 57(1-4), pp.531-535.
53. Karathanos, V.T., Mourtzinou, I., Yannakopoulou, K. and Andrikopoulos, N.K., 2007. Study of the solubility, antioxidant activity and structure of inclusion complex of vanillin with β -cyclodextrin. *Food Chemistry*, 101(2), pp.652-658.
 54. Ficarra, R., Tommasini, S., Raneri, D., Calabro, M.L., Di Bella, M.R., Rustichelli, C., Gamberini, M.C. and Ficarra, P., 2002. Study of flavonoids/ β -cyclodextrins inclusion complexes by NMR, FT-IR, DSC, X-ray investigation. *Journal of pharmaceutical and biomedical analysis*, 29(6), pp.1005-1014.
 55. Mohamad, S., Surikumaran, H., Rao, M., Marimuthu, T., Chandrasekaram, K. and Subramaniam, P., 2011. Conventional study on novel dicationic ionic liquid inclusion with β -cyclodextrin. *International journal of molecular sciences*, 12(9), pp.6329-6345.
 56. Zerrouk, N., Dorado, J.G., Arnaud, P. and Chemtob, C., 1998. Physical characteristics of inclusion compounds of 5-ASA in α and β cyclodextrins. *International journal of pharmaceuticals*, 171(1), pp.19-29.
 57. Sinha, V.R., Anitha, R., Ghosh, S., Nanda, A. and Kumria, R., 2005. Complexation of celecoxib with β -cyclodextrin: Characterization of the interaction in solution and in solid state. *Journal of pharmaceutical sciences*, 94(3), pp.676-687.
 58. Guyot, M., Fawaz, F., Bildet, J., Bonini, F. and Lagueny, A.M., 1995. Physicochemical characterization and dissolution of norfloxacin/cyclodextrin inclusion compounds and PEG solid dispersions. *International journal of pharmaceuticals*, 123(1), pp.53-63.
 59. Marques, H.M.C., 2010. A review on cyclodextrin encapsulation of essential oils and volatiles. *Flavour and fragrance journal*, 25(5), pp.313-326.
 60. Huang, L., Allen, E. and Tonelli, A.E., 1999. Inclusion compounds formed between cyclodextrins and nylon 6. *Polymer*, 40(11), pp.3211-3221.
 61. LIN, S.Z., KOHYAMA, N. and TSURUTA, H., 1996. Characterization of steroid/cyclodextrin inclusion compounds by x-ray powder diffractometry and thermal analysis. *Industrial health*, 34(2), pp.143-148.
 62. Morin, N., Chilouet, A., Millet, J. and Rouland, J.C., 2000. Bifonazole- β -cyclodextrin Inclusion Complexes. Thermal analysis and X-ray powder diffraction study. *Journal of thermal analysis and calorimetry*, 62(1), p.187.
 63. Caira, M.R., Griffith, V.J., Brown, G.R. and Nassimbeni, L.R., 1996. X-ray structures and thermal analyses of new CD/drug inclusion compounds. *Journal of inclusion phenomena and molecular recognition in chemistry*, 25(1-3), pp.141-144.
 64. Rossel, C.V.P., Sepúlveda Carreño, J., Rodríguez-Baeza, M. and Alderete, J.B., 2000. Inclusion complex of the antiviral drug acyclovir with cyclodextrin in aqueous solution and in solid phase. *Quimica Nova*, 23(6), pp.749-752.
 65. Pinto, L.M., Fraceto, L.F., Santana, M.H.A., Pertinhez, T.A., Junior, S.O. and de Paula, E., 2005. Physico-chemical characterization of benzocaine- β -cyclodextrin inclusion complexes. *Journal of pharmaceutical and biomedical analysis*, 39(5), pp.956-963.
 66. Abarca, R.L., Rodriguez, F.J., Guarda, A., Galotto, M.J. and Bruna, J.E., 2016. Characterization of beta-cyclodextrin inclusion complexes containing an essential oil component. *Food chemistry*, 196, pp.968-975.
 67. Wang, J., Cao, Y., Sun, B. and Wang, C., 2011. Physicochemical and release characterisation of garlic oil- β -cyclodextrin inclusion complexes. *Food chemistry*, 127(4), pp.1680-1685.

68. Groom, C.R., Bruno, I.J., Lightfoot, M.P. and Ward, S.C., 2016. The Cambridge structural database. *Acta Crystallographica Section B: Structural Science, Crystal Engineering and Materials*, 72(2), pp.171-179.
69. Saenger, W., Jacob, J., Gessler, K., Steiner, T., Hoffmann, D., Sanbe, H., Koizumi, K., Smith, S.M. and Takaha, T., 1998. Structures of the common cyclodextrins and their larger analogues beyond the doughnut. *Chemical reviews*, 98(5), pp.1787-1802.
70. Lindner, K. and Saenger, W., 1982. Crystal and molecular structure of cyclohepta-amylose dodecahydrate. *Carbohydrate Research*, 99(2), pp.103-115.
71. Lindner, K. and Saenger, W., 1982. Crystal and molecular structures of cyclomaltoheptaose inclusion complexes with HI and with methanol. *Carbohydrate Research*, 107(1), pp.7-16.
72. Makedonopoulou, S. and Mavridis, I.M., 2001. The dimeric complex of cyclomaltoheptaose with 1, 14-tetradecanedioic acid. Comparison with related complexes. *Carbohydrate research*, 335(3), pp.213-220.
73. Udachin, K.A. and Ripmeester, J.A., 1998. A novel mode of inclusion for pyrene in β -cyclodextrin compounds: The crystal structures of β -cyclodextrin with cyclohexanol and pyrene, and with n-octanol and pyrene. *Journal of the American Chemical Society*, 120(5), pp.1080-1081.
74. Mentzafos, D., Mavridis, I.M. and Hursthouse, M.B., 1996. β -Cyclodextrin (Z)-9-Dodecen-1-ol 2: 1 Complex. *Acta Crystallographica Section C*, 52(5), pp.1220-1223.
75. Paulidou, A., Maffeo, D., Yannakopoulou, K. and Mavridis, I.M., 2008. Crystal structure of the inclusion complex of the antibacterial agent triclosan with cyclomaltoheptaose and NMR study of its molecular encapsulation in positively and negatively charged cyclomaltoheptaose derivatives. *Carbohydrate research*, 343(15), pp.2634-2640.
76. Mangolim, C.S., Moriwaki, C., Nogueira, A.C., Sato, F., Baesso, M.L., Neto, A.M. and Matioli, G., 2014. Curcumin- β -cyclodextrin inclusion complex: stability, solubility, characterisation by FT-IR, FT-Raman, X-ray diffraction and photoacoustic spectroscopy, and food application. *Food chemistry*, 153, pp.361-370.
77. Galvão, J.G., Silva, V.F., Ferreira, S.G., França, F.R.M., Santos, D.A., Freitas, L.S., Alves, P.B., Araújo, A.A.S., Cavalcanti, S.C.H. and Nunes, R.S., 2015. β -cyclodextrin inclusion complexes containing Citrus sinensis (L.) Osbeck essential oil: An alternative to control Aedes aegypti larvae. *Thermochimica Acta*, 608, pp.14-19.
78. Papadopoulos, N.D., Karayianni, H.S., Tsakiridis, P.E., Perraki, M. and Hristoforou, E., 2010. Cyclodextrin inclusion complexes as novel MOCVD precursors for potential cobalt oxide deposition. *Applied Organometallic Chemistry*, 24(2), pp.112-121.
79. Ghodke, D.S., Nakhat, P.D., Yeole, P.G., Naikwade, N.S., Magdum, C.S. and Shah, R.R., 2010. Preparation and Characterization of domperidone Inclusion complexes with cyclodextrin: Influence of preparation method. *Iranian Journal of Pharmaceutical Research*, pp.145-151.
80. Kayaci, F., Sen, H.S., Durgun, E. and Uyar, T., 2014. Functional electrospun polymeric nanofibers incorporating geraniol-cyclodextrin inclusion complexes: High thermal stability and enhanced durability of geraniol. *Food research international*, 62, pp.424-431.
81. Uyar, T., Nur, Y., Hacıoğlu, J. and Besenbacher, F., 2009. Electrospinning of functional poly (methyl methacrylate) nanofibers containing cyclodextrin-menthol inclusion complexes. *Nanotechnology*, 20(12), p.125703.

82. Udrescu, L., Sbârcea, L., Fuliş, A., Ledeti, I., Vlase, G., Barvinschi, P. and Kurunczi, L., 2014. Physicochemical analysis and molecular modeling of the fosiopril β -cyclodextrin inclusion complex. *Journal of Spectroscopy*, 2014.
83. Braga, S.S., Ribeiro-Claro, P., Pillinger, M., Gonçalves, I.S., Pereira, F., Fernandes, A.C., Romão, C.C., Correia, P.B. and Teixeira-Dias, J.J., 2003. Encapsulation of sodium nimesulide and precursors in β -cyclodextrin. *Organic & biomolecular chemistry*, 1(5), pp.873-878.
84. Gidley, M.J. and Bociek, S.M., 1988. Carbon-13 CP/MAS NMR studies of amylose inclusion complexes, cyclodextrins, and the amorphous phase of starch granules: relationships between glycosidic linkage conformation and solid-state carbon-13 chemical shifts. *Journal of the American Chemical Society*, 110(12), pp.3820-3829.
85. Pralhad, T. and Rajendrakumar, K., 2004. Study of freeze-dried quercetin–cyclodextrin binary systems by DSC, FT-IR, X-ray diffraction and SEM analysis. *Journal of pharmaceutical and biomedical analysis*, 34(2), pp.333-339.
86. Okada, M., Kamachi, M. and Harada, A., 1999. Preparation and characterization of inclusion complexes of poly (propylene glycol) with methylated cyclodextrins. *The Journal of Physical Chemistry B*, 103(14), pp.2607-2613.
87. Moyano, J.R., Arias-Blanco, M.J., Gines, J.M. and Giordano, F., 1997. Solid-state characterization and dissolution characteristics of gliclazide- β -cyclodextrin inclusion complexes. *International journal of pharmaceuticals*, 148(2), pp.211-217.
88. Sathigari, S., Chadha, G., Lee, Y.P., Wright, N., Parsons, D.L., Rangari, V.K., Fasina, O. and Babu, R.J., 2009. Physicochemical characterization of efavirenz–cyclodextrin inclusion complexes. *Aaps PharmSciTech*, 10(1), pp.81-87.
89. Gao, Y.A., Li, Z.H., Du, J.M., Han, B.X., Li, G.Z., Hou, W.G., Shen, D., Zheng, L.Q. and Zhang, G.Y., 2005. Preparation and characterization of inclusion complexes of β -cyclodextrin with ionic liquid. *Chemistry–A European Journal*, 11(20), pp.5875-5880.
90. Sapkal, N.P., Kilor, V.A., Bhursari, K.P. and Daud, A.S., 2007. Evaluation of some methods for preparing gliclazide- β -cyclodextrin inclusion complexes. *Tropical journal of pharmaceutical research*, 6(4), pp.833-840.
91. Harada, A., Nishiyama, T., Kawaguchi, Y., Okada, M. and Kamachi, M., 1997. Preparation and characterization of inclusion complexes of aliphatic polyesters with cyclodextrins. *Macromolecules*, 30(23), pp.7115-7118.
92. Fernandes, C.M., Vieira, M.T. and Veiga, F.J.B., 2002. Physicochemical characterization and in vitro dissolution behavior of nifedipine–cyclodextrins inclusion compounds. *European journal of pharmaceutical sciences*, 15(1), pp.79-88.
93. Harada, A., Suzuki, S., Okada, M. and Kamachi, M., 1996. Preparation and characterization of inclusion complexes of polyisobutylene with cyclodextrins. *Macromolecules*, 29(17), pp.5611-5614.
94. Baboota, S., Dhaliwal, M. and Kohli, K., 2005. Physicochemical characterization, in vitro dissolution behavior, and pharmacodynamic studies of rofecoxib-cyclodextrin inclusion compounds. Preparation and properties of rofecoxib hydroxypropyl β -cyclodextrin inclusion complex: a technical note. *AAPS PharmSciTech*, 6(1), pp.E83-E90.
95. Okumura, H., Kawaguchi, Y. and Harada, A., 2001. Preparation and characterization of inclusion complexes of poly (dimethylsiloxane) s with cyclodextrins. *Macromolecules*, 34(18), pp.6338-6343.

96. Sri, K.V., Kondaiah, A., Ratna, J.V. and Annapurna, A., 2007. Preparation and characterization of quercetin and rutin cyclodextrin inclusion complexes. *Drug development and industrial pharmacy*, 33(3), pp.245-253.
97. Liu, Y., Chen, G.S., Chen, Y. and Lin, J., 2005. Inclusion complexes of azadirachtin with native and methylated cyclodextrins: solubilization and binding ability. *Bioorganic & medicinal chemistry*, 13(12), pp.4037-4042.
98. Zingone, G. and Rubessa, F., 2005. Preformulation study of the inclusion complex warfarin- β -cyclodextrin. *International journal of pharmaceuticals*, 291(1-2), pp.3-10.
99. Erden, N. and Çelebi, N., 1988. A study of the inclusion complex of naproxen with β -cyclodextrin. *International journal of pharmaceuticals*, 48(1-3), pp.83-89.
100. Ember, K.J., Hoeve, M.A., McAughtrie, S.L., Bergholt, M.S., Dwyer, B.J., Stevens, M.M., Faulds, K., Forbes, S.J. and Campbell, C.J., 2017. Raman spectroscopy and regenerative medicine: a review. *NPJ Regenerative medicine*, 2(1), p.12.
101. Lin-Vien, D., Colthup, N.B., Fateley, W.G. and Grasselli, J.G., 1991. *The handbook of infrared and Raman characteristic frequencies of organic molecules*. Elsevier.
102. Vasko, P.D., Blackwell, J. and Koenig, J.L., 1971. Infrared and raman spectroscopy of carbohydrates: Part I: Identification of O-H and C-H-related vibrational modes for D-glucose, maltose, cellobiose, and dextran by deuterium-substitution methods. *Carbohydrate Research*, 19(3), pp.297-310
103. Wiercigroch, E., Szafraniec, E., Czamara, K., Pacia, M.Z., Majzner, K., Kochan, K., Kaczor, A., Baranska, M. and Malek, K., 2017. Raman and infrared spectroscopy of carbohydrates: a review. *Spectrochimica Acta Part A: Molecular and Biomolecular Spectroscopy*, 185, pp.317-335.
104. Amado, A.M., Moreira da Silva, A.M., Ribeiro-Claro, P.J.A. and Teixeira-Dias, J.J.C., 1994. Meta-substituted styrene molecules included in cyclodextrins: A Raman spectroscopic study. *Journal of Raman spectroscopy*, 25(7-8), pp.599-605.
105. Amado, A.M. and Ribeiro-Claro, P.J., 2000. Selection of substituted benzaldehyde conformers by the cyclodextrin inclusion process: a Raman spectroscopic study. *Journal of Raman Spectroscopy*, 31(11), pp.971-978.
106. García-Zubiri, Í.X., González-Gaitano, G., Sánchez, M. and Isasi, R., 2004. Infrared Study of Solid Dispersions of β -Cyclodextrin with Naphthalene Derivatives. *Journal of inclusion phenomena and macrocyclic chemistry*, 49(3-4), pp.291-302.
107. Nagao, A., Kan-No, A. and Takayanagi, M., 2009. Infrared spectra of monosubstituted toluene derivatives in cyclodextrin: Orientation of guest molecules in included complexes. *Journal of Molecular Structure*, 929(1-3), pp.43-47.
108. Billes, F., Ziegler, I. and Mikosch, H., 2015. Application of quantum chemistry for the interpretation of vibrational spectra. *Structural Chemistry*, 26(5-6), pp.1703-1714.
109. Zvereva, E.E., Shagidullin, A.R. and Katsyuba, S.A., 2010. Ab initio and DFT predictions of infrared intensities and Raman activities. *The Journal of Physical Chemistry A*, 115(1), pp.63-69.
110. Frisch, M.J., Trucks, G.W., Schlegel, H.B., Scuseria, G.E., Robb, M.A., Cheeseman, J.R., Scalmani, G., Barone, V., Mennucci, B., Petersson, G.A. and Nakatsuji, H., 2014. Official Gaussian 09 literature citation.

111. Becke, A.D., 1996. Density-functional thermochemistry. IV. A new dynamical correlation functional and implications for exact-exchange mixing. *The Journal of chemical physics*, 104(3), pp.1040-1046.
112. Lee, C., Yang, W. and Parr, R.G., 1988. Development of the Colle-Salvetti correlation-energy formula into a functional of the electron density. *Physical review B*, 37(2), p.785.
113. O'boyle, N.M., Tenderholt, A.L. and Langner, K.M., 2008. CcLib: a library for package-independent computational chemistry algorithms. *Journal of computational chemistry*, 29(5), pp.839-845.
114. Dennington, R., Keith, T. and Millam, J., 2009. GaussView, version 5. *Semichem Inc.: Shawnee Mission, KS*.
115. Sahra, K., Dinar, K., Seridi, A. and Kadri, M., 2015. Investigation on the inclusion of diclofenac with β -cyclodextrin: a molecular modeling approach. *Structural Chemistry*, 26(1), pp.61-69.
116. Zhang, J.Q., Jiang, K.M., An, K., Ren, S.H., Xie, X.G., Jin, Y. and Lin, J., 2015. Novel water-soluble fisetin/cyclodextrins inclusion complexes: preparation, characterization, molecular docking and bioavailability. *Carbohydrate research*, 418, pp.20-28.
117. Rajendiran, N. and Venkatesh, G., 2015. Micrometer size rod formed by secondary self assembly of omeprazole with α - and β -cyclodextrins. *Spectrochimica Acta Part A: Molecular and Biomolecular Spectroscopy*, 137, pp.832-840.
118. Rajendiran, N. and Siva, S., 2014. Inclusion complex of sulfadimethoxine with cyclodextrins: Preparation and characterization. *Carbohydrate polymers*, 101, pp.828-836.
119. Hanwell, M.D., Curtis, D.E., Lonie, D.C., Vandermeersch, T., Zurek, E. and Hutchison, G.R., 2012. Avogadro: an advanced semantic chemical editor, visualization, and analysis platform. *Journal of cheminformatics*, 4(1), p.17.
120. Nagaraju, M. and Sastry, G.N., 2009. Theoretical studies on inclusion complexes of cyclodextrins. *The Journal of Physical Chemistry A*, 113(34), pp.9533-9542.
121. Tomasi, J., Mennucci, B. and Cancès, E., 1999. The IEF version of the PCM solvation method: an overview of a new method addressed to study molecular solutes at the QM ab initio level. *Journal of Molecular Structure: THEOCHEM*, 464(1-3), pp.211-226.
122. Venkatesh, G., Sivasankar, T., Karthick, M. and Rajendiran, N., 2013. Inclusion complexes of sulphanilamide drugs and β -cyclodextrin: a theoretical approach. *Journal of Inclusion Phenomena and Macrocyclic Chemistry*, 77(1-4), pp.309-318.
123. Politzer, P. and Abu-Awwad, F., 1998. A comparative analysis of Hartree-Fock and Kohn-Sham orbital energies. *Theoretical Chemistry Accounts*, 99(2), pp.83-87.
124. Karelson, M., Lobanov, V.S. and Katritzky, A.R., 1996. Quantum-chemical descriptors in QSAR/QSPR studies. *Chemical reviews*, 96(3), pp.1027-1044.

Chapter-3 Inclusion complexation studies of β CD: Alcohols

3.1 Introduction

This important chapter provides details about all the results obtained and the analysis done for the complexes obtained for β CD and linear aliphatic primary alcohols. Our studies are done with a systematic and fundamental approach in order to gather the maximum information from them. Understanding alcohol's role on inclusion in complexation with β CD is important because their use is mandatory to solvate pure aromatic compounds in the further analysis. Usually people have used only smaller alcohols like methanol and ethanol molecules as co-solvent but using longer alcohol may be a key parameter to allow complexation of new hydrophobic compound. The effect of the nature and length of alcohols on complexation can further be considered as the benchmark of this thesis as this step has to be understood and examined clearly. During literature studies, we found that scientists were focussing on the effect of alcohols (smaller) on the formation of CDs inclusion complexes¹⁻⁶ and some studied CD : ethanol inclusion complexes⁷⁻⁹. So far, only one research article talks about α CD : Undecanol inclusion complex¹⁰. We also found structural data in CSD comprising linear aliphatic primary alcohols which will be discussed in the chapter. To obtain these results, we performed the synthesis of the complex in both solutions (liquid) and solid state. The methods and materials used to prepare and characterize the samples are already being discussed in the second chapter. The first step for this part was to check the phenomenon of inclusion of the hydrophobic part of the linear alcohol inside the β CD cavity by NMR characterization in solutions. The solutions were prepared in the similar fashion as explained before. The spectra were recorded multiple times with fresh solutions prepared each time just to avoid errors and accidental results. The results were further exploited by Job's method to have knowledge about the stoichiometry of the system for each alcohol when inclusion is observed. We proceeded further after getting impressive results in the liquid state. The next step was the preparation of solid complexes by co-precipitation as already explained. The solid complexes were further treated for their thermal behaviour by DSC technique followed by obtaining Powder X-ray diffraction patterns to know about the crystallization properties. The change in vibrational modes occurring due to inclusion complexation (if any) were analysed by Raman Spectroscopy. At last, to have knowledge about the behaviour of molecules in the system, molecular modeling studies were done. Our purpose is to determine which alcohols have to be used in order to obtain inclusion complexes in solution and further channel structures in solid state as we consider that they are most likely to induce pure aromatic guest.

In this chapter, the role of the guest is played by alcohol molecules. The expected results obtained from each technique as concluded from literature listed in the previous chapter for β CD: Guest inclusion complexes:

1. NMR (in solution) :-If there occurs some change in the characteristic position of H3 and H5 protons which are present inside the β CD cavity. To check the extent of displacement occurring.
2. DSC (thermal studies):- The curve obtained for an inclusion complex should have shown appearance of exothermic or endothermic curves due to the properties of the guests in addition to the properties of the newly formed complexed in comparison to the curve of uncomplexed β CD.

3. Powder X-ray Diffraction :- The diffraction pattern obtained for the inclusion complex would reveal the type of crystal structure being possessed by comparing with some reference patterns. The prime focus is on obtaining either cage type crystal formation, as observed in presence of water or/ methanol¹, or channel type in presence of octanol² molecule depending on the size of guest molecule included.
4. Raman Spectroscopy- The vibrational modes of uncomplexed β CD are unique in terms of peak positions and intensity. Any change in the spectrum of an inclusion complex like appearance of guest peaks, absence of peaks corresponding to β CD, change in intensity would indicate complexation.

After interpreting all the results obtained from different techniques, optimized models of the system will be prepared to have better understanding of the behaviour of the molecules during inclusion phenomenon.

3.2 NMR studies of β CD:alcohol complexation

The NMR studies for β CD: alcohol inclusion were performed on the solutions prepared as explained in the previous chapter. The main motive behind this step was to know the ability of linear alcohols to form an inclusion complex inside the cavity by showing the displacement of the H3 (3.84 ppm) and H5 (3.73 ppm) located inside β CD cavity. We prepared solutions with a concentration of 10mM in D₂O with each alcohol separately. For each β CD: alcohol solution, the results were recorded in multiples, every time with freshly prepared solutions. Another reason to perform these studies is to emphasize the behaviour of the different alcohols in relation with their aliphatic chain length in order to choose the ones that will be used to forward our studies. For our convenience and in relation with the first results obtained in solutions, we have divided the homologous series of alcohols into two parts – lower alcohols (<5C) and higher alcohols (\geq 5C). This terminology will be used throughout this chapter. In the literature, researchers were able to find the stoichiometry of the β CD: alcohol inclusion complexes by other techniques like Fluorescence measurements¹¹.

3.2.1 NMR studies of β CD: Lower alcohols Complexation (from methanol to n-butanol)

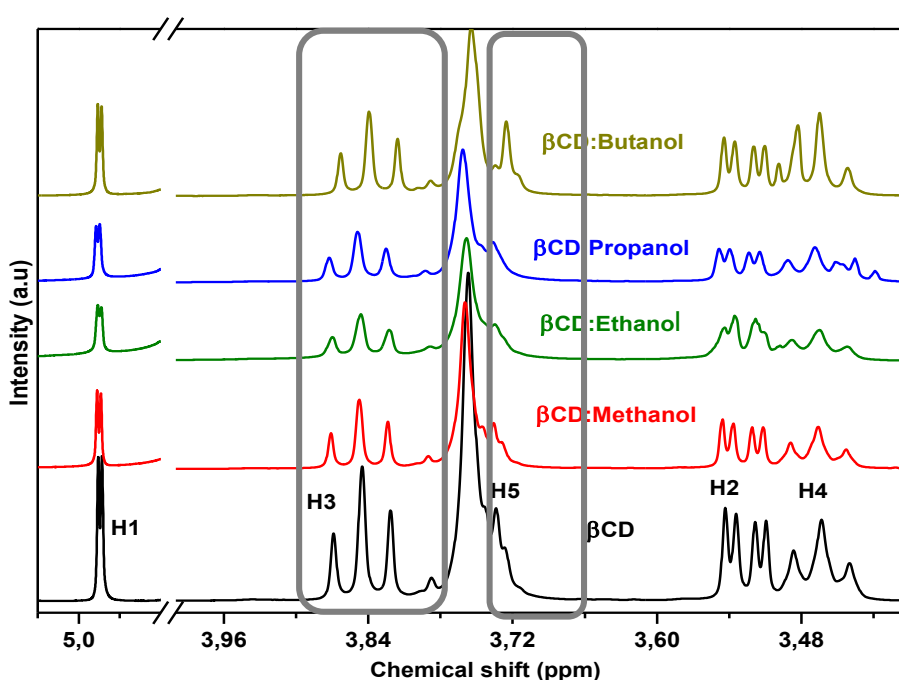


Figure 3.1 : The spectra obtained for β CD: Lower Alcohol for 1:1 volume ratio.

Figure 3.1 shows the spectra obtained for β CD: Lower Alcohol for 1:1 volume ratio. The results shown for lower alcohols do not contain any interesting peak shifts for H3 and H5 protons which are present inside the CD's cavity.

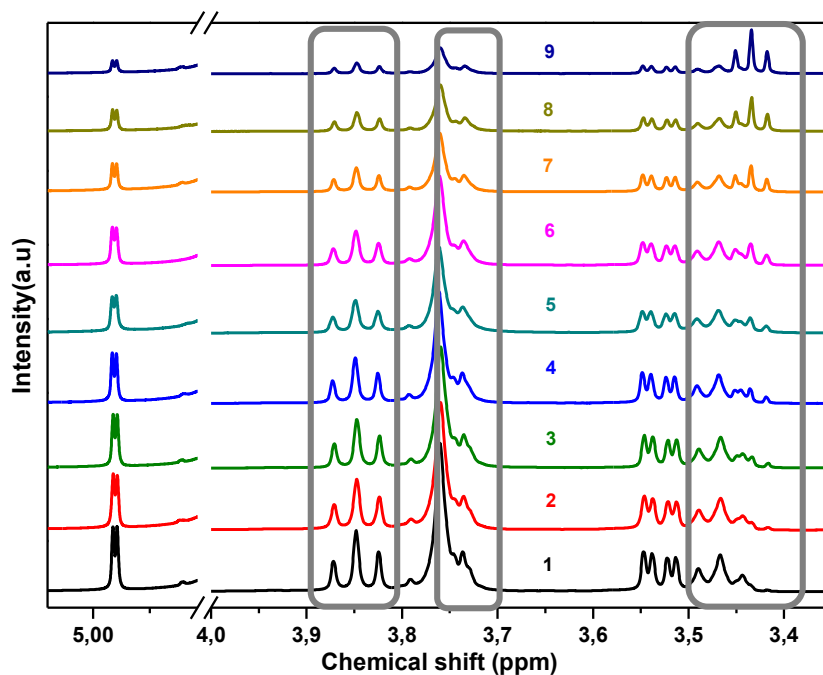


Figure 3.2 : NMR spectra obtained for β CD: Propanol mixture solutions prepared in D_2O .

Figure 3.2 shows as an example the spectra of all the mixtures prepared for β CD and Propanol. The spectra are numbered 1 to 9 in relation with the composition of the mixture. 1st is the spectrum of β CD with volume ratio 0.9 in solution. 9th is the spectrum of β CD with volume ratio 0.1. One can also observe a small shift of the triplet H4 (at 3.4 ppm) located outside the cavity. The same solutions were prepared for other lower alcohols and different results are obtained. The different volume mixtures prepared for this set are shown in the table 3.1. The spectrum number written for each mixture in the Figure 3.2 corresponds to the Sample number in the table.3.1. In presence of lower alcohols, no significant shift of H3 and H5 in β CD are observed indicating a non-inclusion complexation. Those alcohols are small and polar enough to act as water solvent molecules and are randomly present in solution and their molecular organisation in solution is very similar to what is observed in presence of water.

Sample Number	Vol. of β CD (10mM) (μ l)	Vol. of Alcohol (10mM) (μ l)	β CD volume ratio in solution
1	450	50	0.9
2	400	100	0.8
3	350	150	0.7
4	300	200	0.6
5	250	250	0.5
6	200	300	0.4
7	150	350	0.3
8	100	400	0.2
9	50	450	0.1

Table 3.1. Volume of β CD and Alcohols solutions mixed together to form inclusion complexes in D_2O to carry out NMR studies.

3.2.2 NMR studies for β CD: Higher alcohols Complexation

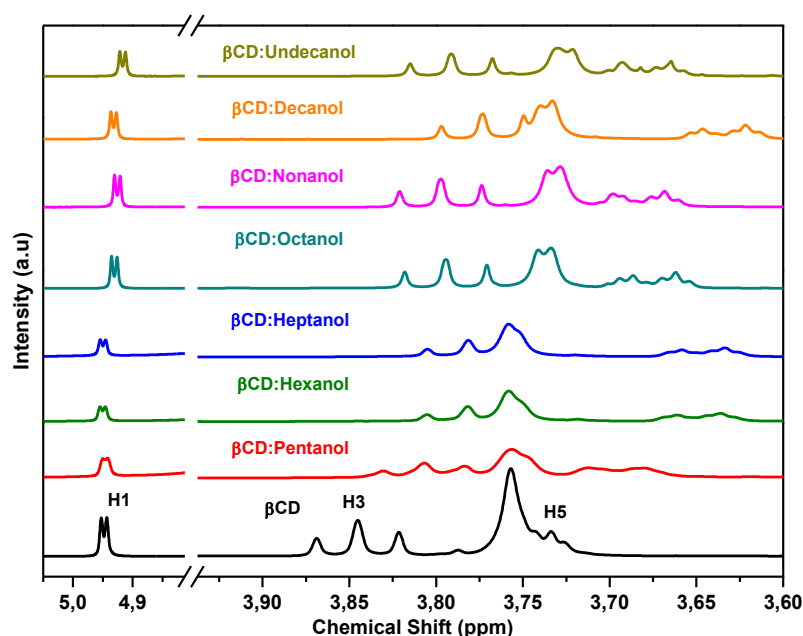


Figure 3.3 : NMR spectra obtained for β CD: Higher alcohols for volume ratio 1:1 prepared in D_2O .

Figure 3.3 shows the spectra obtained for β CD: Higher Alcohol for 1:1 volume ratio. All higher alcohols were able to displace the peaks for H3 and H5 β CD protons. The spectrum for β CD: Pentanol shows the least shift in comparison to others. The appearance of spectra indicate that β CD: Hexanol and β CD:Heptanol and β CD: Decanol show same extent of peak shift, the triplet observed for H3 proton is seen merging with H6 proton peak. The spectra showing same behaviour are also observed for β CD: Octanol and β CD:Nonanol and β CD: Undecanol.

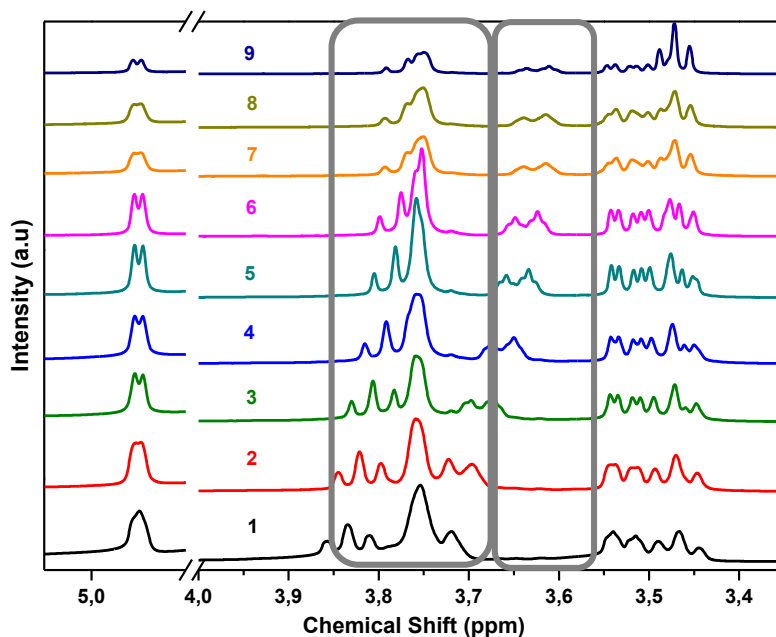


Figure 3.4 : NMR spectra obtained for β CD: Heptanol mixture solutions prepared in D_2O .

Figure 3.4 shows as an example the spectra of all the mixtures prepared for β CD and Heptanol. The same solutions were prepared for other Higher alcohols. The Different volume mixtures prepared for this set are shown in the table 3.1. The spectrum number written for each mixture in the figure corresponds to the sample number in the table.

An important shift of H3 and H5 peaks indicates a variation in the chemical neighbouring of H3 and H5 located in the β CD cavity obtained in the case of the formation of an inclusion complex. The non-polar effect of the aliphatic chain of longer alcohols enforces them to act as guest molecules by inclusion inside the β CD cavity in contrary to what was observed with smaller alcohols. The role herein played by the water molecules is solvation while the alcohols are specifically complexed inside the cavity. The nature of the interaction between longer alcohols starting from n-pentanol is different considering the non-polar behaviour of their aliphatic chain in comparison with smaller alcohol guided by their polar properties.

3.2.3 Criterion to choose appropriate alcohol on the basis of chemical shift

The criterion to choose the appropriate alcohols for inclusion complex formation is based on value of chemical shift (considered in Hertz to give more accurate values) difference obtained for H3 and H5 protons in complex spectrum from the uncomplexed β CD spectrum observed under similar conditions. A significant experimental border value of difference is ≥ 10 Hz. In case of lower alcohols for each solution prepared, the values difference obtained for positions of H3 and H5 are less than 5 Hz in both cases.

The table.3.2 (a) and (b) show the difference obtained for the volume ratio 1:1 (β CD:Lower alcohol) protons present inside the cavity. The further investigation of stoichiometry of the complex by job's plot is based on these values.

Alcohol	Difference between H ₂ O and H5 positions in βCD spectrum (Hz)	Difference between H ₂ O and H5 positions in βCD: alcohol spectrum (Hz)	Difference (Hz)
Methanol	386.01	386.05	0.04
Ethanol	386.01	386.13	0.12
Propanol	385.2	385.34	0.14
Butanol	386.01	389.89	3.88

(a)

Alcohol	Difference between H ₂ O and H3 positions in βCD spectrum (Hz)	Difference between H ₂ O and H3 positions in βCD: alcohol spectrum (Hz)	Difference (Hz)
Methanol	341.44	341.42	0.02
Ethanol	341.44	342.39	0.95
Propanol	341.44	343.5	2.06
Butanol	341.44	344.95	3.51

(b)

Table 3.2 : The significant shifts for the peak positions of (a) H5 and (b) H3 for lower alcohols for the stoichiometry 1:1.

In case of higher alcohols, the value difference observed is always more than 25 Hz. The values are listed in the table 3.3.

Alcohol	Difference between H ₂ O and H5 positions in βCD spectrum (Hz)	Difference between H ₂ O and H5 positions in βCD: alcohol spectrum (Hz)	Difference (Hz)
Pentanol	386.01	408.58	22.57
Hexanol	386.01	425.9	39.89
Heptanol	386.01	426.51	40.5
Octanol	386.01	440.35	54.34
Nonanol	386.01	424.61	38.6
Decanol	386.01	436.04	50.03
Undecanol	386.01	467.81	81.8

(a)

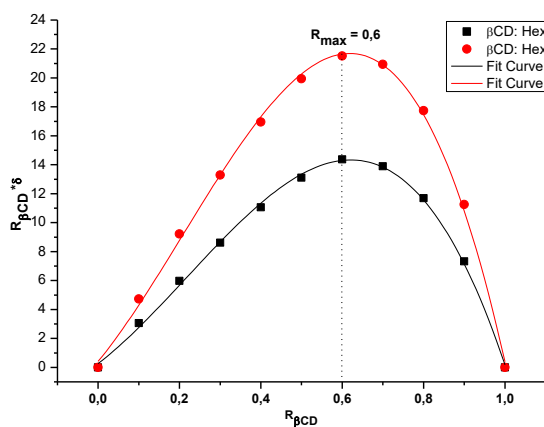
Alcohol	Difference between H ₂ O and H3 positions in β CD spectrum (Hz)	Difference between H ₂ O and H3 positions in β CD: alcohol spectrum (Hz)	Difference (Hz)
Pentanol	341.44	357.83	16.39
Hexanol	341.44	367.66	26.22
Heptanol	341.44	367.38	25.94
Octanol	341.44	377.75	36.31
Nonanol	341.44	367.85	26.41
Decanol	341.44	373.35	31.91
Undecanol	341.44	403.15	61.71

(b)

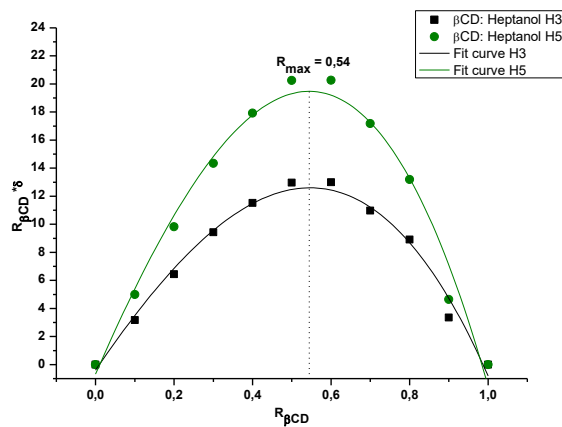
Table 3.3 : The significant shifts for the peak positions of (a) H5 and (b) H3 for higher alcohols for the stoichiometry 1:1.

3.2.4 Job's plot: Stoichiometry of the complex

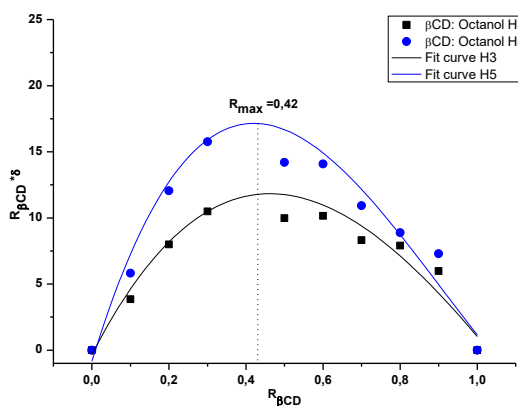
Based on the values of difference in peak positions as explained earlier, the stoichiometry of each β CD: Higher alcohol were calculated by Job's plot¹²⁻¹⁶ method using curve fitting by third degree polynomial method. The method of continuous variation to obtain job's plot are already discussed in the previous chapter. On the basis of the concept of continuous variation, the curve should possess 'bell shape'. Depending on the type of bell shape the real stoichiometry of the complex system in solutions can be determined. The system acquires 1:1 stoichiometry when the highest point on the curve falls at 0.5 value on the x-axis of the curve. The other achieved stoichiometry can be 1:2 (0.3 value on the x-axis) corresponding to 1 β CD molecule in complexation with 2 molecule of a guest or 2:1 (0.7 value on the x-axis), corresponding to 2 β CD molecule in complexation with 1 molecule of a guest depending on the system. We have also obtained job's plot for all β CD: Higher alcohols for H3 and H5 protons. They are represented in the Figure 3.5.



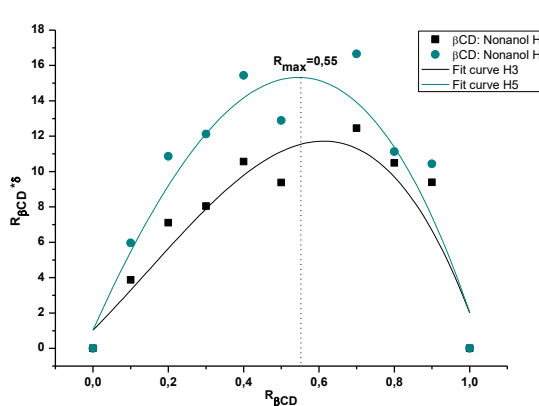
(a)



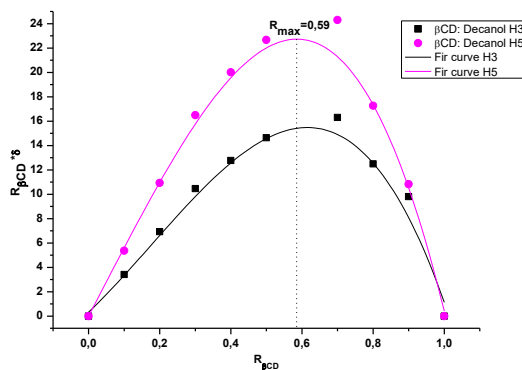
(b)



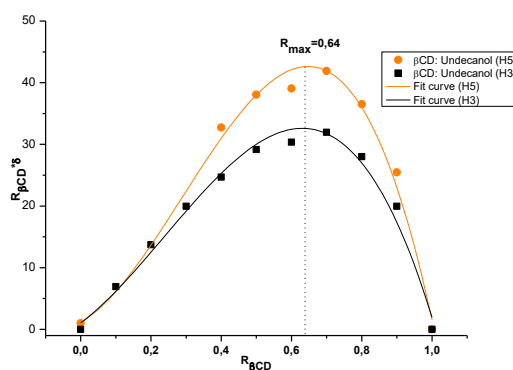
(c)



(d)



(e)



(f)

Figure 3.5 : Job'plot obtained for β CD: Higher alcohol H3 and H5 protons complexes (a) β CD: Hexanol ,(b) β CD: Heptanol, (c) β CD: Octanol , (d) β CD: Nonanol, (e) β CD: Decanol (f) β CD: Undecanol.

Alcohol	R _{max}	Stoichiometry (βCD: Higher Alcohol)
Hexanol	0.6	2:1
Heptanol	0.54	1:1
Octanol	0.42	1:2 or 1:1
Nonanol	0.66	2:1
Decanol	0.59	2:1
Undecanol	0.64	2:1

Table 3.4 : show the observed medium H3 and H5 R_{max} values for each βCD: Higher alcohols and the corresponding stoichiometry.

The values obtained by NMR studies were plotted using polynomial curve fitting method and values of R_{max} were calculated by finding 2nd order derivatives. The R_{max} values and the stoichiometry of the different βCD: Higher Alcohol are given in the table 3.4. It can be observed that the alcohols are behaving differently to each other while forming inclusion complexes with βCD, βCD: Hexanol, βCD: Nonanol, βCD: Decanol and βCD: Undecanol are observed to form 2:1 stoichiometry. βCD: Heptanol and βCD: Octanol form 1:1 and 1:2 stoichiometry respectively.

It is also very evident from plots that the stoichiometry of the complexes is dependent on the length of the hydrophobic chains. The greater curvature in the peaks also leads to evenly distributed equilibrium. This behaviour of the chains adds to the perspectives of our research²¹.

3.3 DSC analysis of the inclusion complexes in the solid state

When we summarize the DSC curve for uncomplexed βCD, the endothermic feature relative to dehydration appears at 115°C in two phases. It can be concluded as the removal of tightly bound water molecules from the βCD cavity. The melting point of βCD is reference as above 260°C but in fact, a decomposition is observed above 280°C. In the case of uncomplexed mixed samples of two compounds, the DSC curve is supposed to be in exact superposition of the two curves of the compounds alone.

3.3.1 DSC studies for βCD: Lower alcohols inclusion complexes

The DSC studies performed on βCD:Lower alcohol are presented in the figure.3.6. In case of βCD: Lower alcohol, the complexes prepared with different alcohols show different endothermic curves indicating the formation of complexed forms. The boiling points for all alcohols are listed in the table 3.5.

Alcohol	Boiling point (°C)
Methanol	65
Ethanol	78
Propanol	97
Butanol	118

Table 3.5 : List of boiling point temperatures of different linear alcohols (from methanol to Butanol) (Source:Wikipedia)

β CD: Lower alcohols DSC curve show endothermic peaks at higher temperature than β CD (Figure 3.6). For β CD, the removal of tightly bound high energy water molecules occurs at temperature upto 120°C. It can be assumed that few of the alcohol molecules have replaced tightly bound water molecules inside the cavity. On forming complexes with methanol, an endothermic peak is observed at temperature 131°C. Similarly, for other lower alcohols the endothermic curves can be seen at temperatures higher than 120°C. None of these temperatures represent the respective boiling points of the alcohol used. The shifts in water/solvent removal peak observed are in relation with the role of co-solvent played by the lower alcohol molecule in direct comparison with the role of water molecules.

At higher temperatures, the curves obtained do not show any significant difference in comparison with the DSC curve obtained with β CD alone.

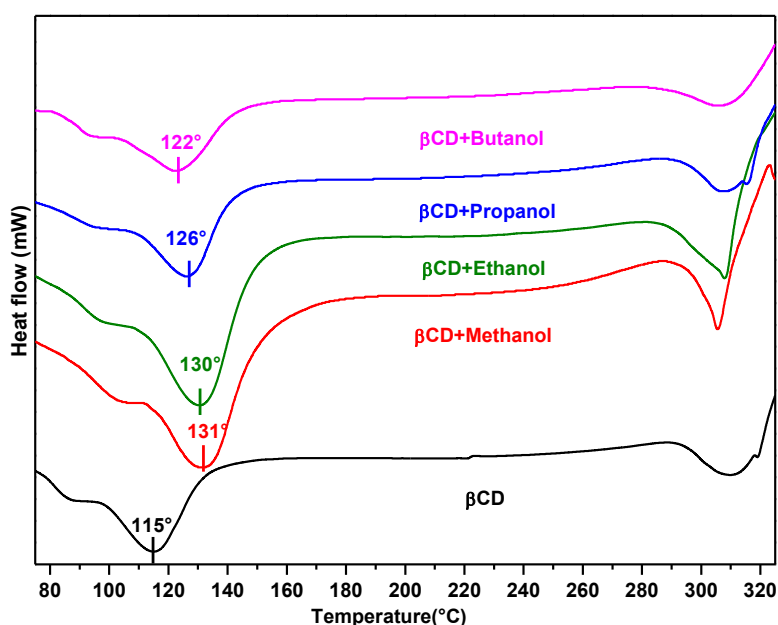


Figure 3.6 : DSC curves for inclusion complex of β CD: lower alcohols in molar ratio 1:1.

3.3.2 DSC studies for β CD: Higher alcohols inclusion complexes

The DSC curves observed for β CD: Higher alcohols complexes show noticing points (figure 3.7). The different boiling temperatures of linear alcohols are listed in the table 3.6.

Alcohol	Boiling Point (°C)
Pentanol	138
Hexanol	157
Heptanol	175
Octanol	195
Nonanol	214
Decanol	230
Undecanol	243

Table 3.6 : List of boiling point temperatures of different linear alcohols (from pentanol to n-Undecanol).

For β CD: pentanol case. we see two endothermic peaks at 104°C and 118°C corresponding to solvent removal in two stages. The curve observed for β CD: Hexanol shows two endothermic patterns at 107°C and 166°C. The value corresponds to the optimum temperature of the peak; the starting temperature of the phenomenon corresponds to the boiling temperature. The β CD: Heptanol curve show multiple endothermic behaviours at 96°C, 109°C, 146°C, 156°C and 186°C. The dips below 120°C corresponds to removal of water molecules relative to their binding inside the cavity. The boiling point of Heptanol is 175°C. The 186°C peak might belong to the boiling point of Heptanol which failed to form the inclusion complex but are still present in the powder sample. At 146°C and 156°C, the melting of different crystalline forms of the inclusion complexes formed might exist.

The β CD: Octanol curve shows only two endothermic curves at 112°C and 127°C corresponding to removal of water molecules in the inclusion complex. No dip is observed at its boiling point temperature around 195°C.

Again, two endothermic dips are observed in case of β CD: Nonanol. The typical removal of water molecules can be seen at 115°C and melting of the inclusion complex formed at 187°C.

The curve for β CD: Decanol shows two endothermic process temperatures at 114°C and 130°C for removal of water molecules in two stages and 176°C for the melting of a new crystalline structures.

In the end, β CD: Undecanol curve has shown two endothermic temperatures, at 124°C and 174°C corresponding to removal of water molecules and melting of inclusion complex formed respectively.

For all those complexes, an endothermic peak is obtained that can be attributed to the melting of a new crystalline form different from the initial form of β CD alone.

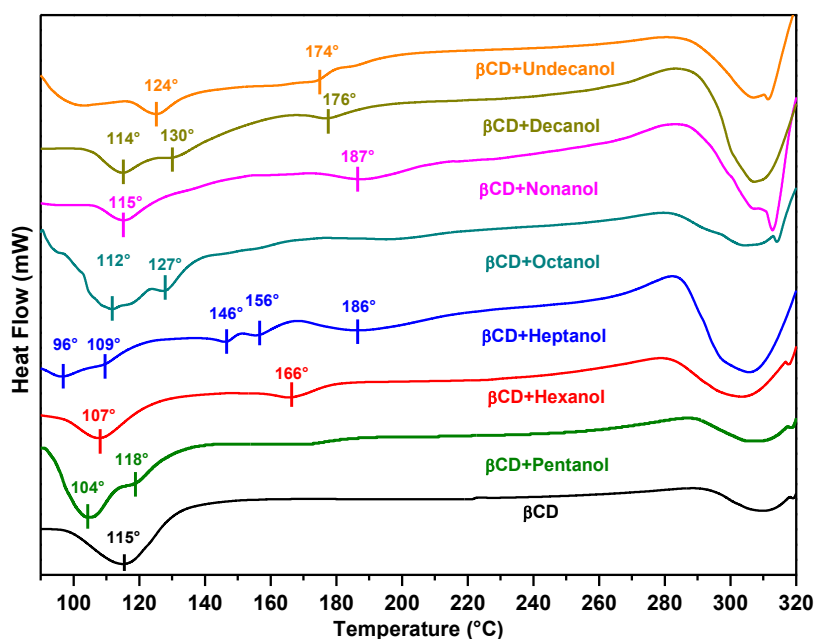


Figure 3.7 : DSC curves for inclusion complex of β CD: Higher alcohols in molar ratio 1:1.

3.4 Powder X-ray diffraction studies of β CD: Alcohol inclusion complexes

3.4.1 For β CD: Lower alcohols Inclusion complexes

The powder X-ray diffraction studies were performed on β CD: Lower alcohols in order to know the type of crystals structure their inclusion forms. Till date, only one group of researchers have studied crystal structures of alcohol inclusion complexes²². On obtaining the patterns, we have noticed them to be very similar to that obtained for β CD (figure 3.8). On comparison with patterns in the literature, they all found to resemble BCDEXD10²³. The position of peaks is same in all the cases. The only change arises due to reduced intensity of some of the peaks.

Variations in intensity are directly related to the atomic positions in the crystalline planes whereas the 2 theta position is in relation with the geometric characteristics of the crystalline cell. CD's spatial organisation in the cell determines its geometry.

The crystal structures obtained in presence of lower linear primary alcohols. From methanol to 1-butanol, the curves present the same herringbone structural type as observed for β CD in the structure CSD REFCODE BCDEXD10 and for β CD (as received). It confirms the solvation role of the alcohol molecules in those structures.

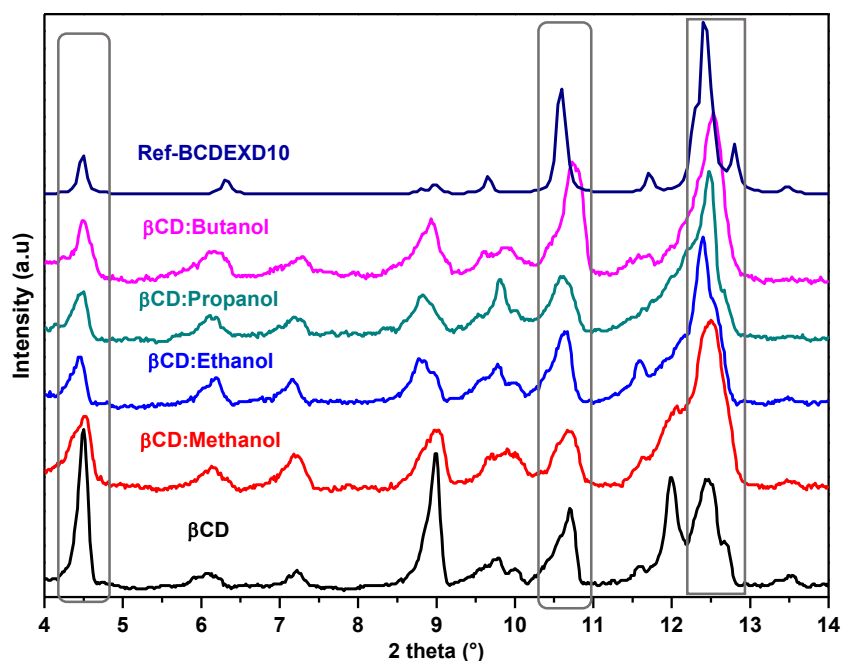


Figure 3.8 : Powder x-ray diffraction for inclusion complex of β CD: lower alcohols in molar ratio 1:1 compared with reference (BCDEXD10).

3.4.2 For β CD: Higher alcohols Inclusion complexes

The diffraction patterns obtained for β CD: higher alcohols complexes are presented in the figure 3.9 and 3.10 in comparison found in the literature with different diffraction patterns as explained in chapter 2.

Complexes pattern obtained for β CD: Pentanol and β CD: Hexanol produced similar pattern to the one already present in the literature, named as PUKPIU²⁴. For these complexes, we

proposed channel type structure which is in accordance with the conclusion made from the proton NMR studies in solution.

The other β CD: higher alcohols patterns resembled CACPOM²⁵. We propose for these complexes, a structure based upon a dimer brick organisation with stoichiometry of 2 CD for 1 alcohol molecule in accordance with the results obtained by proton NMR. This result sustains if we consider that the molecular organisation in the solution constructs the premises of the solid state packing.

The powders seem to have lost their crystalline character and acquired amorphous character²⁶⁻²⁸ in comparison to crystalline pattern obtained for uncomplexed β CD. Only selective sharp peaks are observed for example-The peak at 5.6° and 11.9°. In rest of the pattern, many superimposed peaks are present creating 'a hump' kind of appearance. These superimposed peaks are difficult to be distinguished. This appearance is generally characteristic of a disordered inclusion complex present in the system.

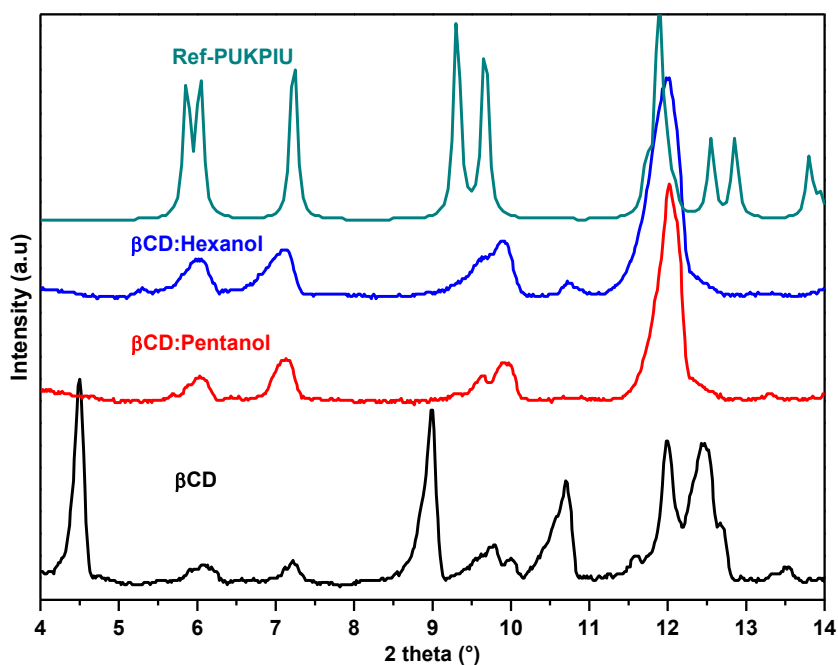


Figure 3.9 : Powder x-ray diffraction for inclusion complex of β CD: Higher alcohols in molar ratio 1:1 compared with PUKPIU.

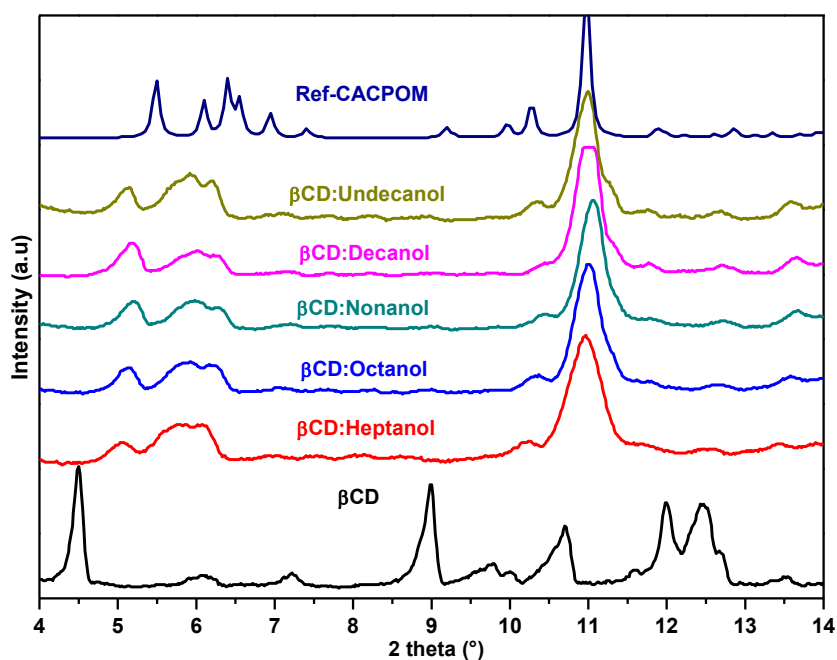


Figure 3.10 : Powder x-ray diffraction for inclusion complex of β CD: Higher alcohols in molar ratio 1:1 compared with reference CACPOM.

3.5 Raman spectroscopic analysis of β CD: Linear alcohol complexes

When inclusion takes place, the spectrum contains the peaks corresponding to both the host and the guest which can be generally shifted in their positions or intensity may be altered. In the solid form of inclusion, the different types of non-covalent interactions such as hydrophobic, Van der Waals interactions and hydrogen bonding lower the energy of the included guest leading to the reduced intensities of the corresponding bands. We have observed Raman Spectra for all β CD: Linear alcohol complexes prepared. All linear alcohols show similar type of Raman Spectra with typical peak positions. They are quickly summarized in the table 3.7.

Alcohol (O-H)	Wavenumber (cm^{-1})	Vibrational mode
O-H (free)	3600-3650	Stretch
O-H (H-bond)	3300-3400	Stretch
C-H	2850-3000	Stretch
CH ₂	2864	Stretch
CH ₂	1400-1450	Bend
C-O-H	1220-1440	Bend
C-O (primary alcohol)	1050 (base value)	Stretch

Table 3.7 : Vibrational regions assigned to alcohols.

3.5.1 Raman Spectral Studies β CD: Lower alcohols

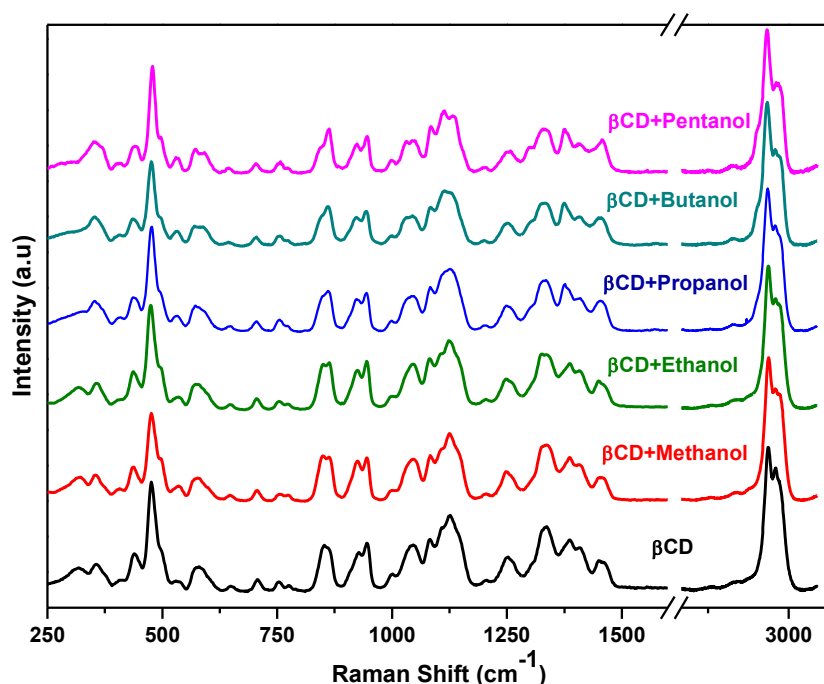


Figure 3.11 : Raman Spectra for inclusion complex of β CD: Lower alcohols in molar ratio 1:1.

The figure 3.11 shows the Raman spectra of all the complexes prepared with lower alcohols. It can be seen that all the spectra obtained are very similar to that of the spectrum obtained for uncomplexed β CD. Appearance of new peaks or disappearance of the characteristic peaks have not been observed. Moreover, the intensity of the peaks remains same. The reason behind this observation is the superposition of β CD and alcohols peaks.

3.5.2 Raman Spectral Studies β CD: Higher alcohols

On moving towards longer alcohols, the spectra have changed at two positions for each β CD: Higher alcohol complex. The changes can be observed between regions $1357\text{-}1488\text{ cm}^{-1}$ and $2814\text{-}2879\text{ cm}^{-1}$ of the spectra (Figure 3.12). These regions fall in the same vibrational regions active for linear alcohols as shown in the table above. Other peaks corresponding to alcohols might be present in the spectra but they remain undetected due to superposition of β CD peaks.

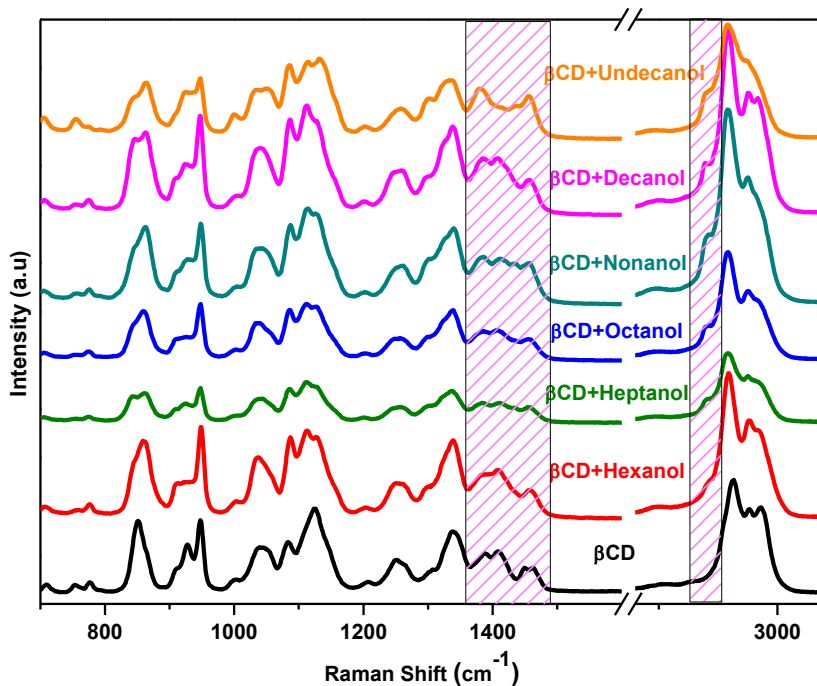


Figure 3.12 : Raman Spectra for inclusion complex of β CD: higher alcohols in molar ratio 1:1.

3.6 Molecular modelling studies of β CD: Alcohol complexes

3.6.1 Stability study of the β CD: alcohol complexes by manual docking

We have investigated systematically the stability of the alcohol-cyclodextrin complexes in water by manual docking using the semi empirical PM3 level of theory as explained in the chapter 2. Convergence of the optimised structures has been checked by computation of positive frequencies. All calculations were done on the MAGI supercomputer of the PARIS 13 university located at Villetaneuse.

The results of inclusion in function of the center mass position along the Z-axis have been compared with the lengths L of the alcohol molecules (from approximately 1.7 Å for methanol to 16 Å for dodecanol with an increment of 1.3 Å for each carbon added) and the thickness T of the β CD molecule (approximately 5 Å along the Z-axis).

We can consider that an alcohol molecule enters in the cavity for the position $\frac{1}{2}(L+T)$ along Z-axis and exists for the position $-\frac{1}{2}(L+T)$ along Z-axis. The zone is highlighted in each graphs presented below. We can consider that the system increases its stability by inclusion when there is a significant decrease of the value of the negative binding energy in this region.

The results obtained with molecular modeling are directly in relation with our experimental observations in solutions by NMR and powder diffraction analysis in the solid state with two major classes : smaller alcohols from methanol with butanol and longer alcohols from pentanol to undecanol.

3.6.1.1 β CD: Methanol complex :

Considering that the length L of the methanol molecule is approximately 1.7 \AA , we can consider that a methanol molecule enters in the cavity for the position $+3.4 \text{ \AA}$ along Z-axis and exits for the position -3.4 \AA along Z-axis (Figure 3.13). Table 3.8 lists all thermodynamic and electronic features of the two orientations considered.

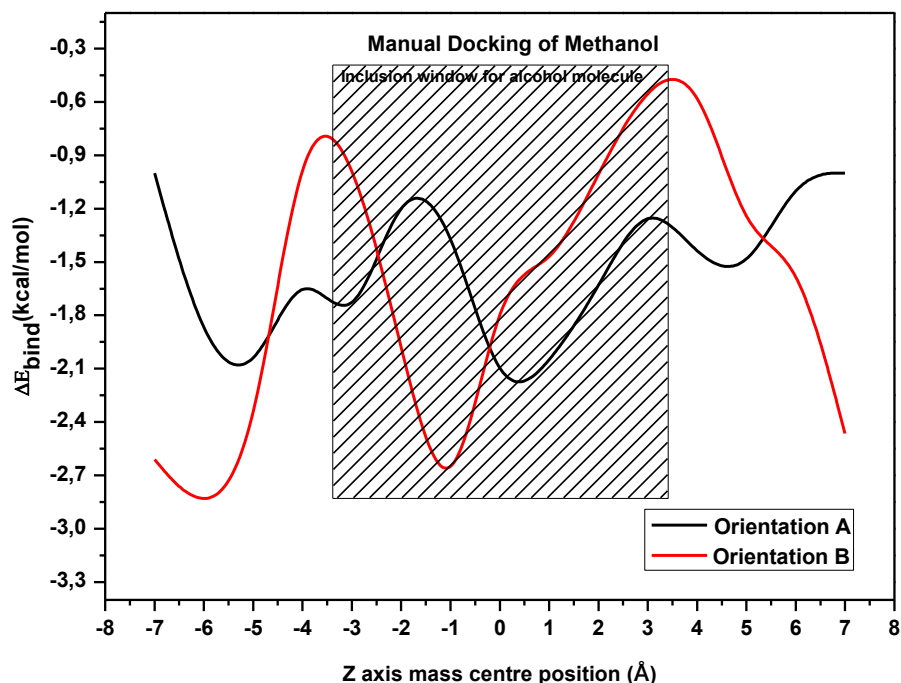


Figure 3.13 : Evolution of the binding energy changes ΔE_{bind} (kcal/mol) in function of the starting position of methanol along Z-axis for the two orientations.

	β CD	Methanol	Complex β CD :Methanol	
			Orientation A	Orientation B
E (kcal/mol)	-695.183	-20.205	-718.486	-717.707
ΔE_{bind} (kcal/mol)			-3.097	-2.319
H (kcal/mol)	-694.591	-19.613	-717.893	-717.115
ΔH (kcal/mol)			-3.690	-2.911
G (kcal/mol)	-815.265	-36.699	-844.185	-844.869
ΔG (kcal/mol)			7.780	7.095
S (kcal/mol.K)	0.405	0.057	0.424	0.428
ΔS (kcal/mol.K)			-0.038	-0.034
E_{HOMO} (Ha)	0.057	0.130	0.057	0.057
E_{LUMO} (Ha)	-0.395	-0.412	-0.395	-0.395
E_{HOMO} (eV)	1.542	3.535	1.545	1.549
E_{LUMO} (eV)	-10.755	-11.207	-10.750	-10.750

G(eV)	12.297	14.742	12.295	12.300
μ (eV)	-4.607	-3.836	-4.602	-4.600
η (eV)	6.149	7.371	6.148	6.150
ω (eV)	1.726	0.998	1.723	1.721
Dipole moment (D)	10.953	1.663	10.786	11.871

Table 3.8: Energies features. thermodynamic and electronic parameters of β CD:methanol complexes by PM3 method for the more thermodynamically favorable complex of each orientation.

3.6.1.2 β CD: ethanol complex:

Considering that the length L of the ethanol molecule is approximately 3 Å, we can consider that an ethanol molecule enters in the cavity for the position +4 Å along Z-axis and exits for the position -4 Å along Z-axis (Figure 3.14). Table 3.13 lists all thermodynamic and electronic features of the two orientations considered.

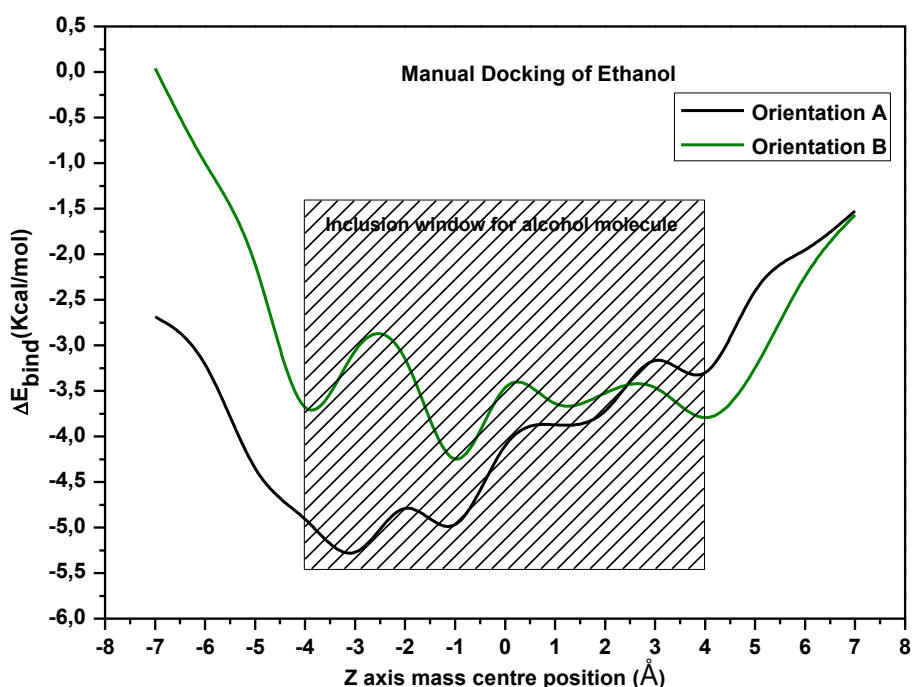


Figure 3.14 : Evolution of the binding energy changes ΔE_{bind} (kcal/mol) in function of the starting position of ethanol along Z-axis for the two orientations.

	β CD	Ethanol	Complex β CD :Ethanol	
			Orientation A	Orientation B
E (kcal/mol)	-695.183	-8.623	-709.398	-708.728
ΔE_{bind} (kcal/mol)			-5.592	-4.922
H (kcal/mol)	-694.591	-8.030	-708.805	-708.136
ΔH (kcal/mol)			-6.184	-5.515

G (kcal/mol)	-815.265	-27.379	-835.341	-834.450
ΔG (kcal/mol)			7.304	8.195
S (kcal/mol.K)	0.405	0.065	0.424	0.424
ΔS (kcal/mol.K)			-0.045	-0.046
E_{HOMO} (Ha)	0.057	0.124	0.057	0.057
E_{LUMO} (Ha)	-0.395	-0.413	-0.395	-0.395
E_{HOMO} (eV)	1.542	3.372	1.548	1.545
E_{LUMO} (eV)	-10.755	-11.247	-10.750	-10.751
G (eV)	12.297	14.619	12.298	12.296
μ (eV)	-4.607	-3.938	-4.601	-4.603
η (eV)	6.149	7.310	6.149	6.148
ω (eV)	1.726	1.061	1.722	1.723
Dipole moment (D)	10.953	1.776	11.364	12.216

Table 3.9: Energies features. thermodynamic and electronic parameters of β CD:ethanol complexes by PM3 method for the more thermodynamically favorable complex of each orientation.

3.6.1.3 β CD: propanol complex:

Considering that the length L of the propanol molecule is approximately 4.3 \AA , we can consider that a propanol molecule enters in the cavity for the position $+4.7 \text{ \AA}$ along Z-axis and exits for the position -4.7 \AA along Z-axis (Figure 3.15). Table 3.10 lists all thermodynamic and electronic features of the two orientations considered.

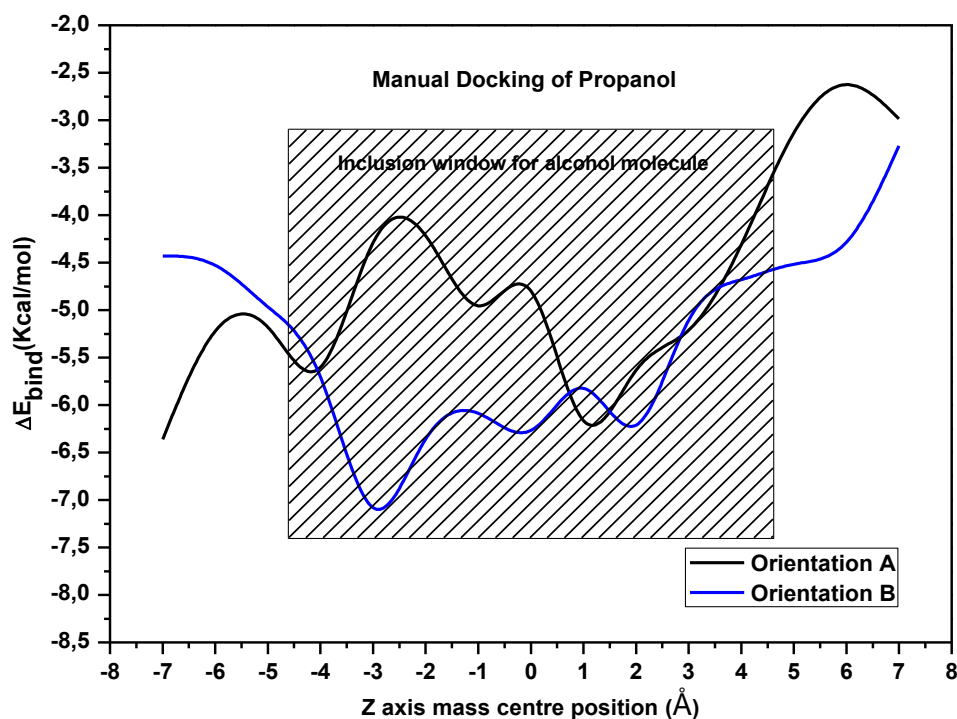


Figure 3.15 : Evolution of the binding energy changes ΔE_{bind} (kcal/mol) in function of the starting position of propanol along Z-axis for the two orientations.

	β CD	Propanol	Complex β CD :Propanol	
			Orientation A	Orientation B
E (kcal/mol)	-695.183	4.403	-697.645	-698.532
ΔE_{bind} (kcal/mol)			-6.865	-7.752
H (kcal/mol)	-694.591	4.996	-697.053	-697.940
ΔH (kcal/mol)			-7.457	-8.345
G (kcal/mol)	-815.265	-16.761	-826.723	-824.716
ΔG (kcal/mol)			5.303	7.310
S (kcal/mol.K)	0.405	0.073	0.435	0.425
ΔS (kcal/mol.K)			-0.043	-0.053
E_{HOMO} (Ha)	0.057	0.119	0.057	0.057
E_{LUMO} (Ha)	-0.395	-0.411	-0.395	-0.395
E_{HOMO} (eV)	1.542	3.247	1.543	1.552
E_{LUMO} (eV)	-10.755	-11.184	-10.749	-10.751
G(eV)	12.297	14.431	12.292	12.303
μ (eV)	-4.607	-3.969	-4.603	-4.600
η (eV)	6.149	7.215	6.146	6.151
ω (eV)	1.726	1.091	1.724	1.720
Dipole moment (D)	10.953	1.771	9.971	10.894

Table 3.10: Energies features. thermodynamic and electronic parameters of β CD:propanol complexes by PM3 method for the more thermodynamically favorable complex of each orientation.

3.6.1.4 β CD: Butanol complex :

Considering that the length L of the butanol molecule is approximately 5.6 Å, we can consider that a butanol molecule enters in the cavity for the position +5.3 Å along Z-axis and exits for the position -5.3 Å along Z-axis(Figure 3.16). Table 3.11 lists all thermodynamic and electronic features of the two orientations considered.

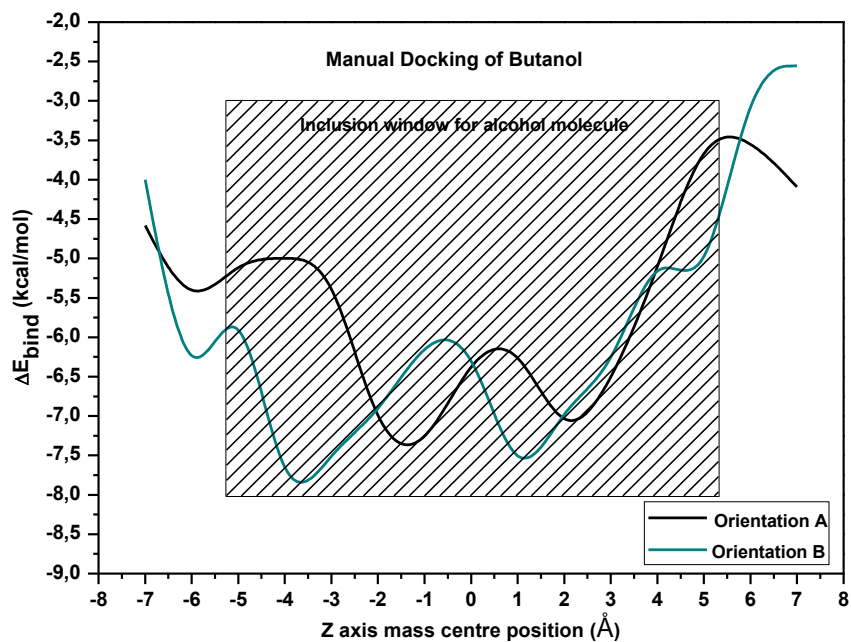


Figure 3.16 : Evolution of the binding energy changes ΔE_{bind} (kcal/mol) in function of the starting position of Butanol along Z-axis for the two orientations.

	β CD	Butanol	Complex β CD :Butanol	
			Orientation A	Orientation B
E (kcal/mol)	-695.183	17.341	-685.336	-686.204
ΔE_{bind} (kcal/mol)			-7.494	-8.362
H (kcal/mol)	-694.591	17.934	-684.744	-685.612
ΔH (kcal/mol)			-8.087	-8.955
G (kcal/mol)	-815.265	-6.068	-815.578	-815.038
ΔG (kcal/mol)			5.756	6.296
S (kcal/mol.K)	0.405	0.081	0.439	0.434
ΔS (kcal/mol.K)			-0.046	-0.051
E_{HOMO} (Ha)	0.057	0.116	0.057	0.057
E_{LUMO} (Ha)	-0.395	-0.412	-0.395	-0.395
E_{HOMO} (eV)	1.542	3.169	1.550	1.546
E_{LUMO} (eV)	-10.755	-11.208	-10.748	-10.752
G(eV)	12.297	14.376	12.298	12.298
μ (eV)	-4.607	-4.019	-4.599	-4.603
η (eV)	6.149	7.188	6.149	6.149
ω (eV)	1.726	1.124	1.720	1.723
Dipole moment (D)	10.953	1.776	10.484	12.074

Table 3.11: Energies features. thermodynamic and electronic parameters of β CD:Butanol complexes by PM3 method for the more thermodynamically favorable complex of each orientation.

3.6.1.5 β CD:Pentanol complex:

Considering that the length L of the pentanol molecule is approximately 6.9 Å, we can consider that a pentanol molecule enters in the cavity for the position +6 Å along Z-axis and exits for the position -6 Å along Z-axis (Figure 3.17). Table 3.12 lists all thermodynamic and electronic features of the two orientations considered.

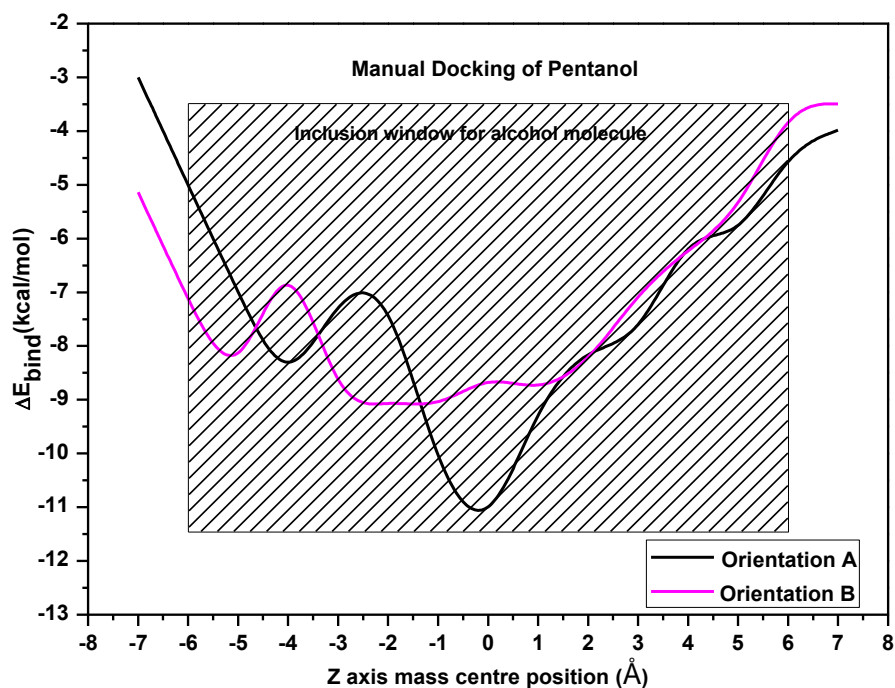


Figure 3.17 : Evolution of the binding energy changes ΔE_{bind} (kcal/mol) in function of the starting position of pentanol along Z-axis for the two orientations.

	β CD	Pentanol	Complex β CD :Pentanol	
			Orientation A	Orientation B
E (kcal/mol)	-695.183	30.235	-676.567	-674.195
ΔE_{bind} (kcal/mol)			-11.618	-9.246
H (kcal/mol)	-694.591	30.827	-675.975	-673.603
ΔH (kcal/mol)			-12.211	-9.839
G (kcal/mol)	-815.265	4.494	-804.589	-803.913
ΔG (kcal/mol)			6.183	6.859
S (kcal/mol.K)	0.405	0.088	0.431	0.437
ΔS (kcal/mol.K)			-0.062	-0.056
E_{HOMO} (Ha)	0.057	0.115	0.057	0.057
E_{LUMO} (Ha)	-0.395	-0.412	-0.396	-0.395
E_{HOMO} (eV)	1.542	3.117	1.539	1.542

EL _{UMO} (eV)	-10.755	-11.206	-10.771	-10.758
G(eV)	12.297	14.323	12.310	12.300
μ (eV)	-4.607	-4.045	-4.616	-4.608
η (eV)	6.149	7.161	6.155	6.150
ω (eV)	1.726	1.142	1.731	1.726
Dipole moment (D)	10.953	1.779	10.045	11.435

Table 3.12: Energies features. thermodynamic and electronic parameters of βCD:pentanol complexes by PM3 method for the more thermodynamically favorable complex of each orientation.

3.6.1.6 βCD:Hexanol complex:

Considering that the length L of the hexanol molecule is approximately 8.2 Å, we can consider that a hexanol molecule enters in the cavity for the position +6.6 Å along Z-axis and exits for the position -6.6 Å along Z-axis (Figure 3.18). Table 3.13 lists all thermodynamic and electronic features of the two orientations considered.

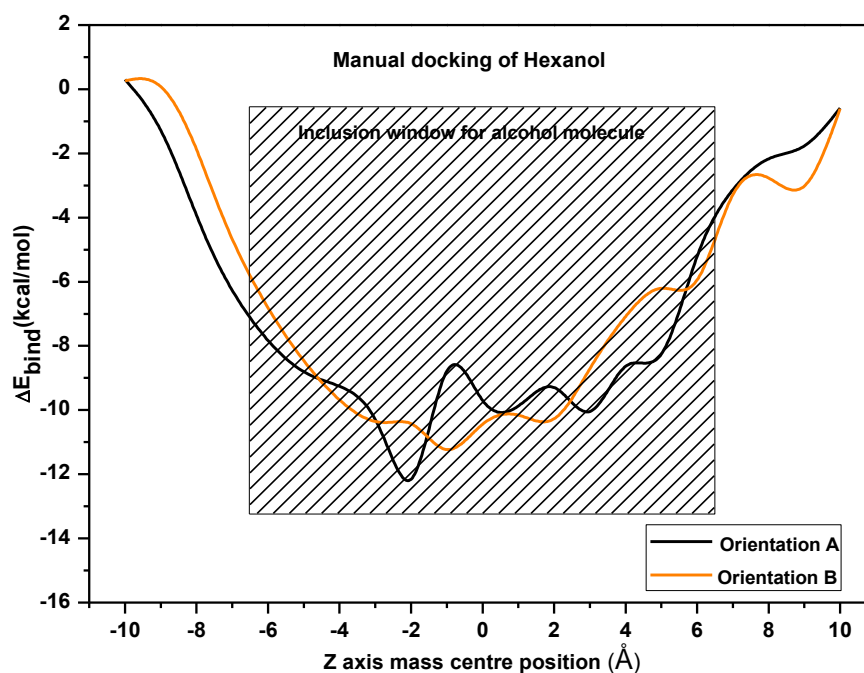


Figure 3.18 : Evolution of the binding energy changes ΔE_{bind} (kcal/mol) in function of the starting position of Hexanol along Z-axis for the two orientations.

	β CD	Hexanol	Complex β CD :Hexanol	
			Orientation A	Orientation B
E (kcal/mol)	-695.183	43.139	-666.239	-663.836
ΔE_{bind} (kcal/mol)			-14.196	-11.792
H (kcal/mol)	-694.591	43.732	-665.646	-663.244
ΔH (kcal/mol)			-14.787	-12.385
G (kcal/mol)	-815.265	15.110	-796.530	-794.790
ΔG (kcal/mol)			3.624	5.365
S (kcal/mol.K)	0.405	0.096	0.439	0.441
ΔS (kcal/mol.K)			-0.062	-0.060
E_{HOMO} (Ha)	0.057	0.113	0.056	0.056
E_{LUMO} (Ha)	-0.395	-0.412	-0.396	-0.395
E_{HOMO} (eV)	1.542	3.081	1.524	1.535
E_{LUMO} (eV)	-10.755	-11.208	-10.782	-10.752
G(eV)	12.297	14.288	12.306	12.287
μ (eV)	-4.607	-4.063	-4.629	-4.608
η (eV)	6.149	7.144	6.153	6.144
ω (eV)	1.726	1.156	1.741	1.728
Dipole moment (D)	10.953	1.779	11.197	10.520

Table 3.13: Energies features. thermodynamic and electronic parameters of β CD:Hexanol complexes by PM3 method for the more thermodynamically favorable complex of each orientation.

3.6.1.7 β CD:Heptanol complex:

Considering that the length L of the heptanol molecule is approximately 9.5 Å, we can consider that a heptanol molecule enters in the cavity for the position +7.3 Å along Z-axis and exits for the position -7.3 Å along Z-axis (Figure 3.19). Table 3.14 lists all thermodynamic and electronic features of the two orientations considered.

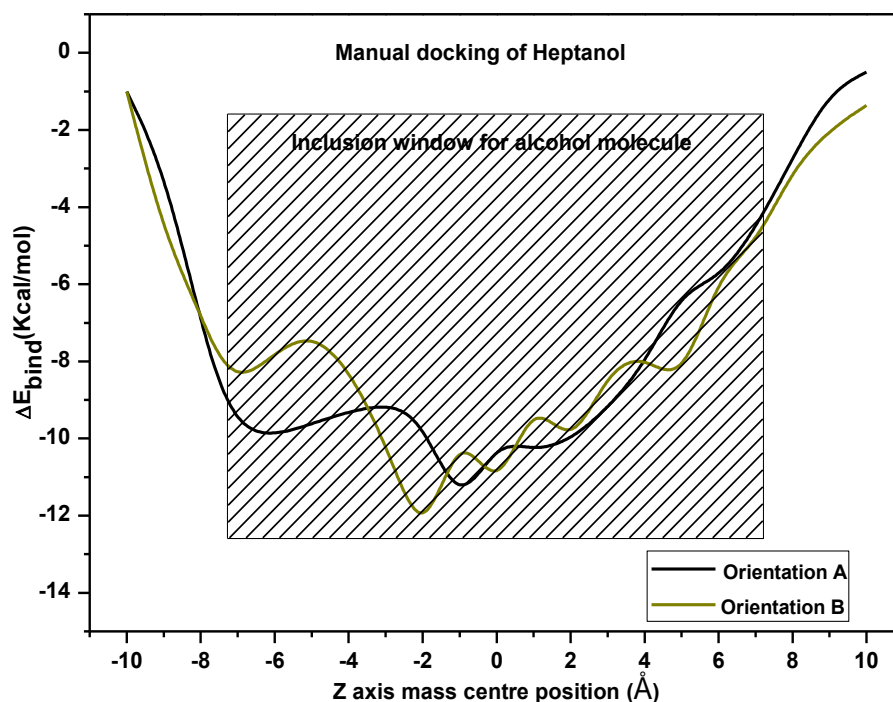


Figure 3.19 : Evolution of the binding energy changes ΔE_{bind} (kcal/mol) in function of the starting position of Heptanol along Z-axis for the two orientations.

	β CD	Heptanol	Complex β CD :Heptanol	
			Orientation A	Orientation B
E (kcal/mol)	-695.183	56.023	-651.083	-652.211
ΔE_{bind} (kcal/mol)			-11.923	-13.051
H (kcal/mol)	-694.591	56.616	-650.490	-651.618
ΔH (kcal/mol)			-12.516	-13.644
G (kcal/mol)	-815.265	25.676	-783.269	-784.592
ΔG (kcal/mol)			6.320	4.997
S (kcal/mol.K)	0.405	0.104	0.445	0.446
ΔS (kcal/mol.K)			-0.063	-0.063
E_{HOMO} (Ha)	0.057	0.112	0.057	0.053
E_{LUMO} (Ha)	-0.395	-0.412	-0.395	-0.396
E_{HOMO} (eV)	1.542	3.056	1.550	1.435
E_{LUMO} (eV)	-10.755	-11.206	-10.758	-10.778
G(eV)	12.297	14.262	12.308	12.214
μ (eV)	-4.607	-4.075	-4.604	-4.672
η (eV)	6.149	7.131	6.154	6.107
ω (eV)	1.726	1.164	1.722	1.787
Dipole moment (D)	10.953	1.781	10.084	11.669

Table 3.14: Energies features. thermodynamic and electronic parameters of β CD:Heptanol complexes by PM3 method for the more thermodynamically favorable complex of each orientation.

3.6.1.8 β CD:Octanol complex:

Considering that the length L of the octanol molecule is approximately 10.8 \AA , we can consider that an octanol molecule enters in the cavity for the position $+7.9 \text{ \AA}$ along Z-axis and exits for the position -7.9 \AA along Z-axis (Figure 3.20). Table 3.15 lists all thermodynamic and electronic features of the two orientations considered.

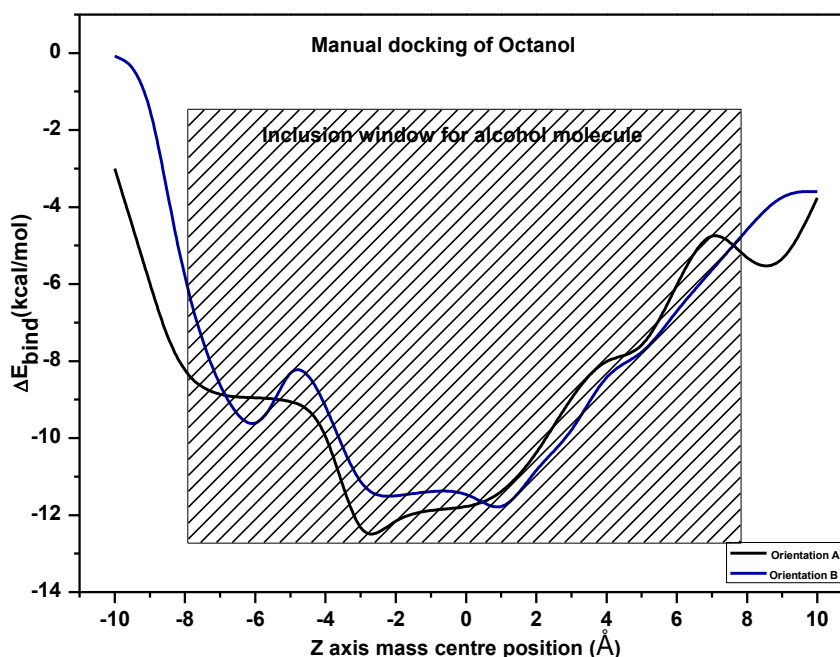


Figure 3.20 : Evolution of the binding energy changes ΔE_{bind} (kcal/mol) in function of the starting position of Octanol along Z-axis for the two orientations.

	β CD	Octanol	Complex β CD :Octanol	
			Orientation A	Orientation B
E (kcal/mol)	-695.183	68.924	-639.429	-638.439
ΔE_{bind} (kcal/mol)			-13.170	-12.180
H (kcal/mol)	-694.591	69.517	-638.836	-637.847
ΔH (kcal/mol)			-13.762	-12.773
G (kcal/mol)	-815.265	36.284	-771.660	-775.514
ΔG (kcal/mol)			7.321	3.467
S (kcal/mol.K)	0.405	0.111	0.445	0.462
ΔS (kcal/mol.K)			-0.071	-0.054
E_{HOMO} (Ha)	0.057	0.112	0.056	0.056

$E_{LUMO}(Ha)$	-0.395	-0.412	-0.396	-0.395
$E_{HOMO}(eV)$	1.542	3.038	1.523	1.534
$E_{LUMO}(eV)$	-10.755	-11.206	-10.763	-10.756
$G(eV)$	12.297	14.244	12.286	12.291
$\mu (eV)$	-4.607	-4.084	-4.620	-4.611
$\eta (eV)$	6.149	7.122	6.143	6.145
$\omega (eV)$	1.726	1.171	1.737	1.730
Dipole moment (D)	10.953	1.780	9.844	11.724

Table 3.15: Energies features. thermodynamic and electronic parameters of β CD:Octanol complexes by PM3 method for the more thermodynamically favorable complex of each orientation.

3.6.1.9 β CD:Nonanol complex:

Considering that the length L of the nonanol molecule is approximately 12.1 Å, we can consider that a nonanol molecule enters in the cavity for the position +8.6 Å along Z-axis and exits for the position -8.6 Å along Z-axis(Figure 3.21). Table 3.16 lists all thermodynamic and electronic features of the two orientations considered.

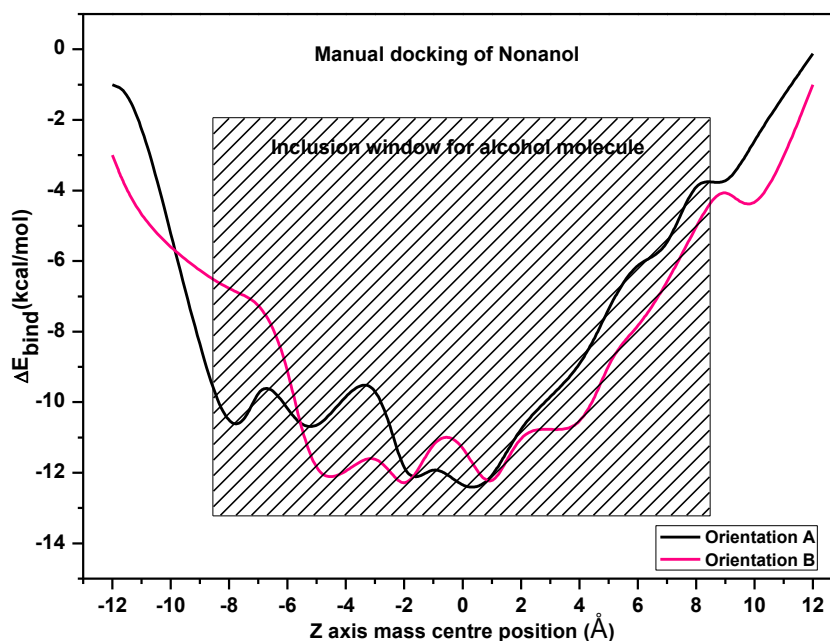


Figure 3.21 : Evolution of the binding energy changes ΔE_{bind} (kcal/mol) in function of the starting position of Nonanol along Z-axis for the two orientations.

	β CD	Nonanol	Complex β CD :Nonanol	
			Orientation A	Orientation B
E (kcal/mol)	-695.183	81.809	-626.155	-626.514
ΔE_{bind} (kcal/mol)			-12.780	-13.139
H (kcal/mol)	-694.591	82.401	-625.562	-625.921
ΔH (kcal/mol)			-13.373	-13.732
G (kcal/mol)	-815.265	46.859	-763.200	-763.038
ΔG (kcal/mol)			5.206	5.368
S (kcal/mol.K)	0.405	0.119	0.462	0.460
ΔS (kcal/mol.K)			-0.062	-0.064
E_{HOMO} (Ha)	0.057	0.111	0.057	0.057
E_{LUMO} (Ha)	-0.395	-0.412	-0.396	-0.396
E_{HOMO} (eV)	1.542	3.024	1.561	1.560
E_{LUMO} (eV)	-10.755	-11.206	-10.769	-10.780
G(eV)	12.297	14.230	12.329	12.339
μ (eV)	-4.607	-4.091	-4.604	-4.610
η (eV)	6.149	7.115	6.165	6.170
ω (eV)	1.726	1.176	1.719	1.722
Dipole moment (D)	10.953	1.781	9.873	11.701

Table 3.16: Energies features. thermodynamic and electronic parameters of β CD:Nonanol complexes by PM3 method for the more thermodynamically favorable complex of each orientation.

3.6.1.10 β CD: Decanol complex:

Considering that the length L of the decanol molecule is approximately 13.4 Å, we can consider that a decanol molecule enters in the cavity for the position +9.2 Å along Z-axis and exits for the position -9.2 Å along Z-axis(Figure 3.22). Table 3.17 lists all thermodynamic and electronic features of the two orientations considered.

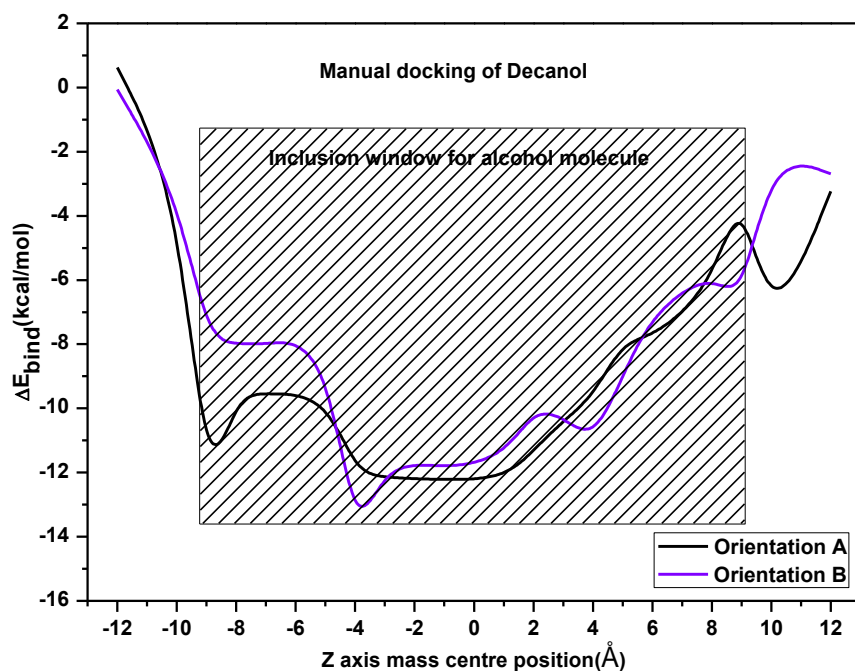


Figure 3.22 : Evolution of the binding energy changes ΔE_{bind} (kcal/mol) in function of the starting position of Decanol along Z-axis for the two orientations.

	β CD	Decanol	Complex β CD :Decanol	
			Orientation A	Orientation B
E (kcal/mol)	-695.183	94.706	-610.027	-614.914
ΔE_{bind} (kcal/mol)			-9.550	-14.437
H (kcal/mol)	-694.591	95.299	-609.435	-614.322
ΔH (kcal/mol)			-10.142	-15.029
G (kcal/mol)	-815.265	57.454	-752.316	-751.178
ΔG (kcal/mol)			5.495	6.633
S (kcal/mol.K)	0.405	0.127	0.479	0.459
ΔS (kcal/mol.K)			-0.052	-0.073
E_{HOMO} (Ha)	0.057	0.111	0.057	0.056
E_{LUMO} (Ha)	-0.395	-0.412	-0.396	-0.396
E_{HOMO} (eV)	1.542	3.013	1.552	1.513
E_{LUMO} (eV)	-10.755	-11.207	-10.769	-10.763
G(eV)	12.297	14.220	12.321	12.277
μ (eV)	-4.607	-4.097	-4.608	-4.625
η (eV)	6.149	7.110	6.160	6.138
ω (eV)	1.726	1.180	1.724	1.742
Dipole moment (D)	10.953	1.780	10.996	11.649

Table 3.17: Energies features. thermodynamic and electronic parameters of β CD:Decanol complexes by PM3 method for the more thermodynamically favorable complex of each orientation.

3.6.1.11 β CD: Undecanol complex:

Considering that the length L of the undecanol molecule is approximately 14.7 Å, we can consider that an undecanol molecule enters in the cavity for the position +9.9 Å along Z-axis and exits for the position -9.9 Å along Z-axis (Figure 3.23). Table 3.18 lists all thermodynamic and electronic features of the two orientations considered.

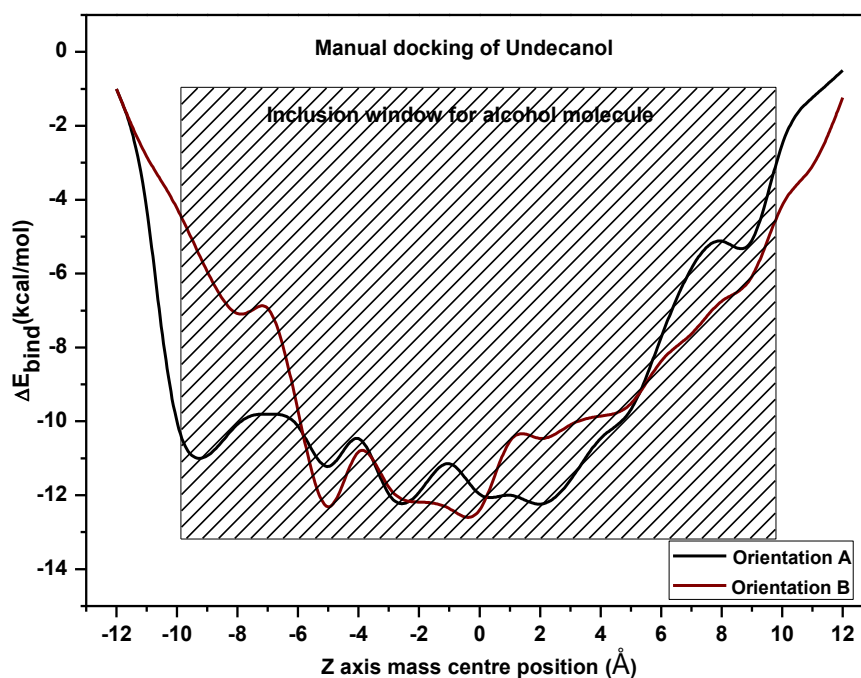


Figure 3.23 : Evolution of the binding energy changes ΔE_{bind} (kcal/mol) in function of the starting position of Undecanol along Z-axis for the two orientations.

	β CD	Undecanol	Complex β CD :Undecanol	
			Orientation A	Orientation B
E (kcal/mol)	-695.18	107.59341	-599.96	-601.20
ΔE_{bind} (kcal/mol)			-12.37	-13.61
H (kcal/mol)	-694.59	108.18578	-599.37	-600.61
ΔH (kcal/mol)			-12.96	-14.20
G (kcal/mol)	-815.27	68.045248	-744.78	-741.51
ΔG (kcal/mol)			2.44	5.71
S (kcal/mol.K)	0.40	0.13	0.49	0.47
ΔS (kcal/mol.K)			-0.05	-0.07

$E_{\text{HOMO}}(\text{Ha})$	0.06	0.11	0.06	0.06
$E_{\text{LUMO}}(\text{Ha})$	-0.40	-0.41	-0.40	-0.40
$E_{\text{HOMO}}(\text{eV})$	1.54	3.01	1.53	1.55
$E_{\text{LUMO}}(\text{eV})$	-10.76	-11.21	-10.76	-10.78
$G(\text{eV})$	12.30	14.21	12.30	12.34
μ (eV)	-4.61	-4.10	-4.61	-4.62
η (eV)	6.15	7.11	6.15	6.17
ω (eV)	1.726	1.183	1.732	1.726
Dipole moment (D)	10.95	1.78	10.6396	11.75

Table 3.18: Energies features. thermodynamic and electronic parameters of βCD : Undecanol complexes by PM3 method for the more thermodynamically favorable complex of each orientation.

3.6.1.12 βCD :dodecanol complex:

Considering that the length L of the dodecanol molecule is approximately 16 \AA , we can consider that a dodecanol molecule enters in the cavity for the position $+10.5 \text{ \AA}$ along Z-axis and exits for the position -10.5 \AA along Z-axis (Figure 3.24). Table 3.19 lists all thermodynamic and electronic features of the two orientations considered.

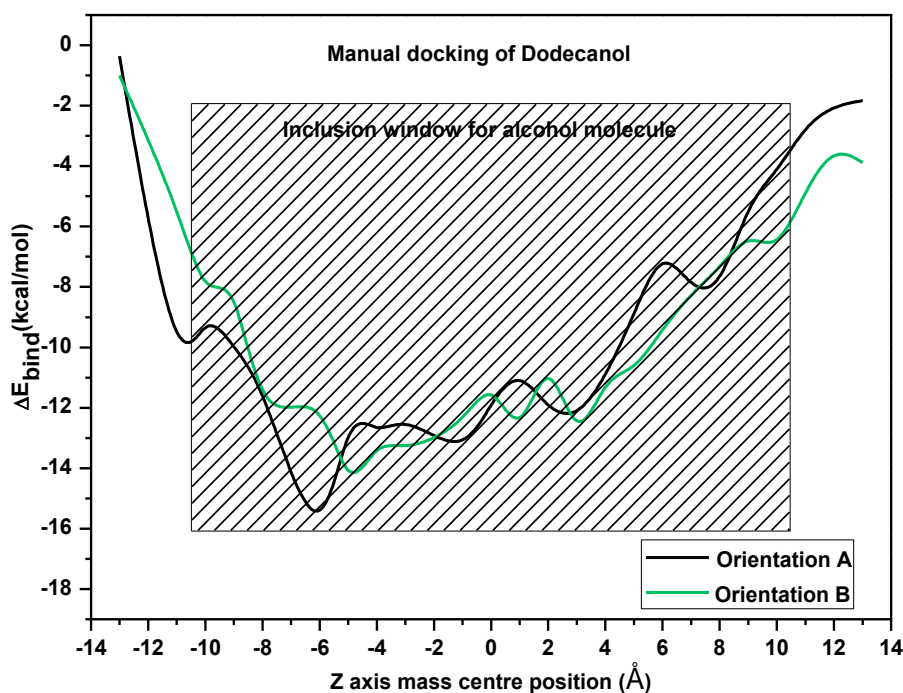


Figure 3.24 : Evolution of the binding energy changes ΔE_{bind} (kcal/mol) in function of the starting position of Dodecanol along Z-axis for the two orientations.

	β CD	Dodecanol	Complex β CD :Dodecanol	
			Orientation A	Orientation B
E (kcal/mol)	-695.18	120.4881	-592.05	-589.76
ΔE_{bind} (kcal/mol)			-17.36	-15.06
H (kcal/mol)	-694.59	121.08	-591.46	-589.16
ΔH (kcal/mol)			-17.95	-15.65
G (kcal/mol)	-815.27	78.63	-732.91	-730.59
ΔG (kcal/mol)			3.72	6.05
S (kcal/mol.K)	0.40	0.14	0.47	0.47
ΔS (kcal/mol.K)			-0.07	-0.07
E_{HOMO} (Ha)	0.06	0.11	0.06	0.06
E_{LUMO} (Ha)	-0.40	-0.41	-0.40	-0.40
E_{HOMO} (eV)	1.54	3.00	1.53	1.52
E_{LUMO} (eV)	-10.76	-11.21	-10.78	-10.76
G(eV)	12.30	14.21	12.31	12.28
μ (eV)	-4.61	-4.10	-4.63	-4.62
η (eV)	6.15	7.10	6.15	6.14
ω (eV)	1.726	1.186	1.739	1.739
Dipole moment (D)	10.95	1.78	11.9769	12.80

Table 3.19: Energies features. thermodynamic and electronic parameters of β CD: Dodecanol complexes by PM3 method for the more thermodynamically favorable complex of each orientation.

3.6.1.13 Discussion

Table 3.20 and figure 3.25 give a synthesis of the energetic features of the more stable complexes obtained during the theoretical study.

Negative values for ΔH and positive values for ΔG indicate that the formation of the complexes are exothermic and non-spontaneous processes. The ΔS for the complexation process makes a very small contribution to the positive value of ΔG in comparison to the heat effect. The entropy effect is generally in relation with the replacement of water molecules by guest molecules, their release outside the cavity and a reorganization in the structures. Our study uses an implicit solvation model that can reduce the energetic effect of this molecular reorganization. Moreover, the docked molecules tend to stay linear after computation although a complete docking process should include entropic variation in the guest conformation. However, this study gives results in accordance with experimental observations.

The electronic energetic and chemical parameters are all very similar in all the complexes and thus their evolution is not significant to a better understanding of the inclusion process.

Complex betaCD with	methano	ethano	propano	butano	pentano	hexano	heptano	octano	nonano	decano	undecano	dodecano
	1	2	3	4	5	6	7	8	9	10	11	12
E (kcal/mol)	-718.49	-709.40	-698.53	-686.20	-676.57	-666.24	-652.21	-639.43	-626.51	-614.91	-601.20	-592.05
ΔE_{bind} (kcal/mol)	-3.10	-5.59	-7.75	-8.36	-11.62	-14.20	-13.05	-13.17	-13.14	-14.44	-13.61	-17.36
H (kcal/mol)	-717.89	-708.81	-697.94	-685.61	-675.97	-665.65	-651.62	-638.84	-625.92	-614.32	-600.61	-591.46
ΔH (kcal/mol)	-3.69	-6.18	-8.34	-8.95	-12.21	-14.79	-13.64	-13.76	-13.73	-15.03	-14.20	-17.95
G (kcal/mol)	-844.18	-835.34	-824.72	-815.04	-804.59	-796.53	-784.59	-771.66	-763.04	-751.18	-741.51	-732.91
ΔG (kcal/mol)	7.78	7.30	7.31	6.30	6.18	3.62	5.00	7.32	5.37	6.63	5.71	3.72
S (kcal/mol.K)	0.42	0.42	0.43	0.43	0.43	0.44	0.45	0.45	0.46	0.46	0.47	0.47
ΔS (kcal/mol.K)	-0.04	-0.05	-0.05	-0.05	-0.06	-0.06	-0.06	-0.07	-0.06	-0.07	-0.07	-0.07

Table 3.20 : Energetic features and thermodynamic parameters for linear alcohol inclusion complexes by PM3 manual docking method.

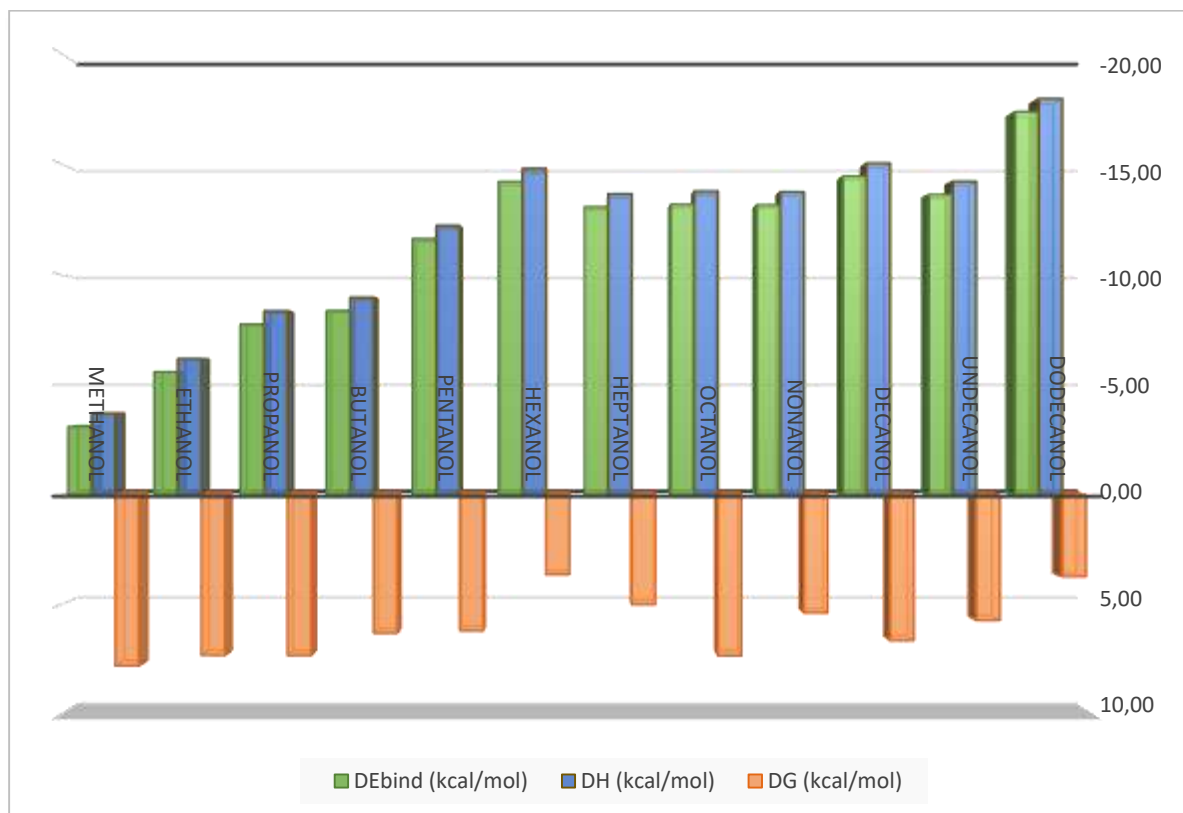


Figure 3.25 : Binding energy ΔE_{bind} (kcal/mol) (in green), ΔH (kcal/mol) (in blue) and ΔG (kcal/mol) (in orange) results from PM3 manual docking of a linear primary alcohol molecule in β CD. Energy axis is inverted to allow a better visualization of the results

Typically, the more negative the binding energy is, the stronger the interaction is between the host and the guest considered. Thus, the stability of the inclusion complexes tends to increase from methanol to hexanol and is then quite similar for hexanol to dodecanol.

The inclusion complexation of the methanol molecule do not change significantly the energy of the system. It confirms that the methanol molecule can randomly replace any water molecule inside or outside the cavity. In all the structures obtained by manual docking, the methanol molecule stay centered in the cavity as in the starting job files.

Behaviours of methanol, ethanol, propanol and butanol are very similar with no significant gain in energy due to the inclusion process in β CD and inclusion of the alcohol molecule aligned with the center of the cavity.

Our experimental results indicating that methanol to butanol tend to have a behaviour comparable to a molecule of water solvent with no choice between a position inside or outside the cyclodextrin cavity. A value of binding energy above -10 kcal/mol may indicate a non significant interaction.

The thickness of the cyclodextrin ring can almost insert the aliphatic chain of the primary alcohol starting from pentanol. In case of inclusion of pentanol in the cavity, there is a little increase of stability with a significant value of the binding energy below -10 kcal/mol . The inside hydrophobic cyclodextrin cavity stabilizes the aliphatic part of the guest molecule from the effect of the polar implicit solvent outside. The optimised docked structures present a

slightly tilted pentanol molecule in the cavity. We have observed inclusion of pentanol with a stoichiometry of 1:1 by NMR and channel structural type by PXRD in accordance with the theoretical result.

In the case of heptanol and longer alcohol molecules, there are more than one starting positions to obtain a minimum value for the binding energy because there are many different possibilities to insert the aliphatic chain in the cavity as it is longer than the thickness of the cyclodextrin cavity. This observation can be put in relation with two facts observed in the solid state structures available: (i) Molecules presenting long length chains are frequently described with a high level of disorder as there are many energetic equivalent possibilities to insert them in the cavity and (ii) Molecules presenting long length chains are frequently complexed by cyclodextrin dimers in brick type structures.

The values obtained for binding energies are equivalent in the case of the inclusion of heptanol and longer alcohol molecules in a β CD when considering an implicit water solvent environment. An interesting extension of this work would consist in the complexation of alcohol by cyclodextrin dimers.

3.7 Conclusion

All the work explained in this chapter has marked as the first step of this thesis. The inclusion complexes of β CD and alcohols have shown interesting results. We have tried to form complexes of β CD along with the homologous series of aliphatic linear alcohols. The complexes prepared were further characterized with different characterization techniques to understand the behaviour and complexation forming ability of each alcohol used. The objective was to know which of the following alcohols form channel type crystal structure arrangement such that the arrangement allows us to capture aromatic hydrocarbons which are generally termed as 'Water Pollutants'.

It has been concluded from all the results obtained in the liquid state as well as the solid state that lower alcohols up to Butanol (=4C) do not show interesting inclusion complexes results with β CD. On interpreting NMR results, it can be concluded that lower alcohols are unable to displace H3 and H5 protons peak because they are not included in the cavity but distributed randomly in the structure to replace solvent water molecules. Therefore, their use to form complexes with aromatic hydrocarbons exhibiting a channel type opened structure is doubtful. On the contrary, the higher alcohols were successful in showing positive displacement results for H3 and H5 protons which is a spontaneous phenomenon while forming inclusion complex. The use of job's plot also revealed the stoichiometry of the systems.

DSC results for lower alcohols showed only one endothermic curve corresponding to removal of tightly bounded water molecules. No other information could be revealed on detailed analysis. The results for higher alcohols have shown multiple endothermic curves for each alcohol which are not related to their respective boiling points. It can be assumed that they occur due to melting of crystals of inclusion complex. In cases, where there are more than two endothermic depths are present indicates the formation of different crystalline structures of the inclusion complexes formed.

On exploitation of XRD results, it can be concluded that the complexes formed with lower alcohols have formed same type of crystal structure as all the diffraction pattern obtained are similar. The complexes prepared with higher alcohols have shown two different pattern types which are different pattern obtained with lower alcohols. Depending on the length of the aliphatic chain in primary linear alcohol, the weak interaction between β CD and alcohol gives rise to different structural types. Lower alcohols, up to butanol, act as water molecules in a herringbone structural type comparable to the structure obtained with β CD (as received). Intermediate alcohols, like 1-pentanol and 1-hexanol, present a channel structure in accordance with the structure obtained in PUKPIU, based upon β CD, pyrene and octanol. Finally, longer alcohols such as 1-heptanol up to 11-undecanol exhibit a dimer brick structural type in accordance with the stoichiometry determined previously by proton NMR.

Inclusion complexes prepared with lower alcohols have shown unnoticeable changes in their vibrational modes as the bands from alcohol molecules and β CD are superimposed. The spectra obtained resemble exactly to β CD spectrum. On moving to higher alcohols, the spectra of the complexes show slight changes in their vibrational modes. Peaks corresponding to alcohols are present in all spectra.

Detailed Molecular modelling studies indicated that lower alcohols behave like water molecule indicating non-significant interaction. Higher alcohols possess lower binding energy values and hence undergoing significant interactions.

At last, on considering all the finding, it can be finally concluded that the higher alcohols should be used for further studies of this thesis in favour to obtain opened channel type structures.

3.8 References

1. Furuta. T., Yoshii. H., Miyamoto. A., Yasunishi. A. and Hirano. H., 1993. Effects of water and alcohol on the formation of inclusion complexes of d-limonene and cyclodextrins. *Supramolecular Chemistry*. 1(3-4). pp.321-325.
2. Pitha. J. and Hoshino. T., 1992. Effects of ethanol on formation of inclusion complexes of hydroxypropylcyclodextrins with testosterone or with methyl orange. *International journal of pharmaceuticals*. 80(1-3). pp.243-251.
3. Nelson. G., Patonay. G. and Warner. I.M., 1988. Effects of selected alcohols on cyclodextrin inclusion complexes of pyrene using fluorescence lifetime measurements. *Analytical Chemistry*. 60(3). pp.274-279.
4. Nelson. G., Patonay. G. and Warner. I.M., 1988. Influence of tert-butyl alcohol on cyclodextrin inclusion complexes of pyrene. *Journal of inclusion phenomena*. 6(3). pp.277-289.
5. Buvári. A., Szejtli. J. and Barcza. L., 1983. Complexes of short-chain alcohols with β -cyclodextrin. *Journal of inclusion phenomena*. 1(2). pp.151-157.
6. Boonyarattanakalin. K., Viernstein. H., Wolschann. P. and Lawtrakul. L., 2015. Influence of ethanol as a co-solvent in cyclodextrin inclusion complexation: a molecular dynamics study. *Scientia pharmaceutica*. 83(2). pp.387-399.
7. Yoshii. H., Kometani. T., Furuta. T., WATANABE. Y., LINKO. Y.Y. and LINKO. P., 1998. Formation of inclusion complexes of cyclodextrin with ethanol under anhydrous conditions. *Bioscience, biotechnology, and biochemistry*. 62(11). pp.2166-2170.
8. Aree. T. and Chaichit. N., 2003. A new crystal form of β -cyclodextrin-ethanol inclusion complex: channel-type structure without long guest molecules. *Carbohydrate research*. 338(15). pp.1581-1589.
9. Matsui. Y. and Mochida. K., 1979. Binding forces contributing to the association of cyclodextrin with alcohol in an aqueous solution. *Bulletin of the Chemical Society of Japan*. 52(10). pp.2808-2814.
10. Gallois-Montbrun. D., Le Bas. G., Mason. S.A., Prange. T. and Lesieur. S., 2013. A highly hydrated α -cyclodextrin/1-undecanol inclusion complex: crystal structure and hydrogen-bond network from high-resolution neutron diffraction at 20 K. *Acta Crystallographica Section B: Structural Science, Crystal Engineering and Materials*. 69(2). pp.214-227.
11. Munoz De La Pena. A., Ndou. T.T., Zung. J.B., Greene. K.L., Live. D.H. and Warner. I.M., 1991. Alcohol size as a factor in the ternary complexes formed with pyrene and β -cyclodextrin. *Journal of the American Chemical Society*. 113(5). pp.1572-1577.
12. Gil. V.M. and Oliveira. N.C., 1990. On the use of the method of continuous variations. *Journal of Chemical Education*. 67(6). p.473.
13. Huang. C.Y., 1982. [27] Determination of binding stoichiometry by the continuous variation method: The job plot. In *Methods in enzymology* (Vol. 87. pp. 509-525). Academic Press.
14. Furlong. W.R., Rubinski. M.A. and Indralingam. R., 2013. The method of continuous variation: a laboratory investigation of the formula of a precipitate. *Journal of Chemical Education*. 90(7). pp.937-940.
15. Renny. J.S., Tomasevich. L.L., Tallmadge. E.H. and Collum. D.B., 2013. Method of continuous variations: applications of job plots to the study of molecular associations

in organometallic chemistry. *Angewandte Chemie International Edition*. 52(46). pp.11998-12013.

16. Olson. E.J. and Bühlmann. P.. 2011. Getting more out of a Job plot: determination of reactant to product stoichiometry in cases of displacement reactions and n: n complex formation. *The Journal of organic chemistry*. 76(20). pp.8406-8412.
17. Bogdan. M.. Caira. M.R.. Bogdan. D.. Morari. C. and Fărcaș. S.I.. 2004. Evidence of a bimodal binding between diclofenac-Na and β -cyclodextrin in solution. *Journal of inclusion phenomena and macrocyclic chemistry*. 49(3-4). pp.225-229.
18. Floare. C.G.. Pirnau. A. and Bogdan. M.. 2013. 1H NMR spectroscopic characterization of inclusion complexes of tolfenamic and flufenamic acids with β -cyclodextrin. *Journal of Molecular Structure*. 1044. pp.72-78.
19. Isnin. R.. Salam. C. and Kaifer. A.E.. 1991. Bimodal cyclodextrin complexation of ferrocene derivatives containing n-alkyl chains of varying length. *The Journal of Organic Chemistry*. 56(1). pp.35-41.
20. Aki. H.. Niiya. T.. Iwase. Y. and Yamamoto. M.. 2001. Multimodal inclusion complexes between barbiturates and 2-hydroxypropyl- β -cyclodextrin in aqueous solution: Isothermal titration microcalorimetry. ^{13}C NMR spectrometry. and molecular dynamics simulation. *Journal of pharmaceutical sciences*. 90(8). pp.1186-1197.
21. Akita. T.. Yoshikiyo. K. and Yamamoto. T.. 2014. Formation of 1: 1 and 2: 1 host-guest inclusion complexes of α -cyclodextrin with cycloalkanols: A 1H and ^{13}C NMR spectroscopic study. *Journal of Molecular Structure*. 1074. pp.43-50.
22. Tanaka. K.. Toda. F. and Mak. T.C.. 1984. Isolation and crystal structure of alcohol inclusion complexes. In *Clathrate Compounds. Molecular Inclusion Phenomena. and Cyclodextrins* (pp. 99-102). Springer. Dordrecht.
23. Lindner, K. and Saenger, W., 1982. Crystal and molecular structure of cyclohepta-amylose dodecahydrate. *Carbohydrate Research*, 99(2), pp.103-115.
24. Udachin, K.A. and Ripmeester, J.A., 1998. A novel mode of inclusion for pyrene in β -cyclodextrin compounds: The crystal structures of β -cyclodextrin with cyclohexanol and pyrene, and with n-octanol and pyrene. *Journal of the American Chemical Society*, 120(5), pp.1080-1081.
25. Makedonopoulou, S. and Mavridis, I.M., 2001. The dimeric complex of cyclomaltoheptaose with 1, 14-tetradecanedioic acid. Comparison with related complexes. *Carbohydrate research*, 335(3), pp.213-220.
26. Loh. G.O.K.. Tan. Y.T.F. and Peh. K.K.. 2016. Enhancement of norfloxacin solubility via inclusion complexation with β -cyclodextrin and its derivative hydroxypropyl- β -cyclodextrin. *asian journal of pharmaceutical sciences*. 11(4). pp.536-546.
27. Charumanee. S.. 2004. Amorphization and dissolution studies of Acetaminophen- β -Cyclodextrin inclusion complexes. *CMU J*. 13(1). pp.13-23.
28. Patil. J.S. and Suresh. S.. 2009. Physicochemical characterization. in vitro release and permeation studies of respirable rifampicin-cyclodextrin inclusion complexes. *Indian journal of pharmaceutical sciences*. 71(6). p.638

Chapter 4 : Inclusion complexes of β CD: Aromatic Hydrocarbons

4.1 Introduction

In the present chapter, we have studied the behaviour of only selected aromatic compounds to form inclusion complexes in absence of linear alcohols. The first information obtained revealed their nature while forming an inclusion complexation. The main idea behind this step is to see their existence in the final solutions prepared or in the crystalline powders. For this purpose, we followed the same procedure of performing NMR studies in the liquid state. The results have cleared the picture about the aromatic compounds which are able to form the inclusion complexes in absence of linear alcohols and the one which failed to do the act. It has been found out that derivatives of BEN and NAP with a polar part like PHE, BA and 2-NAP were able to form complexes with β CD without alcohols. On the other hand, for few aromatic compounds like BEN and TFT, solubility issues of PAH in water do not allow the study of inclusion complexation in solution. Experimental methods are still those explained in the chapter 2.

By preparing co-precipitated crystalline powders, solubility issues are partially raised by the increase of the temperature applied in the sample preparation protocol. After washing of the powders, we are able to detect PAH in some solid state complexes that could not be studied in solution in D_2O by proton NMR.

Here, we have also discussed the solid state studies for these compounds. Thermal studies were performed to observe new events of endothermic or exothermic curves corresponding to inclusion complexes. For the aromatics, already forming inclusion complexes in solution with β CD without the use of linear alcohols show additional curves for melting of the inclusion complexes formed at the respective temperatures. Furthermore, the aromatics considered of not forming inclusion complexes show curves showing the melting/boiling of the uncomplexed guest molecules. Another information revealed here which was not available by NMR studies in solution is the inclusion solid state complex formation by TOL without addition of alcohols.

The XRD studies indicated the types of crystal structures formed by the β CD on inclusion with different aromatic hydrocarbons. The aromatics already showing complexation as interpreted by the other techniques have shown typical XRD pattern as obtained when inclusion complexation occurs. All the patterns are compared with XRD pattern obtained for β CD: Octanol and many others structures from the literature which are used as references for channel inclusion complex structure.

In the last part, the Raman Studies are done to further investigate the vibrational motions of the molecules affected while forming an inclusion complex. The vibrational modes of the guest molecules were calculated by theoretical studies to check the mode of the guest appearing in the inclusion complex system (if occurs) for better understanding.

Our group has previously investigated the inclusion structure of some PAH by β CD¹. In the literature, complexation of derivatives of benzoic acid, phenol and 2-naphthol by β CD have been extensively studied²⁻⁷. A very interesting studies about crystalline alpha and gamma CDs inclusion compounds formed with aromatics guests is also available⁸. Soluble inclusion complexes of aromatic molecules, i.e. styrene⁹, aniline¹⁰, phenol¹¹ and their derivatives¹² with CDs have been reported in the literature. These studies have found that the inclusion of

substituted benzene derivatives in the CD cavities depends on a variety of factors, including their sizes, shapes, substitution position (ortho, meta or para), ionic strength, etc.

4.2 NMR studies of β CD: aromatic hydrocarbons

1D proton NMR studies were also carried out for some aromatic pollutants in order to have some basic idea about inclusion complex formation. The samples were prepared and analysed as explained in chapter 2. The objective for carrying out these studies was to know about any inclusion process occurring when the two compounds were mixed and also to know the stoichiometry of the inclusion complex formed by method of continuous variation (Job's Plot). Aromatic hydrocarbons are slightly soluble in water, but are highly lipophilic. Their solubility in water varies with increase in temperature. Here, we have carried out studies in solution in presence of D₂O at ambient temperature.

For inclusion complex formation, another finding which is very important for the studies is the evolution of proton peaks for aromatic hydrocarbons guest for different solutions prepared. We have also focussed on the same studies for few of our sample in order to understand complexation phenomenon better.

4.2.1 Monocyclic Aromatic hydrocarbons

4.2.1.1 β CD: BEN, β CD: FB and β CD: TFT NMR studies in D₂O

The solutions for those analysis were prepared in D₂O. For each set of solutions, the studies were carried out for a minimum of two times.

In the past, fewer research articles have been published about β CD:BEN¹³⁻¹⁵ complexes but no such type of NMR studies were done. For β CD:BEN (D₂O), the non-existence of BEN in the solution is confirmed by absence of benzene peak at 7.26 ppm due to poor solubility in water (1.84 g/L at 30°C).

Similar results were obtained with FB and TFT. The previously done studies on complexation of FB^{11,16,17} do not reveal any NMR studies for stoichiometry confirmation. TFT does not form any inclusion complex with β CD because of the solubility issues (< 0.1 g/100 ml at 21°C).

For the same reason of poor solubility, we are not able to solubilize other PAH like NAP, TOL, PYR and ANTH in D₂O avoiding the study of their complexation by β CD by proton NMR in solution.

4.2.1.2 β CD: B.A NMR studies in D₂O

Benzoic acid (Figure 4.3) is one such aromatic molecule that forms inclusion complex in solution (D₂O) with β CD. This observation can be confirmed before by the NMR^{18,19} studies. The results obtained during our studies show the formation of 1:1 stoichiometry by job's plot method (Figure 4.2). The Figure 4.1 presents the shifts for H3 and H5 positions due to BA molecule inclusion. The evolution in the peaks due to BA protons is also observed at higher ppm values (Figure 4.4). The stoichiometry was found to be 1:1 when the R_{max} was calculated by polynomial curve fitting method.

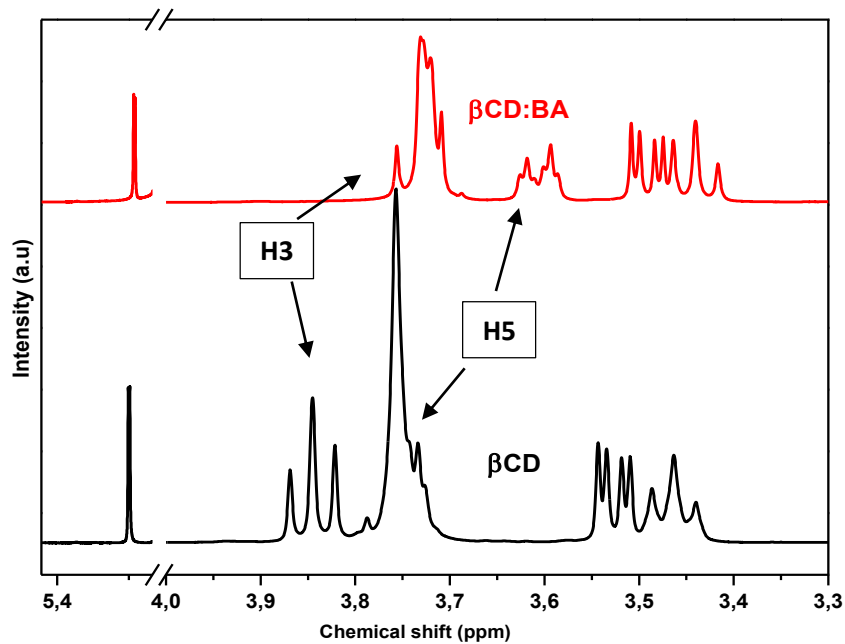


Figure 4.1 : Comparison of NMR spectra of β CD and β CD:BA complex showing shift in H3 and H5 positions.

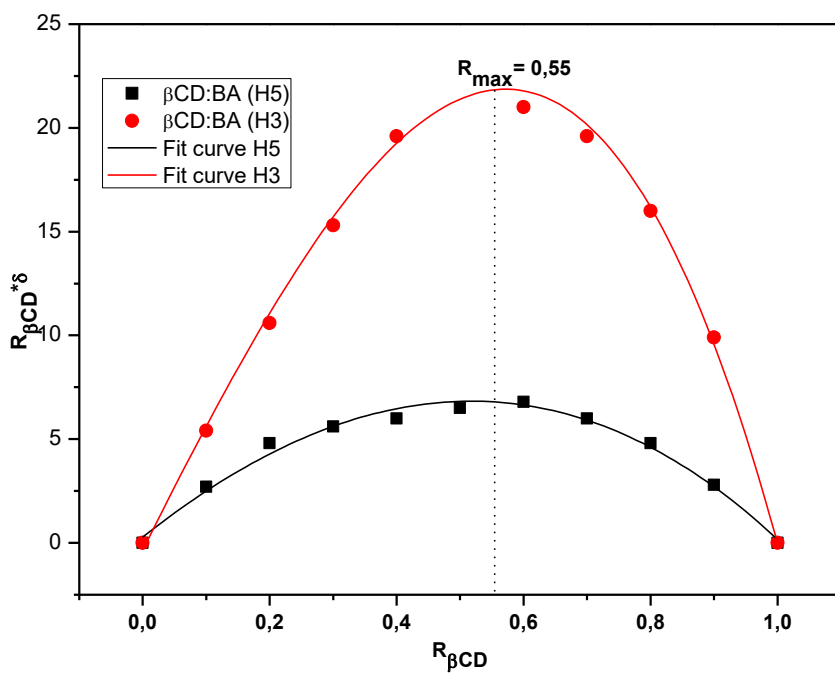


Figure 4.2 : Job's plot for β CD:BA complex in D_2O for β CD protons.

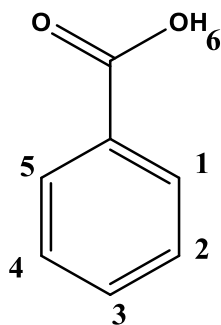


Figure 4.3 : BA molecule with proton labelling.

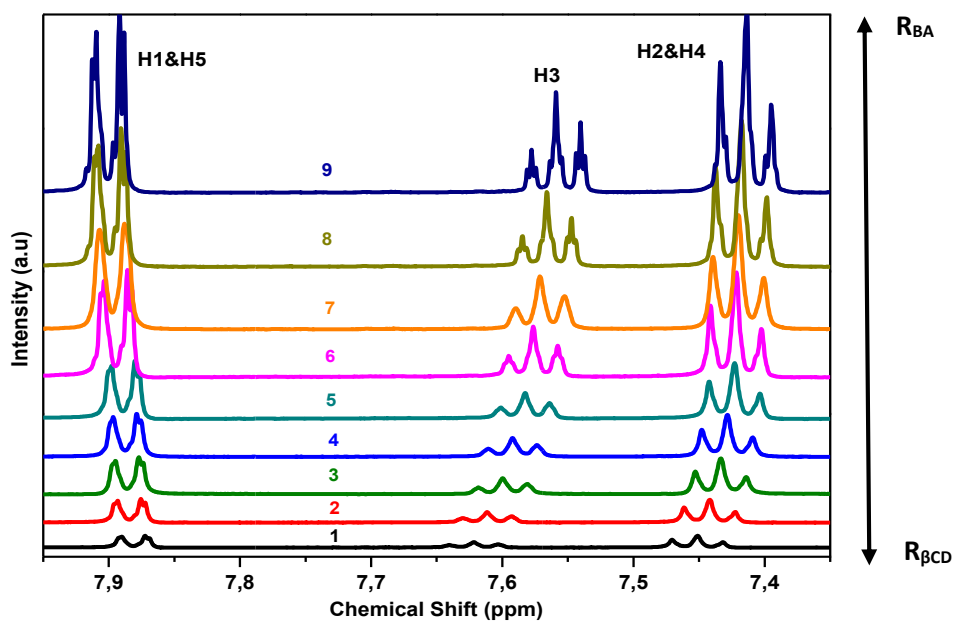


Figure 4.4 : Displacement of peaks of Benzoic acid.

The BA proton peaks at higher ppm value have also shown the deviation from their original positions. The H3 proton of B.A showed the maximum deviation. The job's plot confirmed the stoichiometry of the complex as 1:1 with $R_{\max} = 0.49$ (Figure 4.5) which are in accordance with the previous studies^{2,20} done. The stoichiometry of the complex is found to be 1:1 on considering the job's plot from the different molecules protons study. The number of the spectra in the figure correspond to the series of solution preparation discussed in the previous chapter.

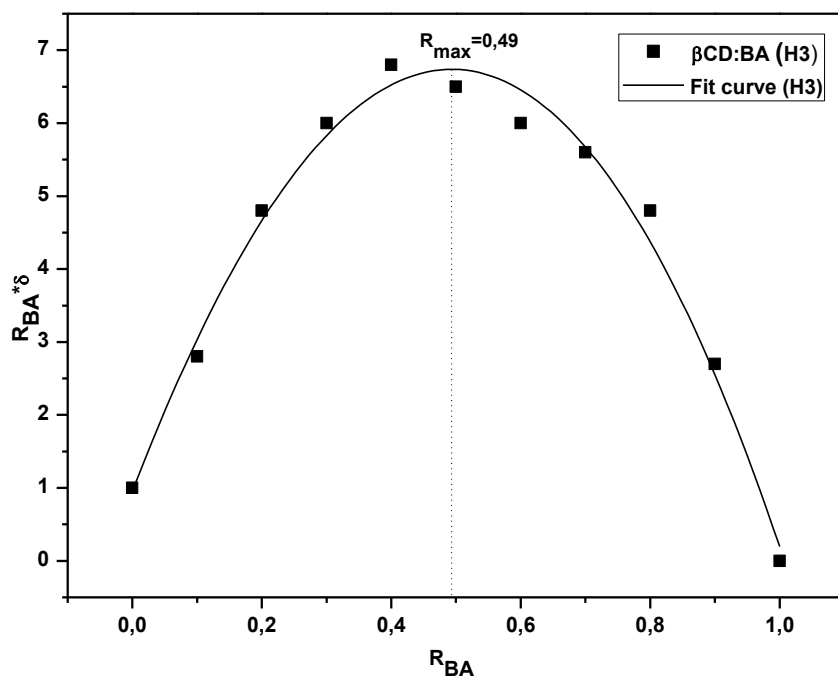


Figure 4.5 : Job's plot for β CD:BA complex in D_2O for BA protons.

4.2.1.3 β CD: PHE NMR studies in D_2O

Phenol (Figure 4.8), being an aromatic alcohol is expected to certainly form inclusion complex with β CD. The behaviour of complex formation can be seen in the Figure 4.6. The results presented in the Figure 4.7 as job's plot suggest formation of 1:1 ($R_{max}=0.5$) inclusion complex. The peaks for H3 and H5 show apparent shifts indicating insertion of phenol molecule inside the β CD cavity.

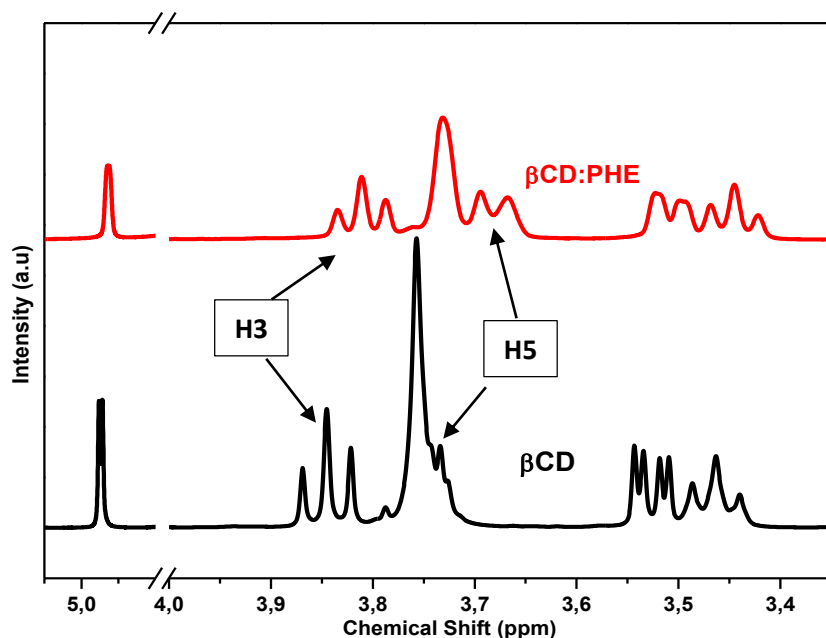


Figure 4.6 : Comparison of NMR spectra of β CD and β CD:PHE complex showing shift in H3 and H5 positions.

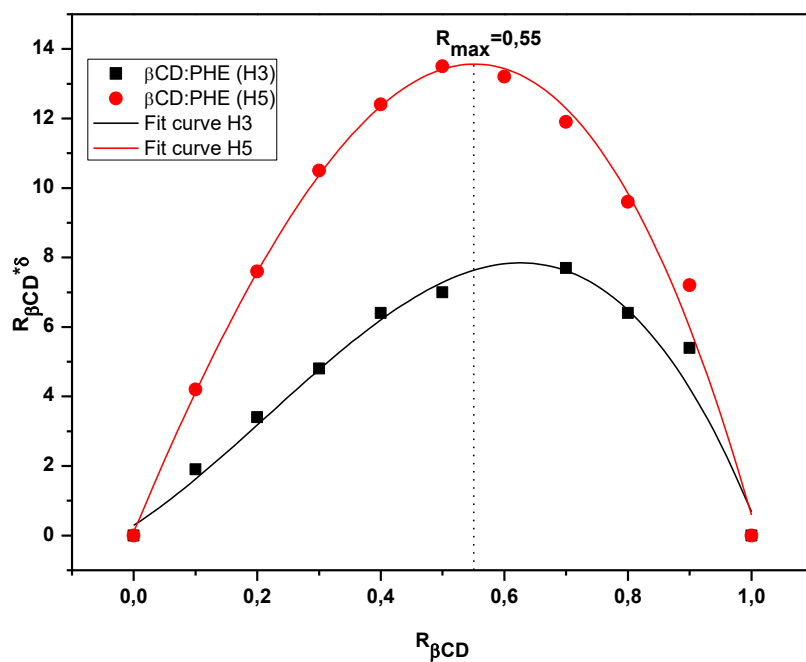


Figure 4.7 : Job's plot for β CD:PHE complex in D_2O .

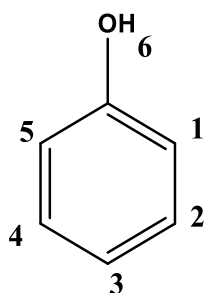


Figure 4.8 : PHE molecule with proton labelling.

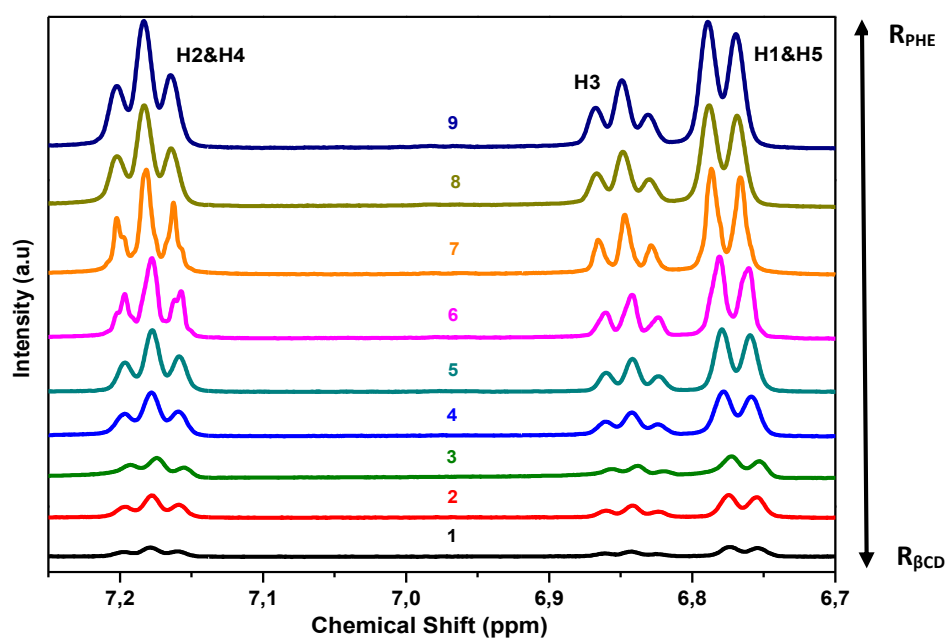


Figure 4.9 : Displacement of peaks of Phenol.

The peaks evolution due to phenol protons can be seen in the Figure 4.9. The number of the spectra in the figure correspond to the series of solution preparation discussed in the previous chapter. They show slight deviation from their original position indicating that phenol is surely inserted in the cavity via its hydroxyl functions not observable in D₂O. These results are in accordance with the theoretical studies²¹ done before.

4.2.2 Bicyclic Aromatic hydrocarbons

4.2.2.1 β CD: 2-NAP NMR studies in D₂O

2-naphthol (Figure 4.12), another bicyclic aromatic alcohol molecule tends to show formation of inclusion complex with β CD. The stoichiometry of the system shows 2:1 ratio (Figure 4.11). The literature finding does not reveal any details about NMR studies of 2-naphthol with β CD. The comparison of the β CD and β CD: 2NAP peaks clearly show the shifting of H3 and H5 (Figure 4.10). From these results we can conclude that 2-naphthol forms inclusion complex with β CD. The value of R_{\max} is observed at 0.3 indicating formation of 2:1 stoichiometry.

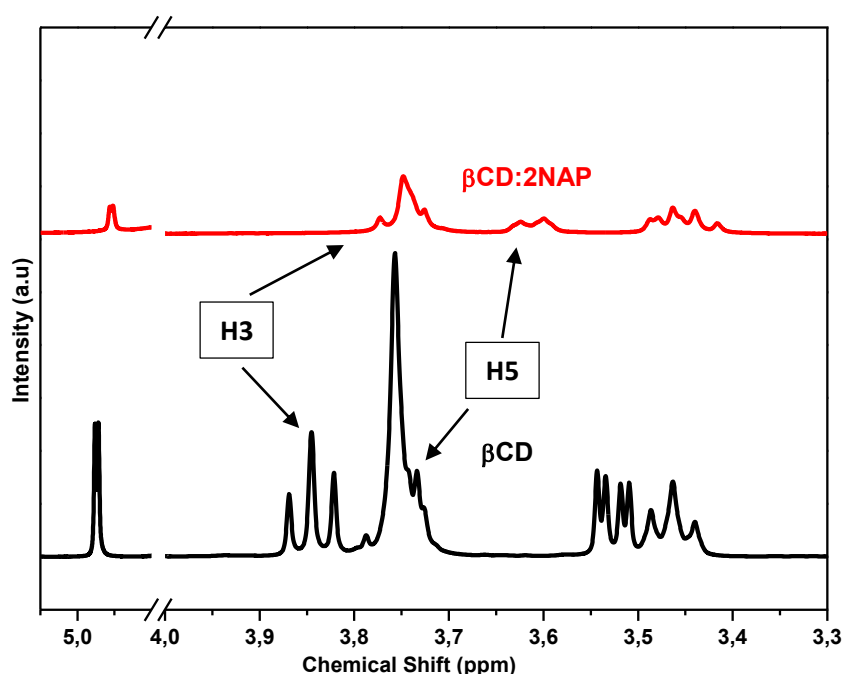


Figure 4.10 : Comparison of NMR spectra of β CD and β CD:2NAP complex showing shift in H3 and H5 positions.

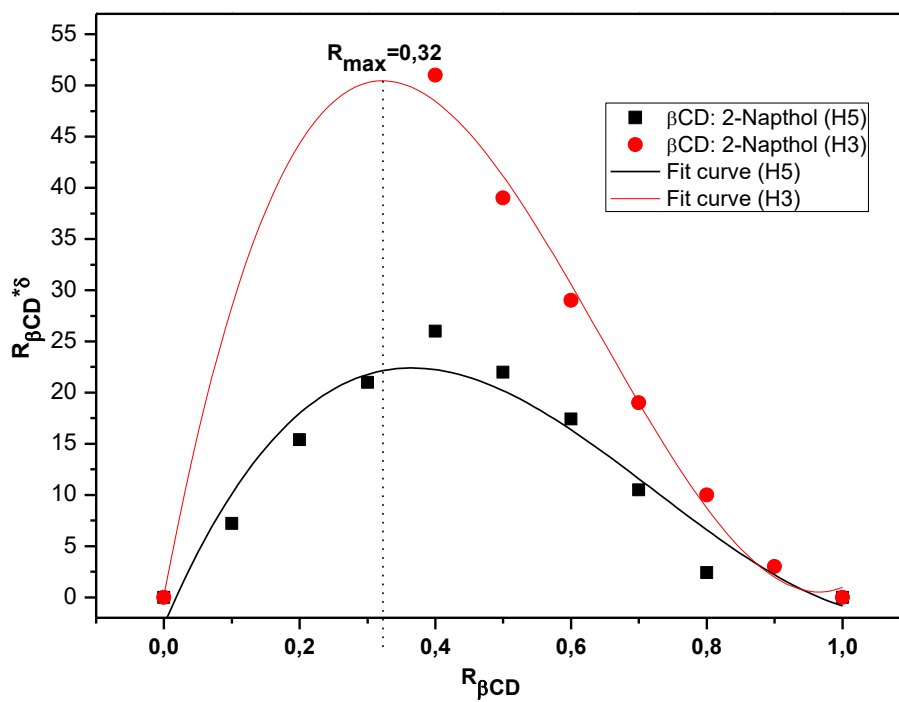


Figure 4.11 : Job's plot for $\beta CD:2NAP$ complex in D_2O .

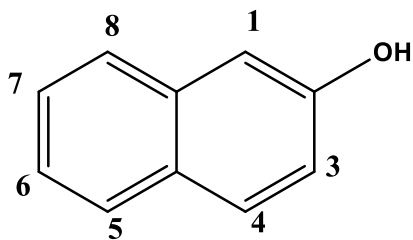


Figure 4.12 : 2-NAP molecule with proton labelling.

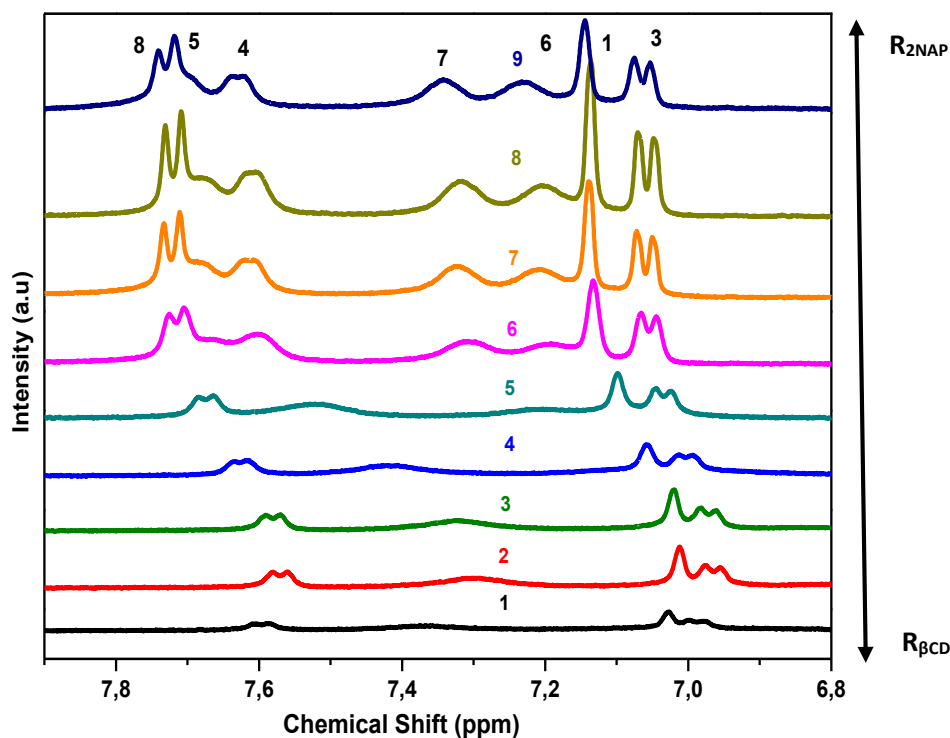


Figure 4.13 : Displacement of peaks of 2-Naphthol.

The 2-naphthol protons, like other molecules discussed above, have tend to show progressive evolution which is shown in the Figure 4.13. The number of the spectra in the figure correspond to the series of solution preparation discussed in the previous chapter. As depicted from the figure, the shift for aromatic protons can be seen only for selected protons like H8, H5, H4 and H3. They show similar amount of shift indicating horizontal encapsulation of the molecule by β CD cavity.

4.3 Thermal studies of β CD: Aromatic hydrocarbons

The powder samples are prepared by co-precipitation, then washed and dried under vacuum as explained in chapter 2. The thermal studies for β CD: Aromatic hydrocarbons were performed for most of the powdered compounds in order to check their complexation ability. Thermal analysis reveals existence of inclusion complex by showing an endothermic peak corresponds to its melting point at a temperature different from the melting temperatures of the host and the guest. For comparison, Table 4.1 provides the melting and boiling point values of all the guests used to carry out thermal studies.

Aromatic hydrocarbon	Physical State	Melting/Boiling Point (°C)
Fluorobenzene	Colorless liquid	85
Toluene	Colorless liquid	110.6
Trifluorotoluene	Colorless liquid	102
Phenol	White crystalline solid	40.5
Benzoic Acid	Colorless crystalline solid	122
Naphthalene	White crystalline solid	80.2
2-Naphthol	Colorless crystalline solid	121-123
Anthracene	Colorless solid	215.7
Pyrene	Colorless solid	145-148

Table 4.1 : list of melting and boiling point values of all the guests

4.3.1 Monocyclic aromatic hydrocarbons

4.3.1.1 Thermal studies of β CD:FB complexes

The thermal studies were carried out for β CD: FB in the molar ratio 1:1 (Figure 4.14). The curve for the complex shows an endothermic curve at temperature 147°C which corresponds to the removal of tightly bound water molecules from the host cavity. The energy involved in this phenomenon is smaller in compared to β CD curve indicating fewer water molecules removal at higher temperature and smaller area involved. There exists exothermic effect which can be observed around 255°C, that hints about crystallization of a new phase. Another features appearing at 273°C corresponds to the onset of decomposition of uncomplexed β CD while rest of the curves remain smooth.

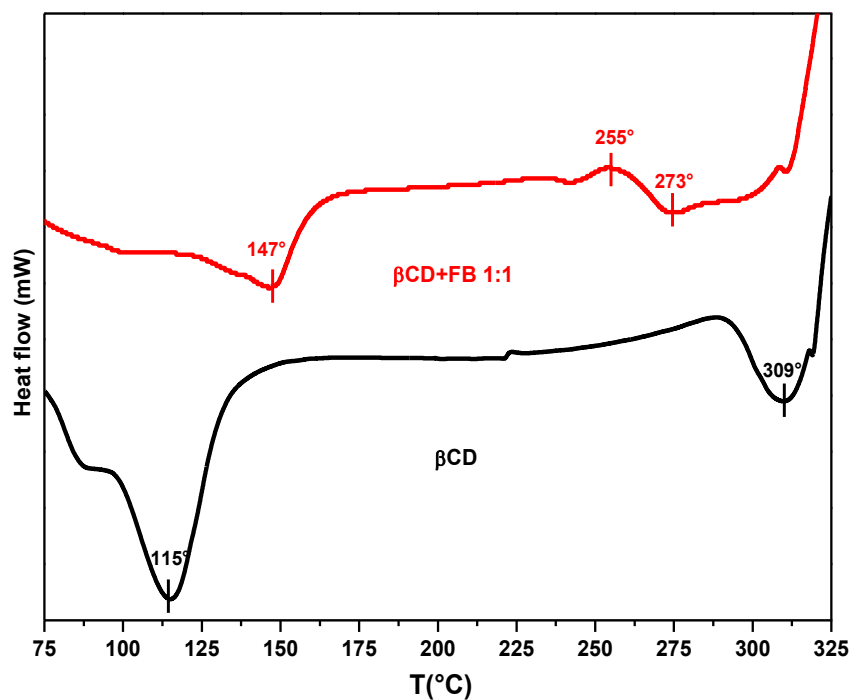


Figure 4.14. DSC curve of β CD and β CD:FB (1:1)

4.3.1.2 Thermal studies of β CD:TOL complexes

The thermal studies carried out for β CD:TOL complexes showed an endothermic peak corresponding to the inclusion complex formed at 158°C apart from the other details like peak at 90°C due to removal of water molecules with different organization in the cavity. This argument is supported by smaller temperature and area involved than in β CD curve. The boiling point of TOL is 110.6 °C which does not appear in the curve obtained (Figure 4.15). An exothermic curve is appeared at 260°C indicating formation of new crystalline phase followed by decomposition of uncomplexed β CD around 290°C.

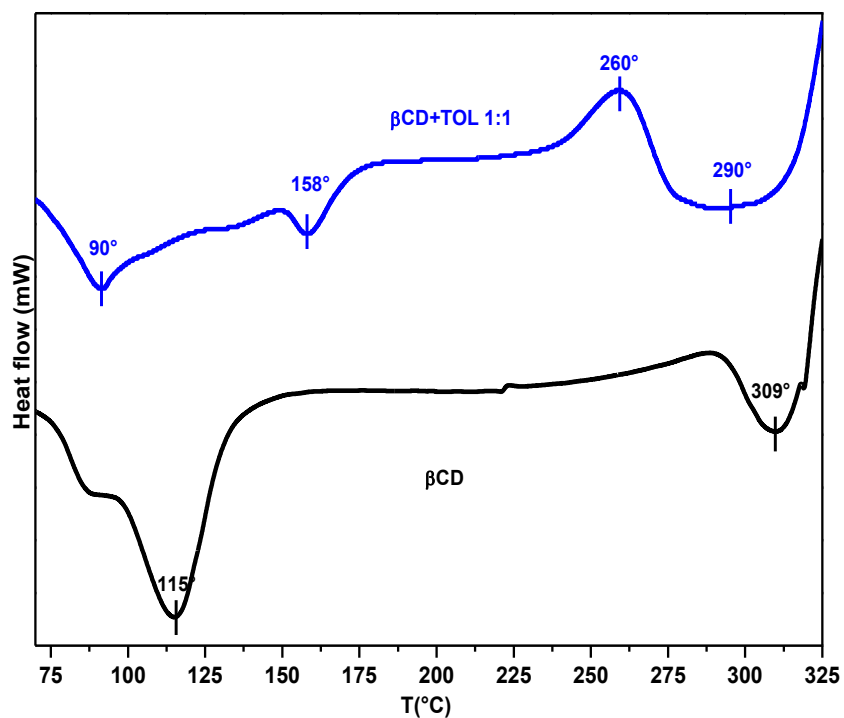


Figure 4.15 : DSC curve of βCD and $\beta\text{CD}:\text{TOL}$ (1:1).

4.3.1.3 Thermal studies of $\beta\text{CD}:\text{TFT}$ complexes

The results obtained by NMR studies of $\beta\text{CD}:\text{TFT}$ have not revealed any complex formation details. On performing thermal studies (Figure 4.16), a small endothermic peak is observed at 167°C which does not correspond to the boiling point of TFT. It could be due to formation of inclusion complex or some impurity in the system. The curve also contains the standard features of removal of water molecules at 110°C that were differently organised in the system, indicated by lower temperature and smaller area. The decomposition of uncomplexed βCD at 271°C has followed another exothermic phenomenon at 251°C. It can be described as formation of new crystalline phase.

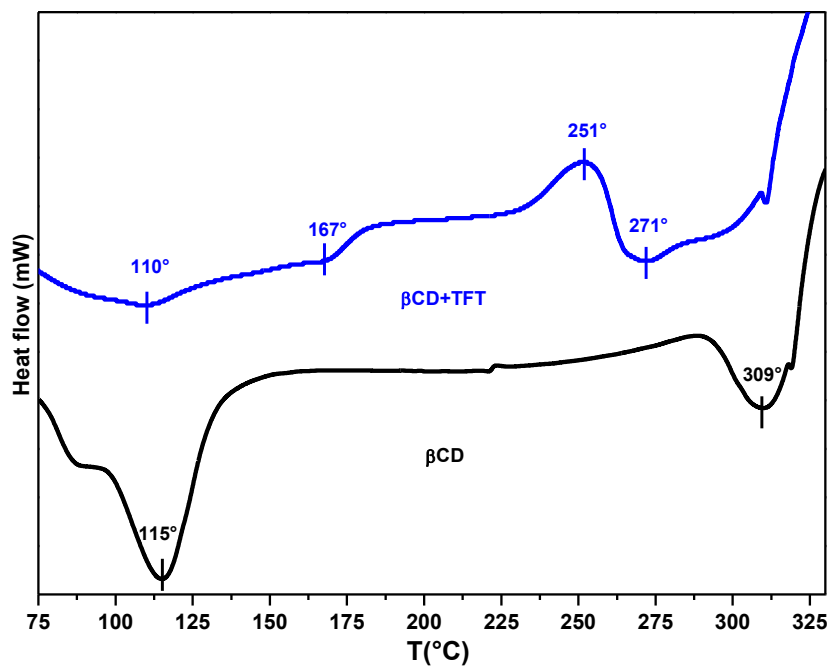


Figure 4.16. DSC curve of β CD and β CD:TFT (1:1)

4.3.1.4 Thermal studies of β CD:PHE complexes

PHE is one of molecules for which positive NMR results are obtained. It does not require use of any alcohol molecule to form inclusion complex. Thermal studies (Figure 4.17) have also showed the existence of inclusion complex whose melting temperature is observed at 144°C. The removal of water molecules from the cavity did not require lot of energy in comparison to β CD and the corresponding peak can be seen at 104 °C.

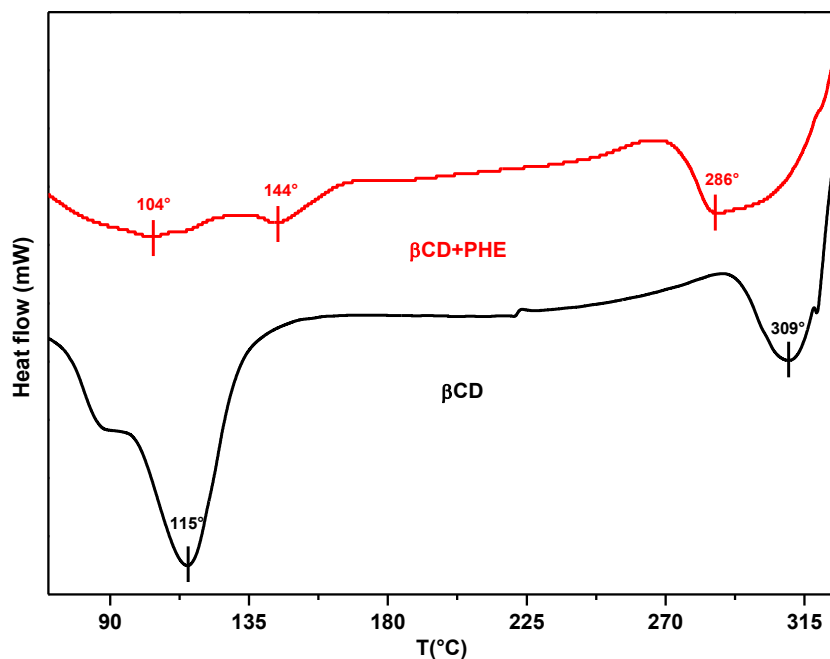


Figure 4.17 : DSC curve of β CD and β CD:PHE (1:1).

4.3.1.5 Thermal studies of β CD:BA complexes

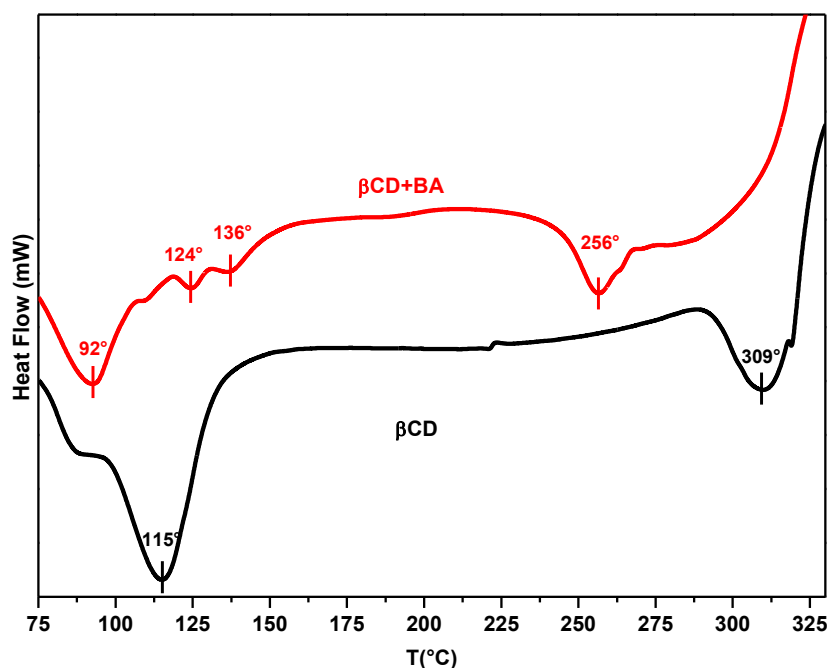


Figure 4.18 : DSC curve of β CD:BA (1:1).

The thermal studies show difference in behaviour for the complexes prepared with β CD:BA^{22,23}. The curve (Figure.4.18) obtained for β CD:BA has many thermal features appearing at different temperatures like 92°, 124°, 136°C and 256°C. The reasons for appearance of each endothermic curve are the removal of tightly bound water molecules, the melting of uncomplexed B.A, melting of different crystal forms of inclusion complexes at 136° and the temperature degradation and oxidation of uncomplexed CDs which have appeared at

relatively lower temperature respectively. The results obtained here are in accordance with NMR studies confirming inclusion complex formation.

4.3.2 Bicyclic aromatic hydrocarbons

4.3.2.1 Thermal studies of β CD:NAP complexes

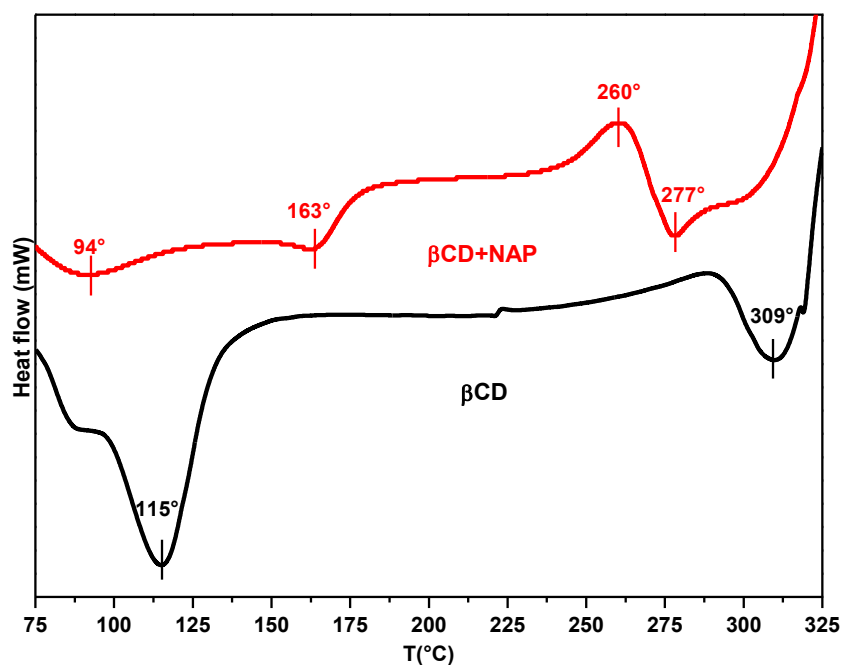


Figure 4.19 : DSC curve of β CD and β CD:NAP (1:1).

The melting point of naphthalene is 80.26°C. The endothermic peak for removal of lesser number of water molecules can be seen at 94°C followed by another endothermic curve at 163°C. This peak may be due to the inclusion complex formed. At 260°C, an exothermic effect can be observed which can be explained as formation of new crystalline system. The decomposition of β CD crystals can be seen at temperature at 277°C (Figure 4.19).

4.3.2.2 Thermal studies of β CD:2-NAP complexes

2-NAP has already proved to form inclusion complex with β CD by NMR studies. The results (Figure 4.20) observed for thermal studies are seem to have in an agreement with NMR results. The melting of the inclusion complex is observed at 260°C which does not correlate with the melting point of neither 2-NAP (m.p-121-123°C) nor β CD. The water molecules removal peak is observed at 106 °C which are lesser in number in comparison to β CD curve. Moreover, additional information that can be revealed is that the structure obtained with β CD:2-NAP is different from β CD containing water molecules inside the cavity.

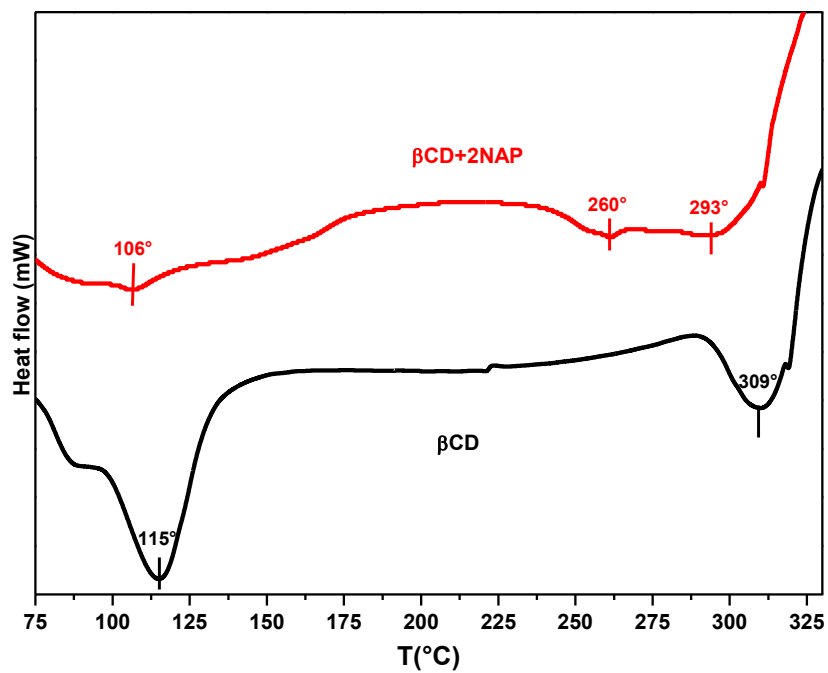


Figure 4.20 : DSC curve of βCD and $\beta\text{CD}:2\text{-NAP}$ (1:1).

4.3.3 Polycyclic aromatic hydrocarbons

4.3.3.1 Thermal studies of $\beta\text{CD}:\text{PYR}$ complexes

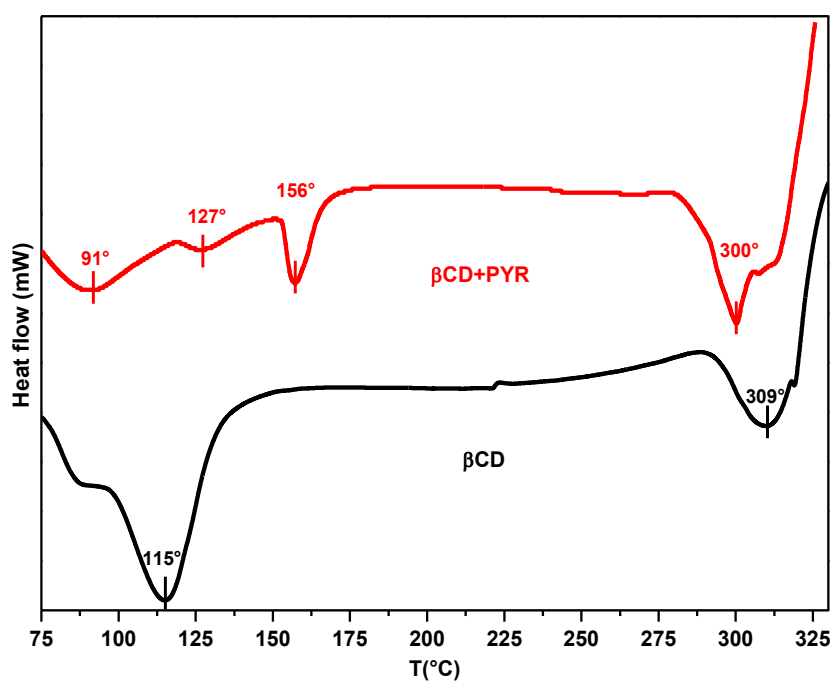


Figure 4.21 : DSC curve of βCD and $\beta\text{CD}:\text{PYR}$ (1:1).

The DSC curve obtained for the β CD:PYR (Figure 4.21) contains the peaks for multistage removal of water molecules at 91°C and 127°C. The melting of uncomplexed PYR represented by a sharp peak can be seen at 156°C. The thermal behaviour of β CD:PYR seems very different from β CD. The features observed are very different in terms of the number of water molecules inside the cavity and the area of energy involved for their removal. It can be concluded that presence of PYR has some influence on the β CD structural organisation.

4.4 Powder X ray diffraction studies of β CD: aromatic hydrocarbon complexes

4.4.1 Monocyclic aromatic hydrocarbons

The XRD patterns (Figure 4.22) obtained for β CD: BEN and β CD:FB look similar to each other in terms of the peak intensities and positions. On considering the literature, they found to follow the diffraction patterns obtained by the CSDCODE PUKPIU²⁴ and POXHUG²⁵ (both have channels along c axis structural arrangement) that are two channel organised structures. The important peaks are observed at positions :6.0°, 7.5°, 9.0°, 9.7°, 11.2°, 11.8°, 12.3° and 13.0°. The peak at 5.2° is seen only in β CD:FB XRD pattern which also existed in reference POXHUG. Table 4.2 lists the assignment of CSD REFCODE to the experimental pattern obtained for β CD: BEN and β CD:FB.

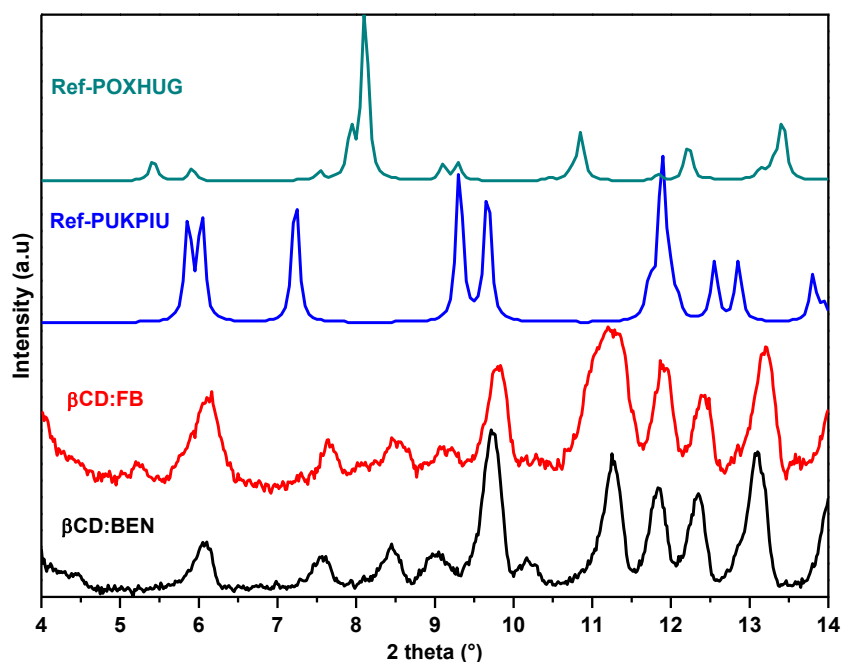


Figure 4.22. Comparison of diffraction patterns of experimentally observed and simulated structures (PUKPIU and POXHUG) from literature of β CD inclusion complexes. The experimentally observed β CD: aromatic hydrocarbon pattern can be seen to show peaks corresponding to both of these structures.

2theta (°)	Relative intensity	Assignment
6.0	31	PUKPIU
7.5	22	POXHUG
9.0	25	PUKPIU+POXHUG
9.7	100	PUKPIU
11.2	82	POXHUG
11.8	64	PUKPIU
12.3	60	POXHUG
13.0	87	POXHUG

Table 4.2. Experimental X-ray pattern of β CD:BEN and β CD:FB with CSD refcode reference assignment.

The aromatics PHE, BA and 2-NAP have hinted formation of inclusion complex in NMR studies. The XRD patterns (Figure 4.23) observed in case of β CD: BA and β CD: PHE are similar whereas β CD: 2-NAP show minor differences. The important peaks are observed at 5.8°, 6.9°, 9.3°, 9.7° and 11.8° for β CD: BA and β CD: PHE (approx.). For β CD: 2-NAP, the peaks can be seen at 5.4°, 6.2°, 6.5°, 10.6°, 11.2° and 11.6°. The literature comparison has revealed their resemblance to CSDCODE PUKPIK²⁴.

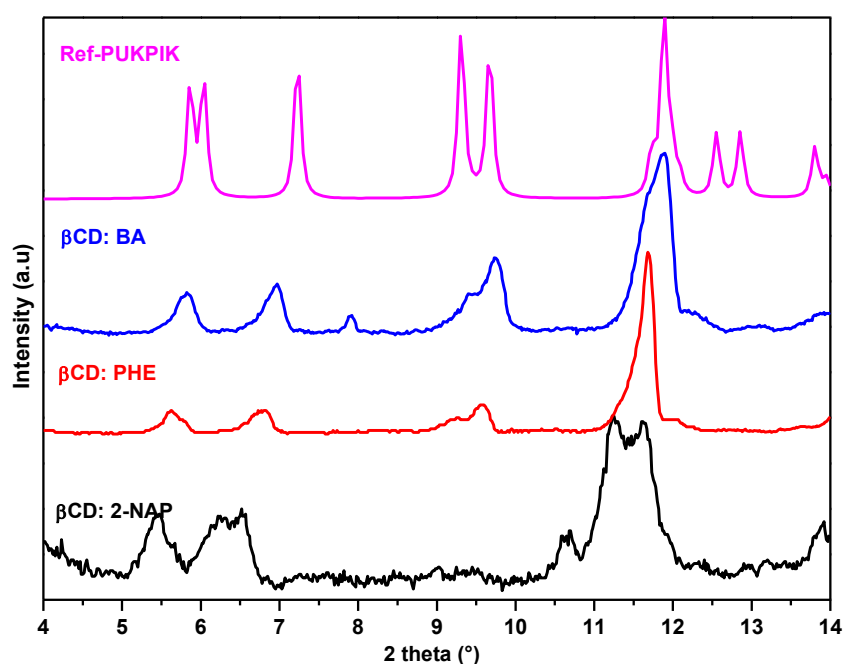


Figure 4.23. Comparison of diffraction patterns of experimentally observed and simulated structures (PUKPIK) from literature of β CD inclusion complexes. The experimentally observed β CD: aromatic hydrocarbon pattern can be seen to show peaks corresponding to the structure.

The XRD results obtained with β CD:TOL, β CD:TFT, β CD:NAP and β CD:PYR (Figure 4.24) complexes look similar to reference CACPOM²⁶ (dimer brick type structural organisation) from the literature. The group of peaks between 6° to 7° in CACPOM are present in the patterns of complexes as a single broad 'hump' indicating merging of the peaks. The peak appearing at 11.4° in β CD:TOL, β CD:TFT and β CD:NAP is the shifted version of peak at 11° in CACPOM whereas the same peak appears as a doublet in β CD:PYR pattern. Moreover, an additional peak at 9.8° which is similar to the reference appears in this case only.

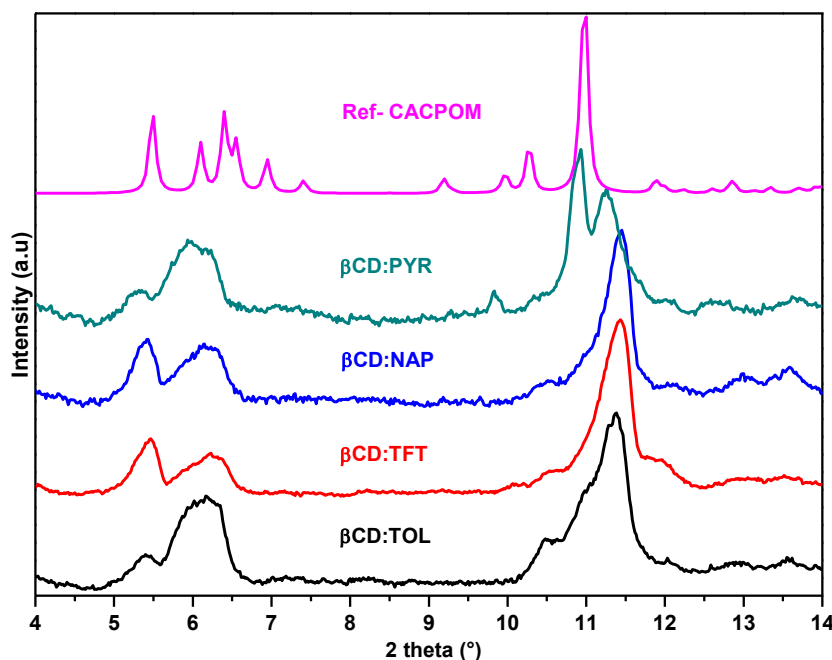


Figure 4.24 . Comparison of diffraction patterns of experimentally observed and simulated structures (CACPOM) from literature of β CD inclusion complexes. The experimentally observed β CD: aromatic hydrocarbon pattern can be seen to show peaks corresponding to the structure.

4.5 Raman Spectroscopy based analysis of β CD: Aromatic hydrocarbon complexes

The complexes at first, were synthesised in molar ratio (1:1) between the two precursors used namely β CD and aromatic hydrocarbon. During the course of the research, the first and the foremost idea was to study the encapsulation behaviour without the addition of long aliphatic chain alcohols. The reason behind these studies was to understand the basic nature of interaction between β CD and AH under consideration. Raman spectra of complexes without addition of alcohols were obtained and studied to determine if there is any kind of encapsulation occurring.

The vibrational properties of organic compounds and cyclic aromatic hydrocarbons have been extensively studied. Infrared and Raman spectra of many monocyclic and PAHs with different functional groups have been obtained with quantum chemical calculations.

Due to advancements in computational chemistry methods and increasing ability of computing hardware, it is now possible to perform theoretical investigation of any type of molecules.

The Raman spectral studies were carried out for β CD: Aromatic hydrocarbon for the molar ratio 1:1. For better understanding of the Raman vibrational modes of the guest molecules, theoretical studies were also performed. The computation of Raman spectrum allows attribution of aromatic peaks. The studies involved two steps, (1) the Optimization of the guest molecule and (2) Frequency calculations. Both the steps were performed using DFT (B3LYP, 3-21G). The Raman activities of the aromatics were calculated again by B3LYP method of DFT with the 6-311G (d,p) basis set. The Raman intensities were computed from activities with GaussSum²⁷ 3.0 using an excitation wavelength of 660 nm for monocyclic aromatics and 785 nm for bicyclics or polycyclics. In order to obtain good agreement with observed frequencies, the calculated harmonic frequencies of C-H vibrations and all other vibrations were scaled by different factors in each case. Gaussview²⁸ 5.0 was used to visualise the participation and direction of atoms in vibrational normal modes for easier band assignments.

4.5.1 Monocyclic aromatic hydrocarbons

4.5.1.1 β CD:BEN Raman studies

The first monocyclic aromatic carbon to be studied was benzene. Benzene has cyclic continuous π bonds between the carbon atoms. It is used as a precursor to manufacture complex structures. For our investigation of complexation¹³⁻¹⁵ between benzene and β CD, the first step was to understand the Raman vibrational modes of the pure precursors followed by the Raman spectral studies of the complexes prepared. The calculated harmonic frequencies of C-H vibrations were scaled by a factor of 0.96 and all other frequencies by 0.98 to allow a good agreement with observed one for BEN alone.

The Raman spectrum of benzene show the important peaks at 606, 990, 1175, 1585, 1605, 2945 and 3057 cm^{-1} . The peak at 606 cm^{-1} represents the C-C-C deformation of the plane, 990 cm^{-1} represents the benzene ring breathing vibration. 1175 cm^{-1} represents the C-H shear vibration mode. The peak at 1585 cm^{-1} represents the CCC stretching vibration mode. The peak at 2945 cm^{-1} represents C-H antisymmetric stretching mode and for the one at 3057 cm^{-1} represents the CH symmetrical stretching vibration mode.

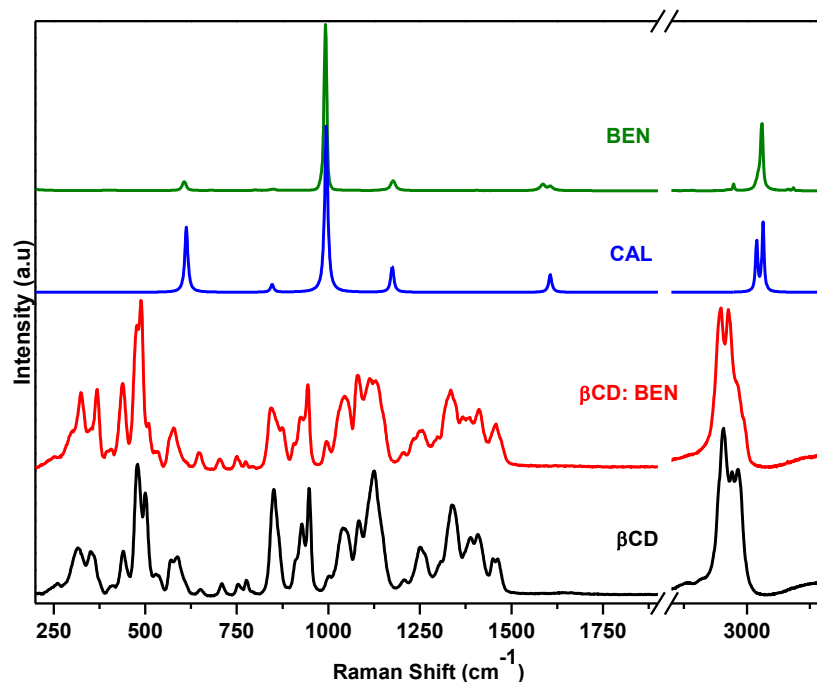


Figure 4.25 : Raman Spectrum of the β CD, BEN and of the inclusion complex obtained after mixing β CD with BEN in the molar ratio of 1:1.

The Raman spectrum (Figure 4.25) of β CD:BEN (1:1) complex does not clearly show any of the benzene peaks, in fact it is very similar to β CD spectrum with slight variations in terms of intensities for example- the peaks at 436 and 478 cm^{-1} in β CD spectra show intensity changes in the complex spectrum, the singlet at 850 cm^{-1} has changed to doublet, the peak at 1000 cm^{-1} is more intense and sharp, the peaks between the range 1300-1500 cm^{-1} have reduced in intensities. The shape of the peak above 3000 cm^{-1} is changed in the spectrum of complex formed. These small changes indicate a complex formation which are in accordance with results obtained by XRD analysis for the same complex. If the inclusion had occurred, the most probable impacted peaks would be the most intense peak in the BEN spectrum i.e the peaks at 990 cm^{-1} and 3057 cm^{-1} . Their expected vibrational modes are shown in the Figure 4.26.

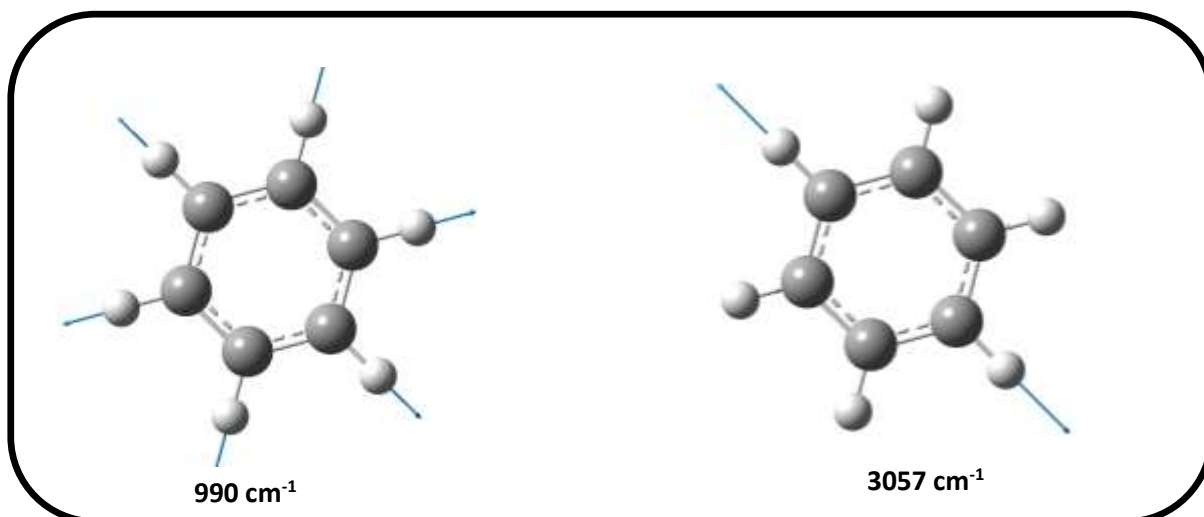


Figure 4.26 : The vibrational modes of BEN which are most intense and have been impacted by the interaction with β CD.

4.5.1.2 β CD:FB Raman studies

Fluorobenzene (FB) is another derivative of benzene where a single fluorine atom is attached to the benzene ring. It is used as an insecticide and as a reagent for plastic and resin polymer. It has been added to the hazardous substance. The literature studies^{11,16,17} show limited investigation about their encapsulation behaviour by β CD.

In the present case, it is used as guest to be encapsulated by the β CD cavity. We have studied the Raman spectrum of FB in order to understand the inclusion complex spectra. The calculated harmonic frequencies of C-H vibrations were scaled by a factor of 0.96 and all other frequencies by 0.98. Several peaks are observed corresponding to different vibrational modes such as: 3074 cm^{-1} corresponding to C-H stretching mode. 1601 cm^{-1} corresponds to C-C in plane stretching. 1217 and 1153 cm^{-1} corresponds to C-H in plane bending. 1004 cm^{-1} corresponds to C-H out of plane bending. 803 cm^{-1} C-H out of plane bending. 611 cm^{-1} corresponds to ring deformation out of plane bending and 517 cm^{-1} matching to C-H out of plane bending

The first step in understanding the encapsulation was to study interaction between β CD and FB. For that, the samples of stoichiometry 1:1 were prepared. The Raman spectra were recorded and are presented in Figure 4.27. Several features corresponding to FB are observed in the spectra with moderate intensities. The peaks found at the positions: 1000, 1606 and 3065 cm^{-1} . The appearance of features corresponding to FB in the inclusion complex spectrum reveals that the vibrational modes of the β CD have changed in presence of FB.

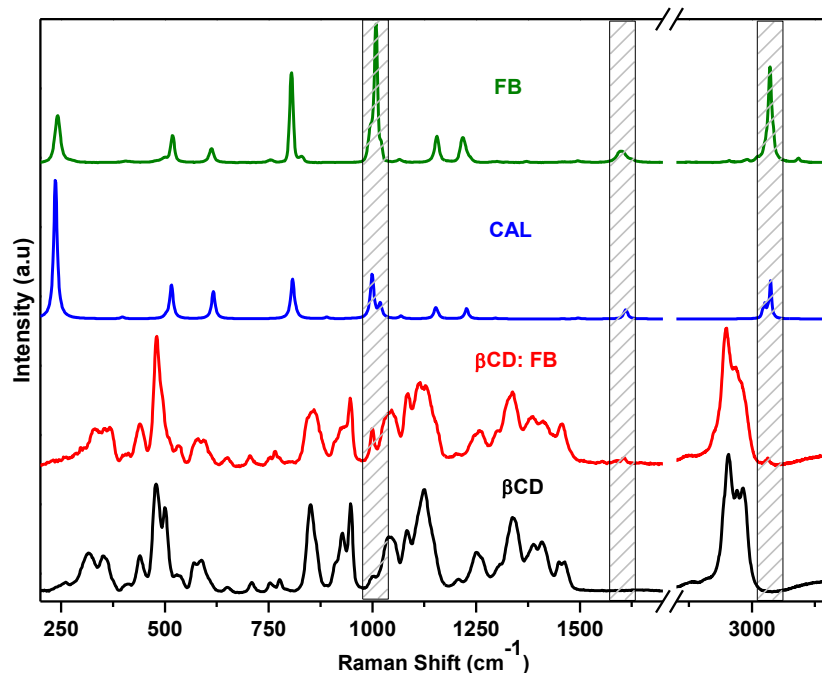


Figure 4.27 : Raman Spectrum of the β CD, FB and of the inclusion complex obtained after mixing β CD with FB in the molar ratio of 1:1

The most impacted vibrational modes are shown in the Figure 4.28. A comparison was made for the FB peaks appearing in the complex and of the same peaks in the observed FB spectrum. It can be concluded that the peaks have changed their positions as well as intensities on complex formation as can be seen in the table 4.3.

FB		Complex	
Peak	Relative Intensity	Peak	Relative Intensity
1004	1.00	1000	0.26
1601	0.08	1606	0.05
3074	0.68	3065	0.05

Table 4.3 : Comparison of FB peak shifts and relative intensities (free FB and inclusion complex with β CD).

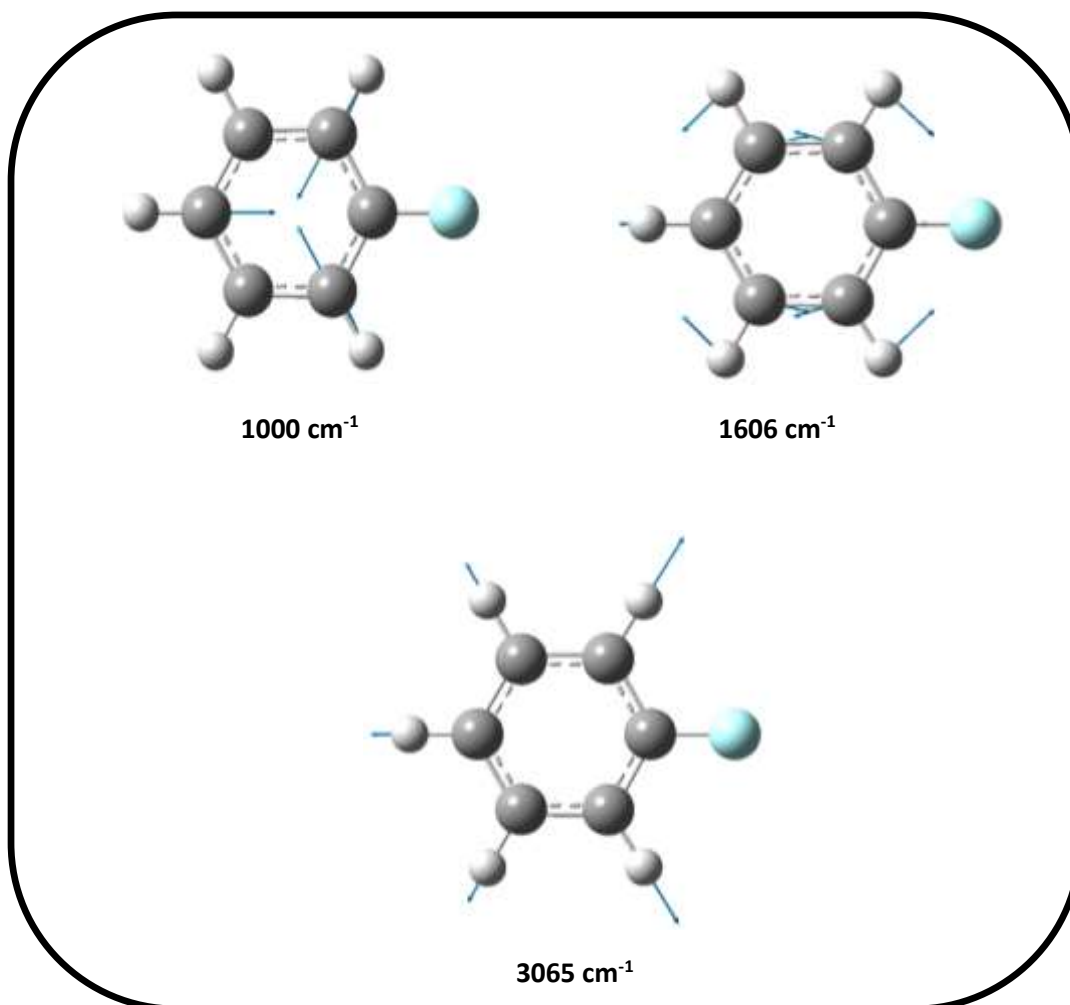


Figure 4.28. The vibrational modes of FB which are most impacted on interaction with β CD.

4.5.1.3 β CD:TOL Raman studies

Toluene^{29,30}- a monosubstituted benzene derivative³¹ consists of a CH₃ group attached to a phenyl group. Because of methyl group, toluene is more reactive than benzene towards electrophiles. It is mostly used as industrial feedstock and solvent. The calculated harmonic frequencies of C-H vibrations were scaled by a factor of 0.96 and all other frequencies by 0.97 in order to get a good agreement to the observed one.

When the complexes were synthesised with toluene, some peaks attributed to TOL were observed in the Raman spectra (Figure 4.29).

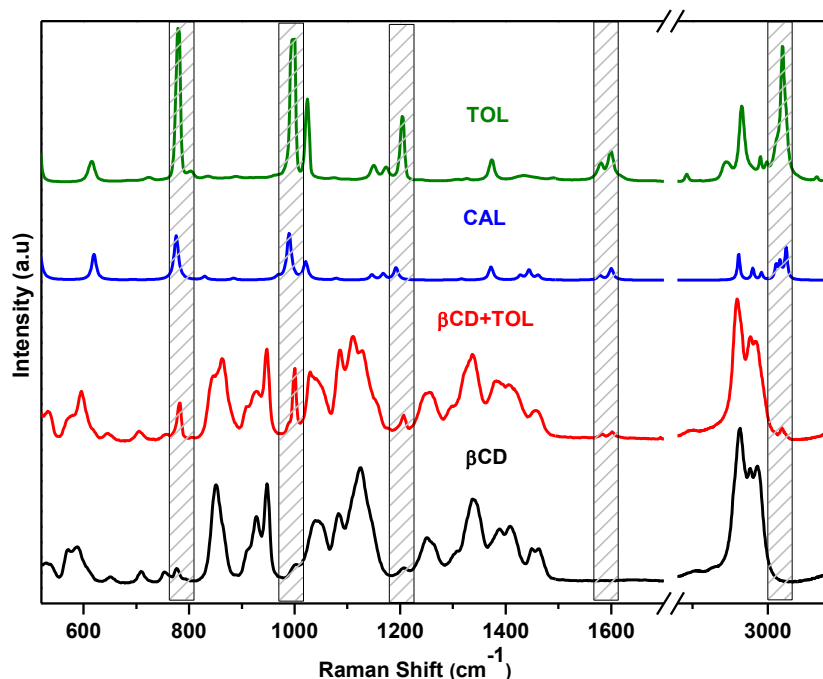


Figure 4.29. Raman Spectrum of the β CD, TOL and of the inclusion complex obtained after mixing β CD with TOL in the molar ratio of 1:1.

The Raman spectrum of toluene show important peaks at positions 618, 780, 996, 998, 1200, 1576, 1596 and 3048 cm^{-1} . The peak at 513 cm^{-1} corresponds to in-plane C-C stretch and ring deformation. The peak around 780 cm^{-1} corresponds to out of plane bending of aromatic C-H. The peaks in the region n 1300-1050 cm^{-1} corresponds to aromatic C-H in plane bending. On moving forward, the peaks in the region 1350-1500 cm^{-1} and 1585 to 1600 cm^{-1} correspond to aromatic C-C stretching. In the functional group region, the peaks can be seen at 3048 cm^{-1} shows aromatic C-H stretches. The complexation of TOL inside the β CD cavity has taken place without the presence of linear alcohol. On referring to the Raman spectrum of β CD: TOL complex, presence of many toluene peaks can be seen.

The peak positions which are evidently seen on complexation with β CD are 597, 785, 998, 1206, 1601 and 3045 cm^{-1} . The peaks are moderately intense giving a hint of interaction between the host and the guest. The vibrational modes of the most affected peaks are shown in the Figure 4.30. The comparison of the TOL peaks in the observed spectrum and peaks observed in the complex formed can be seen in the table 4.4.

TOL		Complex	
Peak	Relative Intensity	Peak	Relative Intensity
618	0.12	597	0.31
780	1.00	785	0.22
998	0.92	998	0.45
1200	0.42	1206	0.15
1596	0.19	1601	0.04
3048	0.88	3045	0.07

Table 4.4 : Comparison of TOL peak shifts and relative intensities (free TOL and inclusion complex with β CD).

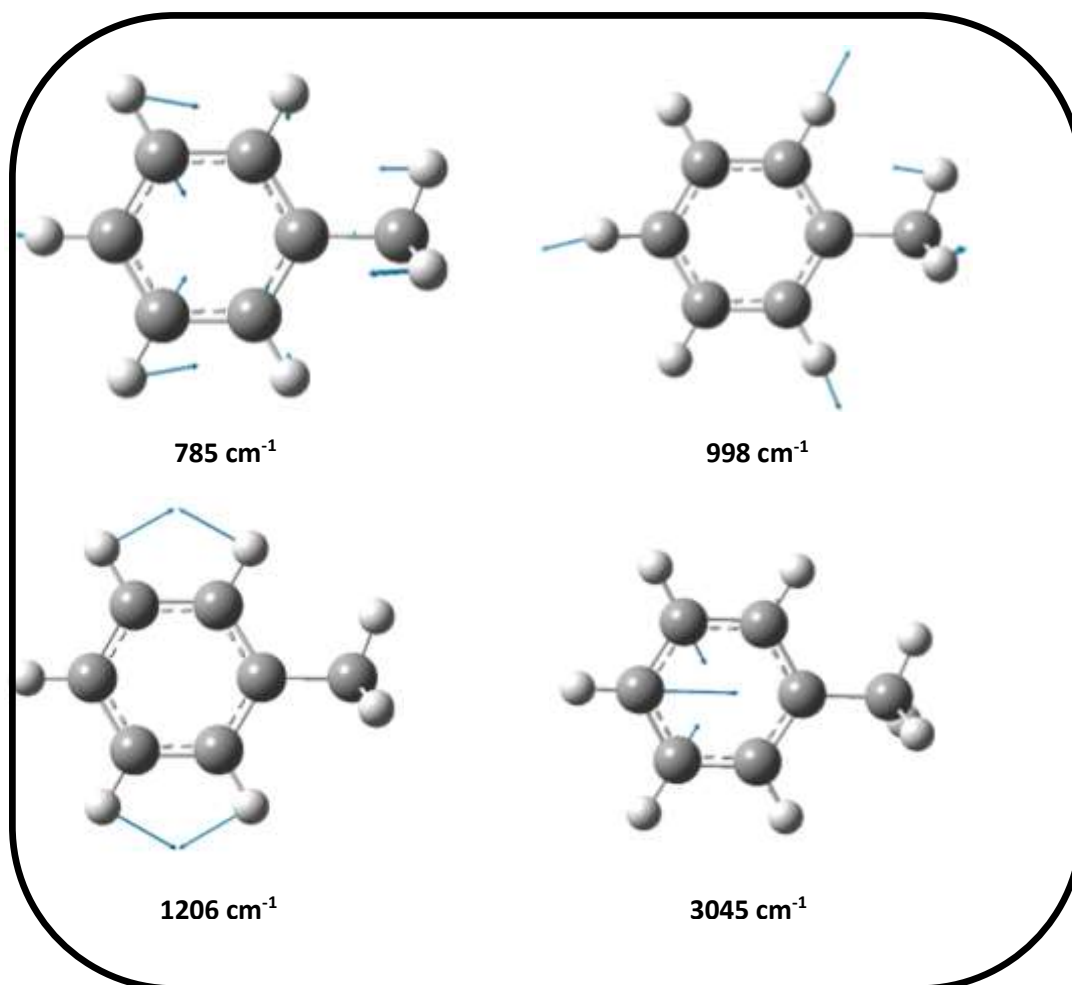


Figure 4.30 : The vibrational modes of TOL which are most impacted by the interaction with β CD.

4.5.1.4 β CD:TFT Raman studies

Another derivative of toluene, α,α,α -trifluorotoluene (TFT) with the formula $C_6H_5CF_3$ has been used to study complexation with β CD. Similar to toluene, TFT used mostly as solvent in organic synthesis and also as intermediate in the production of pesticides and pharmaceuticals.

The case of TFT is very similar to toluene as the only difference is of replacement of three methyl hydrogen by electronegative and heavier element fluorine. The vibrations belong to C-X (X=F, Cl etc.) bonds which are formed between the ring and the halogen atoms, are interesting as mixing of vibrations are possible due to the lowering of molecular symmetry and the presence of heavy atoms. For other heavier halogen atoms like Cl, Br and I, the Raman vibration bands result in strong bands, but for F the bands are comparatively weaker.

The calculated harmonic frequencies of C-H vibrations were scaled by a factor of 0.96 and all other frequencies by 0.99. In the case of CF_3 group, the stretching vibrations are usually observed between 1400 and 1110 cm^{-1} . The C-F symmetric stretching of the molecule is 1163, 1184 and 1322 cm^{-1} and it is assigned to stretching vibration of C-F bond. The bending deformations corresponding to CF_3 group are not active in recorded Raman spectra but can be predicted by theoretical studies.

The C-H stretching vibrations of aromatic ring are observed at 3075 cm^{-1} . The plane due to C-H in-plane bending vibrations are observed in the region 1000-1300 cm^{-1} . The vibrations identified at 1003, 1025, 1063, 1158, 1184 and 1322 cm^{-1} are assigned to C-H in plane bending. C-H out-of-plane bending vibrations are appeared in the region 650-980 cm^{-1} . The C-H out of plane bending vibrations at 757, 663 and 618 cm^{-1} are also present in the characteristic region.

The bands between 1400 and 1650 cm^{-1} in benzene derivatives are usually assigned to C=C stretching modes. The C=C stretching vibrations are found at 1594 and 1611 cm^{-1} . The C-C stretching vibration can be found in the region 1100-1350 cm^{-1} region. The in-plane (CCC) carbon bending vibrations are obtained from the non-degenerate (1010 cm^{-1}) and degenerate (606 cm^{-1}) modes of benzene. The bands assigned for CCC out-of-plane bending vibrations are observed at 492, 398 and 338 cm^{-1} .

On obtaining the Raman spectral studies, simpler spectrum of TFT is obtained in correlation with toluene. On recording the spectrum of inclusion complex formed between TFT and β CD (Figure 4.31) only, some differences of the peaks can be seen. Some kind of interaction is occurring between the two molecules. The most impacted vibrational modes of TFT obtained by theoretical means can be seen in the Figure 4.32.

The appearance of new peaks at different positions: 767, 1002, 1611 and 3065 cm^{-1} are noticed. All these vibrations are mostly due to stretching of the aromatic ring molecules. The comparison of relative intensities of the free TFT and complex peaks can be seen in the table 4.5.

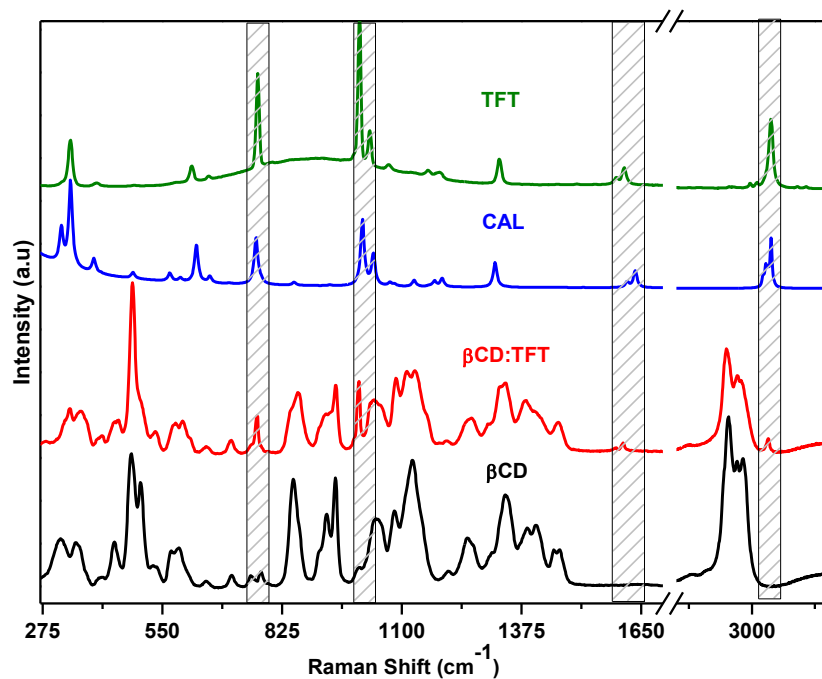


Figure 4.31 : Raman Spectrum of the β CD, TFT and of the inclusion complex obtained after mixing β CD with TFT in the molar ratio of 1:1.

TFT		Complex	
Peak	Relative Intensity	Peak	Relative Intensity
770	0.64	767	0.21
1003	1.00	1002	0.41
1611	0.10	1611	0.05
3075	0.44	3065	0.08

Table 4.5 : Comparison of TFT peak shifts and relative intensities (free TFT and inclusion complex with β CD).

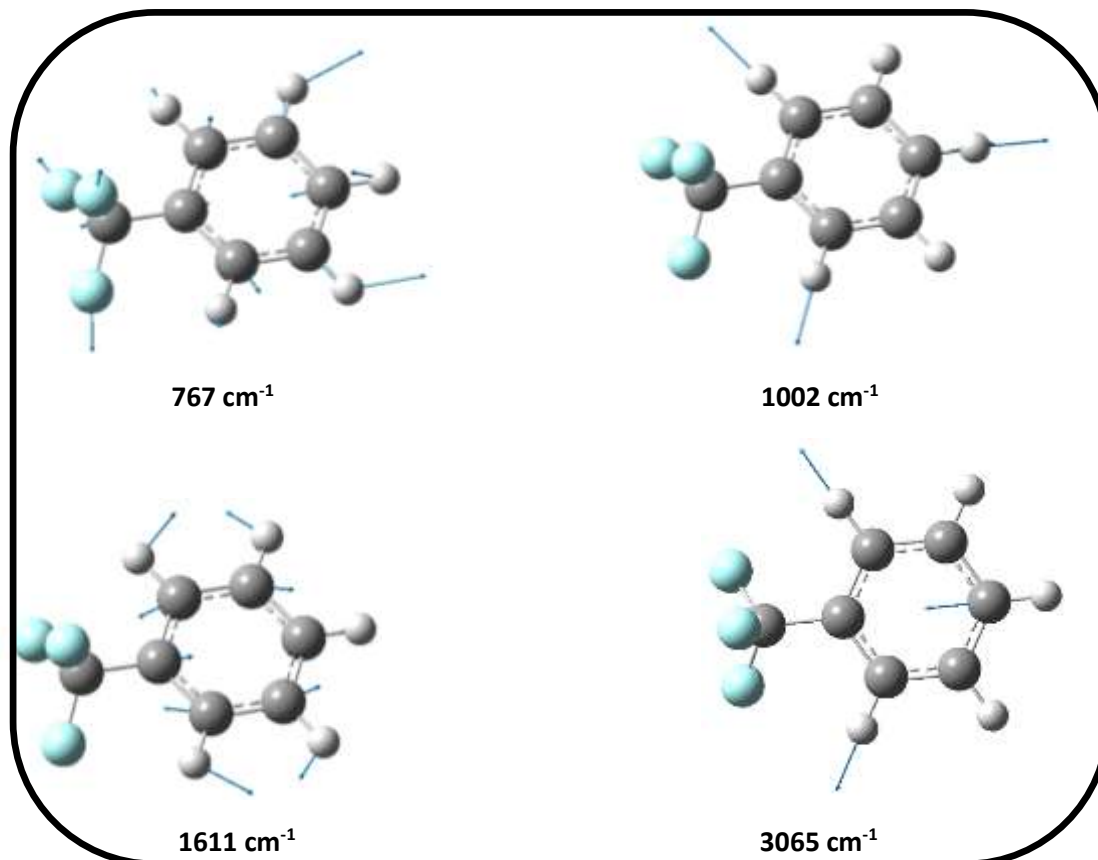


Figure 4.32 : The vibrational modes of TFT which are most impacted by the interaction with β CD.

4.5.1.5 β CD:PHE Raman studies

Phenol (PHE) is an aromatic organic compound where a phenyl group is bonded to a hydroxyl group. It is a derivative of benzene and limited studies have been done for them. Fluorescence studies¹⁴ of native phenol and of derivatives^{32,33} are reported in the literature.

In order to compare our studies, the spectrum of PHE was calculated theoretically. The calculated harmonic frequencies of C-H vibrations were scaled by a factor of 0.96 and all other frequencies by 0.97 to allow a good agreement with observed one for PHE alone.

The Raman spectrum of phenol shows the presence of C-H stretching vibrations in the region 3100–3000 cm⁻¹ which is the predictable region for spotting C-H stretching vibrations. According to the present study, the C-H stretching vibrations are observed at 3060 cm⁻¹. The peaks obtained for the Raman spectrum of phenol are obtained due to mixture of different vibrational modes. For example- the peak at 1606 cm⁻¹ is dominated by C-C stretching but also belongs to C-C-H in plane bending and C-C-C bending by some factor. 1503 cm⁻¹ is the mixture of C-C-H in plane bending and C-C stretching. 1252 cm⁻¹ occurred due to blending of C-O stretch, C-C stretch and C-C-H in-plane bending. 1172 cm⁻¹ corresponds to C-C stretching and OH in plane bending. 1026 cm⁻¹ is again due to C-C stretching and C-C-H in-plane bending. The combination of C-C-C bending and C-C stretching appeared at 998 cm⁻¹ as the most intense peak. The following peaks at 810 and 618 cm⁻¹ are due to C-C stretching, C-C-C bending and C-O stretching. For 537 cm⁻¹, there occurs C-C-C bending, C-O and C-C stretching. 243 and 456 cm⁻¹ are predominantly due to ring torsion, out of plane deformation of C-O and C-H bonds.

The complex prepared for the molar ratio 1:1 (Figure 4.33), after undergoing investigation show some of the phenol peaks. These peaks can be noted at: 233, 527, 815, 1000, 1026, 1596 and 3057 cm^{-1} . The most intense and sharp peak in the complex spectrum is present at position 1000 cm^{-1} . This band corresponds to combined effect of C-C-C bending and C-C stretching of the phenyl ring. Few of the peaks are present with moderate intensity like: 3057, 1596, 815 and 233 cm^{-1} . The peaks at positions 1172 and 1252 cm^{-1} have completely removed from the spectrum. The most influenced vibrational modes of PHE are presented in the Figure 4.34 whereas the comparison of the relative intensities of the PHE peaks in the complex with respect to free PHE are presented in the table 4.6.

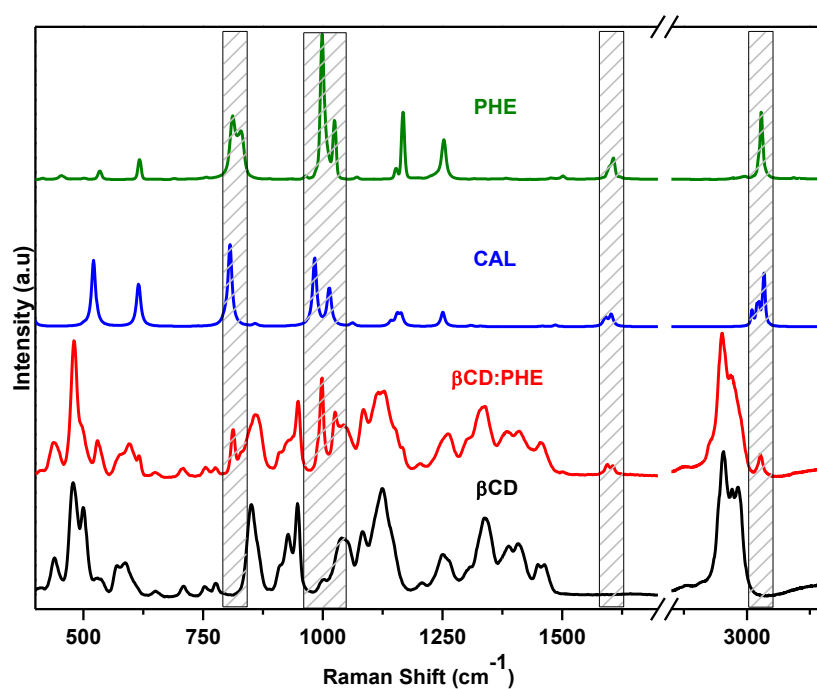


Figure 4.33. Raman Spectrum of the β CD, PHE and of the inclusion complex obtained after mixing β CD with PHE in the molar ratio of 1:1

BA		Complex	
Peak	Rel.Int.	Peak	Rel.Int.
243	0.15	233	0.11
537	0.04	527	0.25
810	0.43	810	0.33
998	1.00	1000	0.69
1606	0.14	1596	0.09
3060	0.45	3057	0.16

Table 4.6: Comparison of PHE peak shifts and relative intensities (free PHE and inclusion complex with β CD).

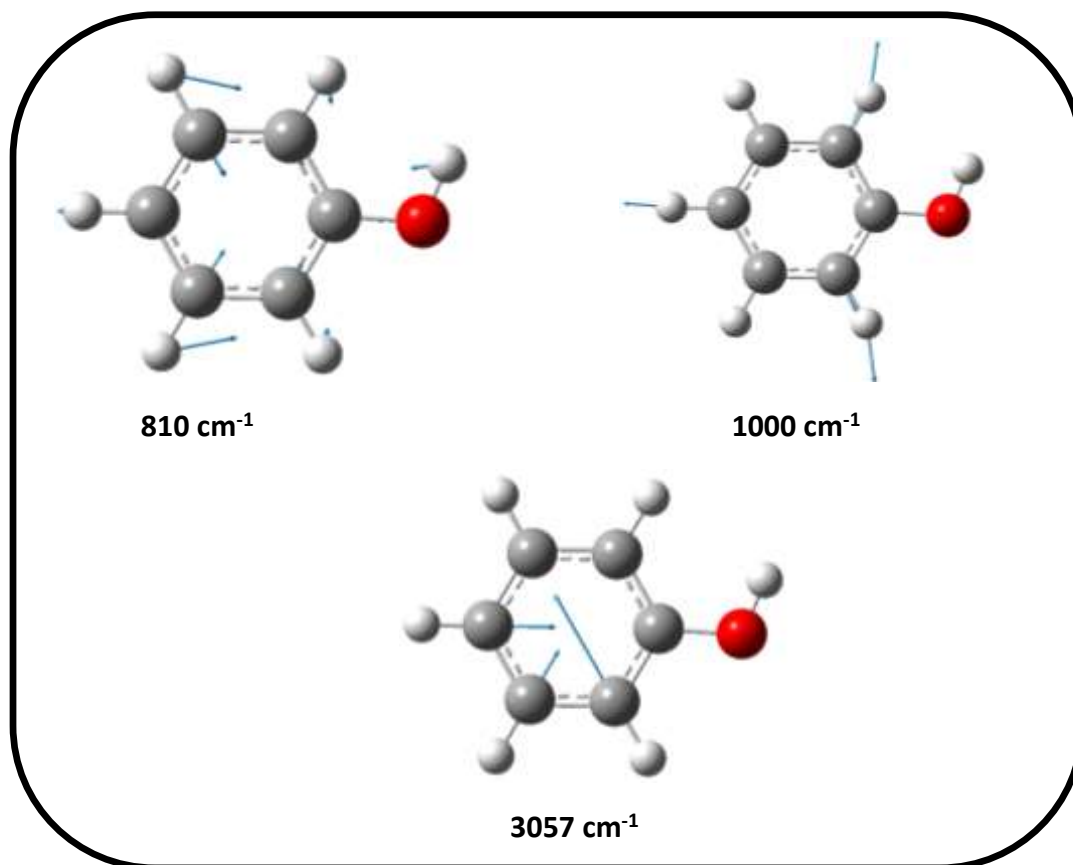


Figure 4.34 : The vibrational modes of PHE which are most impacted by the interaction with β CD.

4.5.1.6 β CD:BA Raman studies

The complexation of benzoic acid (BA) and β CD have already been studied by many scientists^{3,4,18,34–37}. Benzoic acid is the derivative of benzene when a hydrogen of the aromatic ring is replaced by carboxylic group. So the Raman spectrum of benzoic acid shows peaks corresponding to vibrational modes of carboxylic group additionally in comparison to Raman spectrum of benzene.

We calculated the spectrum of BA by theoretical means for further comparison. The calculated harmonic frequencies of C-H vibrations were scaled by a factor of 0.96 and all other frequencies by 0.98. Raman spectrum of benzoic acid contains a band of aromatic ring C–H stretching vibrations (3073 cm^{-1}) and several bands at $1800\text{--}1400\text{ cm}^{-1}$ related to carbonyl group C=O (1793 cm^{-1}) and benzene ring C=C (1601 , 1545 , and 1453 cm^{-1}) stretching vibrations.

For instance, the band at 420 cm^{-1} corresponds to C-C stretching of the benzene ring, while the bands at 614 , 1000 , 1026 and 1438 cm^{-1} are all assigned to ring deformations. And the band at 787 cm^{-1} can also be attributed to the ring deformation, along with the O-C-OH in-plane scissoring. The O-H in-plane bending would be observed in the couple weak bands at 1130 and 1180 cm^{-1} . Both of the bands at 1284 and 1319 cm^{-1} correspond to the combination of O-H and C-H in plane bending. The band at 1602 cm^{-1} can be attributed to the C-C stretching of the benzene ring, whereas the band at 1631 cm^{-1} is assigned to the C=O stretching ($\nu(\text{C=O})$) with accompany of the O-H in-plane bending.

For the complex (1:1) prepared in the absence of alcohols (Figure 4.35), there are several peaks observed for benzoic acid. Those peaks can be found at the positions: 787, 1000, 1602 and 3066 cm^{-1} . The significantly intense peaks are observed at 1000 and 1602 cm^{-1} . The other peaks also show their existence but are very less intense. Few of the β CD peaks also show changes like the intensity of the peak at 478 cm^{-1} has fairly increased. The peaks at 851, 948, 1123, 1335 and 2905 cm^{-1} have decreased in intensity. Very few peaks like 315 and 1408 cm^{-1} have completely vanished or may be only traces are left. The most affected vibrational modes during complexation are shown in the Figure 4.36. Table 4.7 presents the comparison of the free BA and complex peaks in terms of their relative intensities.

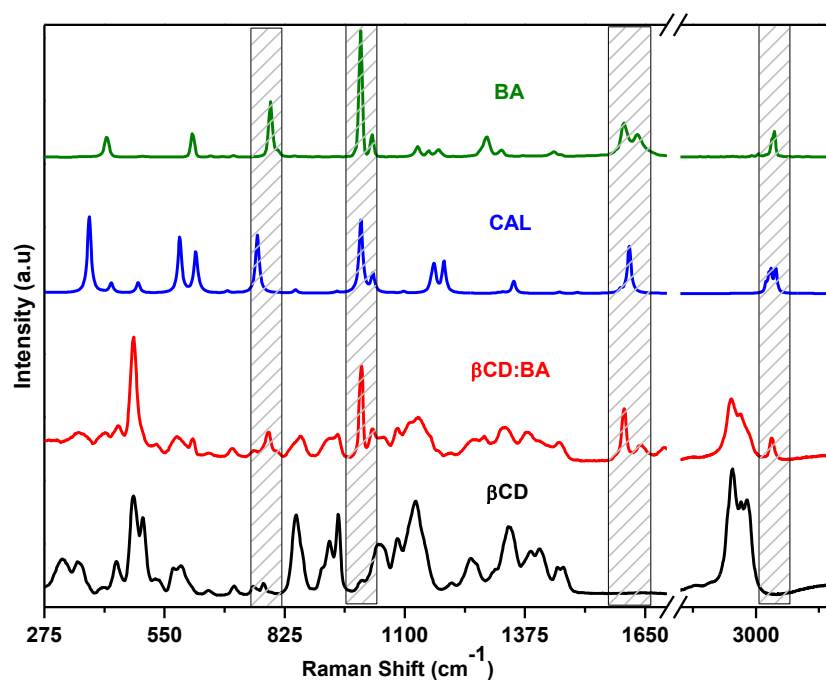


Figure 4.35. Raman Spectrum of the β CD, BA and of the inclusion complex obtained after mixing β CD with BA in the molar ratio of 1:1.

BA		Complex	
Peak	Relative Intensity	Peak	Relative Intensity
790	0.43	787	0.23
998	1.00	1000	0.76
1600	0.26	1602	0.42
3075	0.19	3066	0.19

Table 4.7 : Comparison of BA peak shifts and relative intensities (free BA and inclusion complex with β CD).

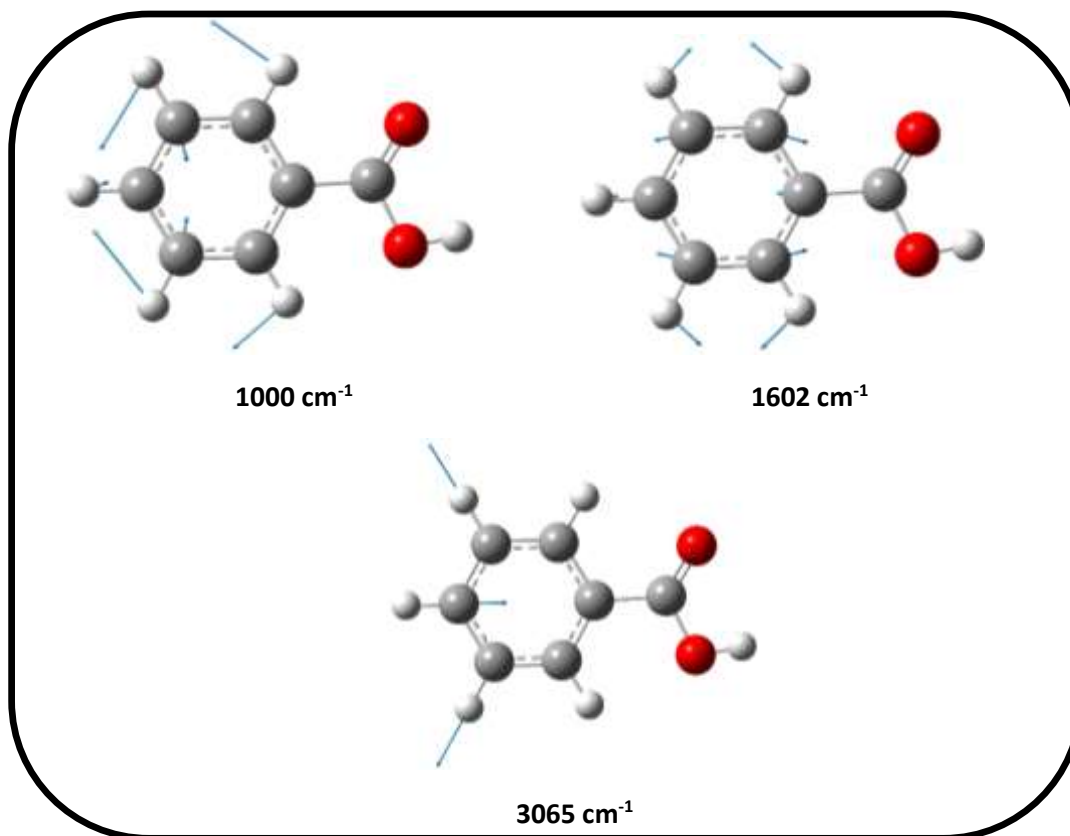


Figure 4.36. The vibrational modes of BA which are most impacted by the interaction with β CD

4.5.2 Bicyclic aromatic hydrocarbons

4.5.2.1 β CD:NAP Raman studies

Naphthalene (NAP) ball commonly known as ‘mothballs’ are used as chemical pesticides and deodorant for storing clothes. They have been classified as carcinogens and are banned in EU. Due to their carcinogenic properties, they are added to the list of PAHs. NAP can also be used as a precursor to other chemical reactions. This versatile nature has been continuously studied by researchers from the past decades and still, the studies are ongoing. Focussing on the complexation studies have revealed the formation of 1:1 complexes with β CD^{38,39}. The advancement in the complexation studies has acquired the detailed information about photo physical properties^{40,41}. The research did not remain limited to native NAP only, many derivatives have also been studied⁴²⁻⁴⁴.

The following figure 4.37 represents the Raman spectra of the native β CD, naphthalene and the of the inclusion complex prepared. To compare the observed spectrum, theoretical calculation was done to obtain spectrum of NAP. The calculated harmonic frequencies of C-H vibrations were scaled by a factor of 0.96 and all other frequencies by 0.98 to allow a good agreement with observed one for NAP alone.

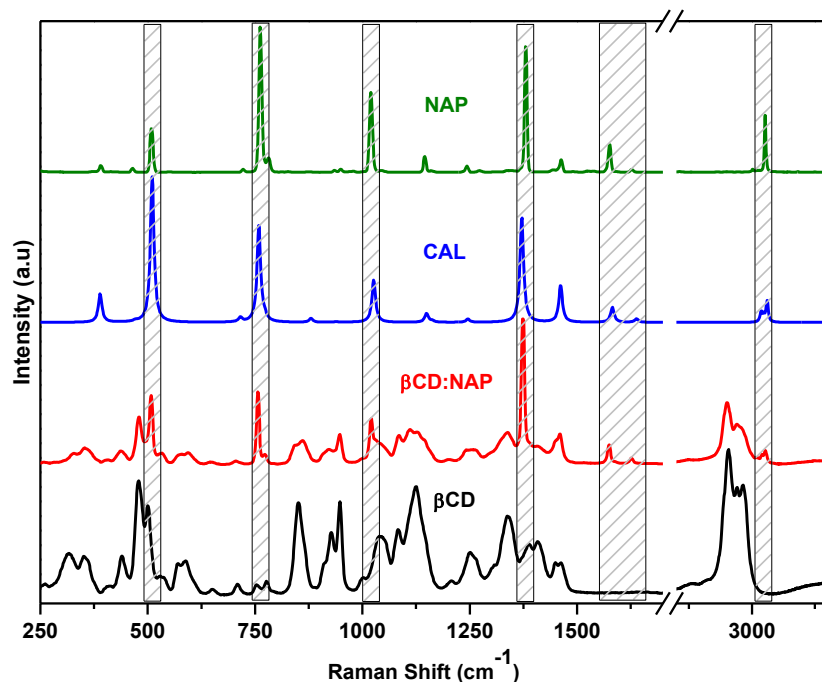


Figure 4.37 Raman Spectrum of the β CD, NAP and of the inclusion complex obtained after mixing β CD with NAP in the molar ratio of 1:1.

NAP		Complex	
Peak	Rel.Int.	Peak	Rel.Int.
507	0.29	507	0.47
760	1.00	755	0.49
1018	0.54	1018	0.31
1378	0.86	1378	1.00
1572	0.18	1576	0.12
3050	0.39	3055	0.09

Table 4.8 : Comparison of NAP peak shifts and relative intensities (free NAP and inclusion complex with β CD).

The peaks corresponding to naphthalene can be easily seen for the inclusion complex spectrum. Furthermore, the relative intensities of the naphthalene peaks observed for the complex, on comparison to that of isolated ones give the proof of molecular interaction and inclusion within the CD cavities clearly (Table 4.8). Also, significant differences in intensities can be observed for several peaks.

The peak located at 760 cm^{-1} , corresponding to ring breathing mode and C-C central stretch, appears as the most intensive peak in the NAP spectrum whereas it is remarkably diminished in the spectra of complexes (755 cm^{-1}). On the contrary, the peak at 1378 cm^{-1} , assigned to a C-C stretching and ring deformation, is becoming the most intense mode when the NAP is embedded into the cavity of the CD. Other modes which are varying after the complex formation are less obvious in the presented graph. An increase of the relative intensity is clearly observed for the C-C-C bending at 507 cm^{-1} . On the contrary, the C-H out of plane stretching mode at 3050 cm^{-1} (3055 cm^{-1} in complex) as well as in plane C=C stretching at 1572

cm^{-1} were less visible when NAP is included into CD (1576 cm^{-1}). The observed change indicates that the stretching mode inducing a potential interaction of H atoms with the CD as well as the radial mode or the C-H stretching exhibit a lower intensity compared to the other modes, which is an evidence of the inclusion of the NAP in the βCD cavity. The most impacted modes during complex formation are presented in the Figure 4.38.

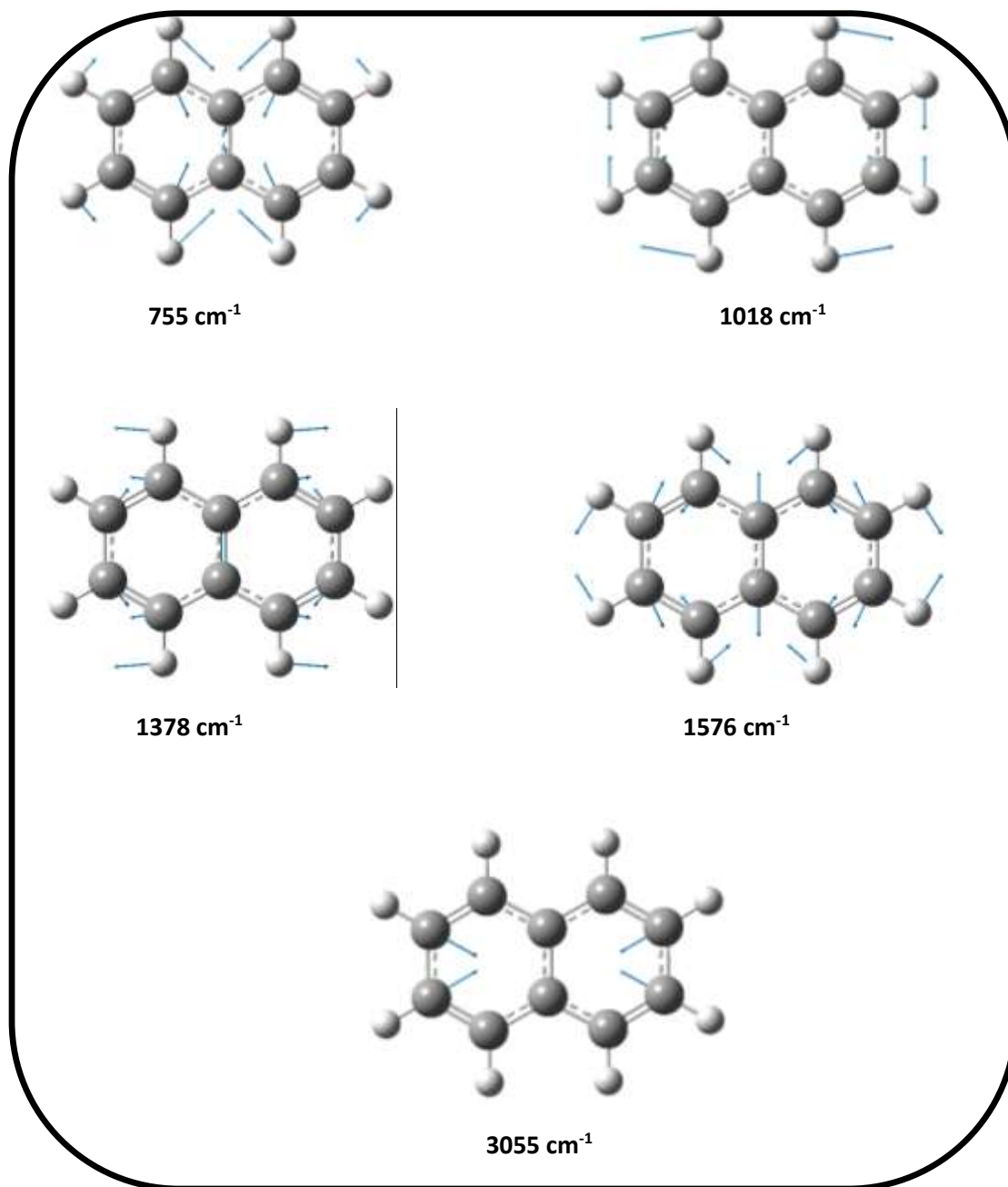


Figure 4.38 : The vibrational modes of NAP which are most impacted by the interaction with βCD .

4.5.2.2 β CD:2-NAP Raman studies

When a hydroxyl group gets attached at beta position of naphthalene ring, 2-naphthol (2-NAP) is formed. They are homologues to phenols but more reactive. In the literature, the research done on β CD:2-NAP complexes focussed mainly on their absorption, fluorescence⁴⁵ properties to study their orientation inside the cavity.

The calculated harmonic frequencies of C-H vibrations were scaled by a factor of 0.96 and all other frequencies by 0.99 to allow a good agreement with observed 2-NAP spectrum.

In case of 2-NAP⁴⁶, the main important bands were observed at 3060, 1636, 1581, 1383, 1013, 770 and 527 cm^{-1} . The strong band at 3056 cm^{-1} is assigned to the C-H stretching modes. The band at 1581 cm^{-1} is assigned to C-C stretching and C-H in plane bending. The second most intense band observed at 1383 is assigned to the ring C-C and C-O stretching mode. The following bands 1170 and 1139 cm^{-1} are attributed to the OH and C-H in-plane bending modes. The 1013 cm^{-1} band is assigned to the C-C-C in-plane bending modes. The very strong peak at 770 cm^{-1} correspond to the OH out-of-plane deformations, whereas the Raman signal at 718 cm^{-1} was assigned to C-C-C in-plane bending mode. Other peak for the C-C-C in-plane deformation appear at 527 cm^{-1} . The in-plane C-OH deformation and C-C-C deformation modes appear at 474, 445 and 406 cm^{-1} .

The spectrum obtained for β CD and 2-NAP shows presence of several peaks corresponding to 2NAP (Figure 4.39). These peaks are present at: 521, 764, 1013, 1378, 1576, 1631 and 3050 cm^{-1} . The two most intense peaks at 764 and 1378 cm^{-1} corresponding to OH out of plane deformation and combination of C-C and C-O stretching modes respectively are present. Other peaks at positions: 521, 1013, 1576, 1631 and 3050 cm^{-1} are moderately intense, clearly justifying their presence. The vibrational modes attributed to these peaks are shown in the Figure 4.40. Table 4.9 presents comparison of relative intensities of the 2-NAP in free state and in complex form.

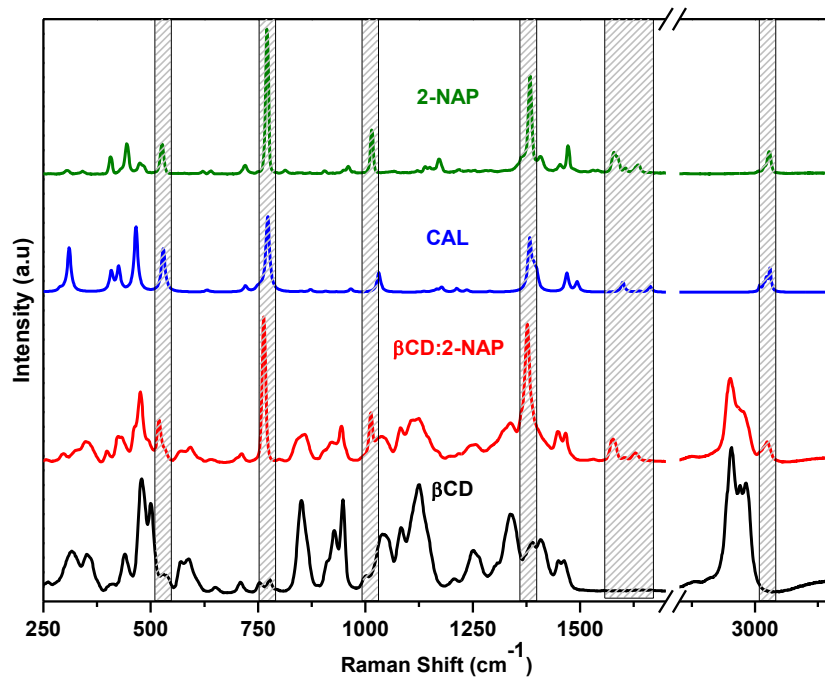


Figure 4.39 : Raman Spectrum of the β CD , 2-NAP and of the inclusion complex obtained after mixing β CD with 2-NAP in the molar ratio of 1:1.

2-NAP		Complex	
Peak	Relative Intensity	Peak	Relative Intensity
527	0.20	521	0.28
770	1.00	764	1.00
1013	0.30	1013	0.33
1383	0.67	1378	0.95
1581	0.14	1576	0.15
1636	0.05	1631	0.06
3060	0.15	3050	0.13

Table 4.9 : Comparison of 2-NAP peak shifts and relative intensities (free 2-NAP and inclusion complex with β CD).

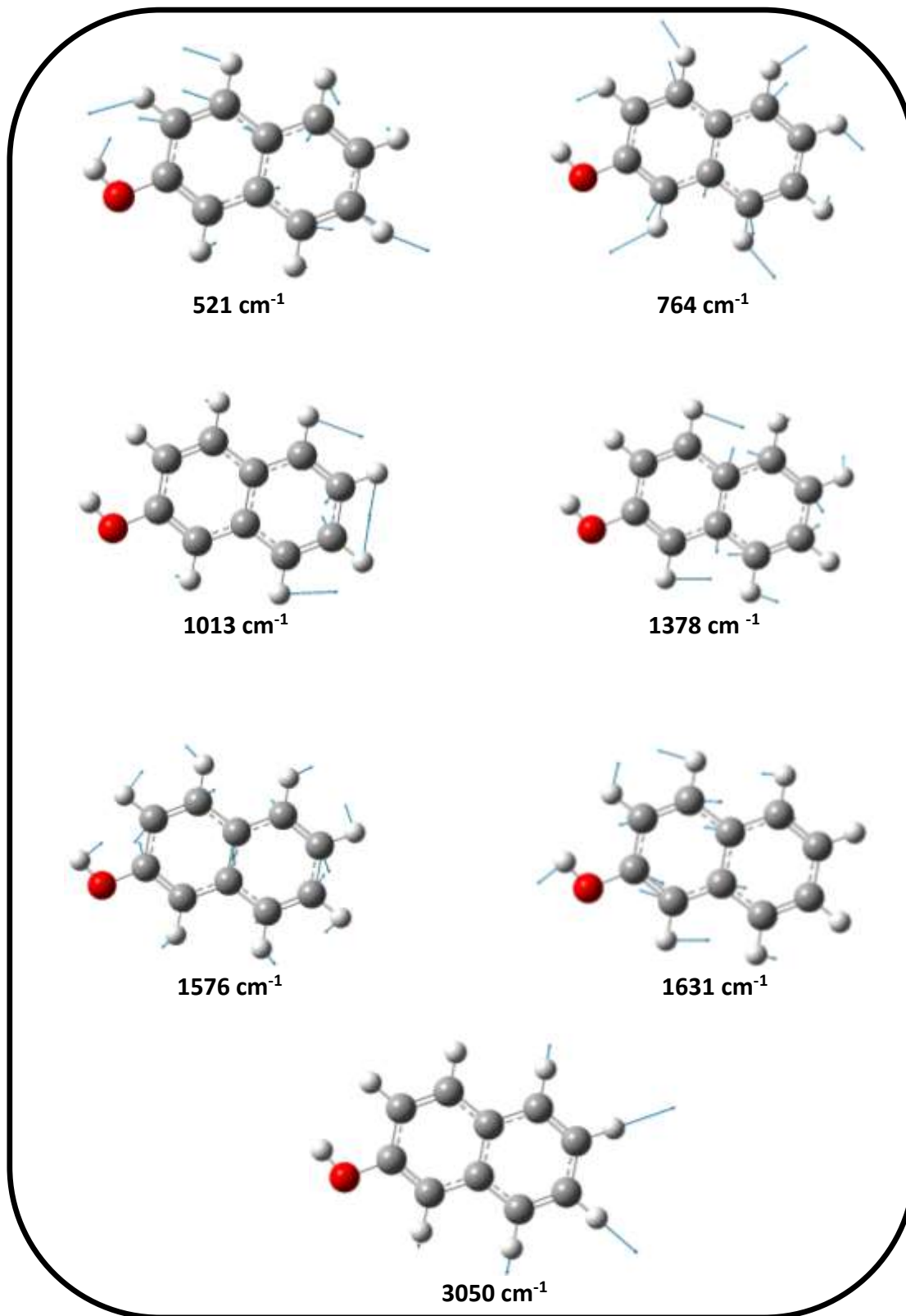


Figure 4.40 : The vibrational modes of 2-NAP which are most impacted by the interaction with β CD

4.5.3 Polycyclic aromatic hydrocarbons

4.5.3.1 β CD: ANTH Raman studies

Anthracene (ANTH), a PAH consists of three fused benzene rings. The main reason behind its occurrence is coal tar and combustion processes. The inclusion complexation have been studied by different techniques namely chromatography⁴⁷ electrochemical methods⁴⁸ etc. Anthracene complexes have also been part of the remediation studies^{49,50} for soil contamination.

The theoretical calculation for ANTH spectrum were performed for further comparison. The calculated harmonic frequencies of C-H vibrations were scaled by a factor of 0.96 and all other frequencies by 0.98.

The Raman spectrum for anthracene⁵¹⁻⁵³ has five distinctive bands which allow the identification of the molecules: 401, 756, 1164, 1403 and 1563 cm^{-1} . The assignment of these bands can be divided into different regions: (1) 1650–1500 cm^{-1} , C–C stretching mode mixed with some CH in-plane bending vibrations; (2) 1500–1350 cm^{-1} , bands are mainly attributed to strong C–C stretching coupled with weak ring-breathing vibrations; (3) 1300–1000 cm^{-1} , bands are mostly CH in-plane bending vibrations; and (4) 1000–600 cm^{-1} , generally CH out-of-plane bends; and (5) bands below 550 cm^{-1} may be due to out-of-plane skeletal deformation vibrations.

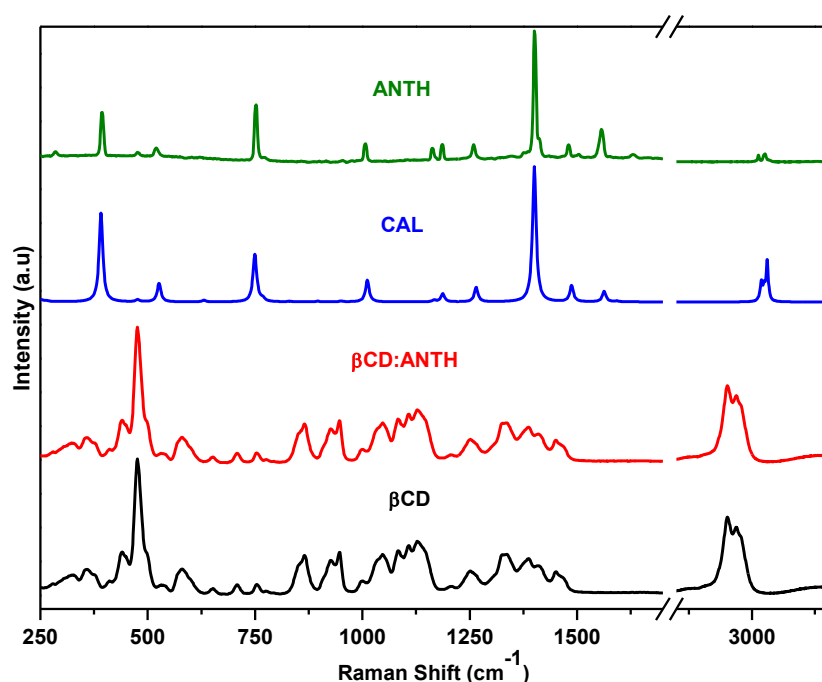


Figure 4.41 : Raman Spectrum of the β CD, ANTH and of the inclusion complex obtained after mixing β CD with ANTH in the molar ratio of 1:1.

The Raman spectrum of the complexes prepared with only β CD and ANTH in the molar ratio 1:1 does not show any of the peaks corresponding to ANTH (Figure 4.41). The spectrum obtained is exactly similar to what we have obtained for β CD. The following result gives a clear indication of failure of inclusion phenomenon. We can thus report that, β CD and anthracene

alone do not form any complex. If the inclusion had occurred the most probable affected peaks corresponding to vibrational modes are present in the Figure 4.42.

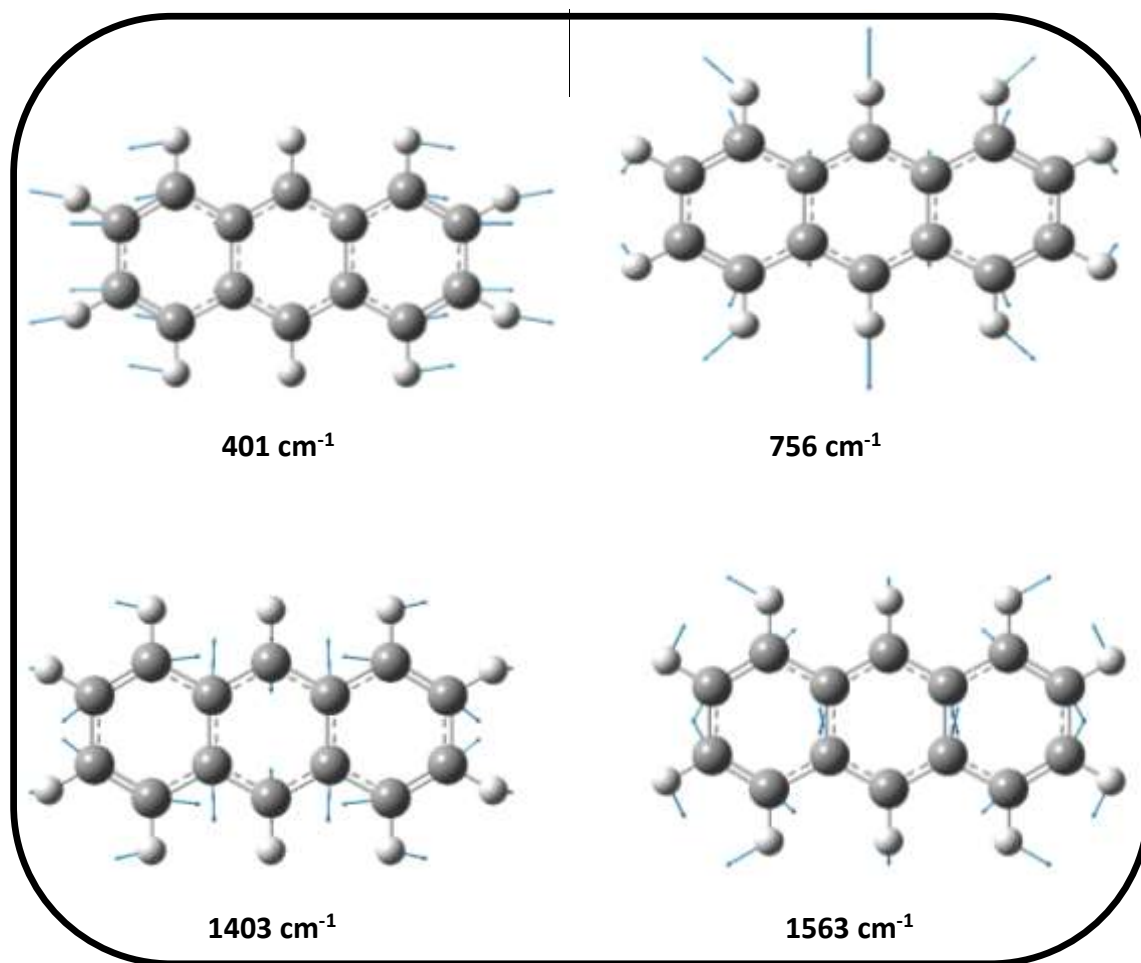


Figure 4.42 : The vibrational modes of ANTH which are most probably impacted by the interaction with β CD.

4.5.3.2 β CD: PYR Raman studies

Pyrene (PYR) consists of four fused benzene rings. It is formed during incomplete combustion of organic compounds. In the past, scientists have tried to study the complexation behaviour^{54,55} of PYR and β CD by different spectroscopic studies⁵⁶. Absorption studies⁵⁷ indicated formation of 1:1:1 inclusion complex with lower primary and cyclic alcohols. Fluorescence studies⁵⁸⁻⁶¹ indicated the size dependency of the components to obtain larger equilibrium constants for the ternary complexes. Some of the scientists from the same groups have also studied the chromatographic studies^{47,62,63} focusing on linear and cyclic alcohols as mobile phase co-modifiers.

FT-Raman spectroscopic studies have not yet been done for β CD:PYR complexes. The complexes reported are studied by different techniques like Surface enhanced Raman Scattering (SERS)⁶⁴ for sensing Polycyclic aromatics. UV Resonance Raman⁶⁵ have also been done to further characterize PAHs.

On Raman Spectroscopy investigation of complexes, peaks corresponding to PYR can be seen in the spectra of all the complexes prepared with β CD (Figure 4.43). The relative intensities of the peaks of native PYR and of the complex formed (Table 4.10), on comparison can further direct towards the hint of molecular interaction and inclusion with the CD cavity. The calculated harmonic frequencies of C-H vibrations were scaled by a factor of 0.95 and all other frequencies by 0.98.

The Raman spectrum of PYR⁵³ can be divided into four important regions (1) 1650-1550 cm^{-1} , the ring stretching mode mixed with little CH in-plane bending; (2) 1500-1350 cm^{-1} bands mainly attributed to strong CH in-plane bending coupled with weak ring breathing. Also (1050-1000 cm^{-1}) belong to the same mode of vibrations. (3) 1300-1000 cm^{-1} , bands are mostly CH bending; and (4) 1000-600 cm^{-1} , generally CH out-of-plane bends. All the bands below 550 cm^{-1} may due to out-of-plane ring bending vibrations. The intense peaks are observed at the peaks positions: 407, 587, 1067, 1247, 1407, 1587, 1629 cm^{-1} in the PYR Raman Spectrum.

The Raman spectrum of the complex prepared in the solid state shows the appearance of new peaks other than β -CD peaks with different intensities. They can be clearly seen at the positions: 409, 594, 1065, 1242, 1412, 1597 and 1630 cm^{-1} .

The different peaks with good intensities like the one located at 409 and 594 cm^{-1} corresponding to out of plane ring bending vibrations and C-H out of plane bending respectively, appear as the most noticeable intensive peak in the PYR spectrum whereas equally intense in the spectra of complex prepared without alcohols. On moving ahead, other peaks like the ones at 1242, 1412, 1597 and 1630 cm^{-1} are dominating the spectrum of the complex. These peaks correlate to different vibrational modes like ring stretching, CH in plane bending and ring breathing modes. The other modes which are varying during complex formation are less obvious.

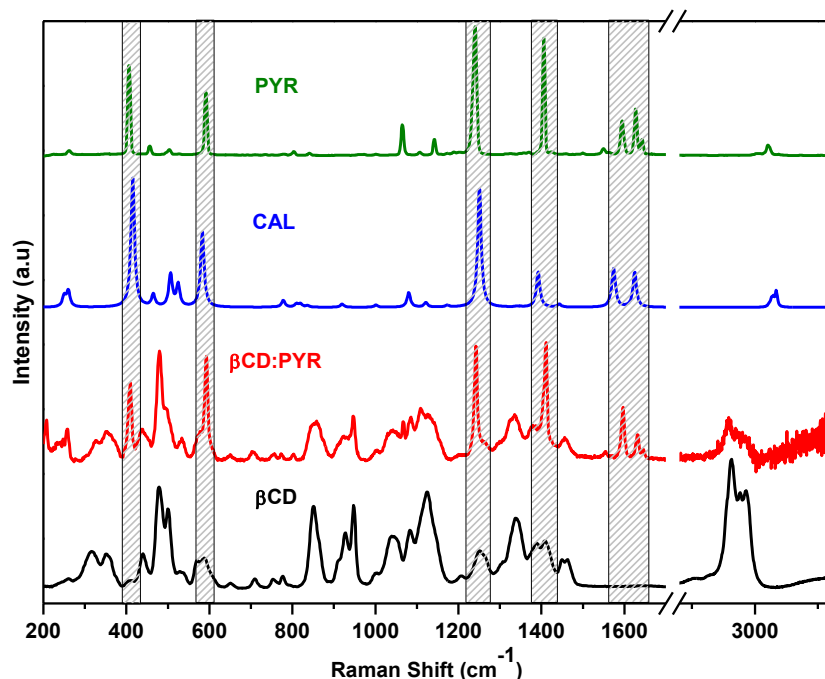


Figure 4.43 : Raman Spectrum of the β CD, PYR and of the inclusion complex obtained after mixing β CD with PYR in the molar ratio of 1:1

Some changes can also be seen in the CD vibrational modes after inclusion complex formation. The relative intensities of many peaks corresponding to different modes of vibrations have significantly reduced. For example- the bending vibration of C-C-C link at 317 cm^{-1} has diminished for the complex. The peaks at 852 cm^{-1} and 1125 cm^{-1} showing breathing vibration of glucose ring and C-C stretching vibration have reduced in intensity. The stretching vibrations of CH and CH₂ in the functional group detection region have also reduced in intensity. The vibrational modes of PYR which are most impacted by the interaction with β CD are shown in the Figure 4.44.

PYR		Complex	
Peak	Relative Intensity	Peak	Relative Intensity
407	0.69	409	0.69
587	0.48	594	0.89
1067	0.23	1065	0.38
1247	1.00	1242	0.97
1407	0.91	1412	1.00
1587	0.26	1597	0.48
1629	0.35	1630	0.28

Table 4.10 : Comparison of PYR peak shifts and relative intensities (free PYR and inclusion complex with β CD)

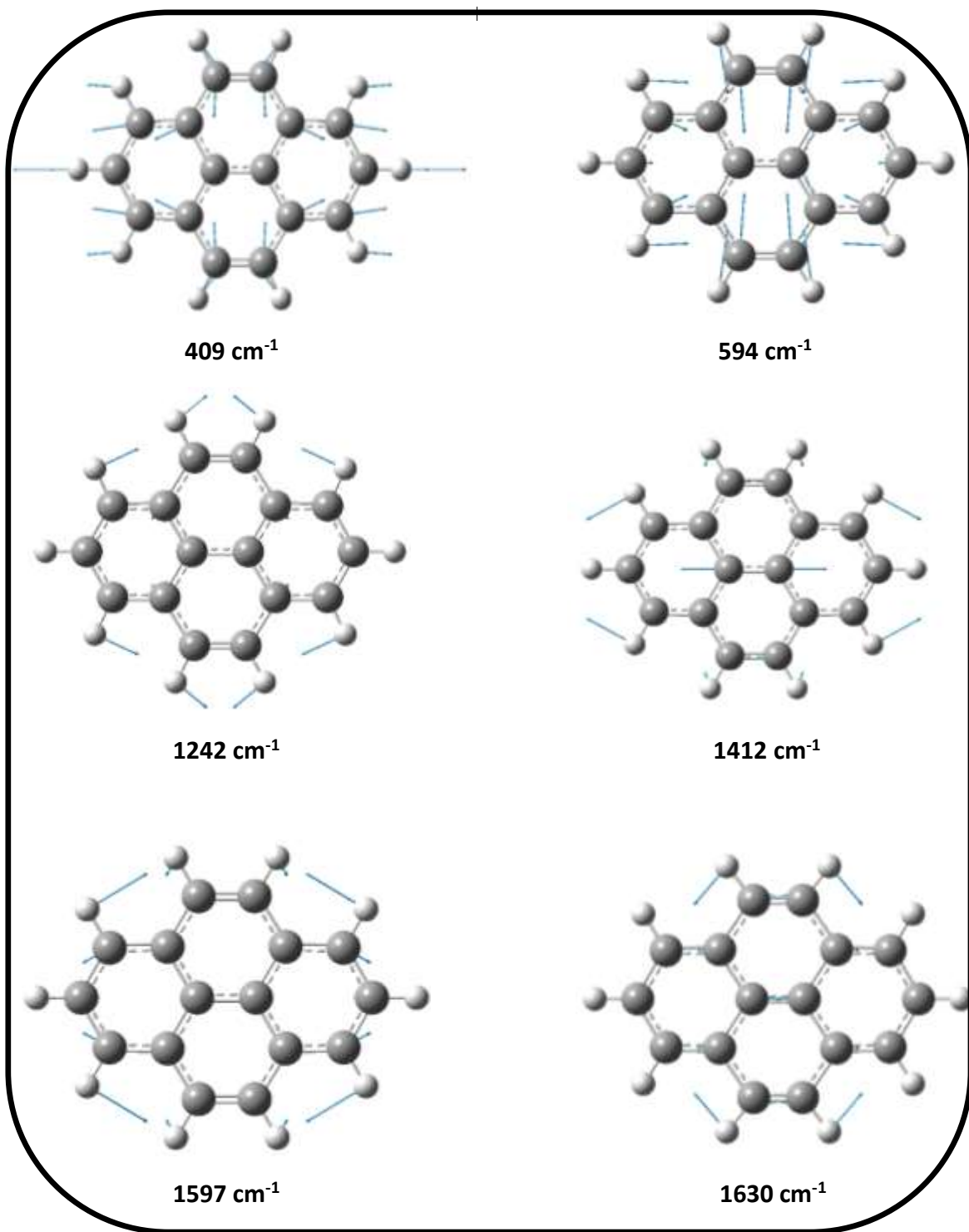


Figure 4.44 : The vibrational modes of PYR which are most impacted by the interaction with β CD.

4.6 Conclusion

The different investigations carried out to check complexation phenomenon by different techniques for β CD: aromatic hydrocarbons in absence of linear alcohols have produced different results. Due to unavailability of some techniques like NMR, the results were not obtained for all aromatic hydrocarbons. Hence for all the cases studied, it can be concluded that BEN, FB and TFT were failed to show any shift for the positions of H3 and H5 peaks on inclusion. Moreover, the bell shape curve from job's plot was violated. On the other hand, aromatics like BA, PHE and 2-NAP (derivatives with polar groups) were able to show the shifts and followed the bell shaped curve. The results obtained by our studies are in accordance with the work done previously. We also investigated the proton peaks corresponding to the aromatics and found progressive evolution in the pattern confirming inclusion complex formation.

The thermal studies were performed for almost all the β CD: Aromatic compounds complexes for the molar ratio 1:1. The results obtained revealed the formation of inclusion complexes in some cases where we observed the endothermic curves corresponding to melting of the inclusion complex formed. Few of the curve which failed to form any successful inclusion showed the melting/boiling curves for the guest molecules used.

On comparison with the literature, the XRD patterns of different β CD: Aromatics shown similarities. Few of patterns showed peaks corresponding to different references indicating existing in two different crystal formation.

The Raman Spectroscopic study has revealed the interesting behaviour of different aromatic molecules under observation. Most of the results obtained have positive aspects, in the sense, the aromatic molecules are forming inclusion complexes with β CD. For better understanding, the computed spectra of aromatic molecules have produced the vibrational modes of molecules for each peak appearing in the spectra of the complexes formed. It can also be concluded that Raman Spectroscopy can be used to check the aromatic inclusion complexation in β CD so this technique can be further used to design new analysis methods.

4.7 References

1. Tijunelyte, I., Dupont, N., Milosevic, I., Barbey, C., Rinnert, E., Lidgi-Guigui, N., Guenin, E. and de la Chapelle, M.L., 2017. Investigation of aromatic hydrocarbon inclusion into cyclodextrins by raman spectroscopy and thermal analysis. *Environmental Science And Pollution Research*, 24(35), pp.27077-27089.
2. Salvatierra, D., Jaime, C., Virgili, A. and Sánchez-Ferrando, F., 1996. Determination of the inclusion geometry for the β -cyclodextrin/benzoic acid complex by NMR and molecular modeling. *The Journal of Organic Chemistry*, 61(26), pp.9578-9581.
3. Aree, T., Chaichit, N. and Engkakul, C., 2008. Polymorphism in β -cyclodextrin–benzoic acid inclusion complex: a kinetically controlled crystal growth according to the Ostwald's rule. *Carbohydrate research*, 343(14), pp.2451-2458.
4. Belyakova, L.A., Varvarin, A.M., Khora, O.V. and Oranskaya, E.I., 2008. The interaction of β -cyclodextrin with benzoic acid. *Russian Journal of Physical Chemistry A, Focus on Chemistry*, 82(2), pp.228-232.

5. van Stam, J., De Feyter, S., De Schryver, F.C. and Evans, C.H., 1996. 2-Naphthol complexation by β -cyclodextrin: influence of added short linear alcohols. *The Journal of Physical Chemistry*, 100(51), pp.19959-19966.
6. Divakar, S. and Maheswaran, M.M., 1997. Structural studies on inclusion compounds of β -cyclodextrin with some substituted phenols. *Journal of inclusion phenomena and molecular recognition in chemistry*, 27(2), pp.113-126.
7. Bodor, N., Huang, M.J. and Watts, J.D., 1996. Theoretical am1 studies of inclusion complexes of α - and β -cyclodextrins with methylated benzoic acids and phenol, and γ -cyclodextrin with buckminsterfullerene. *Journal of inclusion phenomena and molecular recognition in chemistry*, 25(1-3), pp.97-102..
8. Uyar, T., Hunt, M.A., Gracz, H.S. and Tonelli, A.E., 2006. Crystalline cyclodextrin inclusion compounds formed with aromatic guests: Guest-dependent stoichiometries and hydration-sensitive crystal structures. *Crystal growth & design*, 6(5), pp.1113-1119.
9. Storsberg, J., Van Aert, H., Van Roost, C. and Ritter, H., 2003. Cyclodextrins in polymer synthesis: A simple and surfactant free way to polymer particles having narrow particle size distribution. *Macromolecules*, 36(1), pp.50-53.
10. Velusamy, P., Pitchumani, K. and Srinivasan, C., 1996. Selectivity in bromination of aniline and N-substituted anilines encapsulated in β -cyclodextrin. *Tetrahedron*, 52(10), pp.3487-3496.
11. Kamiya, M., Mitsuhashi, S., Makino, M. and Yoshioka, H., 1992. Analysis of the induced rotational strength of mono- and disubstituted benzenes included in β -cyclodextrin. *The Journal of Physical Chemistry*, 96(1), pp.95-99.
12. Bertrand, G.L., Faulkner Jr, J.R., Han, S.M. and Armstrong, D.W., 1989. Substituent effects on the binding of phenols to cyclodextrins in aqueous solution. *The Journal of Physical Chemistry*, 93(18), pp.6863-6867.
13. Köhler, J.E.H. and Grzelschak-Mick, N., 2013. The β -cyclodextrin/benzene complex and its hydrogen bonds—a theoretical study using molecular dynamics, quantum mechanics and COSMO-RS. *Beilstein journal of organic chemistry*, 9, p.118.
14. Hoshino, M., Imamura, M., Ikehara, K. and Hama, Y., 1981. Fluorescence enhancement of benzene derivatives by forming inclusion complexes with β -cyclodextrin in aqueous solutions. *The Journal of Physical Chemistry*, 85(13), pp.1820-1823.
15. Trofymchuk, I.M., Belyakova, L.A. and Grebenyuk, A.G., 2011. Study of complex formation between β -cyclodextrin and benzene. *Journal of Inclusion Phenomena and Macrocyclic Chemistry*, 69(3-4), pp.371-375.
16. Yamaguchi, H. and Abe, S., 1981. Vibrational structures in circular dichroism of monosubstituted benzenes included in β -cyclodextrin. *The Journal of Physical Chemistry*, 85(12), pp.1640-1643.
17. Cai, W.S., Xia, B.Y., Shao, X.G., Guo, Q.X., Maigret, B. and Pan, Z.X., 2000. Stability and geometry prediction for the inclusion complexes of mono- or 1, 4-disubstituted benzenes and β -cyclodextrin using a genetic algorithm. *Chemical Physics Letters*, 319(5-6), pp.708-712.
18. Salvatierra, D., Jaime, C., Virgili, A. and Sánchez-Ferrando, F., 1996. Determination of the inclusion geometry for the β -cyclodextrin/benzoic acid complex by NMR and molecular modeling. *The Journal of Organic Chemistry*, 61(26), pp.9578-9581.

19. Terekhova, I., Koźbiał, M., Kumeev, R. and Gierycz, P., 2011. Complex formation of native and hydroxypropylated cyclodextrins with benzoic acid in aqueous solution: Volumetric and ¹H NMR study. *Chemical Physics Letters*, 514(4-6), pp.341-346.
20. Belyakova, L.A. and Lyashenko, D.Y., 2008. Complex formation between benzene carboxylic acids and β-cyclodextrin. *Journal of Applied Spectroscopy*, 75(3), pp.314-318.
21. Huang, M.J., Watts, J.D. and Bodor, N., 1997. Theoretical studies of inclusion complexes of α-and β-cyclodextrin with benzoic acid and phenol. *International Journal of Quantum Chemistry*, 65(6), pp.1135-1152.
22. Rotich, M.K., Brown, M.E. and Glass, B.D., 2003. Thermal studies on mixtures of benzoic and salicylic acids with cyclodextrins. *Journal of thermal analysis and calorimetry*, 73(2), pp.671-686.
23. Cloudy, P., Letoffe, J.M., Germain, P., Bastide, J.P., Bayol, A., Blasquez, S., Rao, R.C. and Gonzalez, B., 1991. Physicochemical characterization of cholesterol-beta cyclodextrin inclusion complexes. *Journal of thermal analysis*, 37(11-12), pp.2497-2506
24. Udachin, K.A. and Ripmeester, J.A., 1998. A novel mode of inclusion for pyrene in β-cyclodextrin compounds: The crystal structures of β-cyclodextrin with cyclohexanol and pyrene, and with n-octanol and pyrene. *Journal of the American Chemical Society*, 120(5), pp.1080-1081.
25. Paulidou, A., Maffeo, D., Yannakopoulou, K. and Mavridis, I.M., 2008. Crystal structure of the inclusion complex of the antibacterial agent triclosan with cyclomaltoheptaose and NMR study of its molecular encapsulation in positively and negatively charged cyclomaltoheptaose derivatives. *Carbohydrate research*, 343(15), pp.2634-2640.
26. Makedonopoulou, S. and Mavridis, I.M., 2001. The dimeric complex of cyclomaltoheptaose with 1, 14-tetradecanedioic acid. Comparison with related complexes. *Carbohydrate research*, 335(3), pp.213-220.
27. O'Boyle, N.M., GaussSum 2.1, 2007.
28. Dennington, R.D., Keith, T.A. and Millam, J.M., 2008. GaussView 5.0. 8. *Gaussian Inc.*
29. Gerloczy, A., Fonagy, A. and Szejtli, J., 1983. Reduction of Residual Toluene Content in beta-Cyclodextrin through Preparing Inclusion Complexes. *Starch-Stärke*, 35(9), pp.320-322.
30. Cai, Y., Tarr, M.A., Xu, G., Yalcin, T. and Cole, R.B., 2003. Dication induced stabilization of gas-phase ternary beta-cyclodextrin inclusion complexes observed by electrospray mass spectrometry. *Journal of the American Society for Mass Spectrometry*, 14(5), pp.449-459.
31. Mavridis, I.M. and Hadjoudis, E., 1992. The crystal structure of the inclusion complex of cyclomaltoheptaose (β-cyclodextrin) with 4-tert-butyltoluene. *Carbohydrate research*, 229(1), pp.1-15.
32. Monti, S., Koehler, G. and Grabner, G., 1993. Photophysics and photochemistry of methylated phenols in. beta.-cyclodextrin inclusion complexes. *The Journal of Physical Chemistry*, 97(49), pp.13011-13016.
33. Marconi, G., Monti, S., Mayer, B. and Koehler, G., 1995. Circular Dichroism of Methylated phenols Included in. beta.-Cyclodextrin. An Experimental and Theoretical study. *The Journal of Physical Chemistry*, 99(12), pp.3943-3950.
34. Aree, T. and Chaichit, N., 2003. Crystal structure of β-cyclodextrin–benzoic acid inclusion complex. *Carbohydrate research*, 338(5), pp.439-446.

35. Méndez, S.G., Espinar, F.J.O., Alvarez, A.L., Longhi, M.R., Quevedo, M.A. and Zoppi, A., 2016. Ternary complexation of benzoic acid with β -cyclodextrin and aminoacids. Experimental and theoretical studies. *Journal of Inclusion Phenomena and Macrocyclic Chemistry*, 85(1-2), pp.33-48.
36. Fatiha, M. and Djameleddine, K., 2009. Molecular modeling study of para amino benzoic acids recognition by β -cyclodextrin. *Orbital: The Electronic Journal of Chemistry*, 1(1), pp.26-37.
37. Fan, Z., Guo, M., Dong, B., Diao, C., Jing, Z. and Chen, X., 2010. Different self-assembly behaviors of mono-modified β -cyclodextrin substituted by benzoic acid derivatives. *Science China Chemistry*, 53(5), pp.1089-1094.
38. Evans, C.H., Partyka, M. and Van Stam, J., 2000. Naphthalene complexation by β -cyclodextrin: influence of added short chain branched and linear alcohols. *Journal of inclusion phenomena and macrocyclic chemistry*, 38(1-4), pp.381-396.
39. Jiang, H., Sun, H., Zhang, S., Hua, R., Xu, Y., Jin, S., Gong, H. and Li, L., 2007. NMR investigations of inclusion complexes between β -cyclodextrin and naphthalene/anthraquinone derivatives. *Journal of Inclusion Phenomena and Macrocyclic Chemistry*, 58(1-2), p.133.
40. Grabner, G., Rechthaler, K., Mayer, B., Köhler, G. and Rotkiewicz, K., 2000. Solvent influences on the photophysics of naphthalene: Fluorescence and triplet state properties in aqueous solutions and in cyclodextrin complexes. *The Journal of Physical Chemistry A*, 104(7), pp.1365-1376.
41. Gravett, D.M. and Guillet, J.E., 1993. Synthesis and photophysics of a water-soluble, naphthalene-containing. beta.-cyclodextrin. *Journal of the American Chemical Society*, 115(14), pp.5970-5974.
42. Inoue, Y., Hakushi, T., Liu, Y., Tong, L., Shen, B. and Jin, D., 1993. Thermodynamics of molecular recognition by cyclodextrins. 1. Calorimetric titration of inclusion complexation of naphthalenesulfonates with. alpha.-, beta.-, and. gamma.-cyclodextrins: enthalpy-entropy compensation. *Journal of the American Chemical Society*, 115(2), pp.475-481.
43. Park, J.W. and Song, H.J., 1989. Association of anionic surfactants with. beta.-cyclodextrin: fluorescence-probed studies on the 1: 1 and 1: 2 complexation. *The Journal of Physical Chemistry*, 93(17), pp.6454-6458.
44. Catena, G.C. and Bright, F.V., 1989. Thermodynamic study on the effects of. beta.-cyclodextrin inclusion with anilinonaphthalenesulfonates. *Analytical chemistry*, 61(8), pp.905-909.
45. Yorozu, T., Hoshino, M., Imamura, M. and Shizuka, H., 1982. Photoexcited inclusion complexes of. beta.-naphthol with. alpha.-, beta.-, and. gamma.-cyclodextrins in aqueous solutions. *The Journal of Physical Chemistry*, 86(22), pp.4422-4426.
46. Pei, Z., Li, L., Sun, L., Zhang, S., Shan, X.Q., Yang, S. and Wen, B., 2013. Adsorption characteristics of 1, 2, 4-trichlorobenzene, 2, 4, 6-trichlorophenol, 2-naphthol and naphthalene on graphene and graphene oxide. *Carbon*, 51, pp.156-163.
47. Anigbogu, V.C., Munoz de la Pena, A., Ndou, T. and Warner, I.M., 1992. Determination of formation constants for. beta.-cyclodextrin complexes of anthracene and pyrene using reversed-phase liquid chromatography. *Analytical Chemistry*, 64(5), pp.484-489.

48. Dang, X.J., Nie, M.Y., Tong, J. and Li, H.L., 1998. Inclusion of the parent molecules of some drugs with β -cyclodextrin studied by electrochemical and spectrometric methods. *Journal of Electroanalytical Chemistry*, 448(1), pp.61-67.
49. Sánchez-Trujillo, M.A., Morillo, E., Villaverde, J. and Lacorte, S., 2013. Comparative effects of several cyclodextrins on the extraction of PAHs from an aged contaminated soil. *Environmental pollution*, 178, pp.52-58.
50. Landy, D., Mallard, I., Ponchel, A., Monflier, E. and Fourmentin, S., 2012. Remediation technologies using cyclodextrins: an overview. *Environmental chemistry letters*, 10(3), pp.225-237.
51. Bree, A. and Kydd, R.A., 1969. The raman spectrum of anthracene-d10. *Chemical Physics Letters*, 3(6), pp.357-360.
52. Abasbegović, N., Vukotić, N. and Colombo, L., 1964. Raman spectrum of anthracene. *The Journal of Chemical Physics*, 41(9), pp.2575-2577.
53. Shinohara, H., Yamakita, Y. and Ohno, K., 1998. Raman spectra of polycyclic aromatic hydrocarbons. Comparison of calculated Raman intensity distributions with observed spectra for naphthalene, anthracene, pyrene, and perylene. *Journal of molecular structure*, 442(1-3), pp.221-234.
54. Muñoz De La Peña, A., Ndou, T., Zung, J.B. and Warner, I.M., 1991. Stoichiometry and formation constants of pyrene inclusion complexes with. beta.-and. gamma.-cyclodextrin. *The Journal of Physical Chemistry*, 95(8), pp.3330-3334.
55. Patonay, G., Shapira, A., Diamond, P. and Warner, I.M., 1986. A systematic study of pyrene inclusion complexes with. alpha.-, beta.-, and. gamma.-cyclodextrins. *The Journal of Physical Chemistry*, 90(9), pp.1963-1966.
56. Will, A.Y., De La Peña, A.M., Ndou, T.T. and Warner, I.M., 1993. Spectroscopic studies of the interaction of tert-butylamine and n-propylamine with the β -cyclodextrin: pyrene complex. *Applied spectroscopy*, 47(3), pp.277-282.
57. Hamai, S., 1989. Inclusion compounds in the systems of. beta.-cyclodextrin-alcohol-pyrene in aqueous solution. *The Journal of Physical Chemistry*, 93(5), pp.2074-2078.
58. Munoz De La Pena, A., Ndou, T.T., Zung, J.B., Greene, K.L., Live, D.H. and Warner, I.M., 1991. Alcohol size as a factor in the ternary complexes formed with pyrene and. beta.-cyclodextrin. *Journal of the American Chemical Society*, 113(5), pp.1572-1577.
59. Yorozu, T., Hoshino, M. and Imamura, M., 1982. Fluorescence studies of pyrene inclusion complexes with. alpha.-, beta.-, and. gamma.-cyclodextrins in aqueous solutions. Evidence for formation of pyrene dimer in. gamma.-cyclodextrin cavity. *The Journal of Physical Chemistry*, 86(22), pp.4426-4429.
60. Cummings, E.A., Ndou, T.T., Smith, V.K. and Warner, I.M., 1993. Spectroscopic study of the ternary complex of beta-cyclodextrin, pyrene, and triton X-100. *Applied spectroscopy*, 47(12), pp.2129-2134.
61. Nelson, G., Patonay, G. and Warner, I.M., 1989. The utility of time-resolved emission spectroscopy in the study of cyclodextrin-pyrene inclusion complexes. *Talanta*, 36(1-2), pp.199-203.
62. Munoz de la Pena, A., Ndou, T.T., Anigbogu, V.C. and Warner, I.M., 1991. Solution studies of. beta.-cyclodextrin-pyrene complexes under reversed-phase liquid chromatographic conditions: effect of alcohols as mobile-phase comodifiers. *Analytical Chemistry*, 63(10), pp.1018-1023.

63. De Feyter, S., van Stam, J., Boens, N. and De Schryver, F.C., 1996. On the use of dynamic fluorescence measurements to determine equilibrium and kinetic constants. The inclusion of pyrene in β -cyclodextrin cavities. *Chemical physics letters*, 249(1-2), pp.46-52.
64. Xie, Y., Wang, X., Han, X., Xue, X., Ji, W., Qi, Z., Liu, J., Zhao, B. and Ozaki, Y., 2010. Sensing of polycyclic aromatic hydrocarbons with cyclodextrin inclusion complexes on silver nanoparticles by surface-enhanced Raman scattering. *Analyst*, 135(6), pp.1389-1394.
65. Rumelfanger, R., Asher, S.A. and Perry, M.B., 1988. UV resonance Raman characterization of polycyclic aromatic hydrocarbons in coal liquid distillates. *Applied spectroscopy*, 42(2), pp.267-272.

Chapter 5. Inclusion complexes of β CD:Linear alcohols:aromatic hydrocarbons

5.1 Introduction

The studies performed in this chapter aimed at encapsulation of aromatic hydrocarbons in β CD cavity in presence of linear alcohols (Figure 5.1). The inspiration to perform this research came from the previously published work¹ on inclusion of PYR molecules inside the cavity with n-octanol and also is the continuation of the similar work done in our team² focussing on inclusion of other aromatic hydrocarbons inside the cavity in absence of linear alcohols. Other studies were also performed with α CD to understand the α CD: undecanol³ complexation behaviour but the techniques used for further investigation are completely different from the techniques available in our lab. After evaluating the results obtained for the different complexes preparation and interpretation about β CD: linear alcohols and β CD: Aromatics as explained in the previous chapters, the next step was to add aromatic hydrocarbons. The reason for using linear alcohols as part of the studies because of the two reasons:

1. The solubility of aromatic hydrocarbons is very low in water. Therefore, alcohols were used to increase their solubility.
2. Most of the linear alcohols are water soluble. The solubility decreases as the hydrophobic carbon chain length increases. The higher alcohol molecules can be present in ground water^{4,5} and can be treated as 'pollutant'. So, these linear alcohols acting as pollutants can also be entrapped inside the CD cavity.

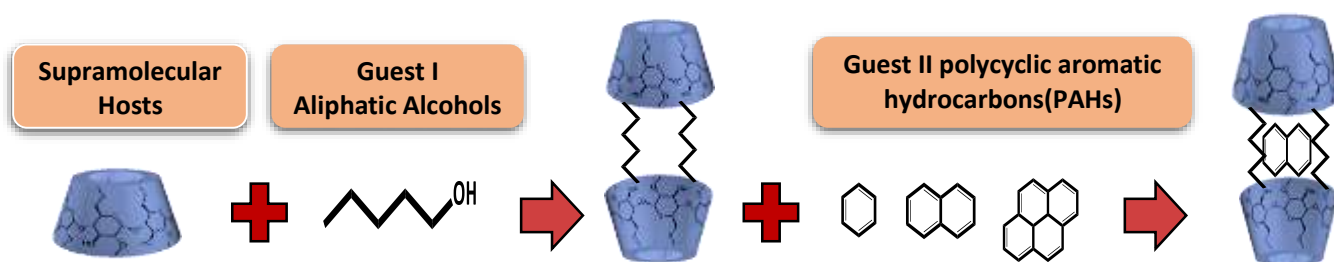


Figure 5.1 : Chronological order representation of aims and objectives of the thesis. (P.S- the images used are only for better understanding of the reader about the concept).

In continuation with the studies performed in the previous chapter in the absence of alcohols, firstly the NMR studies were performed with EtOD (deuterated ethanol) as co-solvent. We were not able to perform the studies for each aromatic hydrocarbon because of availability issues of the NMR instrument in the lab. To have better knowledge about the inclusion phenomenon, the thermal studies were done using DSC technique. Because of time and instrument unavailability, we were able to focus only on the results of ternary complexes prepared with Octanol and Nonanol for most of the samples. The reason for choosing only the complexes prepared with only these two alcohols is the similar studies done with different techniques in the literature which were used as base of this thesis. The next step was to study the ternary complexes by powder XRD studies to confirm their inclusion. The last characterization technique used was the Raman spectroscopy to check the vibrational

motions of the molecules in collaboration with theoretical studies. Furthermore, to check the possibility of using this technique for detection of aromatic pollutants in presence of alcohols.

As we have already seen in the previous chapter, that some of the aromatic hydrocarbons do not require linear alcohols to form inclusion complexes we still continued their studies in the presence of linear alcohols in order to check their behaviour in presence of linear alcohols. Moreover, as these kinds of studies are not done in the past it would have been interesting to know if they form new kind of inclusion complex with different crystal structures when linear alcohols are added.

The conclusion from the results will be summarised at the end of the chapter.

5.2 NMR studies: Ternary complexation in presence of co-solvent

5.2.1 β CD: BEN NMR studies in EtOD as co-solvent

On adding the EtOD as co-solvent (50%), the results (Figure 5.2) show appearance of remarkable shift for the hydrogens present inside the β CD's cavity. The same results have produced the deviation for the benzene peak (7.26 ppm indicating inclusion complex formation). The Figure 5.3 shows the evolution of H3 and H5 peaks on addition of 50% EtOD. The solutions prepared with different volume mixtures of β CD and BEN are presented the table 5.1 and correspond to each serial number for each H3 and H5 evolution BEN peak evolution.

Serial number	Vol. of β CD solution (10mM) (μ l)	Vol. of Aromatic hydrocarbon solution (10mM) (μ l)	β CD volume ratio in solution
1	450	50	0.9
2	400	100	0.8
3	350	150	0.7
4	300	200	0.6
5	250	250	0.5
6	200	300	0.4
7	150	350	0.3
8	100	400	0.2
9	50	450	0.1

Table 5.1 : Volume of β CD and Aromatic hydrocarbons solutions mixed together to form inclusion complexes in EtOD as co-solvent to carry out NMR studies.

The job's plot results (Figure 5.4) could be obtained only for H3 peaks deviation as the H5 peak was difficult to distinguish from the other protons existing during inclusion complexes formation due to superposition with hydrogen residual deuterated ethanol peaks. Moreover, the aromatic hydrogen peaks are highly influenced by the complexation indicating their neighbouring evolution in presence of β CDs by insertion inside the cavity. The R_{max} is observed at 0.69 in this case. The stoichiometry of the complex is found to be 2:1 (β CD:BEN).

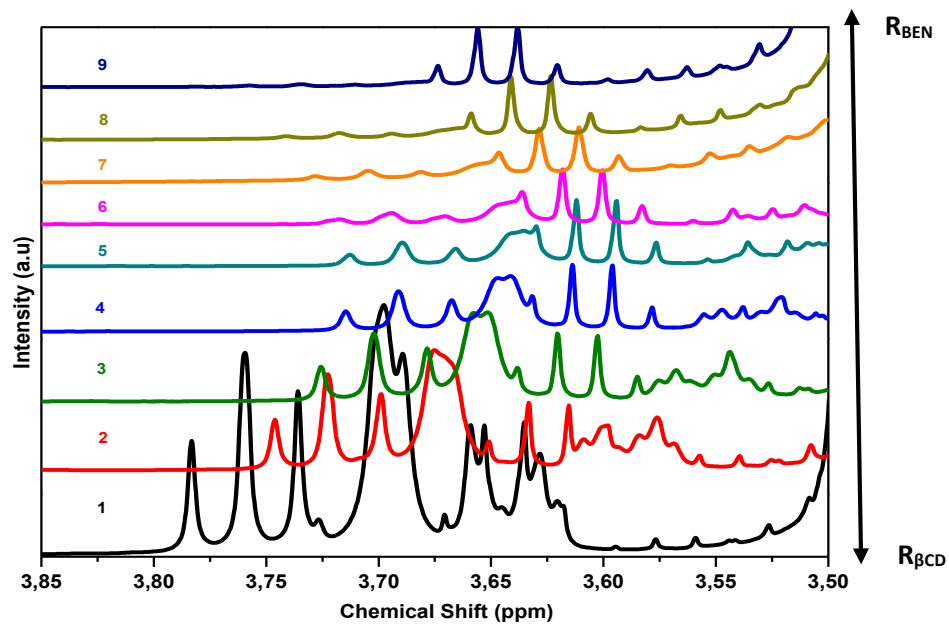


Figure 5.2 : Evolution of H3 and H5 peaks of β CD:BEN complexes when dissolved in 50% EtOD.

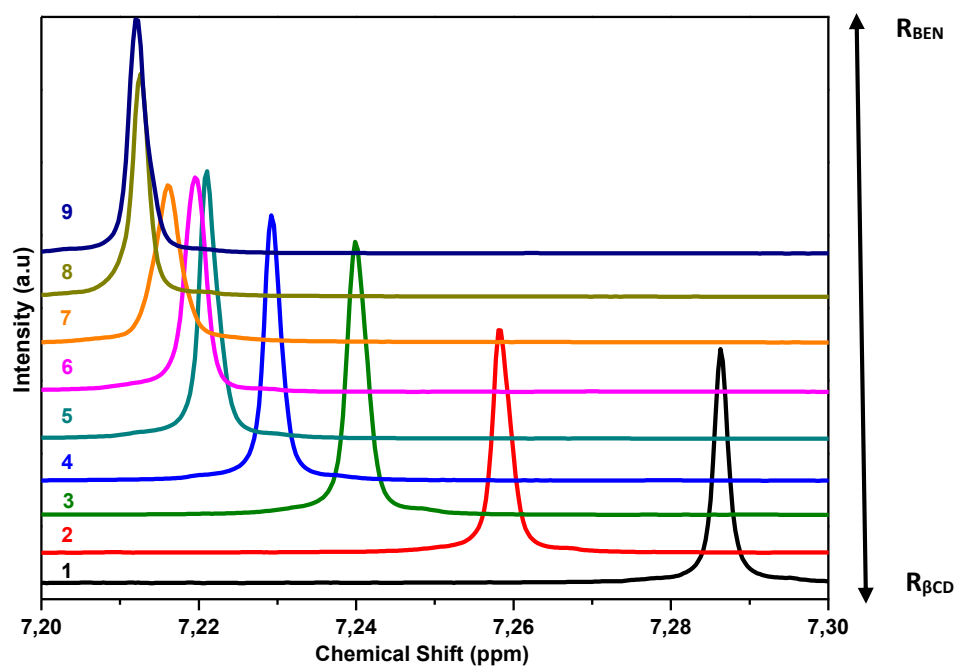


Figure 5.3 : Evolution of BEN peak when dissolved in 50% EtOD.

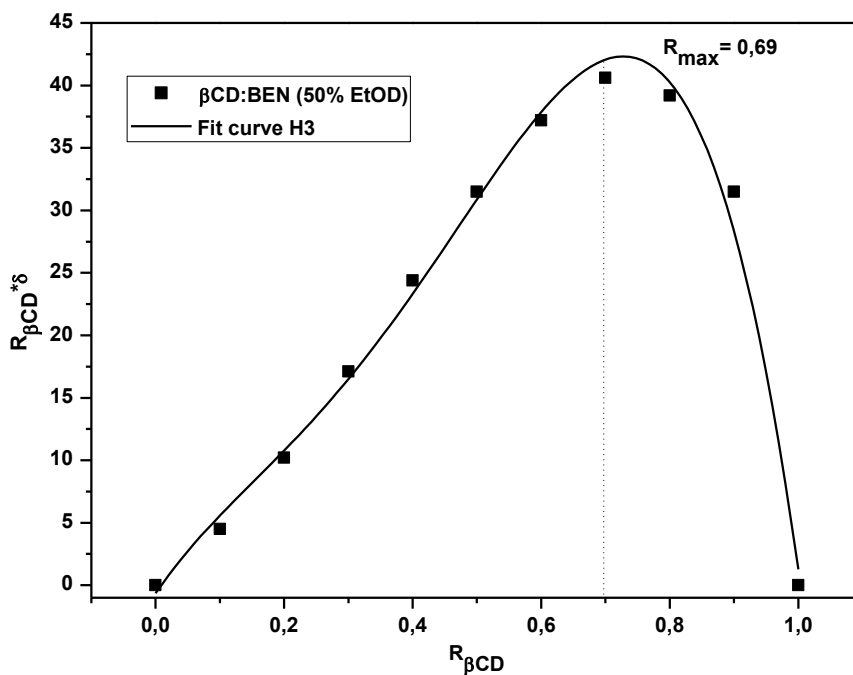


Figure 5.4 : job's plot for βCD : BEN complex in EtOD as co-solvent.

5.2.2 βCD : TFT NMR studies in ETOD as co-solvent

The solutions prepared with 30 % EtOD as co-solvent have obtained different results from solutions prepared in D_2O . The hydrogens present inside the CD's cavity (H3 and H5) have undergone deviation from their original position (Figure 5.5). The peak corresponding to TFT (Figure 5.6) have also shown deviation indicating inclusion complex formation.

The job's plots studies (Figure 5.7) were only performed for H3 peak deviation as the environment of H5 peak changed during complex formation and proton identification became difficult. The R_{max} is observed at 0.63. It further indicates the formation of 2:1 (βCD : TFT) complex.

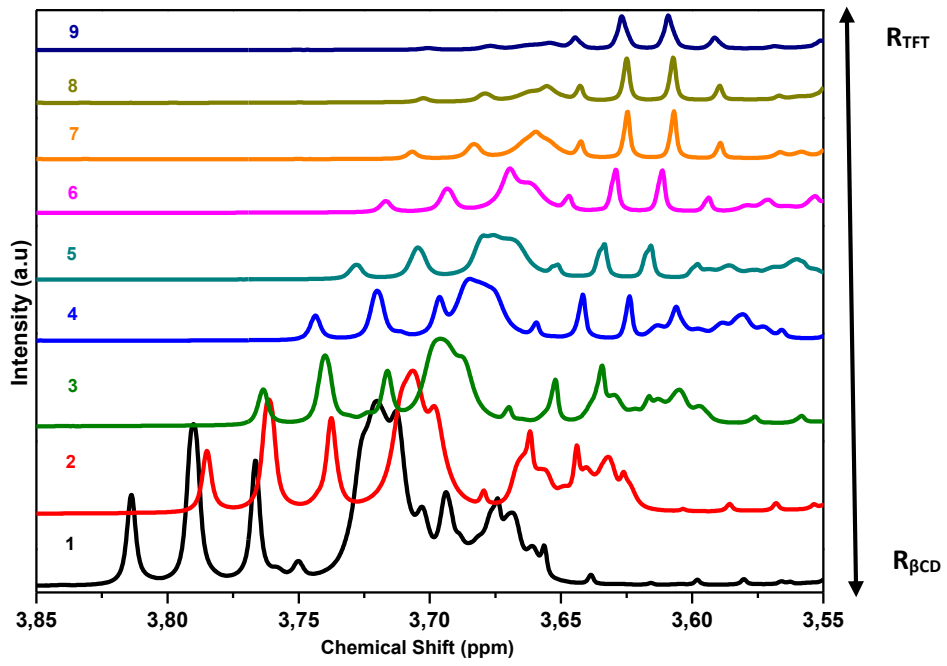


Figure 5.5 : Evolution of H3 and H5 β -CD: TFT complexes peaks when dissolved in 30% EtOD.

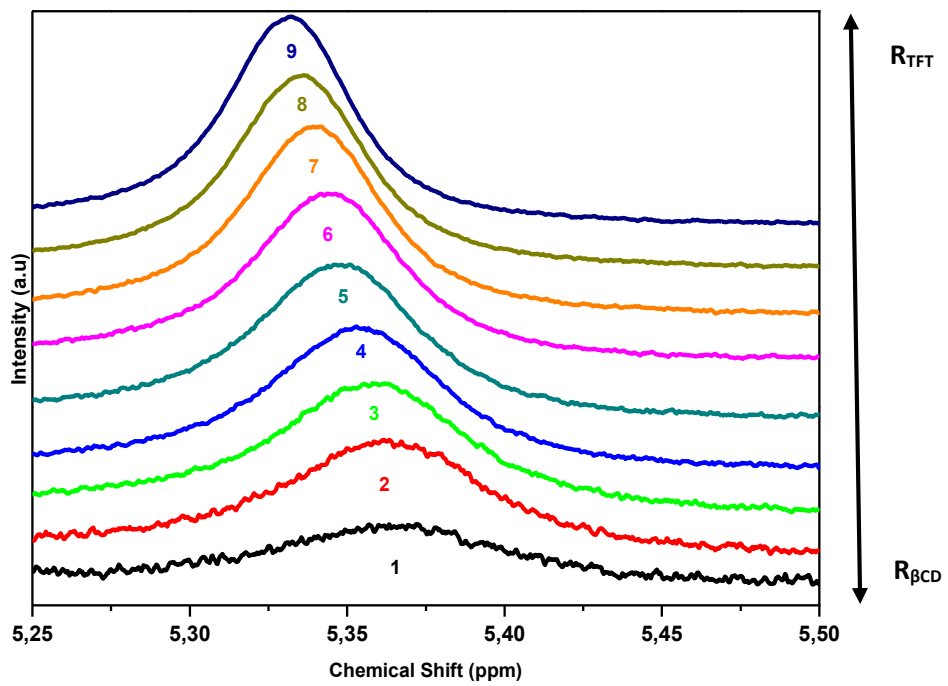


Figure 5.6 : Evolution of TFT peak when dissolved in 30% EtOD.

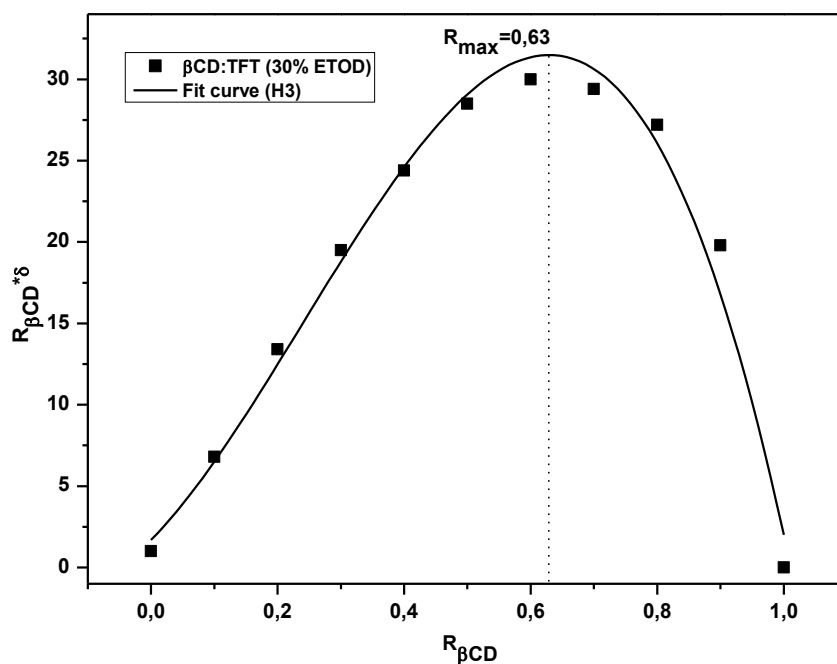


Figure 5.7 : job's plot for βCD : TFT complex in EtOD as co-solvent.

5.3 Thermal studies of βCD : alcohol: aromatic hydrocarbon complexes

The thermal studies were carried out only for ternary complexes prepared with Octanol and Nonanol with stoichiometry 1:1:1 in each case because of the time and instrument unavailability. The reason behind choosing only these alcohols is the publication we inspired from to do this thesis. They used Octanol to encapsulate PYR molecules inside βCD . In this part, we have compared the thermal results obtained as ternary complex with complexes prepared in the previous chapters i.e βCD complexes prepared with different linear alcohols and also the complexes prepared with aromatics in absence of alcohols. The main idea behind this comparison is to check if the similarities or differences occurring in the curves obtained for ternary complexes and the binary complexes prepared in chapter-2 and chapter-3. By such type of analysis, it would be easier to understand the reasons behind the features of the ternary complexes obtained. The melting/boiling point and physical states are listed in the table 5.2. For all aromatic hydrocarbons used.

Aromatic hydrocarbon	Physical State	Melting/Boiling Point (°C)
Benzene	Colorless liquid	80
Fluorobenzene	Colorless liquid	85
Toluene	Colorless liquid	110
Trifluorotoluene	Colorless liquid	102
Phenol	White crystalline solid	40
Benzoic Acid	Colorless crystalline solid	122
Naphthalene	White crystalline solid	80
2-Naphthol	Colorless crystalline solid	121-123
Anthracene	Colorless solid	215
Pyrene	Colorless solid	145-148

Table 5.2. Physical states and melting/ boiling points of the aromatic hydrocarbons.

5.3.1 Monocyclic aromatic hydrocarbons

5.3.1.1 Thermal studies of β CD: alcohol: BEN (1:1:1) complexes

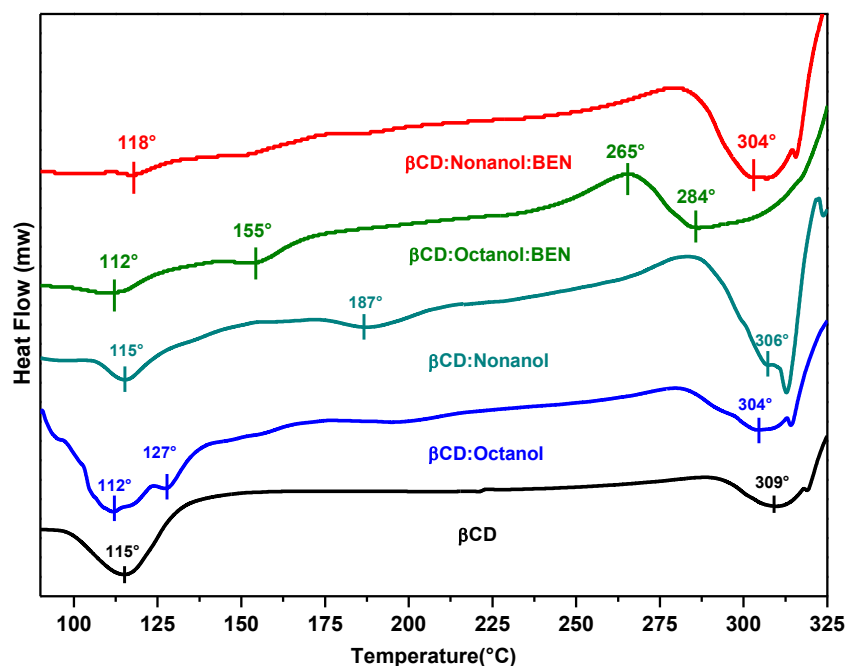


Figure 5.8 : DSC curve of β CD and β CD:alcohol:BEN (1:1:1).

Figure 5.8 represents the thermograms obtained for β CD: Alcohol: BEN complexes. The curve for the ternary complexes obtained with Octanol and Nonanol appear very similar in terms of the different endothermic curves observed and their temperatures. The β CD: Octanol: BEN result shows the appearance of a exothermic curve corresponding to new crystallization phase around 265°C. The high temperature degradation and oxidation phenomenon of uncomplexed CDs in air starting at 250°C in solid phase followed by liquid state fusion occurring at around 300°C. For β CD:Octanol:BEN it appears at 284°C and for β CD:Nonanol:BEN at 304°C. The 'waterloss' i.e removal of tightly bound water molecules is observed at 112°C and 118°C respectively for octanol and nonanol containing ternary complexes. The smaller

curves for the water loss indicates there are very loss or no more molecules to be removed from the cavity, indicating a different structural composition of the cavity than observed for uncomplexed β CD. The curves observed for binary systems in presence of octanol and nonanol show different behaviour to ternary complexes curves except for the water loss temperatures which seem to exist at similar temperature. The only difference arises is for the energy and number of water molecules involved. The β CD:Octanol:BEN curve shows another step for water removal at 155°C followed by an exothermic curves at 265°C indicating the formation of new crystalline phase.

5.3.1.2 Thermal studies of β CD: alcohol: FB (1:1:1) complexes

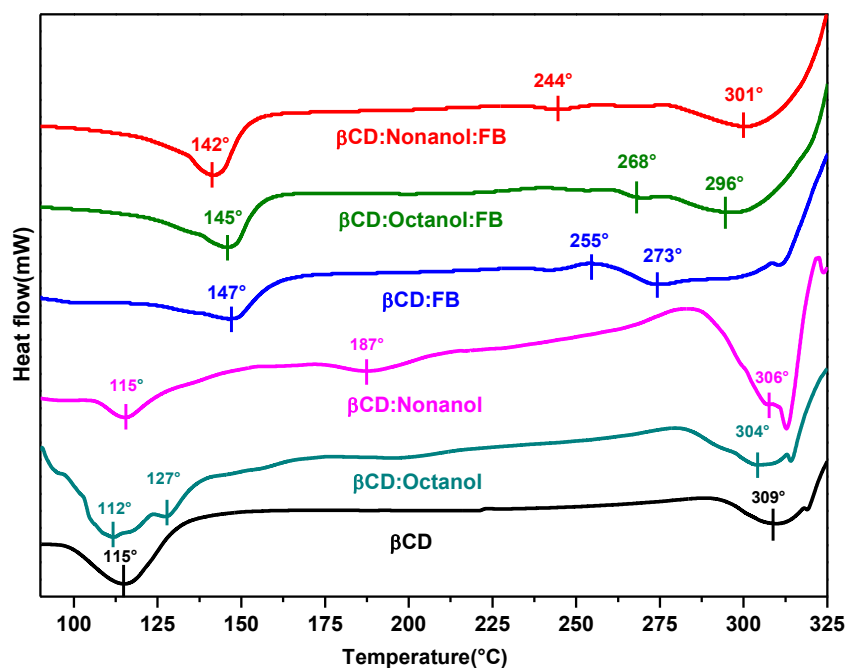


Figure 5.9 : DSC curve of β CD and β CD:alcohol:FB (1:1:1).

The thermogram of β CD:alcohol:FB shows different behaviour from the typical β CD curve (Figure 5.9). The curves obtained for β CD:Octanol:FB and β CD:Nonanol:FB look very similar in appearance to β CD:FB as discussed in the previous chapter. The first curve for the complexes can be seen at slight temperature difference i.e. at 145°C and 142°C for β CD:Octanol:FB and β CD:Nonanol:FB respectively which are not very different from 147°C obtained for β CD:FB where the reason of their appearance could be the removal of water molecules from the host cavity. Other small endothermic feature in complexes can be seen at temperatures between 240°C and 270°C which do not correspond to boiling point temperatures for any of the guest molecules. These points on the curves can be assumed to be related to melting temperatures of the inclusion complex formed. The only difference possessed by alcohol containing curves is the high temperature degradation and oxidation of uncomplexed CDs which are observed in the former cases at 296° and 301° respectively. The ternary complex curves are different from the curves obtained for binary complexes prepared with octanol and nonanol.

5.3.1.3 Thermal studies of β CD: alcohol: TOL (1:1:1) complexes

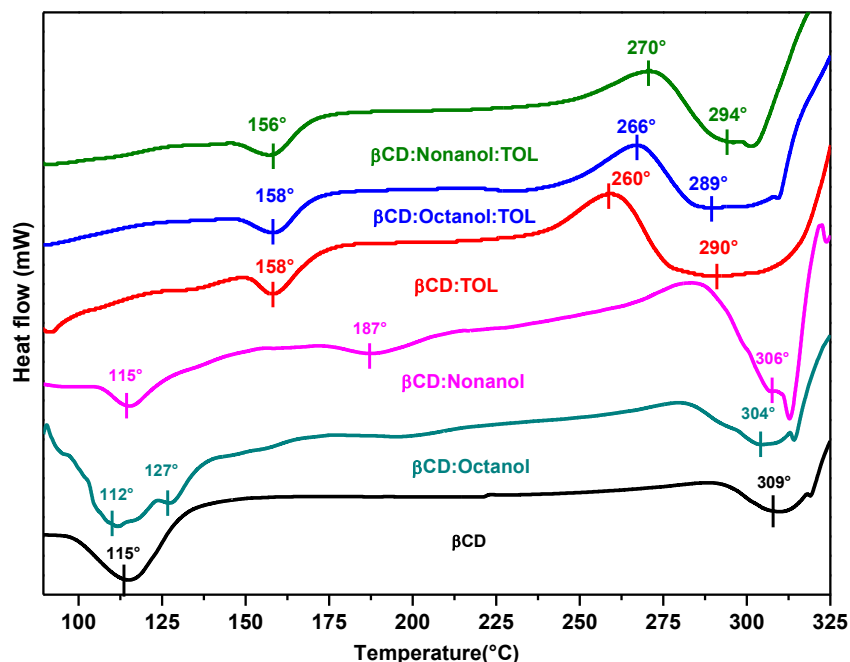


Figure 5.10 : DSC curve of β CD and β CD:alcohol:TOL (1:1:1)

The complexes containing octanol and Nonanol show similar thermal behaviour to the complexes prepared in absence of alcohols (Figure 5.10). The events occurring in all the three curves are appearing at temperature difference of 3-4° approximately from each other. The event occurring due to removal of tightly bound water molecules is shifted to a lower temperature than observed in case of β CD. Moreover, the amount of energy involved is very similar in both the cases. They are appearing at temperatures 86° and 88° for β CD:Octanol:TOL and β CD:Nonanol:TOL respectively(chapter-4). The melting of the inclusion complex (158° C and 156°C) formed exist at almost similar temperatures in the complexes. An exothermic curves related to new crystallization phase can be seen at 266 ° and 270°C involving liberation of similar amount of energy in both the cases. The ternary complexes curves show different behaviour from binary curves obtained with octanol and nonanol. Furthermore, the temperature degradation and oxidation of uncomplexed CDs are observed with not a lot temperature difference at 289° and 294°C respectively. On examining the whole behaviour, it can be concluded that the presence of linear alcohols does not really make a difference in their thermal properties.

5.3.1.4 Thermal studies of β CD: alcohol:TFT (1:1:1) complexes

On discussing about the complexes prepared with alcohols (Figure 5.11), the curves appear very similar to what we have observed for β CD:TFT. For β CD:Octanol:TFT the same events are observed at 92°C, 161°C and 275°C respectively. Similarly for β CD:Nonanol:TFT at 96°, 154° and 276°C. The boiling point of TFT is 102°C, so the curves appearing at 161°C and 154°C might be due to some inclusion complex formation. The ternary complex curves are different from the curves obtained for binary complexes prepared with octanol and nonanol. The appearance of exothermic curve related to formation of new crystallization phase can be seen at 258°C and 276°C in the respective cases. These curves are different in terms of energies involved. Another important point to be noted is the β CD degradation temperature which appears at comparatively lower temperature than other curves.

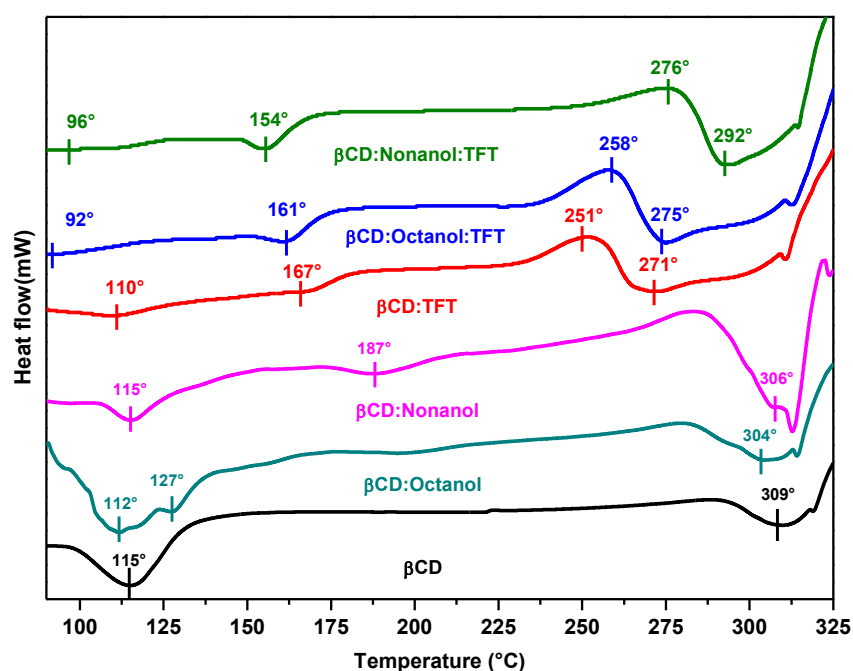


Figure 5.11 : DSC curve of β CD and β CD:alcohol:TFT (1:1:1).

5.3.2 Bicyclic aromatic hydrocarbons

5.3.2.1 Thermal studies of β CD: alcohol: NAP (1:1:1) complexes

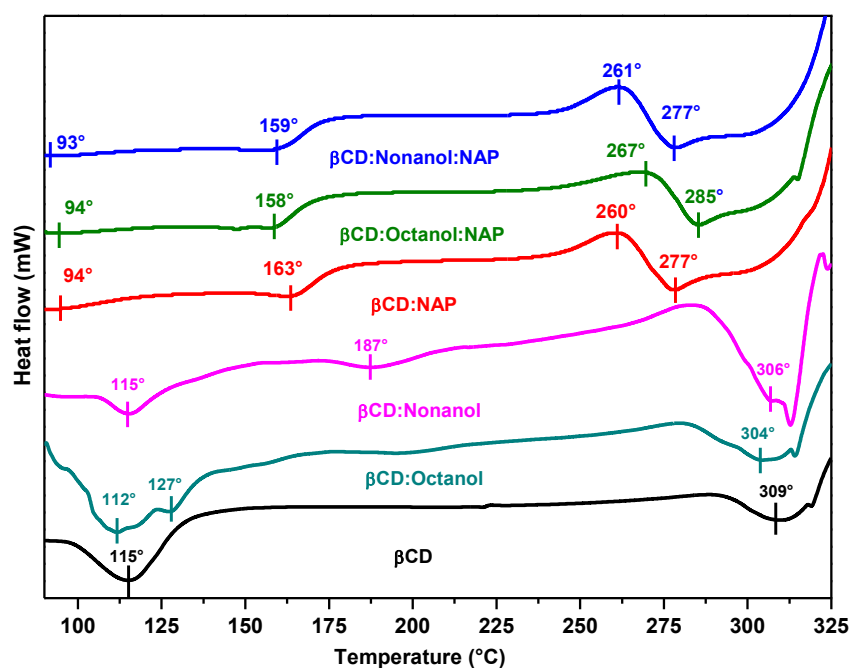


Figure 5.12 : DSC curve of β CD and β CD:alcohol:NAP (1:1:1).

The curves appeared for the three complexes comprising with and without alcohol are similar with respect to all the events occurring during thermal studies (Figure 5.12). Again, the temperature difference observed for all the three complexes for each event is only 3- 4°C. The different endothermic events observed are the removal of water molecules, melting of inclusion complexes formed and the temperature degradation and oxidation of uncomplexed CDs which are occurring for β CD:NAP, β CD:Octanol: NAP and β CD:Nonanol: NAP at temperatures (91°, 94°, 93°), (163°, 158°, 159°) and (278°, 285°, 277°C) respectively. The binary curves observed for complexes prepared with octanol and nonanol seem different with respect to all the features appearing in case of ternary complexes. The exothermic curves involving formation of new crystalline phase are appearing at 267° and 261° differ only by the amount of energy involved in both these cases. The presence of alcohol in the system does not have really impacted the thermal properties.

5.3.3 Polycyclic aromatic hydrocarbons

5.3.3.1 Thermal studies of β CD: alcohol: ANTH (1:1:1) complexes

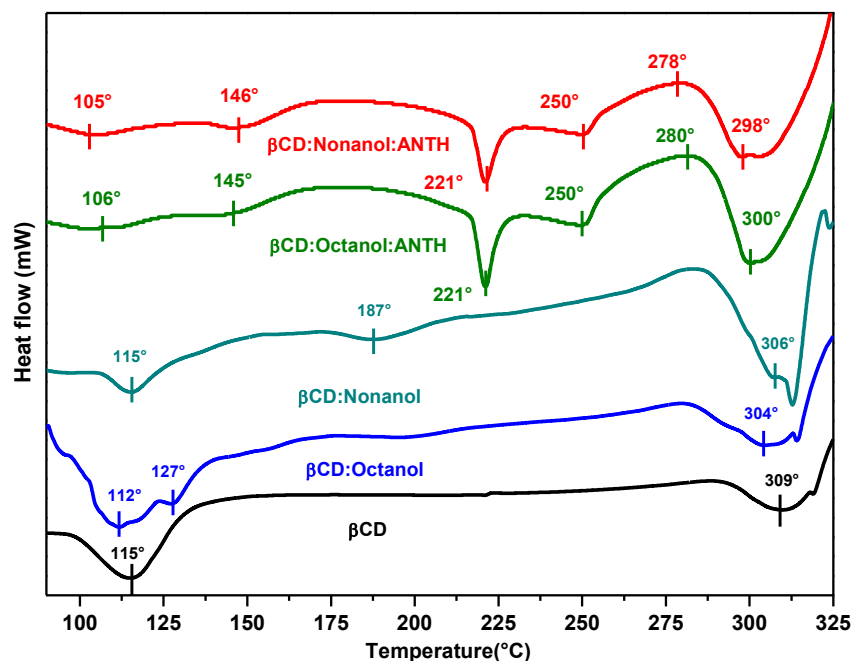


Figure 5.13 : DSC curve of β CD and β CD:alcohol:ANTH (1:1:1).

The thermal studies performed for ANTH inclusion complexes with alcohols have produced similar results (Figure 5.13). The appearance of the thermal events occurring in the curve are present at same temperatures in both the cases. These include curves at temperatures 106°, 145°, 221°, 250° and 300°C. The curves below 120°C are due to removal of high energy water molecules present in the β CD cavity. The curves appearing at 145° and 250° are must be due to melting of different forms of inclusion complex structures. The sharp peak observed in both the cases at the same temperature are due to melting of uncomplexed anthracene molecules. On comparison with the binary system complex obtained with octanol and nonanol, ternary system show completely different thermal curve. A large exothermic curve is observed in both the cases (280° and 278°C respectively) involving similar amount of energies liberated indicating formation of new crystalline phases. Lastly, the temperature degradation and oxidation of uncomplexed CDs exist around 300°C in both the cases. The addition of alcohols has produced many changes in the thermal properties which were absent in native β CD and β CD: alcohol complexes.

5.3.3.2 Thermal studies of β CD: alcohol: PYR (1:1:1) complexes

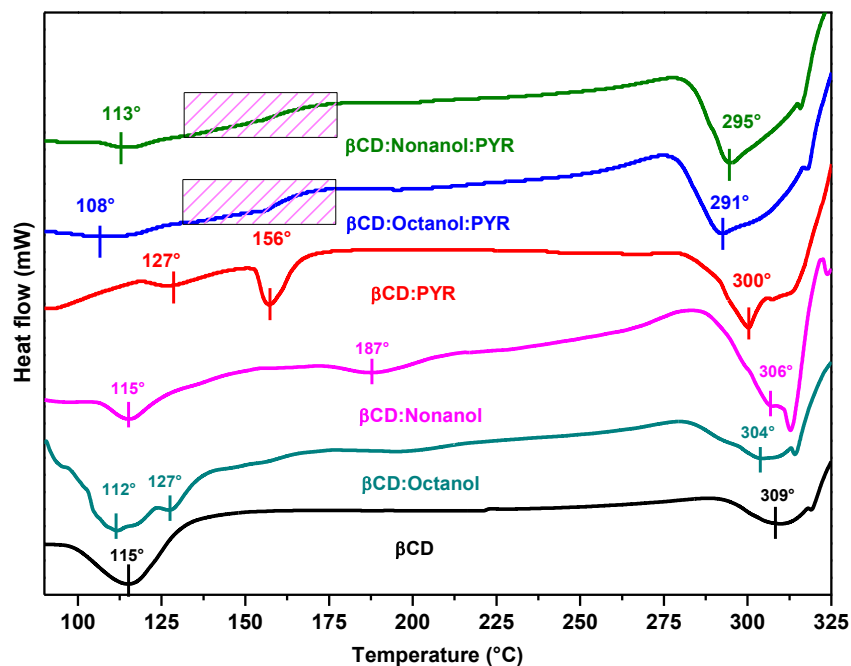


Figure 5.14 : DSC curve of β CD and β CD:alcohol:PYR (1:1:1).

The thermal studies curve obtained for β CD:alcohol:PYR has shown some different features from the curves obtained for complexes prepared with β CD:PYR (Figure. 5.14). The curves observed for complexes containing alcohols are similar to each other but different from β CD:PYR curve (chapter-4). The event for removal water molecules occurs at temperature less than 120°C i.e at 108° for octanol complex and at 113°C for Nonanol complex. No existence of peak at 156°C has been observed. Moreover, the curves between 125° and 175°C show linearly increasing curve instead of a smooth curve. The curves obtained for β CD: Octanol and β CD: Nonanol show very different events occurring to β CD: PYR and β CD: Alcohols:PYR curves. The temperature degradation and oxidation of uncomplexed CDs feature has existed at temperatures above 290°C for all the three cases. The addition of alcohol to the β CD:PYR inclusion complex system have produced remarkable changes.

5.4 Structural studies of β CD: alcohol: aromatic hydrocarbon complexes

5.4.1 Monocyclic aromatic hydrocarbons

5.4.1.1 Structural studies of β CD:alcohol:BEN (1:1:1) complexes

Figure 5.15 shows diffraction pattern for β CD:alcohol:BEN (1:1:1) and β CD:BEN inclusion complexes. As subsequently evident in the figure, the complex β CD:BEN exhibits a diffraction pattern characteristic mixture of β CD channel type (PUKPIU¹ and POHXUG⁶) crystal structure reported in the literature⁷. On the other hand, when the linear aliphatic alcohols are involved, the diffraction pattern shows peaks similar to CACPOM⁸. The peaks obtained in both the cases have lost their crystalline character. The similar appearance of pattern was also seen in case of patterns obtained for β CD: alcohol (chapter 3). We have compared the patterns with β CD: octanol to confirm the similarity between the different cases.

The other stoichiometries for β CD:alcohol:BEN (1:2:1 and 1:1:2) have also obtained the same diffraction patterns as for β CD:alcohol:BEN (1:1:1).

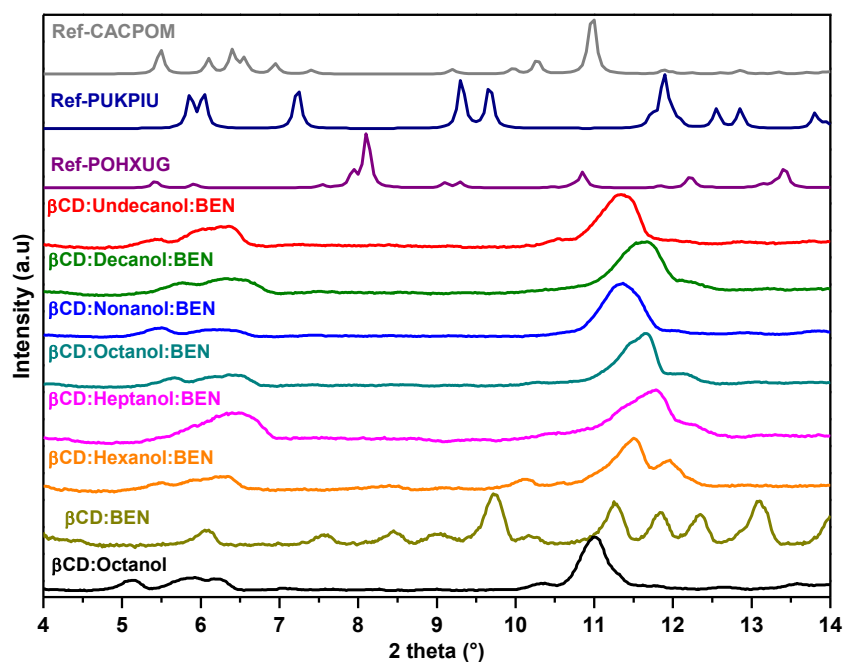


Figure 5.15 : Powder diffraction pattern of β CD:BEN and β CD:alcohol:BEN (1:1:1) in comparison to the references from the literature (CACPOM, PUKPIU and POHXUG).

5.4.1.2 Structural studies of β CD:alcohol:FB (1:1:1) complexes

The diffraction pattern obtained for β CD:FB and β CD:alcohol:FB (1:1:1) (Figure 5.16) inclusion complexes show similar kind of peaks as obtained for β CD:BEN. The literature study comparison indicates the resemblance of the mixture pattern to ref PUKPIU and POHXUG forming channel type pattern. We compared the patterns obtained for the ternary complex to β CD: octanol which shows similarity to REF CODE CACPOM. The complexes are crystalline in nature. The other stoichiometries (1:2:1 and 1:1:2) have produced similar diffraction patterns.

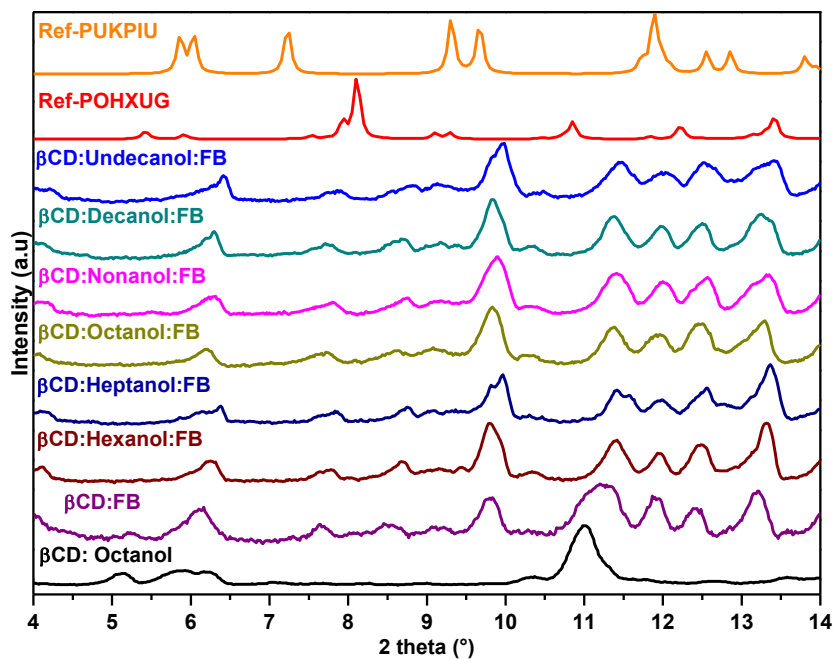


Figure 5.16 : Powder diffraction pattern of β CD:FB and β CD:alcohol:FB (1:1:1) in comparison to the references from the literature (PUKPIU and POHXUG).

5.4.1.3 Structural studies of β CD:alcohol:TOL (1:1:1) complexes

The diffraction patterns for β CD: TOL and β CD: alcohol: TOL (1:1:1) inclusion complex is shown in the Figure 5.17. Both patterns with and without alcohol obtained similar results which on comparison to the literature resemble to ref- CACPOM. The molecular arrangement is channel type. On comparison with β CD: octanol pattern, it can be noticed that the pattern is similar in terms of intensity of the peaks but their positions are slightly shifted. The other stoichiometries of β CD: alcohol: TOL (1:2:1 and 1:1:2) have produced similar results.

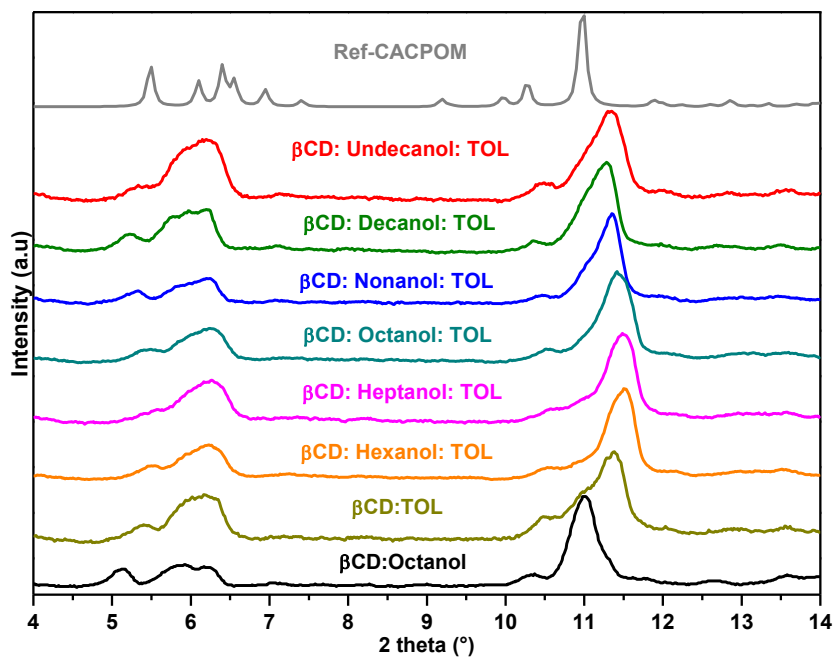


Figure 5.17 : XRD diffraction pattern of β CD:TOL and β CD:alcohol:TOL (1:1:1) in comparison to the references from the literature (CACPOM).

5.4.1.4 Structural studies of β CD:alcohol:TFT (1:1:1) complexes

The diffraction pattern (Figure 5.18) obtained for β CD: TFT and β CD: alcohol: TFT (1:1:1) have resembled channel type arrangement similar to Ref- CACPOM from the literature. Other stoichiometries for β CD: alcohol: TFT (1:2:1 and 1:1:2) have produced similar results. The pattern obtained for β CD:Octanol shows similar intense peaks but the only difference arises is the slight shifting of the peaks.

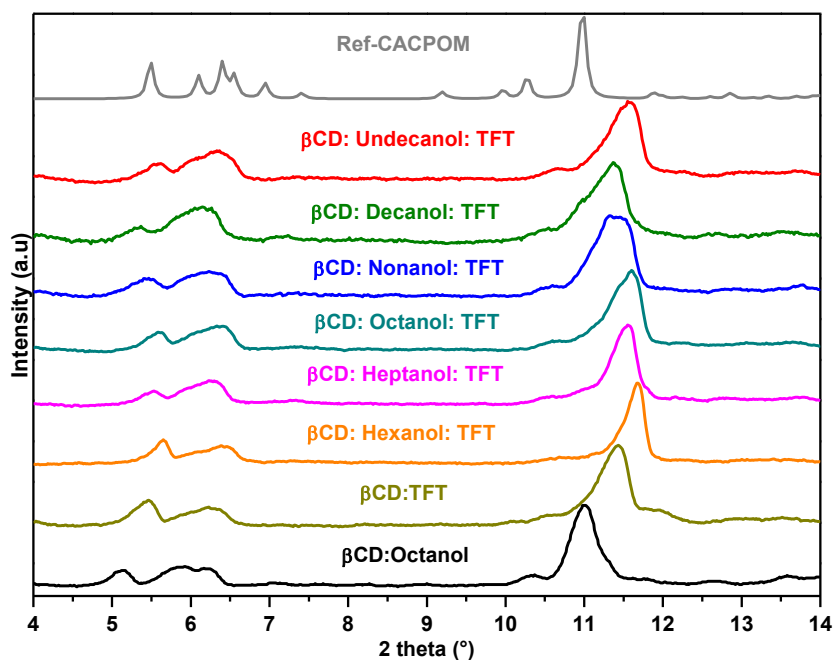


Figure 5.18 : XRD diffraction pattern of β CD:TFT and β CD:alcohol:TFT (1:1:1) in comparison to the references from the literature (CACPOM).

5.4.2 Bicyclic aromatic hydrocarbons

5.4.2.1 Structural studies of β CD:alcohol:NAP (1:1:1) complexes

The diffraction pattern obtained for β CD: NAP and β CD: alcohol: NAP (1:1:1) (Figure 5.19) have resembled channel type arrangement similar to Ref- CACPOM from the literature. Other stoichiometries for β CD: alcohol: NAP (1:2:1 and 1:1:2) have produced similar results. The patterns obtained with ternary complexes are similar to pattern obtained with β CD: octanol in terms of intensity but slight position difference is also observed.

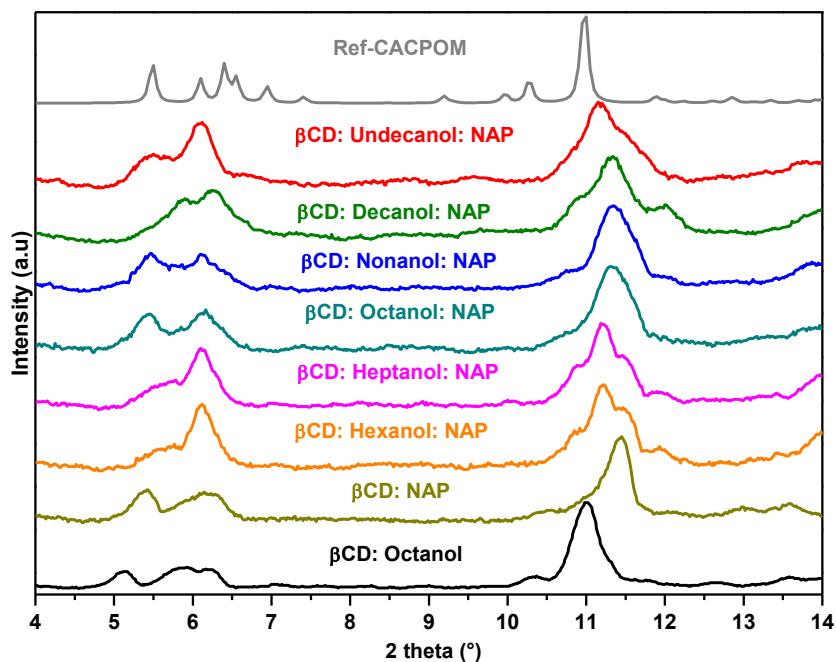


Figure 5.19 : XRD diffraction pattern of β CD:NAP and β CD:alcohol:NAP(1:1:1) in comparison to the references from the literature (CACPOM).

5.4.3 Polycyclic aromatic hydrocarbons

5.4.3.1 Structural studies of β CD:alcohol:ANTH (1:1:1) complexes

The diffraction pattern (Figure 5.20) obtained for β CD: alcohol: ANTH (1:1:1) have resembled channel type arrangement similar to Ref- PUKPIU from the literature. Other stoichiometries for β CD: alcohol: ANTH (1:2:1 and 1:1:2) have produced similar results. The patterns obtained with ternary complexes show different behaviour to β CD: Octanol pattern which resembles REF CODE CACPOM.

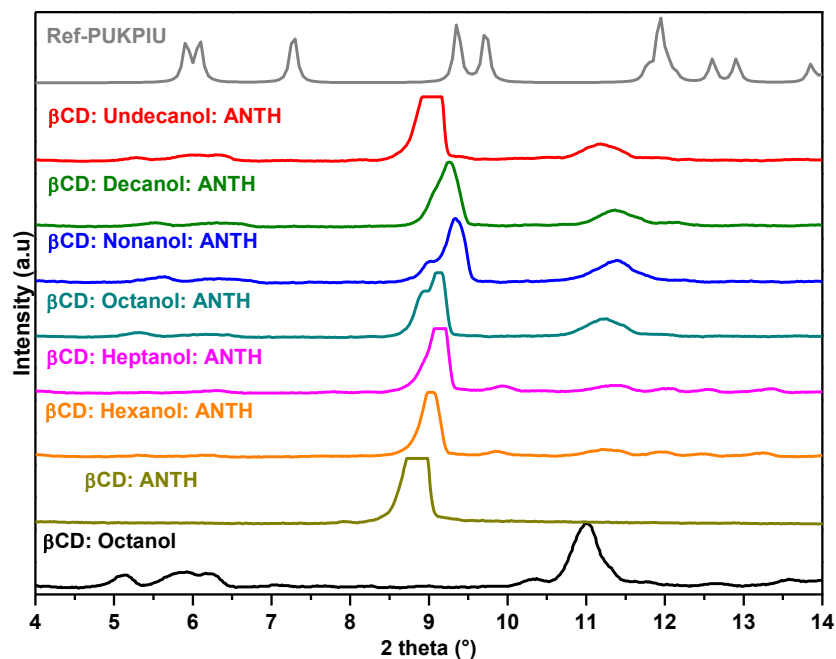


Figure 5.20 : XRD pattern β CD:alcohol:ANTH (1:1:1) in comparison to the references from the literature (PUKPIU).

5.4.3.2 Structural studies of β CD:alcohol:PYR (1:1:1) complexes

The diffraction pattern obtained for β CD: alcohol: PYR (1:1:1) and β CD: PYR (Figure 5.21) have resembled channel type arrangement similar to Ref- CACPOM from the literature. Other stoichiometries for β CD: alcohol: PYR (1:2:1 and 1:1:2) have produced similar results. The β CD: octanol pattern also shows the same peaks.

Another comparison (Figure 5.22) of β CD: alcohol: PYR (1:1:1, 1:2:1 and 1:1:2) with native β CD, β CD: Hexanol and β CD: PYR are shown to explain the similar results obtained by other stoichiometries (1:2:1 and 1:1:2) for all the cases discussed in this section.

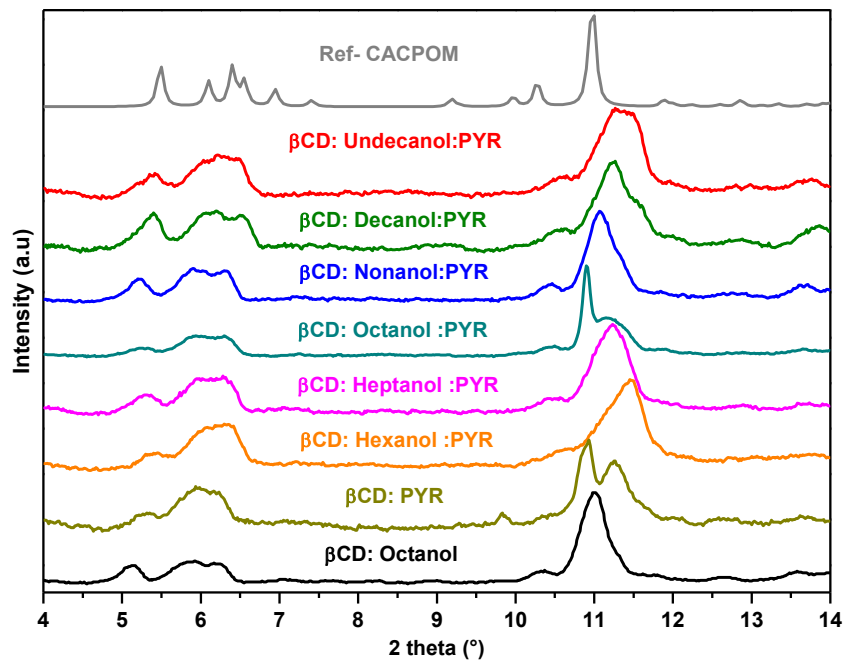


Figure 5.21. XRD pattern of β CD: PYR and β CD:alcohol:PYR (1:1:1) in comparison to the references from the literature (CACPOM).

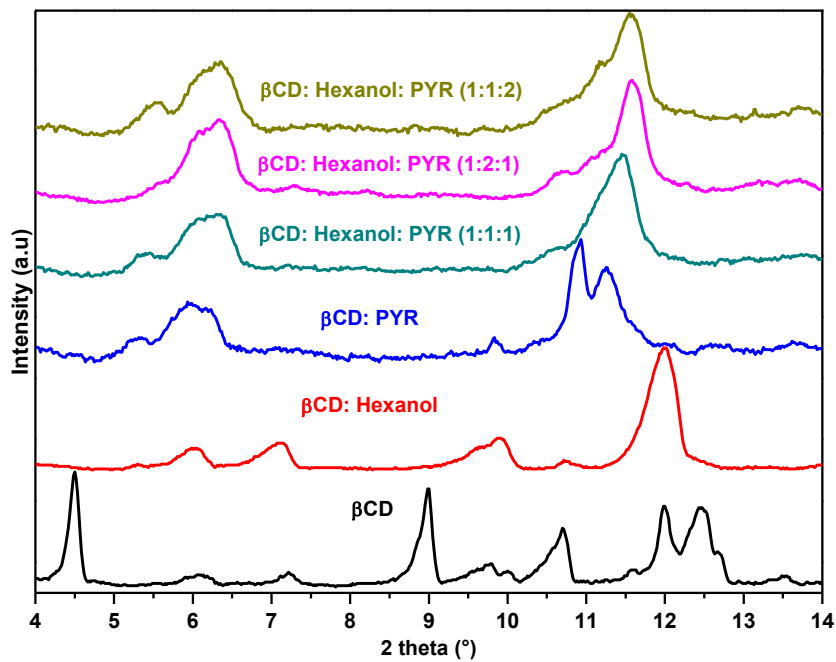


Figure 5.22 : XRD pattern comparison of β CD, β CD: Hexanol, β CD:PYR and β CD: Hexanol: PYR (1:1:1, 1:2:1 and 1:1:2).

5.5 Raman spectroscopic studies of β CD: alcohol: aromatic hydrocarbon complexes

In the previous chapter, we have discussed the Raman spectral studies for β CD: Aromatics. For most of the β CD: Aromatics complexes prepared in this thesis showed the appearance of peaks corresponding to respective aromatics where the complexes were prepared with β CD. There were only two aromatics: BEN and ANTH which failed to show any complexation and hence no peaks corresponding to them in the complexes were recorded. In this part of the chapter, we have shown the results of the complexes prepared in presence of linear aliphatic alcohols.

We also prepared complexes for other aromatics in order to expect new structure formation but we found similar to the results obtained in chapter – 4 where the complexes were prepared in absence of linear alcohols. Due to alcohol addition, the only change occurred is the appearance of C-H vibrational modes of alcohols existing above $2800\text{-}2900\text{ cm}^{-1}$. We have also compared all the ternary complex spectra to spectrum obtained for β CD: octanol that clearly shows the C-H vibrational mode. We have presented results only for stoichiometry 1:1:1 for β CD:Alcohol:Aromatic as other stoichiometries have shown the similar results.

5.5.1 Monocyclic aromatic hydrocarbons

5.5.1.1 Raman Spectral studies of β CD: Alcohol: BEN (1:1:1) complexes

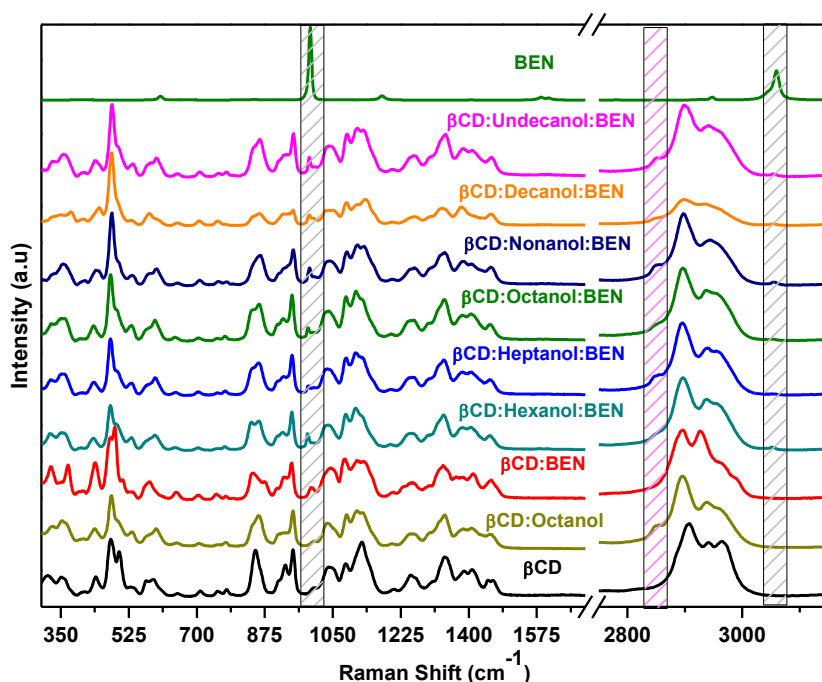


Figure 5.23 : Raman spectra of β CD, β CD: Octanol, β CD: BEN and β CD: alcohol: BEN inclusion complexes (1:1:1).

On introduction of linear aliphatic alcohols to the β CD: BEN system (Figure 5.23), the Raman Spectral studies showed the appearance of peaks corresponding to BEN at the positions 990 and 3057 cm^{-1} with reduced intensities. Here we have shown positive results obtained in presence of different linear aliphatic alcohols.

All other stoichiometries for β CD: alcohol: BEN (1:2:1 and 1:1:2) have produced similar results.

5.5.1.2 Raman Spectral studies of β CD: Alcohol:FB (1:1:1) complexes

After the addition of alcohols, for the new stoichiometry 1:1:1 (Figure 5.24) reveals appearance of few of the peaks with reduced intensities corresponding to FB which were also obtained in absence of alcohols. These peaks are shown in highlighted rectangles with grey fill pattern. The other information indicating the presence of alcohols is the appearance of C-H vibrational modes between 2800 and 2900 cm^{-1} (highlighted rectangles with pink fill pattern).

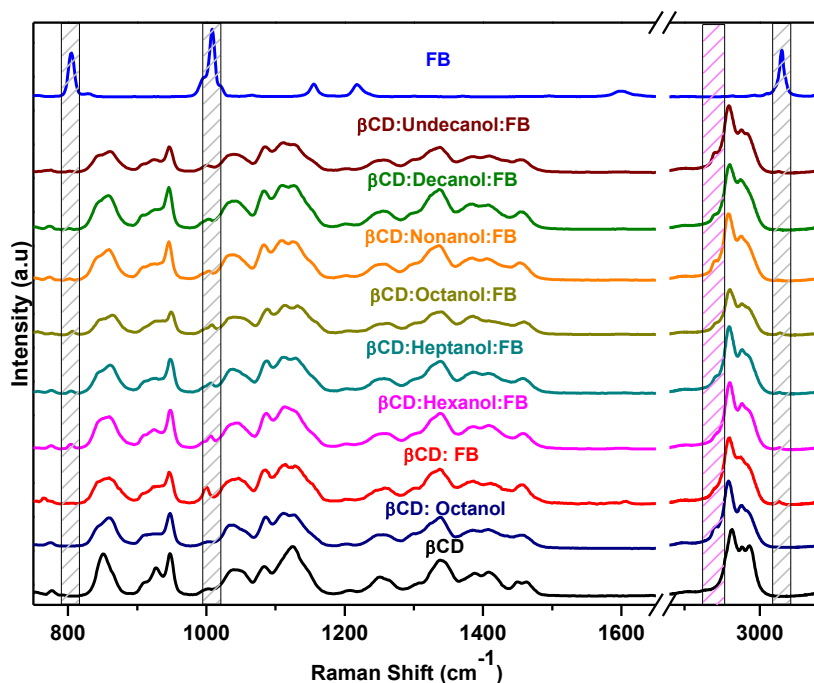


Figure 5.24 : Raman spectra of β CD, β CD: Octanol, β CD:FB and β CD: alcohol: FB inclusion complexes (1:1:1).

5.5.1.3 Raman Spectral studies of β CD: Alcohol:TOL (1:1:1) complexes

On preparing complexes in presence of different linear alcohols, TOL peaks can be seen in all the spectra of the complexes obtained for each alcohol used in different molar ratios. For example- for stoichiometry $1\beta\text{CD}:1\text{alcohol}:1\text{TOL}$ (Figure 5.25), appearance of toluene peaks at the same positions as in the case of $1\beta\text{CD}:1\text{TOL}$ complex spectrum are observed. Moreover, all the spectra also contain the peaks due to CH stretching modes from linear alcohol spectrum.

The TOL peaks are highlighted in rectangles with grey fill pattern whereas the CH vibrational mode of alcohols is highlighted with pink fill pattern.

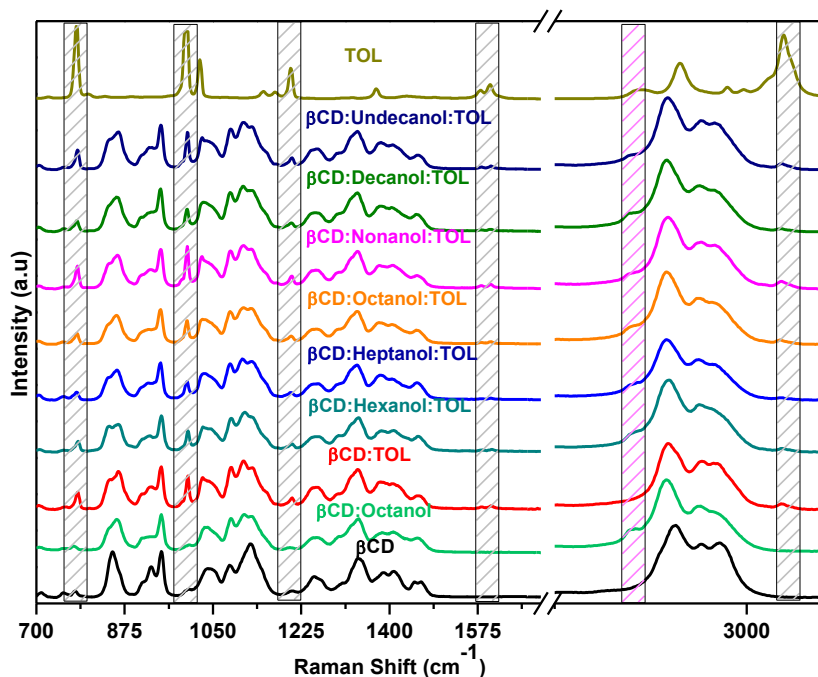


Figure 5.25 : Raman spectra of β CD, β CD: Octanol, β CD:TOL and β CD: alcohol: TOL inclusion complexes (1:1:1).

5.5.1.4 Raman Spectral studies of β CD: Alcohol:TFT (1:1:1) complexes

The spectra of complexes of the stoichiometry 1:1:1 (Figure 5.26) show appearance of the TFT peaks at the same positions. Also, the band due to C-H stretching of the aliphatic alcohols is also present.

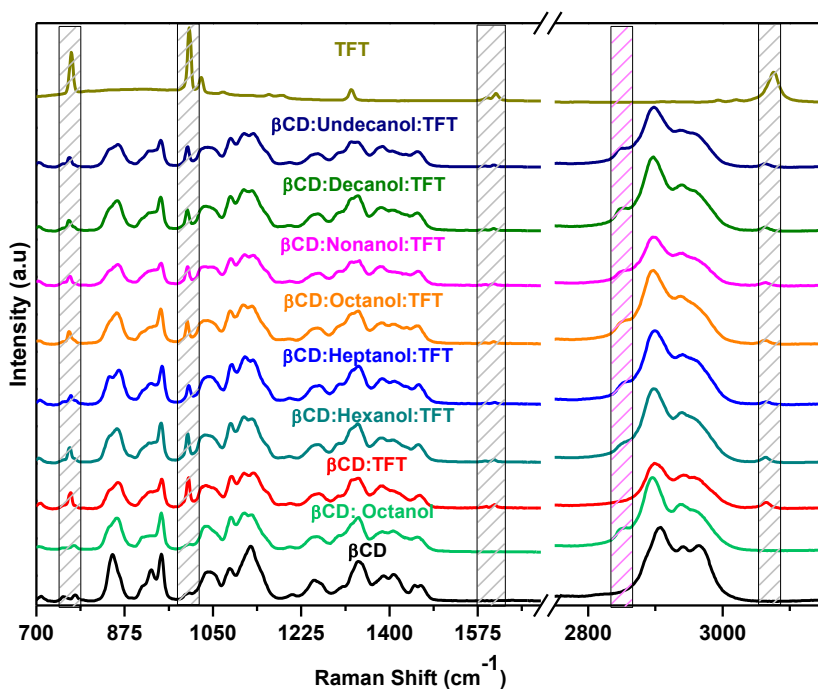


Figure 5.26 : Raman spectra of β CD, β CD: Octanol, β CD:TFT and β CD: alcohol: TFT inclusion complexes (1:1:1).

5.5.2 Bicyclic aromatic hydrocarbons

5.5.2.1 Raman Spectral studies of β CD: Alcohol:NAP complexes

The peaks corresponding to NAP (Figure 5.27) can be easily seen for the inclusion complex spectrum. Furthermore, the relative intensities of the naphthalene peaks observed for the complex, on comparison to that of isolated ones give the proof of molecular interaction and inclusion within the CD cavities clearly. Also, significant differences in intensities can be observed for several peaks. The results obtained during our studies are in accordance with the work done with naphthalene done in the team previously².

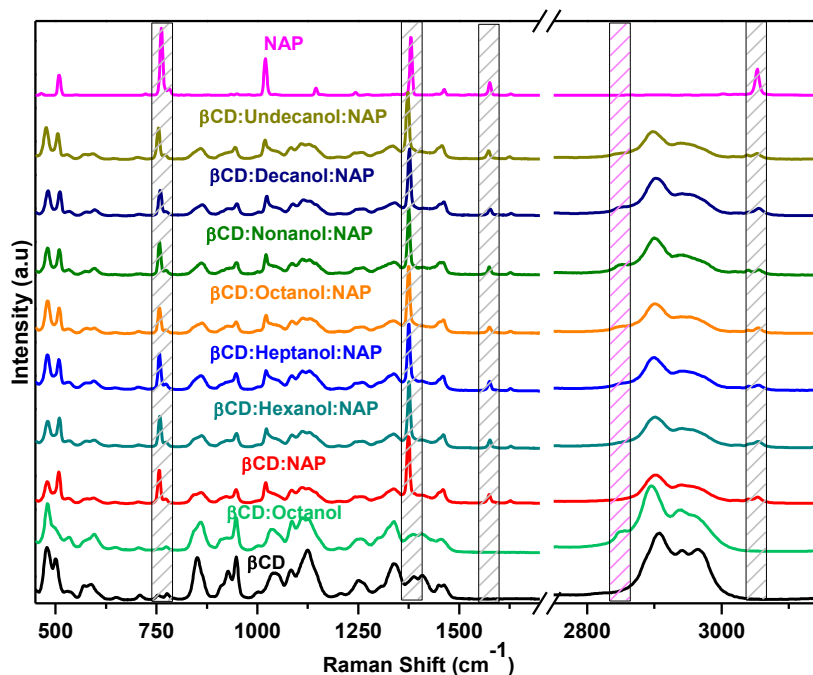


Figure 5.27 : Raman spectra of β CD, β CD: Octanol, β CD:NAP and β CD: alcohol: NAP inclusion complexes (1:1:1).

5.5.3 Polycyclic aromatic hydrocarbons

5.5.3.1 Raman Spectral studies of β CD: Alcohol:ANTH (1:1:1) complexes

On adding alcohols to the mixture, the β CD:Alcohol:ANTH (Figure 5.28) spectra have showed the peaks attributed to anthracene. The sharp, slightly intense peaks can be identified for the positions- 401,756, 1403 and 1563 cm^{-1} . Other peaks with reduced intensities are also present at positions 1006, 1185 and the doublet around 3050 cm^{-1} . All other stiochiometries for β CD: alcohol: ANTH (1:2:1 and 1:1:2) have produced similar results. These results indicate that ANTH forms ternary inclusion complexes in presence of alcohols.

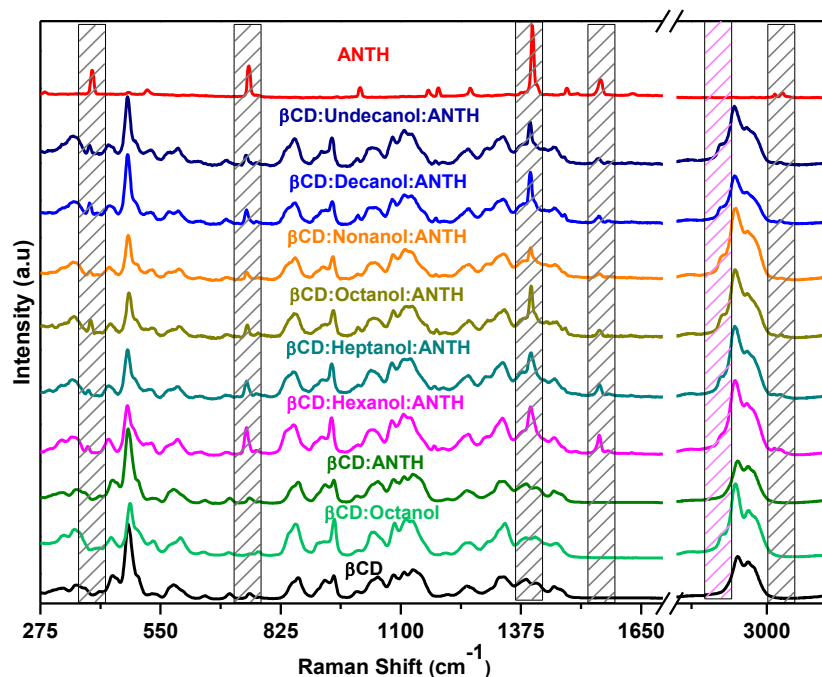


Figure 5.28 : Raman spectra of β CD, β CD: Octanol, β CD:ANTH and β CD: alcohol: ANTH inclusion complexes (1:1:1).

5.6 Conclusions

On analysis of all the results obtained for inclusion complexes prepared in presence of alcohols it can be concluded that we are successful in encapsulating some of the aromatic hydrocarbons in presence of alcohols in different stoichiometry.

The NMR studies performed for β CD with BEN and TFT where deturated ethanol was used as co-solvent showed desired shifts in the values of the proton peaks positions (H3 and H5). Evolution in the proton peaks of guest molecules was also observed. Furthermore, job's plot showed bell shape curve in both the cases indicating inclusion complexation.

The thermal results done with DSC technique obtained mixed results in the sense that some of the aromatics behaved in a similar way as in absence of alcohols i.e no exceptional changes occurred in their thermal properties. For few aromatics, the DSC curve observed are different from the curve obtained for β CD: aromatics in the absence of alcohol. Furthermore, the ternary complex curves seem different when compared with curves observed for β CD:Octanol and β CD:Nonanol thermal curves.

XRD patterns obtained for the complexes obtained with different aromatics prepared in presence of linear aliphatic alcohols showed resemblance to the channel type molecular arrangement in most of the cases when compared to the structures available in the literature. The similar pattern is obtained for β CD:Octanol.

Raman spectroscopic studies for BEN and ANTH containing ternary complexes indicated appearance of peaks corresponding to the guest molecules in the spectrum due to change in their vibrational motions. For the two cases, alcohols have played important role in

encapsulation. Moreover, all the spectra showed C-H vibrational mode peak indicating existence of alcohols in the system.

It can also be concluded that the different stoichiometries prepared for β CD: Alcohol: Aromatics complexes (1:1:1, 1:2:1 and 1:1:2) have obtained similar results indicating independency with respect to number of molecules taking part while formation of stable inclusion complex.

5.7 References

1. Udachin, K.A. and Ripmeester, J.A., 1998. A novel mode of inclusion for pyrene in β -cyclodextrin compounds: The crystal structures of β -cyclodextrin with cyclohexanol and pyrene, and with n-octanol and pyrene. *Journal of the American Chemical Society*, 120(5), pp.1080-1081.
2. Tijunelyte, I., Dupont, N., Milosevic, I., Barbey, C., Rinnert, E., Lidgi-Guigui, N., Guenin, E. and de la Chapelle, M.L., 2017. Investigation of aromatic hydrocarbon inclusion into cyclodextrins by raman spectroscopy and thermal analysis. *Environmental Science And Pollution Research*, 24(35), pp.27077-27089.
3. Gallois-Montbrun, D., Le Bas, G., Mason, S.A., Prange, T. and Lesieur, S., 2013. A highly hydrated α -cyclodextrin/1-undecanol inclusion complex: crystal structure and hydrogen-bond network from high-resolution neutron diffraction at 20 K. *Acta Crystallographica Section B: Structural Science, Crystal Engineering and Materials*, 69(2), pp.214-227.
4. Beihoffer, J. and Ferguson, C., 1994. Determination of Selected Carboxylic Acids and Alcohols in Groundwater by GC—MS. *Journal of chromatographic science*, 32(3), pp.102-106.
5. Belanger, S.E., Sanderson, H., Fisk, P.R., Schaefer, C., Mudge, S.M., Willing, A., Kasai, Y., Nielsen, A.M., Dyer, S.D. and Toy, R., 2009. Assessment of the environmental risk of long-chain aliphatic alcohols. *Ecotoxicology and Environmental safety*, 72(4), pp.1006-1015.
6. Paulidou, A., Maffeo, D., Yannakopoulou, K. and Mavridis, I.M., 2008. Crystal structure of the inclusion complex of the antibacterial agent triclosan with cyclomaltoheptaose and NMR study of its molecular encapsulation in positively and negatively charged cyclomaltoheptaose derivatives. *Carbohydrate research*, 343(15), pp.2634-2640.
7. Uyar, T., Nur, Y., Hacaloglu, J. and Besenbacher, F., 2009. Electrospinning of functional poly (methyl methacrylate) nanofibers containing cyclodextrin-menthol inclusion complexes. *Nanotechnology*, 20(12), p.125703.
8. Makedonopoulou, S. and Mavridis, I.M., 2001. The dimeric complex of cyclomaltoheptaose with 1, 14-tetradecanedioic acid. Comparison with related complexes. *Carbohydrate research*, 335(3), pp.213-220.

Conclusions and perspectives

Within the scope of the thesis, different complexation studies were done in order to understand the behaviour on encapsulation of aromatic hydrocarbons by β CD under different conditions. During this study, we followed different steps to achieve the motive of the thesis, which were as follows: (i) to study the complexation behaviour of β CD and linear aliphatic alcohols. (ii) to study the complexation behaviour of aromatic hydrocarbons in absence of alcohols and lastly (iii) to understand their behaviour in presence of linear aliphatic alcohols. All the complexes prepared were characterized by two spectroscopic techniques like NMR, Raman followed by thermal and structural studies performed with DSC and PXRD techniques. In order to have more information about the results obtained, molecular modelling studies were done for better understating of the science and to support our findings.

After gathering all the knowledge and information about different types of CDs, their physical/chemical properties, their inclusion properties and their versatile applications from the literature and the research done till date, we found that only 2 structures involving CDs and Polycyclic aromatic hydrocarbons are available in the CSD which were prepared in presence of Octanol or cyclohexanol. This number added our curiosity to further explore this field of application. The search for β CD structural characteristics in the literature provided us further details about different structures existing in the CSD. The β CD used for this thesis is found to be similar to mixture of two CSD REFCODE namely BCDEXD10 (herringbone structure type) and ZUZXOH (channels with tilted molecules). The other structures found were PUKPIU (channel structure type) and CACPOM (dimer brick type). Since the complexes with polycyclic aromatics were prepared in presence of Octanol, the PXRD pattern obtained for β CD:Octanol was found similar to the CSD REFCODE CACPOM for further comparison.

To begin our thesis, the first step as mentioned above was to study the complexation chemistry between linear aliphatic alcohols.

The results obtained for β CD:Linear alcohol studies in liquid as well as solid states by different characterization techniques revealed interesting results. For NMR studies in the liquid state, the complexes prepared for 1:1 volume ratio with lower alcohols in the homologous series upto to butanol (=4C) failed to show interesting chemical shifts for H3 and H5 β CD protons. By observing such behaviour, we concluded that those alcohols are small and polar enough to act as water solvent molecules and are randomly present in solution. Moreover, their molecular organisation in solution is very similar as obtained in presence of water. The results obtained for the complexes prepared with higher member of the homologous series i.e from Pentanol (5C) to Undecanol (11C) have shown significant chemical shifts for H3 and H5 β CD protons. The criterion to choose appropriate length of alcohol to form successful inclusion is based on the value of difference of chemical shift (in Hertz) The threshold value of difference is ≥ 10 Hz. For lower alcohols, the value obtained is less than 5 Hz. On the other hand, the value obtained for higher alcohols is always greater than 25 Hz. By solution studies, another features to be discovered for β CD:Linear alcohol is the stoichiometry of the complex by Job's plot method. The stoichiometry in most of the cases is found to be 2:1 and 1:1 in few cases.

During solid state studies, the thermal studies of the β CD:Linear alcohol complex by DSC studies obtained distinctive features. For β CD: Lower alcohol complexes, the curves shown similar behaviour to β CD curve except for the higher values of temperatures for the

endothermic phase related to tightly bound water molecules removal. For β CD: Higher alcohol complexes, the individual curves showed additional endothermic curve corresponding to inclusion complexes and also the 'water molecules loss' curve.

On comparing the literature, the structural studies performed by PXRD technique revealed the similarities between β CD: Lower alcohol complexes and CSD REFCODE BCDEXD10 which represents herringbone structural type indicating the 'solvation' role of the alcohol molecules in these structures. The β CD: Higher alcohol complexes have shown different structural types with different alcohols used. For β CD: Pentanol and β CD: Hexanol complexes, the structures were found to be similar to CSD REFCODE PUKPIU showing channel type structures. The rest of the β CD: higher alcohols patterns resembled CSD REFCODE CACPOM showing dimer brick type structures.

The vibrational mode studies by Raman Spectroscopy indicated the changes in the vibrational modes on forming an inclusion complex. The results obtained for β CD: Lower alcohol complexes failed to show any changes and were found to follow the same spectra as obtained for β CD. The β CD: Higher alcohol complexes have shown changes in the regions 1357-1488 cm^{-1} and 2814-2879 cm^{-1} of the Raman Spectra. The superposition of β CD peaks might be the reason for failure of detection of more peaks corresponding to higher linear alcohols.

To further support our finding, molecular modelling studies were performed for β CD:Linear alcohol complexes by manual docking using the semi empirical PM3 method. A model was created for each complex where an alcohol molecule is located inside the cavity between $\frac{1}{2}$ (L+T) and $-\frac{1}{2}$ (L+T) along Z-axis with length of the molecule and thickness as the two parameters considered. Each structure obtained was optimised and converged to obtain thermodynamic and electronic energy features. The value of binding energy defines the strength of the interaction of the host and the guest. For lower alcohols, the behaviour observed was similar with no significant gain in energy on inclusion. They all behaved in a manner comparable to water molecule with binding energy above -10 kcal/mol. On inserting higher alcohols inside the cavity, the value of binding energy tends to decrease and became equivalent, starting from heptanol to other longer alcohols. All results obtained with different techniques are summarised in the table (a) below:

βCD:Linear alcohol complexes				
βCD:Lower alcohol complexes (upto Butanol (4C))				
NMR	DSC	XRD	Raman	Molecular Modelling
- No significant chemical shift for H3 and H5 protons observed for complexes.	- thermal curves similar to βCD were observed with water loss occurring at higher temperature.	- the patterns obtained are found similar to CSD REFCODE BCDEXD10 which represents herringbone structural type.	- no peaks corresponding to alcohols were observed. The spectra obtained were similar to the Raman Spectrum of βCD.	- no significant change in binding energy on inclusion.
βCD:Higher alcohol complexes (pentanol (5C) to Undecanol (11C))				
- the significant chemical shift for H3 and H5 protons proved the validity of method of continuous variation: job's plot. - the stoichiometry for most of the βCD: Higher alcohol complexes were found to be 2:1.	- the thermal curves showed additional feature corresponding to formation of inclusion complex and the typical water loss endothermic curve.	- the patterns obtained were found similar to CSD REFCODE PUKPIU which represents channel structural type for βCD: Pentanol and βCD: Hexanol complexes. - rest of the βCD: higher alcohols patterns resembled CSD REFCODE CACPOM showing dimer brick type structures.	- The βCD: Higher alcohol complexes have shown changes in the regions 1357-1488 cm ⁻¹ and 2814-2879 cm ⁻¹ of the Raman Spectra.	- the value of binding energy tends to decrease on inclusion.

Table (a): Summary of the results obtained for βCD:Linear alcohol inclusion complexes.

It can be concluded after monitoring all the results, that Pentanol behaves as a borderline molecule to form inclusion complex. The values obtained by different characterizing techniques look less promising for further analysis of the inclusion complexes obtained with aromatic hydrocarbons in presence of Pentanol. On the basis of these results, we have not included pentanol for the next step studies.

All the results obtained for higher alcohols revealed that they form stable inclusion complexes with β CD and form different crystal structures with corresponding alcohols on inclusion.

The studies of β CD: Aromatic Hydrocarbons were performed again in the solid and the liquid state. For poor solubility of most of the aromatic hydrocarbons proton NMR studies could not be performed. For other aromatic hydrocarbons like BA, PHE and 2-NAP; the H3 and H5 peaks showed significant displacement. All the three aromatics were found to form 1:1 stoichiometry. The results obtained are in accordance with the work previously done.

The thermal studies revealed different features in different cases. But three typical features were observed in most of the cases were (i) removal of tightly bound water molecules, (ii) formation of new crystalline phase around 255-260°C (iii) decomposition of uncomplexed β CD. Some of the results have also shown curve related to inclusion complex.

Again, XRD literature comparison for β CD: Aromatic Hydrocarbons indicated the existence of similar patterns. β CD: BEN and β CD: FB were found similar to mixture of CSD REFCODE PUKPIU and POXHUG whereas the aromatics obtained 1:1 stoichiometry with NMR studies which are BA, PHE and 2-NAP were found to be similar to CSD REFCODE PUKPIU. The leftover aromatics-TOL, TFT, NAP and PYR were found to form similar structures to CSD REFCODE CACPOM.

The vibrational mode studies for β CD: Aromatic Hydrocarbons for most of the cases contained the peaks of the aromatic molecules in the spectra of the complexes except for the case of BEN and ANTH. For β CD: BEN system, the spectrum of the complex does not contain any intense peak corresponding to BEN, in fact few changes occurring in the spectrum for β CD peaks are hinting about inclusion complex formation. For β CD: ANTH, neither peaks of ANTH were observed not any changes in the spectrum occurred indicating a complete failure of formation of inclusion complex. The theoretical spectra were also calculated for aromatics for comparison with the observed values. Moreover, most impacted vibration modes on inclusion were also taken into account.

The results obtained are summarised in the table (b) :

βCD:Aromatic hydrocarbons complexes			
NMR	DSC	XRD	Raman
<p>-Inclusion complexes of stoichiometry 1:1 with BA, PHE and 2-NAP were obtained.</p> <p>- due to poor solubility of most of the aromatics no NMR results were obtained.</p>	<p>- inclusion complexes with TOL, TFT, PHE, BA, NAP, 2-NAP showed endothermic curves corresponding to inclusion complexes.</p> <p>- formation of new crystalline phase was also observed in few cases.</p>	<p>- complexes with FB and BEN showed similarities to the mixture of CSD REFCODES PUKPIU and POXHUG (both channel type structures).</p> <p>- complexes with BA, PHE and 2-NAP showed similar structures to CSD REFCODE PUKPIU.</p> <p>- complexes with TOL, TFT, NAP and PYR showed similar pattern to CSD REFCODE CACPOM (dimer brick type structures).</p>	<p>- Most of the results showed peaks of the corresponding the aromatics.</p> <p>- BEN and ANTH complexes did not show their peaks clearly.</p>

Table (b): Summary of the results obtained for βCD: Aromatic hydrocarbons inclusion complexes.

It can be concluded from all the results that aromatics containing polar groups easily formed inclusion complexes with βCD. For other aromatics, solid state studies revealed inclusion complex formation in most of the cases whereas for very few cases ternary complexes with linear alcohols would have given better results.

The formation of ternary complexes revealed surprising results. We were able to perform liquid state studies for limited cases where we used EtOD as co-solvent. On obtaining the results with BEN, we were able to see shifts for H3 and H5 βCD proton. The stoichiometry was found to be 2:1. Similar results were obtained for TFT.

The complexes for the solid states were prepared in different stoichiometries (βCD:Alcohol:Aromatic-1:1:1, 1:2:1 and 1:1:2). These stoichiometries showed similar results indicating no impact of the stoichiometry while inclusion complex formation. The studies were then focussed on 1:1:1 stoichiometry. The thermal studies obtained only for complexes prepared with octanol and nonanol showed interesting results in some case and some revealed the same behaviour as observed in absence of alcohols.

The structural studies obtained results to CSD REFCODE CACPOM for βCD:alcohol:BEN complexes. For aromatics like FB, TOL, TFT and NAP the patterns are similar to βCD:Aromatic cases for respective aromatics. Complexes with ANTH and PYR were found similar to PUKPIU and CACPOM respectively.

The Raman spectral studies showed sharper peak of BEN and ANTH in presence of alcohols in the complex spectra. Rest of the aromatics showed similar Raman spectra as observed in absence of alcohols. All the spectra contained only CH peak corresponding to alcohols whereas other peaks become invisible due to superposition of β CD and aromatics peaks.

All the results are summarised into the table (c) :

βCD: Linear Alcohol:Aromatic hydrocarbons			
NMR	DSC	XRD	Raman
<p>- βCD:BEN and βCD:TFT showed significant shifts for H3 and H5 βCD protons when EtOD was used as co-solvent.</p> <p>- the stoichiometry 1:1 were observed in both the cases.</p>	<p>- complexes prepared with octanol and nonanol with FB, TOL, TFT, NAP have produced similar results as observed in absence of alcohols.</p> <p>- complexes with BEN, ANTH and PYR showed different features in terms of energies and inclusion complexation involved.</p>	<p>- complexes with BEN and PYR were found to form similar structures to CSD REFCODE CACPOM.</p> <p>- FB, TOL, TFT, NAP containing complexes obtained similar patterns as observed in absence of alcohols.</p> <p>- ANTH complexes found to be similar to CSD REFCODE PUKPIU.</p>	<p>- complexes of BEN and ANTH showed their sharp peaks.</p> <p>- all other aromatics behaved in the similar manner as observed in absence of alcohols.</p>

Table (c): Summary of the results obtained for β CD:Linear alcohol: Aromatic hydrocarbon inclusion complexes.

After summarising all the results obtained, it can be finally concluded that linear alcohols do form stable inclusion complexes with β CD. For most aromatics in the solid state studies, it can be revealed that they tend to form inclusion complex with β CD without use of alcohols. But some of them have showed remarkable results when alcohols were used in the ternary complex. All the research previously done is in accordance with the results obtained in this thesis.

The perspectives of the thesis includes:

1. Proton NMR studies should be further performed for all the aromatics with alcohol as co-solvent. 2D NMR would be able to reveal further details about the complexation occurring.
2. Thermal studies should be performed for the complexes containing other alcohols also. Moreover, TGA analysis would reveal step by step mass loss in the systems.
3. Molecular mechanics studies should be performed with β CD:Aromatics and β CD:Alcohol:Aromatic complexes to gather better information about the system.
4. The complexes should also be prepared and studied with other CDs available.

Additional informations

β CD:Aromatics and β CD:Alcohols:Aromatics complexes Normalised subtracted spectra

Another observation that could reveal the existence of guest molecules in the complex and which could also reveal the extent of complexation is by calculating the subtracted spectrum of the reference from the spectrum obtained for the binary or ternary complex. Moreover, many CD vibrational modes were strongly modified by the interaction with the aromatic molecules for binary complexes and by both aromatic and alcohol molecules for ternary complexes. Here, we have obtained the subtracted spectra of all the β CD:Aromatics and β CD:Alcohols:Aromatics where β CD spectrum was taken as reference. The resulted spectrum for each complex has produced minute details about the peaks of aromatic guest molecules. We have compared the spectra with negative β CD spectrum for better representation of the changes observed in the resulted normalised subtracted spectra of β CD:Aromatics. These changes in the respective spectra caused due to presence of aromatic peaks are represented by **pink** fill pattern and other apparent changes in the vibrational modes by **grey** fill pattern.

Monocyclic aromatic inclusion complexes

β CD:BEN and β CD:Alcohols:BEN complex Normalised subtracted spectrum

The normalised spectrum obtained for β CD:BEN has shown (Figure 1) slight appearance of the most intense BEN peak in the spectrum at 990 cm^{-1} . This signifies that there existed a weak interaction between the host and the guest in absence of alcohols. Furthermore, other changes in the spectrum can be seen at positions 370 , 500 , 1314 and 2960 cm^{-1} . The peaks at 370 and 1314 cm^{-1} show appearance of new peaks whereas at 500 and 2960 cm^{-1} we observe change in the intensity of the peaks.

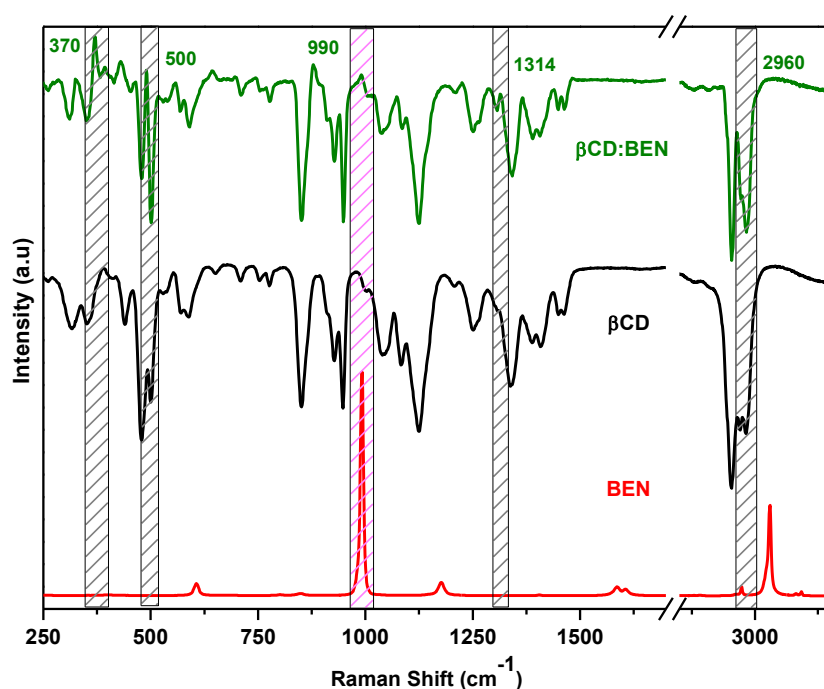


Figure 1. Normalised Raman Spectrum obtained after β CD spectrum subtraction from β CD:BEN (1:1) in comparison with Raman spectrum of BEN.

The normalised subtracted spectra of all the β CD:Alcohol:Aromatics are presented in the Figure 2. The comparison of all the ternary complex is done with spectrum of binary complex to understand the effect of alcohol addition on the overall system. It can be seen that the BEN peaks at 1000 and 3057 cm^{-1} have become more evident in ternary complex than in binary complex indicating a successful interaction between the host and guest systems. All the spectra obtained with different alcohols are similar except for the peaks between 450-550 cm^{-1} .

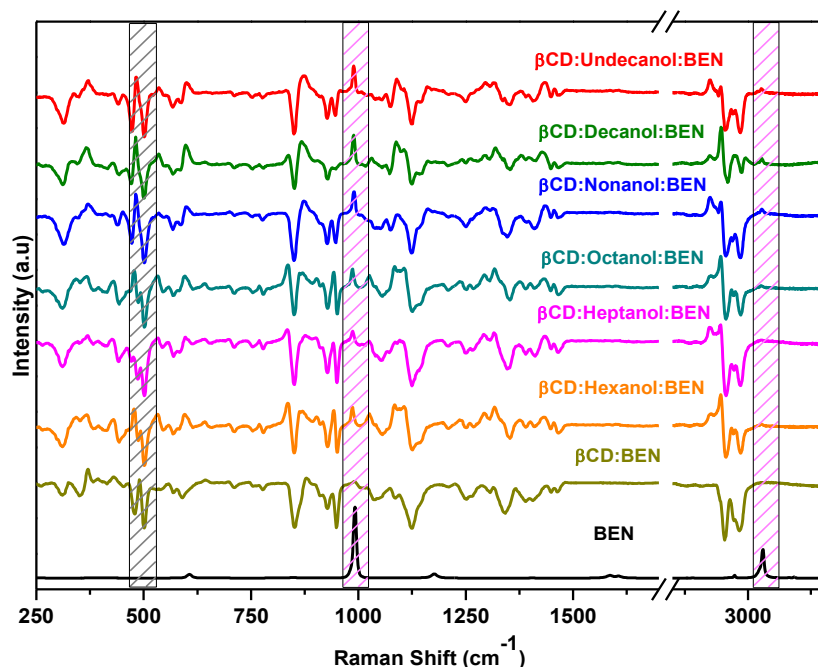


Figure 2. Normalised Raman Spectra obtained after β CD spectrum subtraction from β CD:BEN (1:1) and β CD:Alcohol:BEN (1:1:1) in comparison with Raman spectrum of BEN.

β CD:FB and β CD:Alcohols:FB complex Normalised subtracted spectrum

The normalised spectrum obtained for β CD:FB (Figure 3) has shown slight appearance of the peaks at positions- 1000, 1606 and 3065 cm^{-1} . The other changes in the spectra can be seen at positions- 500, 765 and 1316 cm^{-1} . For all these three positions, intensity changes for the corresponding peaks are observed. It can be concluded that FB had interacted with β CD molecules by changing some vibrational modes in absence of alcohols.

The normalised subtracted spectra obtained with β CD:Alcohol:FB (Figure 4) show differences from β CD:FB spectrum for the cases in which the complexes were prepared with Hexanol, Nonanol and Undecanol. The differences can be seen mainly for the positions between 450-550, 2890 cm^{-1} . The addition of alcohols have not affected the same vibrational modes of β CD resulting in different observations of the spectra. The FB peaks are appearing at the same positions as observed in case of β CD:FB but becoming slightly intense with alcohol addition.

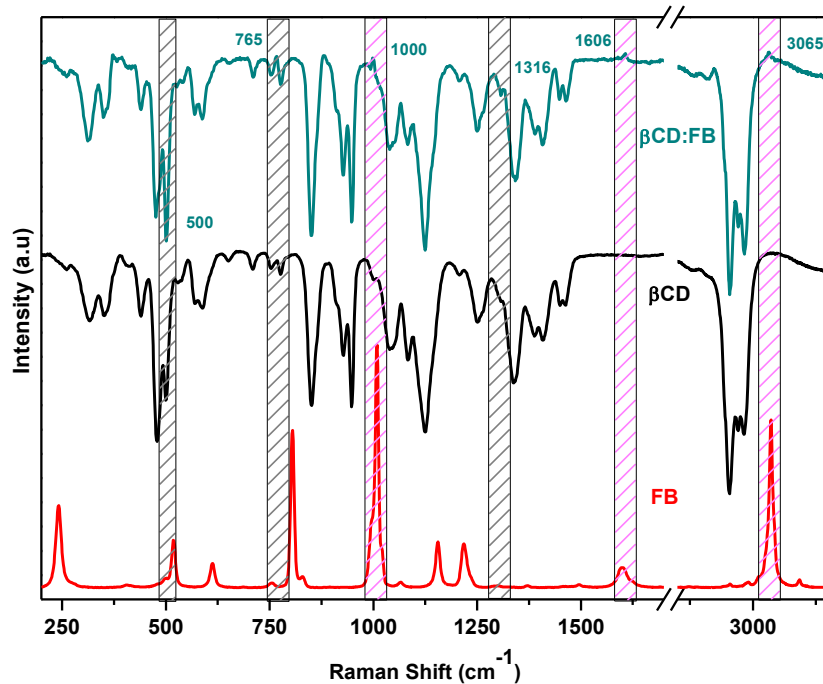


Figure 3. Normalised Raman Spectrum obtained after β CD spectrum subtraction from β CD:FB (1:1) in comparison with Raman spectrum of FB.

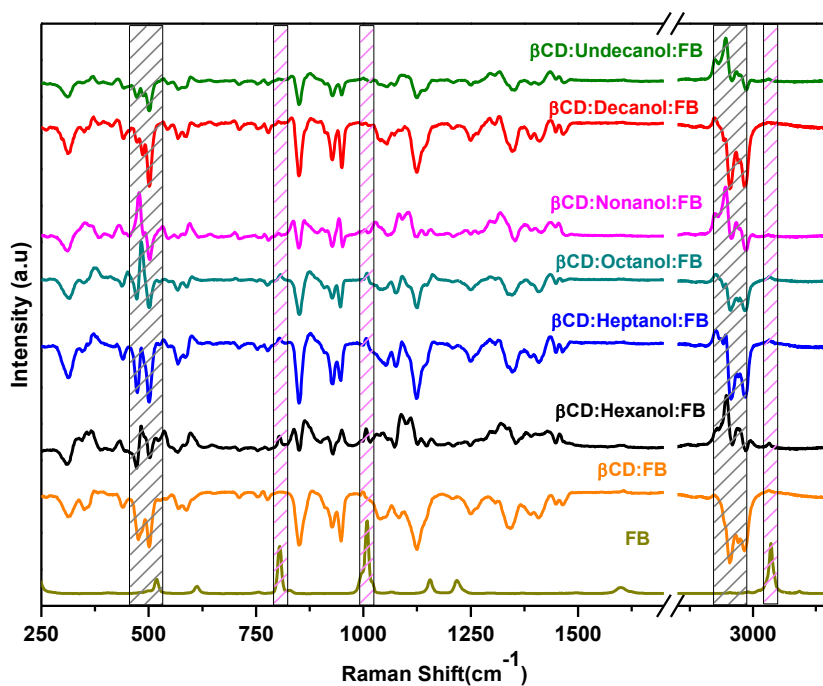


Figure 4. Normalised Raman Spectra obtained after β CD spectrum subtraction from β CD:FB (1:1) and β CD:Alcohol:FB (1:1:1) in comparison with Raman spectrum of FB.

β CD:TOL and β CD:Alcohols:TOL complex Normalised subtracted spectrum

The normalised subtracted spectrum for β CD:TOL (Figure 5) has shown intense peaks corresponding to TOL indicating strong bonding interaction happening between the host and the guest. The peaks can be seen at the positions -785, 998, 1206 and 3046 cm^{-1} . Most of the vibrational modes of β CD have got affected on complexation. The main changes can be seen at positions-365, 478, 952 and 1320 cm^{-1} .

The peaks of TOL observed in normalised subtracted spectrum of β CD:Alcohol:TOL (Figure 6) complexes have become intense for the cases complexes prepared with Nonanol and Undecanol. All the spectra are very similar to the one obtained for β CD:TOL except for the changes observed between 450-550 and 2890 cm^{-1} .

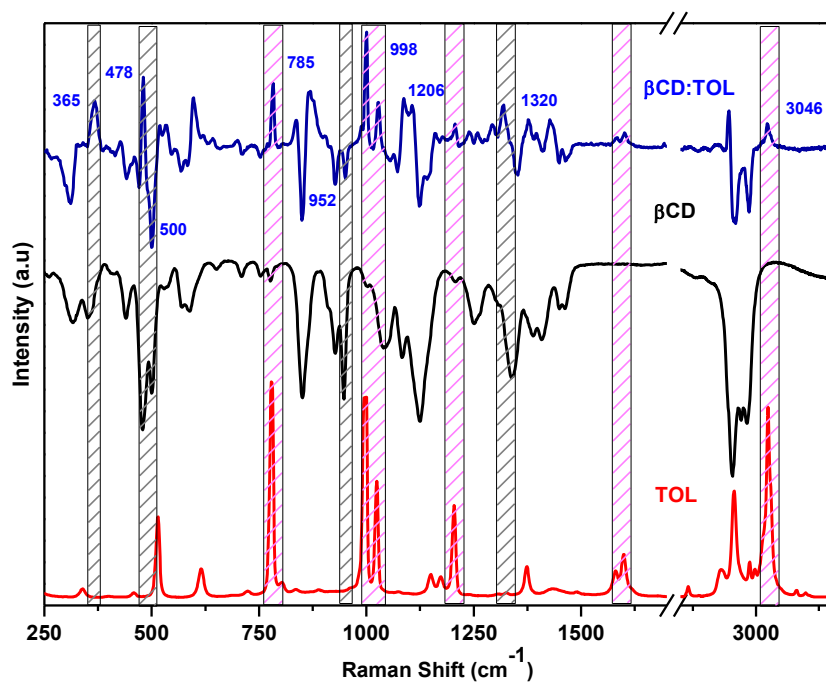


Figure 5. Normalised Raman Spectrum obtained after β CD spectrum subtraction from β CD:TOL (1:1) in comparison with Raman spectrum of TOL.

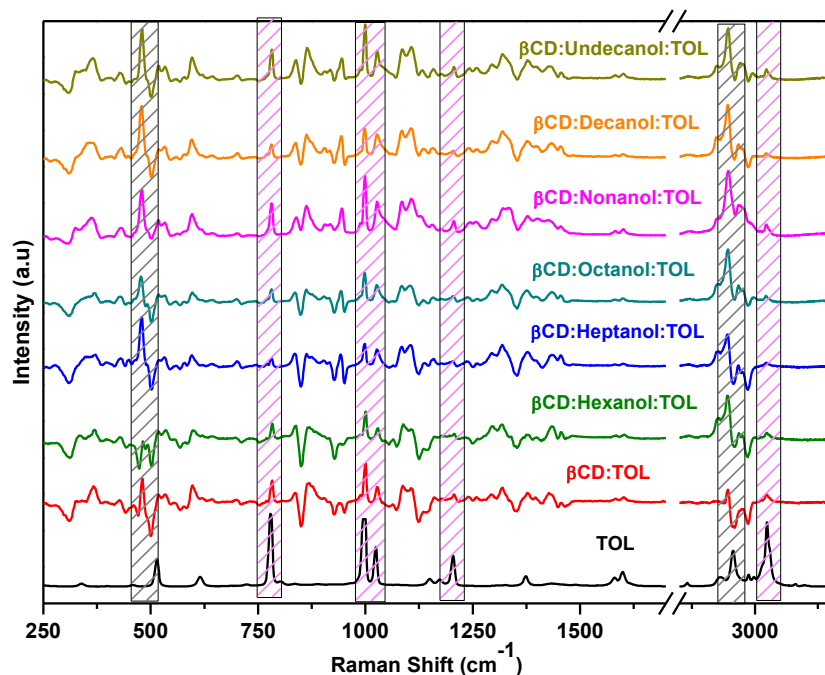


Figure 6. Normalised Raman Spectra obtained after β CD spectrum subtraction from β CD:TOL (1:1) and β CD:Alcohol:TOL (1:1:1) in comparison with Raman spectrum of TOL.

β CD:TFT and β CD:Alcohols:TFT complex Normalised subtracted spectrum

The normalised subtracted spectrum of β CD:TFT (Figure 7) contains intense peaks corresponding to TFT at positions 767, 1002, 1320, 1611 and 3065 cm^{-1} . The intensity of the peaks indicates strong interactions between the host and the guest. The other changes in the vibrational modes mainly of the intensity changes can be seen at positions 482, 500 and 1092 cm^{-1} .

The normalised subtracted spectra observed for β CD:Alcohol:TFT (Figure 8) with Hexanol, Octanol, Decanol and Undecanol seem different from β CD:TFT for the peaks between 450-550 and at 2890 cm^{-1} . The intensity of the peaks has changed while the rest remains the same.

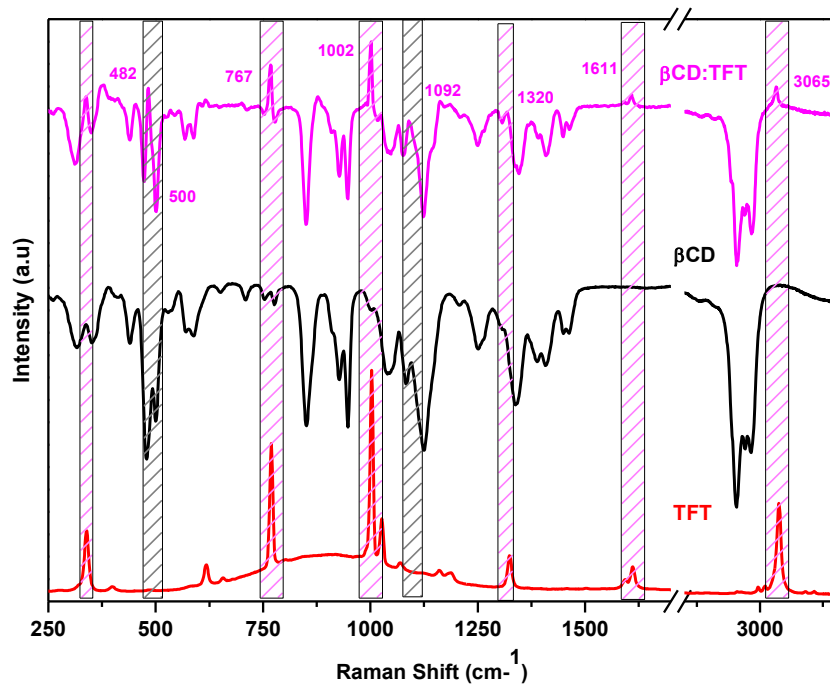


Figure 7. Normalised Raman Spectrum obtained after β CD spectrum subtraction from β CD:TFT (1:1) in comparison with Raman spectrum of TFT.

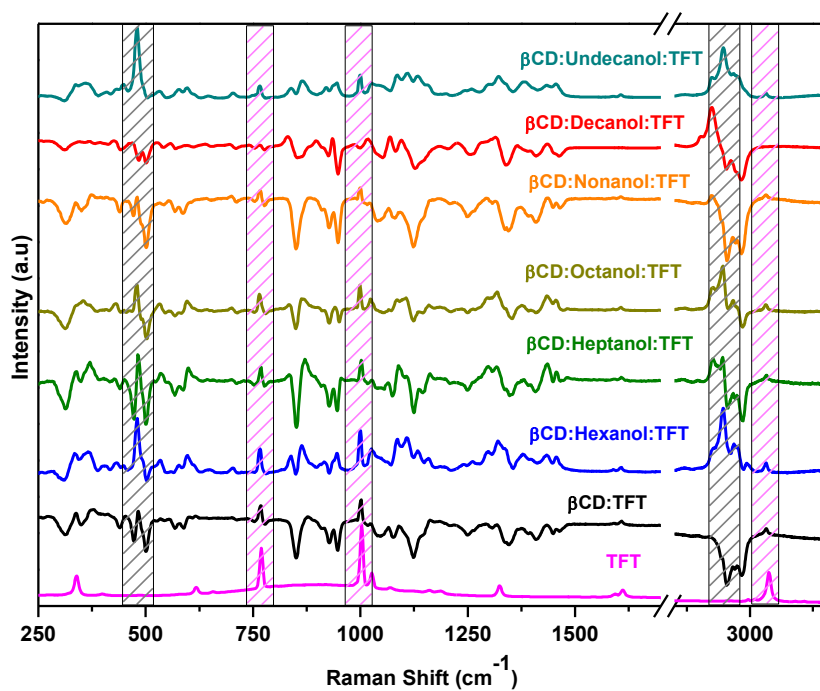


Figure 8. Normalised Raman Spectra obtained after β CD spectrum subtraction from β CD:TFT (1:1) and β CD:Alcohol:TFT (1:1:1) in comparison with Raman spectrum of TFT.

β CD:PHE complex subtracted spectrum

The normalised spectrum (Figure 9) has shown intense peaks corresponding to PHE at positions – 810, 1000, 1596 and 3057 cm^{-1} . The changes in the vibrational modes indicates strong interaction between the host and the guest. The other vibrational motion changes can be seen at positions-362, 482, 500 and between 2850-2980 cm^{-1} .

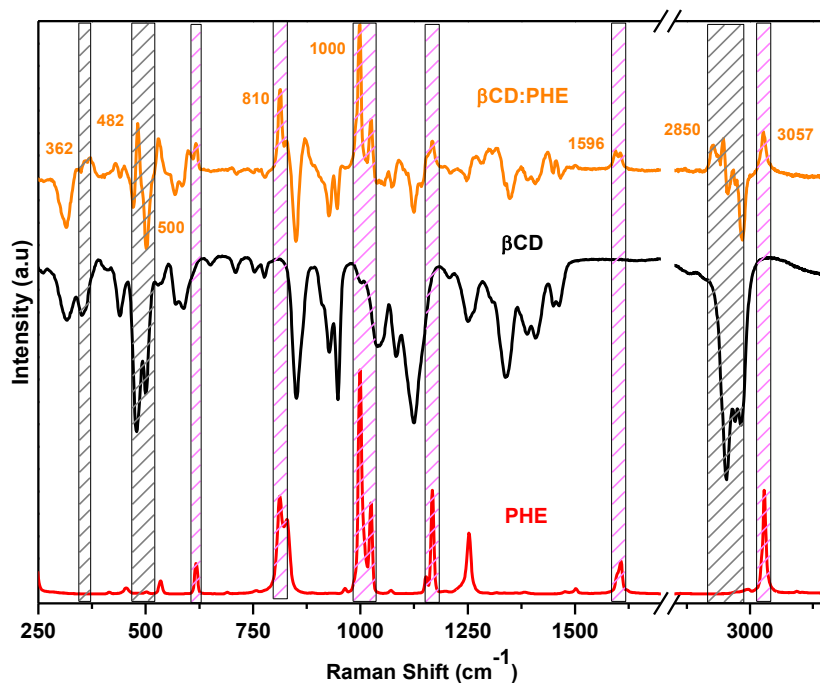


Figure 9. Normalised Raman Spectrum obtained after β CD spectrum subtraction from β CD:PHE (1:1) in comparison with Raman spectrum of PHE.

β CD:BA complex subtracted spectrum

The normalised results (Figure 10) obtained have shown intense BA peaks at positions: 616, 787, 1000, 1602 and 3066 cm^{-1} . The existence of most of the peaks of the guest in the subtracted spectrum indicates strong interaction with the host. The other changes occurring in the vibrational modes of β CD can be seen at positions at 500 and 2959 cm^{-1} .

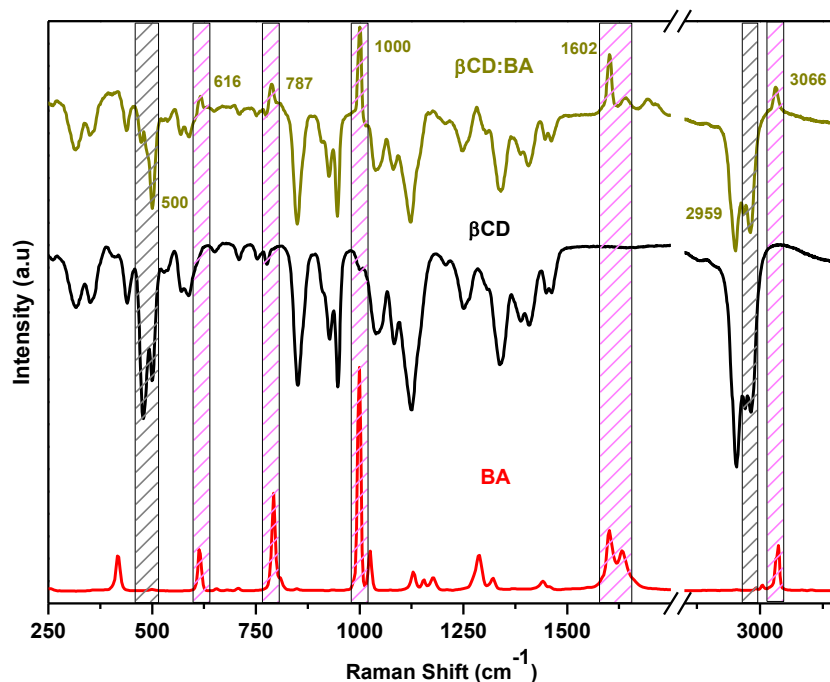


Figure 10. Normalised Raman Spectrum obtained after β CD spectrum subtraction from β CD:BA (1:1) in comparison with Raman spectrum of BA.

Bicyclic aromatic inclusion complexes

β CD:NAP and β CD:Alcohols:NAP complex Normalised subtracted spectrum

The resulted normalised spectrum (Figure 11) has shown very intense peaks of NAP in the complex at positions: 507, 755, 1018, 1378, 1576 and 3055 cm^{-1} . The complexation has strongly affected most of the vibrational modes of β CD. The behaviour is in accordance with the details obtained by our previous team members for the same system. Since most of the modes are strongly impacted, we are mentioning few of them for positions- 352 and between 2890-2970 cm^{-1} .

The normalised subtracted spectrum obtained for β CD:Decanol:NAP (Figure 12) seems to contain more of β CD character instead of NAP. The rest of the spectra contain NAP contain more indicating strong inclusion complexation.

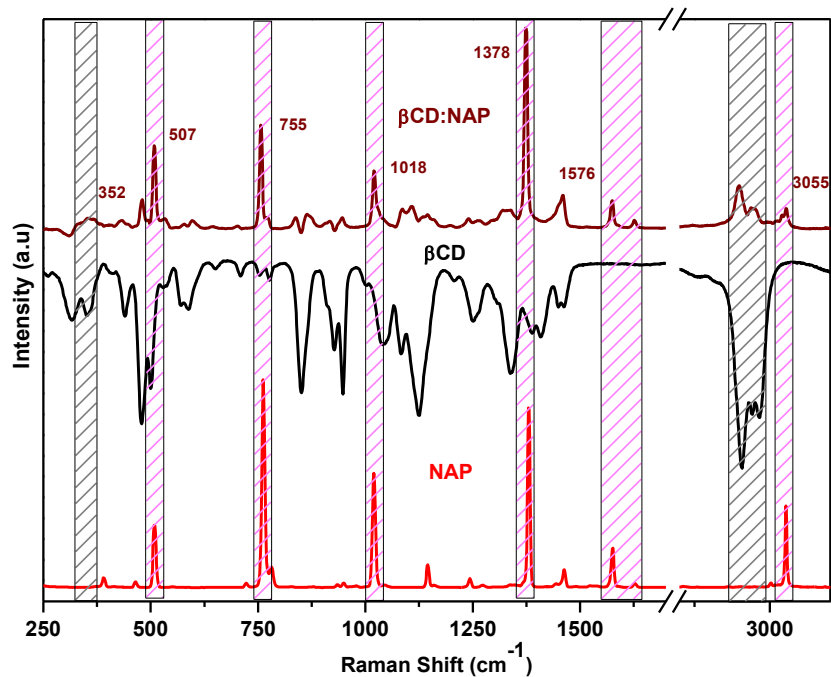


Figure 11. Normalised Raman Spectrum obtained after β CD spectrum subtraction from β CD:NAP (1:1) in comparison with Raman spectrum of NAP.

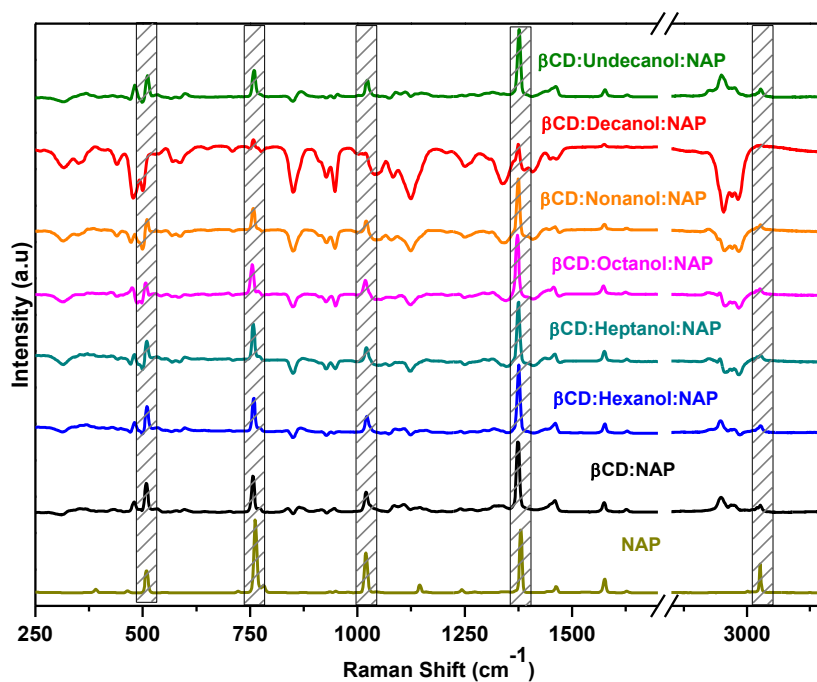


Figure 12. Normalised Raman Spectra obtained after β CD spectrum subtraction from β CD:NAP (1:1) and β CD:Alcohol:NAP (1:1:1) in comparison with Raman spectrum of NAP.

β CD:2-NAP complex subtracted spectrum

The peaks of 2-NAP in the normalised subtracted spectrum (Figure 13) can be seen at the positions: 521, 764, 1013, 1381, 1576, 1631 and 3050 cm^{-1} . The intensity of the peaks indicates strong interaction between the host and the guest. The strong impact has shown few more changes in the vibrational modes of β CD at 346 and 2893 cm^{-1} .

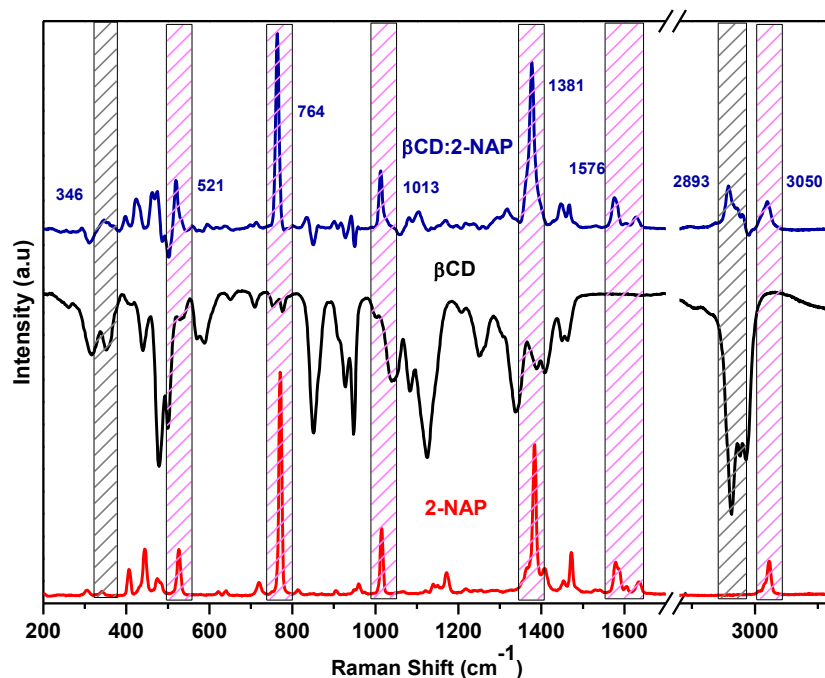


Figure 13. Normalised Raman Spectrum obtained after β CD spectrum subtraction from β CD:2-NAP (1:1) in comparison with Raman spectrum of 2-NAP.

Polycyclic aromatic inclusion complexes

β CD:ANTH and β CD:Alcohols:ANTH complex Normalised subtracted spectrum

The normalised spectrum (Figure 14) obtained does not show any of the ANTH peaks, in fact inverted spectrum of the reference i.e. β CD is obtained. This indicates no interaction between the host and the guest molecules.

The normalised subtracted spectra observed for β CD:Alcohol:ANTH complexes (Figure 15) have shown peaks of ANTH in all the cases which is completely different the spectrum obtained for β CD:ANTH where none of the peaks of ANTH were observed. The apparent changes can be seen between 2850-2980 cm^{-1} .

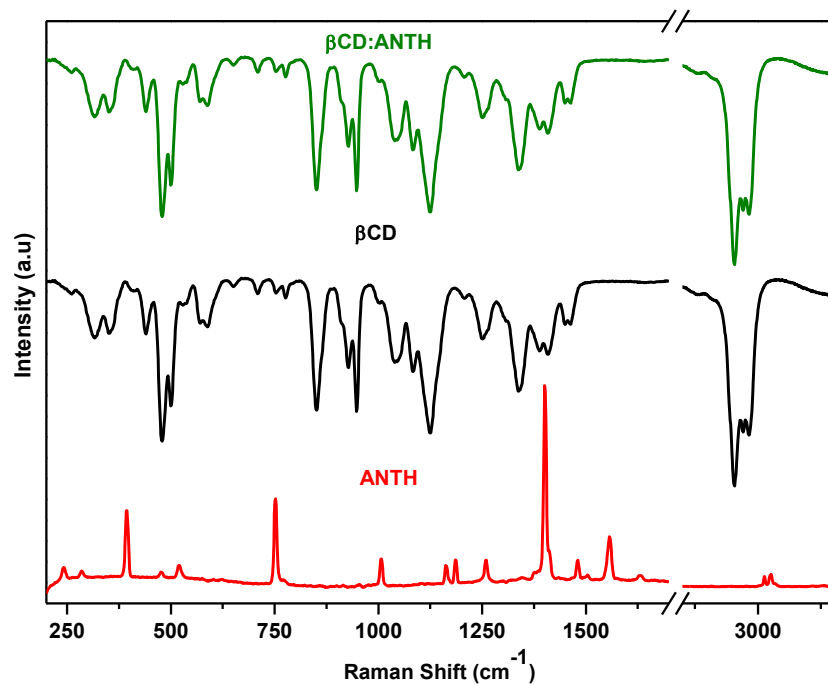


Figure 14. Normalised Raman Spectrum obtained after β CD spectrum subtraction from β CD:ANTH (1:1) in comparison with Raman spectrum of ANTH.

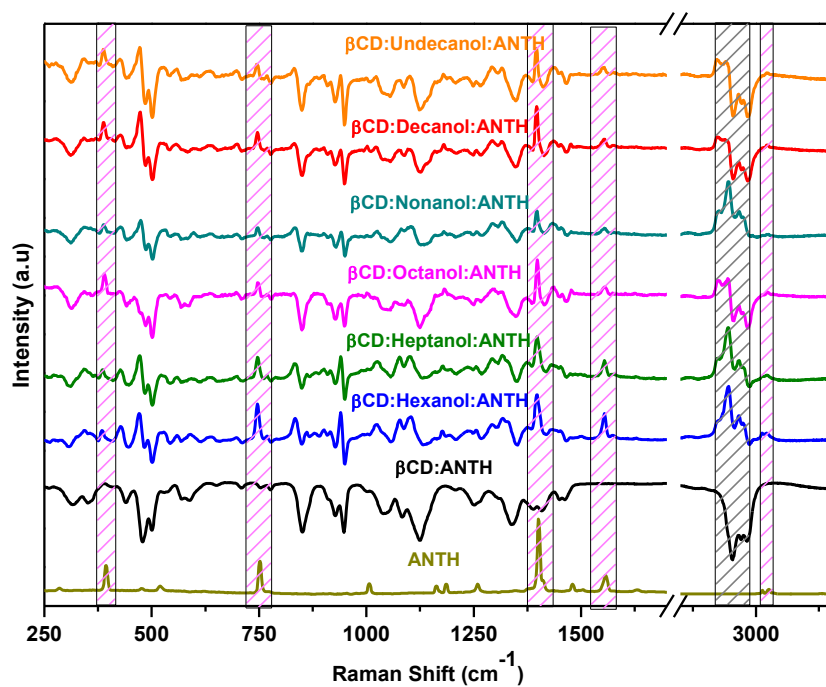


Figure 15. Normalised Raman Spectra obtained after β CD spectrum subtraction from β CD:ANTH (1:1) and β CD:Alcohol:ANTH (1:1:1) in comparison with Raman spectrum of ANTH.

β CD:PYR and β CD:Alcohols:PYR complex Normalised subtracted spectrum

The normalised spectrum shows the medium intense peaks of the PYR (Figure 16) in the system. These peaks can be observed at positions: 594, 1242, 1412, 1597 and 1630 cm^{-1} . The strong interaction between the host and the guest has created many changes in the β CD vibrational modes. Few of those changes can be seen at positions-400, 482, 936 and 1100 cm^{-1} .

The normalised subtracted spectra observed for β CD:Alcohol:PYR complexes (Figure 17) have shown peaks of PYR in all the cases similar to the spectrum obtained for β CD:PYR . The PYR peaks observed are similar in intensity in most of the cases except for Undecanol where the peaks have become slightly intense than the rest.

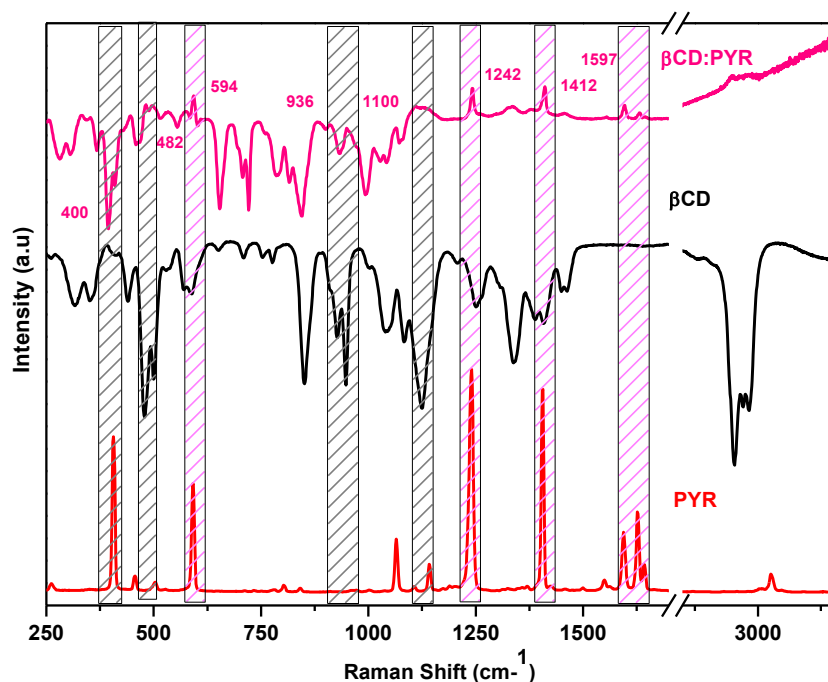


Figure 16. Normalised Raman Spectrum obtained after β CD spectrum subtraction from β CD:PYR (1:1) in comparison with Raman spectrum of PYR.

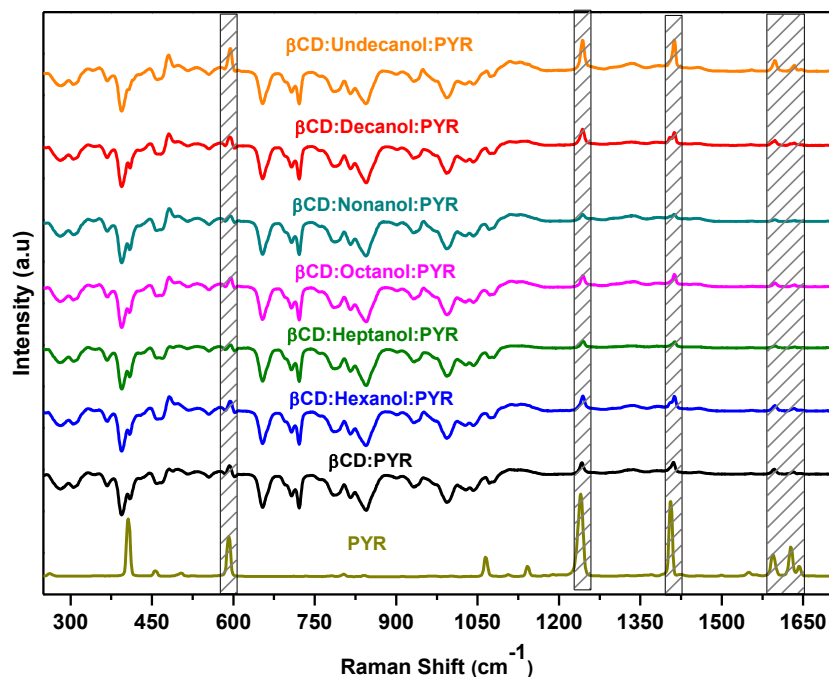


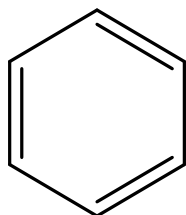
Figure 17. Normalised Raman Spectra obtained after β CD spectrum subtraction from β CD:PYR (1:1) and β CD:Alcohol:PYR (1:1:1) in comparison with Raman spectrum of PYR.

Conclusion

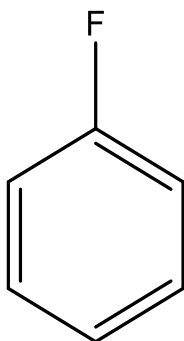
This study of normalised subtracted spectra revealed the existence of the aromatic guest peaks in the complex by highlighting all aromatic peaks when reference β CD spectrum was subtracted. The results are in accordance with the studies done before indicating strong inclusion complexation occurring between the host and the guest in most of the cases. The strong interactions also induced further changes in the vibrational modes of β CD indicating successful inclusion.

The normalised results obtained for ternary complexes obtained for β CD:Alcohols:Aromatics have shown results similar to the results observed for β CD:Aromatics in most of cases. For binary and ternary complexes prepared with BEN and ANTH showed results different from each other in the two cases indicating the effect of alcohols in complexation.

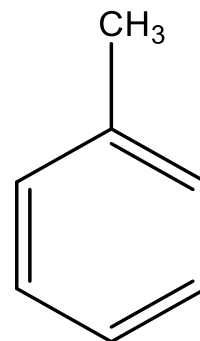
Chemical structures of the aromatics used



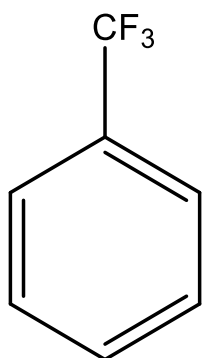
BENZENE



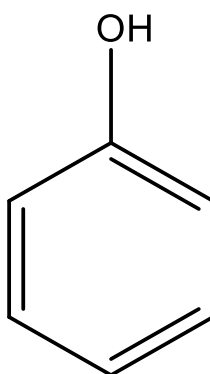
FLUOROBENZENE



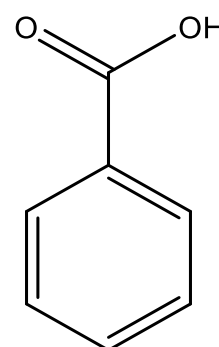
TOLUENE



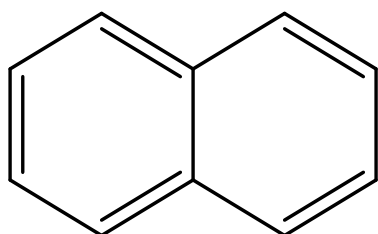
TRIFLUOROTOLUENE



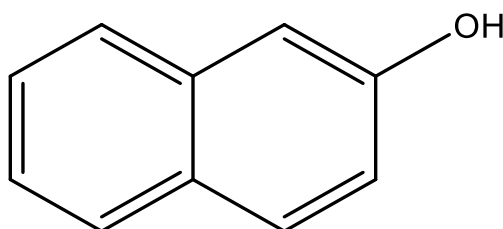
PHENOL



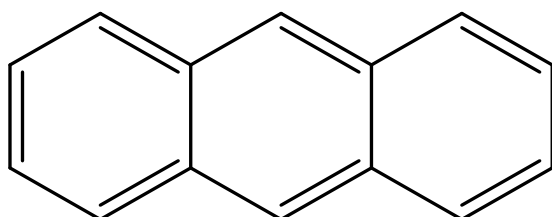
BENZOIC ACID



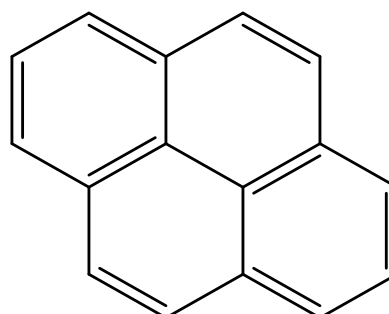
NAPHTHALENE



2-NAPHTHOL



ANTHRACENE



PYRENE

Abstract

Environmental water pollution by organic compound has become a major worldwide concern. Aromatic molecules like benzene rings and their derivatives have gained considerable attention due to officially documented toxicity and carcinogenicity. Mostly used in supramolecular chemistry, Cyclodextrins are truncated cone-shaped molecular structures having a hydrophilic outer surface and a hydrophobic cavity. Thus, they can theoretically encapsulate a large number of hydrophobic organic molecules to form water-soluble inclusion complexes. This complexation property has potential application in the field of detection and quantification of aromatic polycyclic pollutants in environmental water by portable spectroscopic means. We are interested in understanding this phenomenon of inclusion by combining theoretical and experimental approaches applied to solid state and in solution. It has been observed that only a few crystalline structures of cyclodextrin- pure aromatic molecule complexes appear in the structural databases after a brief review. Therefore, the main objective of our research is to focus more precisely on the interactions between the aliphatic alcohols and cyclodextrin molecules. For this purpose, to correlate our experimental and theoretical studies, the results obtained were monitored by various spectroscopic techniques in a systematic manner to observe the interaction between the molecules. Moreover, the powders and crystals obtained by varying the solubility of the mixtures were further subjected to physico-chemical analysis, X-ray diffraction, and DSC monitoring to support our findings. This work also includes modeling of inclusion complexes using different approaches like combining semi-empirical methods of quantum chemistry (DFT / TD-DFT) and polarizable molecular mechanics. Calculations were carried out on homemade clusters, which will allow the implementation of evidence of structural and energetic factors for complexation.

Keywords: β -Cyclodextrins, Aliphatic alcohols, Aromatic hydrocarbons, Encapsulation, NMR, PXRD, DSC, RAMAN, Molecular modelling

Résumé

La pollution de l'environnement par les composés organiques est devenue une préoccupation mondiale majeure. Les molécules aromatiques comme les cycles benzéniques et leurs dérivés ont attiré une attention considérable en raison de la toxicité reconnue et de la cancérogénicité. Principalement utilisées en chimie supramoléculaire, les cyclodextrines sont des structures moléculaires en forme de cône tronqué ayant une surface externe hydrophile et une cavité hydrophobe. Ainsi, ils peuvent théoriquement encapsuler un grand nombre de molécules organiques hydrophobes pour former des complexes d'inclusion solubles dans l'eau. Cette propriété de complexation a une application potentielle dans le domaine de la détection et de la quantification des polluants polycycliques aromatiques dans les eaux environnementales par des moyens spectroscopiques portables. Nous souhaitons comprendre ce phénomène d'inclusion en combinant des approches théoriques et expérimentales appliquées à l'état solide et en solution. Il a été observé que seules quelques structures cristallines de complexes de cyclodextrines, molécules aromatiques pures, apparaissent dans les bases de données structurales après un court examen. L'objectif principal de nos recherches est donc de nous concentrer plus précisément sur les interactions entre les alcools aliphatiques et les molécules de cyclodextrine. Pour cela, afin de corréliser nos études expérimentales et théoriques, les résultats obtenus ont été suivis de manière systématique par différentes techniques spectroscopiques afin d'observer l'interaction entre les molécules. De plus, les poudres et les cristaux obtenus en faisant varier la solubilité des mélanges ont été soumis à une analyse physico-chimique, à une diffraction des rayons X et à une surveillance DSC pour étayer nos résultats. Ce travail comprend également la modélisation de complexes d'inclusion en utilisant différentes approches, comme la combinaison de méthodes semi-empiriques de la chimie quantique (DFT / TD-DFT) et de la mécanique moléculaire polarisable. Des calculs ont été effectués sur des clusters internes, ce qui permettra de mettre en évidence des facteurs structurels et énergétiques de complexation.

Mots clés: β -cyclodextrines, alcools aliphatiques, hydrocarbures aromatiques, encapsulation, RMN, PXRD, DSC, RAMAN, modélisation moléculaire